FACULTY OF MEDICINE AND HEALTH SCIENCES

Towards a bio-active tissue engineered heart valve

Annelies Roosens

AY 2017-2018

Promotor: prof. dr. Ria Cornelissen
Co-promotor: dr. Pamela Somers

Thesis submitted in fulfilment of the requirement for the degree of
DOCTOR OF HEALTH SCIENCES

GHENT UNIVERSITY

Department of Basic Medical Sciences
Tissue Engineering Group

EXAMINATION COMMITTEE

prof. dr. Jolanda van Hengel (Chairman)
Department of Basic Medical Sciences
Ghent University, Belgium

prof. dr. Filip De Somer
Department of Surgery
Ghent University, Belgium

dr. Elien Gevaert
Department of Oto-rhino-laryngology and Logopaedic-audiologic Sciences
Ghent University, Belgium

dr. Sarah Glorieux
Tissue Bank
Ghent University Hospital, Belgium

prof. dr. Lieven Thorrez
Department of Development & Regeneration
University of Leuven, Belgium

dr. Maurizio Pesce
Tissue Engineering Research Unit
Centro Cardiologico Monzino, IRCCS, Milan, Italy

TABLE OF CONTENTS

LIST OF ABBREVIATIONS

A	
α-gal	Galactoseα1-3galactose
α-SMA	α-Smooth muscle actin
AA	Ascorbic acid-2-phosphate
AB	Alcian Blue
Alg	Alginate
AR	Aortic regurgitation
AS	Aortic stenosis
AV	Aortic valve
aVIC	Activated valvular interstitial cells
AVL	Aortic valve leaflet
B	
b	bovine
BHV	Bioprosthetic heart valves
BM	Bone marrow
BM-MSC	Bone marrow derived mesenchymal stem cells
BU-TE	Bottom-Up Tissue Engineering
C	
c	Canine
CVD	Cardiovascular diseases
D	
d	Days
DA	Diacrylate
DAPI	4',6-diamidino-2-phenylindole
E	
EC	Endothelial cells
ECM	Extracellular Matrix
Egr-1	Early growth response protein 1
EM	Elastic modulus
eNOS	Endothelial nitric oxide synthase
ENZ	Enzyme treatment: DNase + RNase
EXT	Extension
F	
Fb	Fibroblasts
FBS	Fetal bovine serum
FGF	Fibroblast growth factor
Flk-1	Fetal Liver Kinase 1
FSP-1	Fibroblast-specific protein 1
G	
GA	Glutaraldehyde
GAG	Glycosaminoglycans
Gel	Gelatin
Gel-MOD	Methacrylated modified gelatin
GF	Growth factor
H	
H	Height
h	Human
HA	Hyaluronic acid, hyaluronan

HA-MA	Methacrylated hyaluronic acid
HE	Hematoxylin Eosin
HV	Heart valve
HVD	Heart valve diseases
HVL	Heart valve leaflet
I	
Irg	Irgacure 2959; 2-Hydroxy-1-[4-(2-hydroxyethoxy) phenyl]-2-methyl-1-propanone
K	
KDR	Kinase insert domain receptor
L	
l	Lapine
LF	Lamina fibrosa
LS	Lamina spongiosa
LV	Lamina ventricularis
M	
m	Months
MFb	Myofibroblast
MHC	Major histocompatibility complex
MHV	Mechanic heart valves
ML	Maximum load
MMP	Matrix metalloproteinases
MNC	Mononuclear cells
MSC	Mesenchymal stem cells
N	
N/A	Not applicable
N/I	Not investigated
NVP	1-vinyl-2-pyrrolidinone
O	
o	Ovine
obVIC	Osteoblastic valvular interstitial cells
OCN	Osteocalcin
P	
p	Porcine
PEG	Polyethylene glycol
PEGDA	Polyethylene glycol diacrylate
PEG-diMA	Polyethylene glycol dimethacrylate
PEGnb	Polyethylene glycol norbornene
PER	Pericardium
PG	Proteoglycans
PGA	Polyglycolic acid
PI	Photoinitiator
PLA	Polylactic acid
PLGA	Polylactic-co-glycolic acid
PR	Picrosirius Red
PV	Pulmonary valve
pVIC	Progenitor valvular interstitial cells
PVL	Pulmonary valve leaflet
Q	
qVIC	Quiescent valvular interstitial cells

R	
r	Rat
RGD	Tripeptide Arg-Gly-Asp
Runx2	Runt-related transcription factor 2
S	
SDC	Sodium deoxycholate
SDS	Sodium dodecyl sulfate
SEM	Scanning electron microscopy
SIS	Small intestine submucosa
SMC	Smooth muscle cells
ST	Stiffness
T	
T	Thickness
TD-TE	Top-Down Tissue Engineering
TE	Tissue Engineering
TEA	Triethanolamine
TEHV	Tissue Engineered Heart Valves
TGF-β1	Transforming growth factor-beta 1
TIMP	Tissue inhibitor of matrix metalloproteinases
TRYP	Trypsin treatment
U	
UV	Ultra violet
V	
VA	VA-0186; 2,2'-Azobis[2-methyl-N-(2-hydroxyethyl)propionamide]
VEC	Valvular endothelial cells
VIC	Valvular interstitial cells
vWF	von Willebrandfactor
W	
w	Weeks
W	Width
WTML	Work to maximum load
Y	
y	Years

SUMMARY/SAMENVATTING

Valvular heart diseases represent a major healthcare issue causing significant morbidity and mortality worldwide. Clinical treatment of end-stage valvulopathy still primarily relies on mechanical or bioprosthetic heart valve replacements, but none of them are ideal valve substitutes. Mechanical valves are durable but are made of artificial biomaterials, therefore, patients with mechanical heart valves require a life-long anti-coagulation treatment due to the substantial risk of thromboembolisms. On the other hand, bioprosthetic valves, for example glutaraldehyde-treated porcine valves or cryopreserved human donor valves, have better hemodynamic characteristics and patients do not face anticoagulation therapy. The drawback of this type is that they have a limited durability due to premature degeneration and calcification. Yet the main disadvantage of all these currently available heart valve substitutes is that they are non-living structures and lack the ability to grow, repair and remodel within the patient.

To overcome the shortcomings of these current treatment options, heart valve tissue engineering approaches have emerged, all with the same goal: to engineer a bio-active, living autologous heart valve with regeneration, remodeling and growth potential, which is especially needed for younger patients as they outgrow valve replacements, resulting in multiple re-operations.

Heart valve tissue engineering is an evolving field of research, which faces several critical issues, including scaffold and cell selection as well as appropriate conditions to accomplish repopulation. **PART A** of this thesis focused on the generation of bio-active cardiac tissues by repopulating xenogeneic tissues (a top-down approach). As it is known that xenogeneic cells can evoke an immunologic response in human recipients, it was important to remove all cellular components before using xenogeneic tissues as a scaffold material. In **SECTION I** the efficacy of cell removal of different decellularization protocols (SDC or Triton X-100 based protocols) and their impact on porcine heart valve leaflets (HVL) and pericardia (PER) was evaluated. Based on the three minimal criteria for acellularity, it was shown that decellularization with Triton X-100+ENZ+TRYP was more effective than with SDC and resulted in cell free HVL as well as PER. In addition, it was demonstrated that the decellularization procedure had less impact on the extracellular matrix (ECM) components of HVL than of PER. Although glycosaminoglycans were lost and a small increase of leaflet stiffness was observed, collagen and elastin fibers were preserved. In **SECTION II**, a static two-stage seeding protocol was used for the repopulation of Triton X-100 decellularized HVL and PER. First, the interstitium was repopulated with valvular interstitial cells (VIC) or stem cells (BM-MSC or ADSC). Secondly, endothelial cells (EC) were used to generate an endothelium layer. The suitability of BM-MSC, once cultivated in the presence of ascorbic acid, and VIC for the complete repopulation of the interstitium of HVL was demonstrated *in vitro*. Compared with ADSC, BM-MSC showed greater migratory potential and recolonized HVL more efficient than PER tissue. In general, it was shown that

within 14 days, the interstitium of HVL could be recolonized and that it was also possible to co-culture endothelial cells on the surface to obtain a continuous endothelium layer.

Although the last 20 years, much progress has been made with the top-down approach, a bio-active living tissue engineered heart valve is still not developed and alternative approaches should be explored. Such an alternative approach could be the generation of bio-active valvular tissue from the bottom-up, which was the main focus of **PART B** of this thesis. Bottom-up tissue engineering aims to create biomimetic tissues by mimicking native microstructural functional tissue blocks and using these modular units as building blocks to engineer larger tissue constructs. In **SECTION I**, a scaffold-free high throughput microwell system was used for the formation of microscale tissue building blocks from VIC in a low shear force environment. This completely cell driven 3D approach generated high-quality valvular microtissues (Ø 150µm) which resembled the native valve composition and contained native-like quiescent VIC that were able to produce and to remodel the ECM. Because the next step is to assemble these microtissues into larger valvular tissue constructs by 3D bioprinting, a cell friendly and printable material was needed. Therefore, in **SECTION II**, modified gelatin (Gel-MOD) hydrogels were evaluated as a microtissues-carrier material/bio-ink for future bioprinting applications. It was evidenced that microtissues remained viable within Gel-MOD hydrogels during the complete study duration. Moreover, they were still able to produce valve related ECM components while remaining in a quiescent state. In addition, a proof of concept was given for the formation of larger valvular tissues by showing that microtissues were able to randomly assemble and to fuse into larger microtissues (Ø 150-1400µm) in soft Gel-MOD hydrogels.

In conclusion, the feasibility of generating bio-active tissues through repopulation of xenogeneic tissues or through biofabrication of valvular microtissue from the bottom-up was demonstrated. Yet, future efforts should be made to 1) repopulate whole porcine heart valves with BM-MSC and EC, 2) biofabricate a larger-scale valvular macrotissue through directed assembly by bioprinting microtissues-laden Gel-MOD, in order to generate a bio-active tissue engineered heart valve.

Hartklepaandoeningen zorgen wereldwijd voor een significante morbiditeit en mortaliteit en maken een groot deel uit van de gezondheidszorg. Klinische behandeling van ernstige valvulopathie gebeurt nog steeds door mechanische of bioprosthetische hartklepvervangingen, maar geen van hen zijn ideale klepvervangers. Mechanische kleppen zijn duurzaam maar zijn vervaardigd uit kunstmatige biomaterialen. Patiënten met deze kleppen hebben een levenslange anti-coagulatiebehandeling nodig door het aanzienlijk verhoogde risico op thrombo-embolismen. Anderzijds hebben bioprosthetische kleppen, zoals glutaaraldehyde gefixeerde varkenskleppen of cryo-gepreserveerde humane donorkleppen, betere hemodynamische eigenschappen maar een beperktere duurzaamheid door vroegtijdige degeneratie en verkalking. Het voordeel is dat patiënten met dit soort kleppen geen anti-coagulatietherapie vereisen. Een groot nadeel van alle hartklepprothesen in het algemeen is dat het om niet-levende structuren gaat, en het vermogen om te groeien of te herstellen of te remodelleren in patiënten ontbreekt.

Om de tekortkomingen van deze huidige behandelingsopties op te lossen, zijn er verschillende methoden van hartklepweefsel-engineering ontstaan, allemaal met hetzelfde doel: een bio-actieve, levende autologe hartklep ontwikkelen die kan groeien, zich kan herstellen bij schade en zich kan aanpassen aan de behoeften van het lichaam. Dit is voornamelijk van belang voor jongere patiënten aangezien zij de klepvervangingen ontgroeien en vaak herhaalde operaties nodig hebben.

Hartklepweefsel-engineering is een snel evoluerend onderzoeksveld, dat verschillende kritische problemen ondervindt, waaronder de selectie van de ideale scaffold en cel bron, alsmede passende omstandigheden om repopulatie van de scaffold te bereiken. **DEEL A** van dit proefschrift heeft betrekking op de generatie van bio-actieve cardiale weefsels d.m.v. cel repopulatie van xenogene weefsels (een *top-down* benadering). Doordat bekend is dat xenogene cellen na transplantatie in humane recipiënten een immunologische respons kunnen uitlokken, is het van belang al deze cellulaire componenten te verwijderen alvorens xenogene weefsels als scaffold-materiaal gebruikt kunnen worden. In **SECTIE I** werd de efficiëntie van cel verwijdering van verschillende decellularisatie-protocols (SDC- of Triton X-100-gebaseerde protocols) en hun impact op porciene hartklepblaadjes (HVL) en pericardia (PER) geëvalueerd. Op basis van de drie minimale criteria voor acellulariteit bleek dat decellularisatie met Triton X-100+ENZ+ TRYP effectiever was dan wanneer SDC werd gebruikt en resulteerde in cel vrije HVL en PER. Bovendien werd aangetoond dat de decellularisatie procedure minder impact had op de extracellulaire matrix (ECM) componenten van HVL dan PER. Hoewel glycosaminoglycanen werden weggewassen en er een kleine toename van de stijfheid van klepbladen werd waargenomen, bleven collageen- en elastine vezels bewaard. In **SECTIE II** werd een statisch tweestaps-bezaaiingsprotocol gebruikt voor de repopulatie van Triton X-100 gedecellulariseerde HVL en PER. Eerst werd het interstitium gerepopuleerd met valvulaire

interstitiële cellen (VIC) of stamcellen (BM-MSC of ADSC). Vervolgens werden endotheelcellen (EC) gebruikt om een endotheel laag te genereren. De geschiktheid van BM-MSC, gecultiveerd in de aanwezigheid van ascorbinezuur, en VIC voor de volledige repopulatie van het interstitium van HVL, werd aangetoond *in vitro*. BM-MSC, vergeleken met ADSC, vertoonden meer migratiecapaciteit en repopuleerden HVL efficiënter dan PER weefsel. In het algemeen werd aangetoond dat binnen 14 dagen het interstitum van HVL volledig gerepopuleerd kan worden en dat het ook mogelijk is om endotheliale cellen op het oppervlak te co-cultiveren en een confluente endotheliumlaag te verkrijgen.

Hoewel de afgelopen 20 jaar veel vooruitgang is geboekt met de *top-down* benadering, is een bio-actieve levende weefsel geëngineerde hartklep nog niet ontwikkeld en is er nood aan alternatieve benaderingen. **DEEL B** van dit proefschrift heeft betrekking op zo een alternatieve aanpak en focuste op de biofabricatie van bio-actief klepweefsel van de *bottom-up*. *Bottom-up* weefselengineering heeft tot doel biomimetische microweefsels te creëren en deze modulaire eenheden te gebruiken als bouwstenen om grotere weefselconstructen te biofabriceren. In **SECTIE I** werd een agarose-microwell systeem gebruikt voor de vorming van microweefsel bouwstenen vertrekkende van VIC. Deze volledig cel-aangestuurde 3D-aanpak genereerde snel hoge kwaliteitsvolle valvulaire microweefsels (Ø 150µm), die lijken op de native klep compositie en *native-like quiescent* VIC bevatten die in staat waren om ECM te produceren en te remodelleren. Aangezien de volgende stap is om deze microweefsels te assembleren in grotere valvulaire weefselconstructies d.m.v. 3D bioprinting, was er een cel compatibel en printbaar materiaal nodig. In **SECTIE II** werden gemodificeerde gelatine (Gel-MOD) hydrogels geëvalueerd als microweefsel-*carrier* materiaal (bio-inkt). Er werd aangetoond dat de valvulaire microweefsels gedurende de volledige studieduur viabel bleven in Gel-MOD. Bovendien konden ze nog steeds hartklep gerelateerde ECM componenten produceren en hun *quiescent* toestand bleef ongewijzigd. Daarnaast werd ook aangetoond dat grotere valvulaire weefsels (Ø 150-1400µm) gegenereerd konden worden door fusie van microweefsels in zachte Gel-MOD hydrogels.

In het algemeen werd aangetoond dat de generatie van bio-actief hartklepweefsel kan bekomen worden d.m.v van repopulatie van xenogene hartklepblaadjes of door biofabricatie van valvulaire microweefsels. Er dienen echter nog inspanningen gedaan te worden om 1) een volledige porciene hartklep te repopuleren met BM-MSC en EC, 2) een grotere valvulair macroweefsel te biofabriceren door middel van gerichte assemblage door bioprinting van microweefsels met Gel-MOD, om zo mogelijks in de toekomst een volledige bio-actieve hartklep te genereren.

CHAPTER I

General introduction

1. The human aortic valve

1.1 Anatomy (Macrostructure)

The heart valves (HV) play a key role in the unidirectional blood flow regulation of the body. The mitral and tricuspid valve are atrioventricular valves located between the atria and the ventricles, while the pulmonary and aortic valve are semilunar valves located between the ventricles and the great arteries **(Fig.1)** [1].

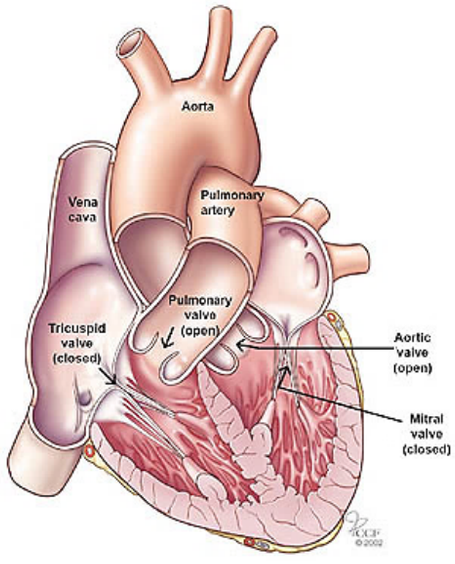

Fig.1: Gross anatomy of the human heart (valves) during systole
(Retrieved from: https://my.clevelandclinic.org/health/articles/women-valve-disease)

Heart valve diseases (HVD) are believed to be 'the next cardiac epidemic' [2]. An estimated 2.5% of the population in developed countries suffer from HVD. One of the most commonly affected and frequently transplanted valves is the aortic valve [3].

The aortic valve closes after each systole, preventing backflow of blood into the ventricle. The opening and closing of the valve is a passive process induced by the pressure gradient over the valve. On average, the valve opens and closes 70 times per minute, $1.03*10^5$ times each day, which adds up to $37*10^6$ times a year [4].

The aortic valve allows the left ventricle outflow and is situated in the aortic root, which is the transition part from the left ventricle to the ascending aorta [1]. The valve consists of three semilunar heart valve leaflets (HVL) and the aortic root is composed of the annulus or ventriculo-aortic junction, the sinotubular junction, the leaflet attachment site, three sinuses of Valsalva, three interleaflet triangles and three commissures **(Fig.2)**. Each leaflet has a free edge with a thickened circular node (nodule of Arantius), which provides the coaptation area to the corresponding neighboring valve leaflets, a leaflet "*belly*" and a basal part attached to the aortic root [5, 6]. The

annulus or ventriculo-aortic junction of the aortic root is a virtual ring defined by the nadirs (basal attachments) of the leaflets. The leaflet attachment sites are U-shaped and form a crown-like structure [5, 7]. The three commissures are located at the apical part of the leaflet attachment site and are the points where two leaflets touch each other at the level of the sinotubular junction. Under each commissure lies one of the three interleaflet triangles. The three bulges of the aortic wall are named the sinuses of Valsalva. They are limited proximally by the attachments of the valve leaflets and distally by the sinotubular junction [7]. The sinotubular junction separates the aortic root from the ascending aorta and is a tubular structure formed by the distal part of the sinuses together with the commissures [5-7].

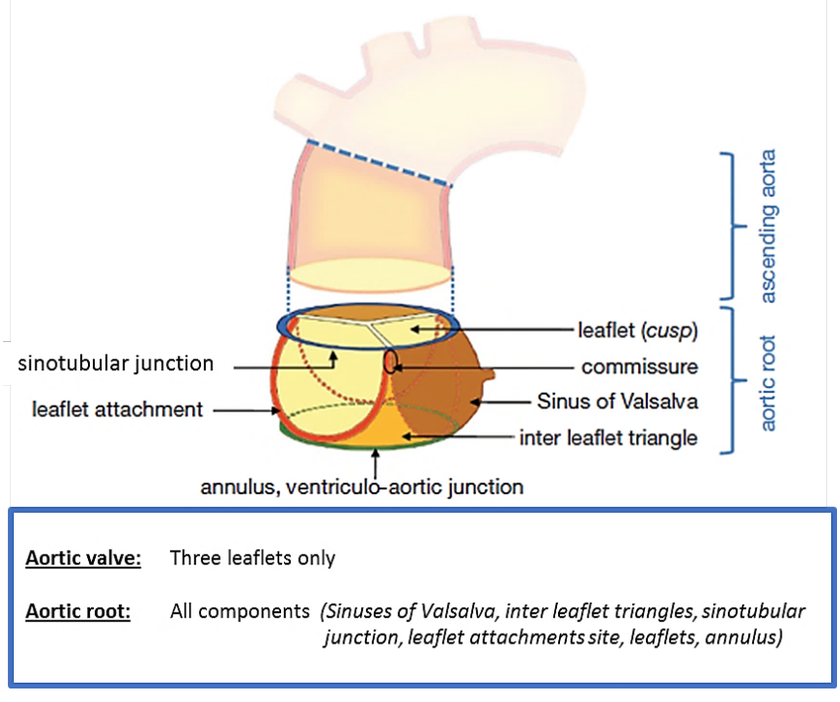

Fig.2: Terminology of the aortic valve and root components (one sinus of Valsalva is excised) (adapted from [5])

1.2 Histology (Microstructure)

1.2.1 Different layers and components of heart valve leaflets

Microscopically, the aortic heart valve leaflet (HVL), as shown in **Figure 3**, is composed of three distinct layers that adapt to biomechanical changes and provide optimal opening and closing during the cardiac cycle: the lamina fibrosa (LF), spongiosa (LS), and ventricularis (LV) [8, 9].

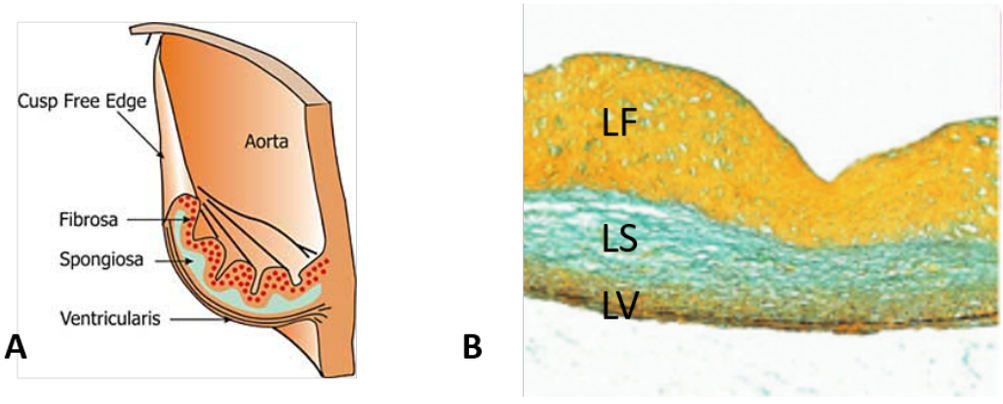

Fig.3: The three-layered architecture of an aortic heart valve leaflet

A: Schematic overview of the three-layered heart valve leaflet structure. A cutaway through the leaflet and aortic wall showing the internal configuration of the lamina fibrosa, spongiosa and ventricularis (adapted from [8]). **B:** Movat pentachrome staining of a decellularized aortic valve leaflet showing the three-layered structure. The LF is the nearest to the aortic side of the valve, contains type I and III fibrillar collagens, and serves a load-bearing function. The LS contains glycosaminoglycans (GAG) that lubricate the fibrosa and ventricularis layers as they shear and deform during the cardiac cycle. The LV contains elastin fibers to decrease radial strain. Yellow, dense collagen; black, elastin fibers; blue, soluble matrix proteins (GAG). L, lamina; F, fibrosa; S, spongiosa; V, ventricularis (adapted from [10]).

The LF is the stiffest layer with elastic moduli ranging from 0.5 to 13.02 kPa [11, 12]. It is located nearest to the outflow, at the atrial side and is primarily composed of densely packed, circumferentially aligned collagen I fibers [4, 13]. The collagen bundles are responsible for the strength and stiffness of the leaflets by applying resistance against the diastolic tension during valve closure. They extend during diastole, maintain coaptation and transfer the load, which the leaflets are exposed to when the valve is closed, to the adjacent aortic root **(Fig.4)** [6, 14].

The LS is the middle layer and is mainly composed of glycosaminoglycans (GAG) and loosely arranged collagen fibers [15, 16]. The LS has a gelatinous consistency due to the hydrophilicity of these GAG, which are capable of absorbing water. This layer is thus easily deformed and not quickly compressed by shear forces during the cardiac cycle [17, 18].

The LV is the layer facing the ventricular cavity, and is primarily composed of radially aligned elastin fibers [6, 13]. The abundancy of elastin provides the elasticity needed for the leaflets to extend, which increases the coaptation area during diastole, and to contract against the wall by pulling the collagen fibers of the LF, which results in the formation of corrugations on the surface of the leaflets and reduces the surface area during systole **(Fig. 4)** [19, 20]. The elastic moduli of this layer are ranging from 0.25 to 7.41 kPa [11, 12].

Healthy, normal valve leaflets are traditionally thought to be avascular and the presence of blood vessels in leaflets to be pathologic [21, 22]. However, it has been shown that normal valve leaflets

can contain a vascular bed where tissue thickness is the greatest [23]. Leaflets are approximately 300-700µm thick and thought to rely on the diffusion of nutrients and oxygen to support normal function. The presence of a vasculature suggests that the metabolic activity of the leaflets is greater than can be supported by diffusion from the leaflet surface alone, but the exact route of oxygen delivery is still unclear [6, 23].

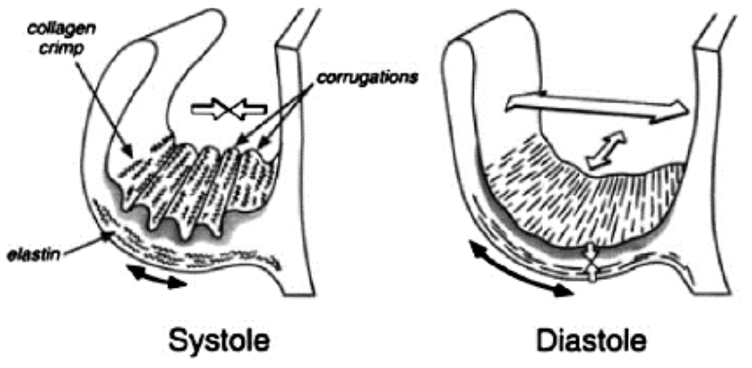

Fig.4: Role of elastin and collagen microstructure in mediating valve leaflet deformation (adapted from [24])
The leaflet behaves relatively inelastically in diastole (supported by the lamina fibrosa), and elastically in systole (supported by the lamina ventricularis). During opening, elastin contracts at minimal load during the extension of the collagen crimp and corrugations. During closing, the collagen fibers completely unfold and the load-bearing element shifts from elastin to collagen.

The overall proportion of collagen, proteoglycans (PG), and elastin in the human heart valves is 60%, 30%, and 10%, respectively, of the dry weight [13]. Collagen type I (74%) is predominantly found in the LF, whereas collagens type III (24%) and V (2%) are present throughout the complete leaflet [25]. PG consist of one or more linear, negatively charged polysaccharide GAG chain(s), covalently attached to a serine residue of a core protein [17]. PG are present in all layers of the leaflets, however, they are more concentrated in the LS. The major PG in valve tissue are biglycan, decorin, and versican. These PG consist of chondroitin sulfate and/or dermatan sulfate GAG side chains [26]. Total GAG composition in the valve is approximately 30% chondroitin-4-sulfate/chondroitin-6-sulfate, 15% dermatan sulfate, and 55% hyaluronic acid (HA) [27]. HA is the only GAG that does not bind to a core protein and is exclusively non-sulfated [28].

The quantity and quality of each of these extracellular matrix (ECM) components is determined by the valvular interstitial cells (VIC) [4, 29].

1.2.2 Different cell types of heart valve leaflets

There are two main cell types present in HVL: valvular endothelial cells (VEC) cover the surfaces of the leaflets, and VIC can be found throughout the entire interstitium **(Fig.5)** [14].

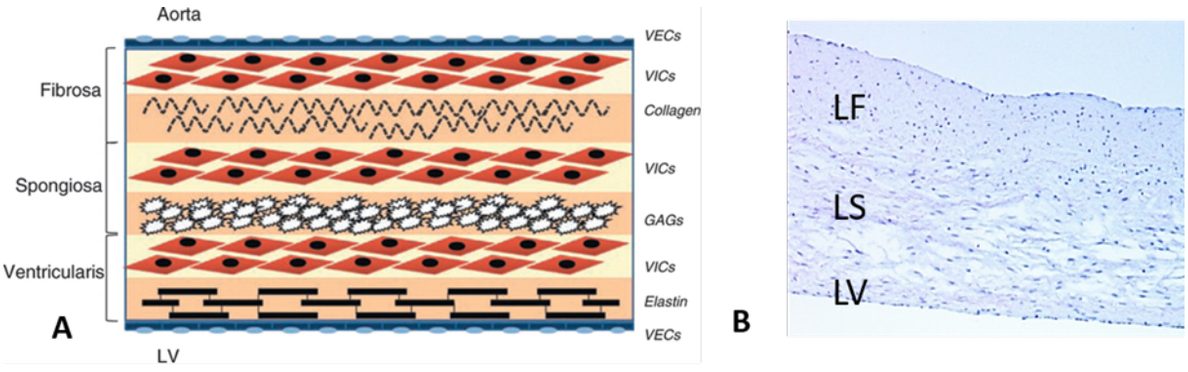

Fig.5: Three layered valve leaflet with valvular endothelial and interstitial cells

A: Schematic overview of the cellular architecture of the aortic valve. Valvular endothelial cells (VEC) line the outer surface of the valve and function as a barrier to limit inflammatory cell infiltration and lipid accumulation. The three middle layers contain valve interstitial cells (VIC) as the predominant cell type, which play an active role in the normal function of the aortic valve and undergo geometric alterations during the cardiac cycle (adapted from [9]). **B:** Hematoxylin Eosin (HE) staining of a native heart valve leaflet. L, lamina; F, fibrosa; S, spongiosa; V, ventricularis

The continuous monolayer of VEC plays a significant role in thrombogenesis prevention during blood contact, immune and inflammatory modulation, nutrient supply, as well as biochemical transmission to the underlying VIC [22, 30]. In contrast to the arrangement of endothelial cells (EC) elsewhere, the arrangement of the VEC is perpendicular to the direction of flow and similar to the alignment of the collagen fibers. It has been suggested that biaxial force, rather than shear stresses which occur in all blood vessels, might be responsible for this arrangement [30, 31]. VEC also behave differently based on their location on the leaflets. Simmons et al. identified a total of 584 genes as differentially expressed in situ by the endothelium on the aortic side versus ventricular side of normal aortic valves. The disease-prone aortic side of the valve expressed significantly less inhibitors of cardiovascular calcification [32].

Between the ECM components reside VIC, which are the most abundant cell type in HVL and are responsible for ECM synthesis, repair and remodeling [14]. During embryonic development, VIC arise from the transformation of the endothelial cells (EC) on the endocardial cushion, which is known as the endothelial-mesenchymal transition (EMT) [1, 14]. VIC can also origin from progenitor cells (pVIC), which are present in HVL, in the blood circulation and in bone marrow **(Fig.6).** pVIC have a high proliferative capacity which is important to repair the injured heart valve. However, the availability of pVIC is very limited and further studies on the influence of these cells during valve repair are necessary [14].

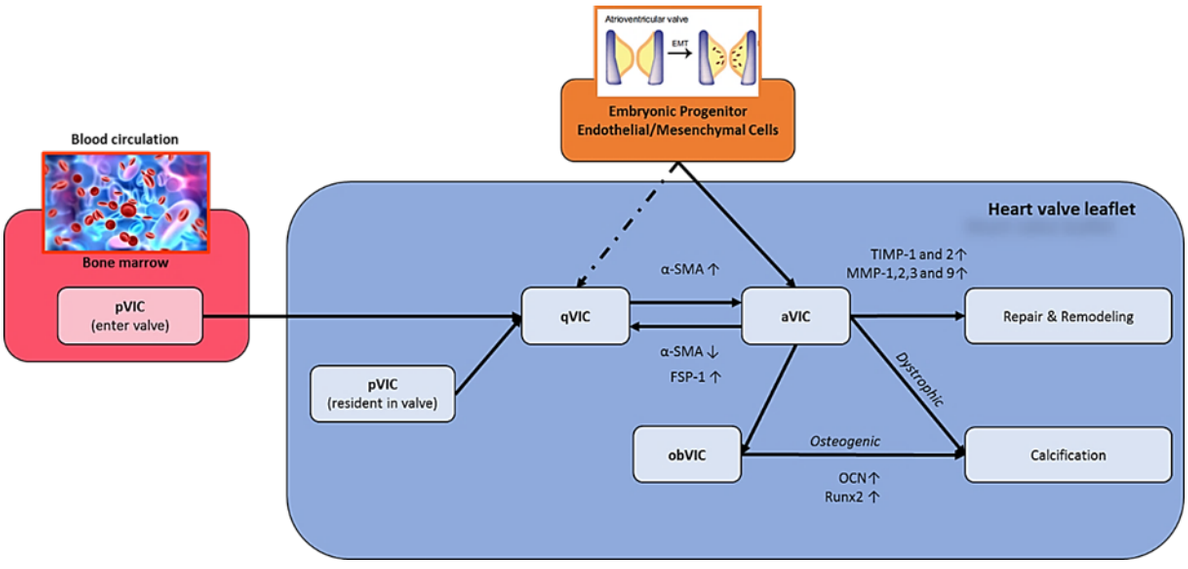

Fig.6: Schematic overview of the proposed VIC phenotype conversions

VIC play an active role in the normal function of the aortic valve and can undergo phenotypic conversions **(Fig.6).** In normal heart valve tissue, the majority of VIC are in a quiescent state (qVIC) and have a fibroblast-like phenotype, low proliferation capacity, minimal activity and express high vimentin and low alpha smooth muscle actin (α-SMA) [33-35]. VIC remain in this quiescent state in the absence of disease throughout life to maintain ECM homeostasis [36-38].

Studies suggest that qVIC can become activated (aVIC) during valve injury and repair or under pathological conditions. These aVIC are more contractile, have a higher proliferation rate and upregulate the myofibroblast (MFb) marker α-SMA [33, 37]. aVIC also secrete proteolytic enzymes that mediate matrix degradation and remodeling: matrix metalloproteinases (MMP)-1, 2, 3 and 9 [39, 40], and their inhibitors 1 and 2 (tissue inhibitor of MMP = TIMP) [41]. Only a small population of aVIC or in some cases no α-SMA positive cells are present in normal heart valve tissue [36-38]. Latif et al. estimate the number of myofibroblastic aVIC in normal valve leaflets to be <5% [37, 42, 43]. Reversal of the activated state leads to a decrease in α-SMA expression and an increase of fibroblast-specific protein 1 (FSP-1 or also known as S100A4) [44].

VIC can also differentiate towards a more osteoblast-like phenotype (obVIC), which are thought to be responsible for valve calcification. There is evidence that in calcified valves the levels of calcification-associated proteins such as osteopontin and osteocalcin (OCN) [45], as well as the expression of chondrogenesis and osteogenesis-associated transcription factors: Sox9 [46, 47] and runt related transcription factor 2 (Runx2 or also known as Cbfa1) [45-47] are elevated. In addition, Hjortnaes et al. recently showed that qVIC differentiate into obVIC by first undergoing myofibroblast differentiation [48].

The calcification process of VIC in HVL is a very complex and still not completely unraveled process. To date, two hypotheses of calcification from the resident VIC population dominate current thinking: the dystrophic/apoptotic calcification theory (calcification of dead or damaged cells, a passive process) and the ossification theory (phenotype conversion to a more osteoblast-like VIC, an active process) **(Fig.7)** [45, 49].

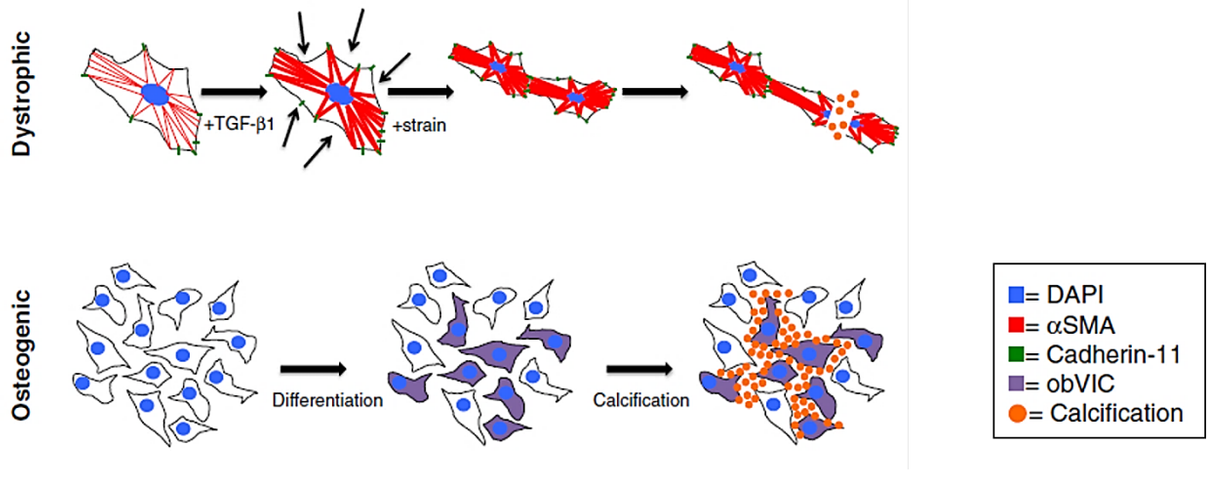

Fig.7: Schematic overview of the proposed mechanisms of valve calcification (adapted from [49])
The dystrophic pathway is mediated by a transforming growth factor-beta 1 (TGF-β1) mediated increase in α-SMA (differentiation into aVIC) and cadherin-11, which increases the cells' contractility and strengthens their connections to each other. Under pathological strain, the increased and uneven tension tears cells apart, leading to passive calcification via apoptosis. The osteogenic pathway proceeds by osteogenic differentiation into obVIC. These obVIC actively form mineralized deposits.

2. Aortic valve diseases

2.1 Epidemiology

Cardiovascular diseases (CVD) represent a major healthcare issue causing significant morbidity and mortality worldwide [50]. The heart disease and stroke statistics—2017 update reported that on the basis of the National Health and Nutrition Examination Survey 2011 to 2014 data, an estimated 92.1 10^6 American adults (>1 in 3; 36.6%) have ≥1 type of CVD. By 2030, 43.9% of the United States' population is projected to have some form of CVD [51]. In every year since 1919, CVD accounted for more deaths than any other major cause of death [52], and on the basis of 2014 mortality data, CVD, listed as the underlying cause of death, accounted for 30.8% of all deaths in the United States [51].

The age-adjusted prevalence of clinically diagnosed heart valve diseases (HVD) is 1.8% in the US, but the overall prevalence of heart diseases in the Western World is estimated to be 2.5% [50, 53]. Aortic valve diseases (0.9%) bring a certain contribution to the total HVD. The two most prevalent aortic valve diseases are aortic stenosis (AS, 0.4%) and aortic regurgitation (AR, 0.5%) **(Fig.8)** [50].

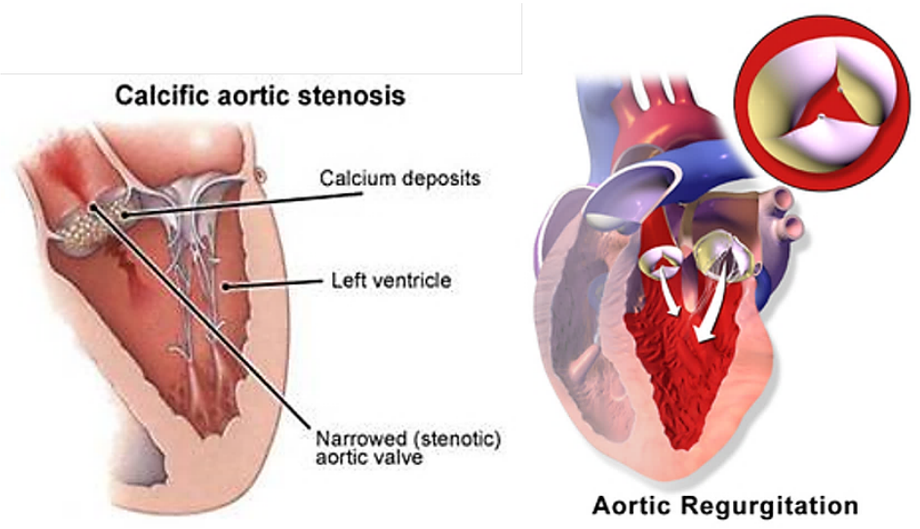

Fig.8: Aortic valve stenosis and regurgitation

Aortic valve diseases can be divided into two groups: aortic stenosis (narrowing of the aortic valve, impeding forward blood flow) and aortic regurgitation (aortic valve insufficiency, allowing backward blood flow). (Retrieved from: http://www.impact-r.com/en/tag/aortic-stenosis/ and Blausen.com staff (2014). "Medical gallery of Blausen Medical 2014")

2.2 Pathologies

2.2.1 Aortic stenosis

AS refers to the thickening of aortic valve leaflets which results in the narrowing of the AV opening and in abnormal leaflet motion. This impedes the forward blood flow from the left ventricle, and leads to left ventricle concentric hypertrophy due to progressive high-pressure overload. The most common causes of AS are calcification of the normal tricuspid or congenital bicuspid valve and rheumatic disease [19, 54].

The calcific disease causes a reduction in leaflet motion and effective valve area without commissural fusion. It is an active disease process characterized by lipid accumulation, inflammation and calcification, with many similarities with atherosclerosis, which mostly occurs in the elderly [55]. Congenital malformations of the valve, e.g. bicuspid valve, can also result in stenosis and is the most common cause in young adults [54, 56]. Rheumatic heart disease is a well-known, and late inflammatory complication of group A, streptococcal pharyngitis. Rheumatic AS is due to thickened and fused leaflets, dominated by fibrosis and calcification. It is less common in the Western World and invariably accompanied by mitral valve disease [57].

2.2.2 Aortic regurgitation

AR, also known as aortic insufficiency, is a condition in which the AV is incompetent and blood flows passively backwards to the heart [58]. AR can either be acute or chronic. Aortic root dilatation, congenital bicuspid valve and rheumatic fever can produce chronic AR. Chronic AR has a prolonged

asymptomatic phase, with a slow insidious left ventricle dilatation (eccentric left ventricle hypertrophy), which increases the forward stroke volume, thereby compensating for the backward regurgitation [56, 59]. Acute AR can result in sudden catastrophic elevation of left ventricle filling pressures and reduction in output and can be caused by infective endocarditis, aortic dissection and trauma [54, 56].

3. Heart valve replacements

A diseased or malfunctioning heart valve increases the chance of death related to a CVD by 50% [51]. The cure of aortic valve diseases by pharmaceuticals is still in early stages and treatment has limited success, leaving surgical replacement as the only treatment option [16]. In 2003, 290 000 patients required heart valve replacement, this number is estimated to triple over 850 000 by 2050 [60]. Heart valve prostheses should possess: excellent durability, biocompatibility, non-thrombogenic surface properties, appropriate hemodynamic performance, and ease of implantation with low morbidity rate [61]. Dysfunctional heart valves are currently being replaced by mechanical or biological prostheses [58].

3.1 Mechanical valves

Mechanical heart valves (MHV) are manufactured of artificial biomaterials (e.g. titanium, cobalt, LTI carbon, Delrin, Teflon, Dacron, etc.). [58]. Over the past 60 years, researchers have developed several designs (caged-ball, tilting-disc and bileaflet valves) each one consisting of a valve ring, a suture ring, one or more struts, and one or more discs or movable stop **(Fig.9.A-C)** [61, 62].

The first MHV was developed in 1952 by inserting a Plexiglas cage containing a ball occluder into the descending thoracic aorta [63, 64]. In 1960, the caged-ball or Starr-Edwards valves were the first valves implanted in the anatomic position. These valves consist of a metal cage with a silicone ball **(Fig.9.C)**. The durability of these prostheses have been proven [65]. However, caged-ball valves can cause health problems due to inappropriate hemodynamics and high pressure drop in the open position, caused by the centrally obstruction design [66]. They also have a relatively large-profile which increases the possibility of interference with anatomical structures after implantation [58].

In the mid-1960s, low-profile tilting-disc (monoleaflet) valves were developed which consist of a single pyrolytic-carbon disc fastened by metal struts **(Fig.9.B)** [58, 61]. Although these MHV mimic the natural blood flow better, resulting in less hemodynamic problems than caged-ball valves, stent fractures and other complications are still present [67].

Since the 1970s, bileaflet valves are the leading design of MHV. These prostheses are based on a similar design as the tilting-disc valves and have a pair of semicircular discs that rotate on struts and are anchored by hinges to the valve ring **(Fig.9.A)** [61, 68]. Compared to the precedent monoleaflet MHV, these prostheses do not disturb the normal laminar blood flow and do not have a negative impact on the natural hemodynamics. These newer-generation valves require a lower level of anti-coagulation compared with older models. Nevertheless, hemorrhagic and thromboembolic complications related to anti-coagulation can still occur, especially around the hinge area of the valves due to shear stress of the blood flow. For this reason, patients with MVH still require a life-long anti-coagulation therapy [62, 68]. Despite this thrombogenicity, MHV are very durable and can function well for 20-30 years [69].

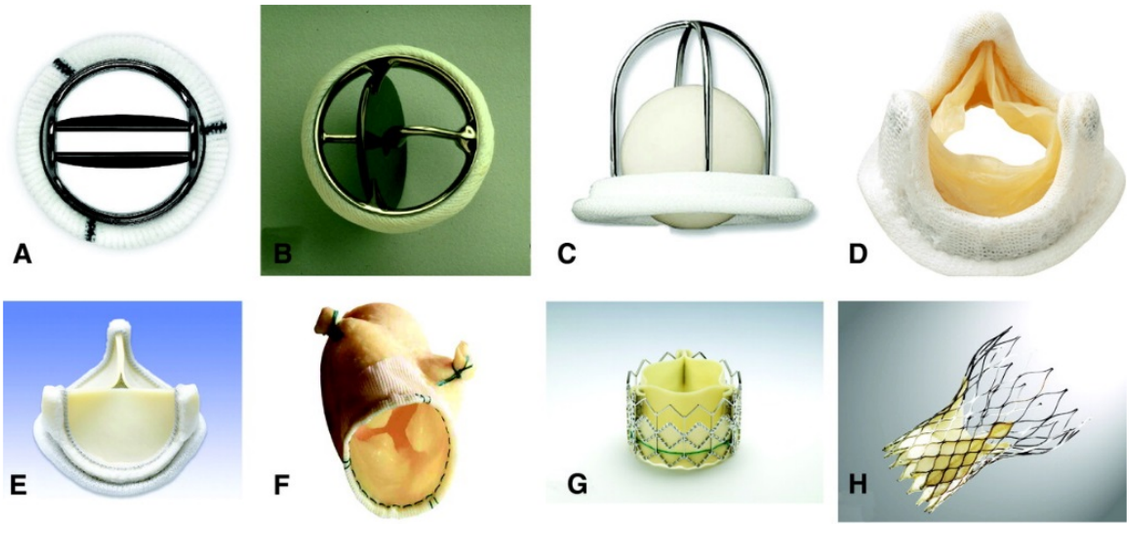

Fig.9: Heart valve prostheses [61]

A-C Mechanical valve replacements: (A) Bileaflet valve (B) Tilting-disc valve (C) Caged-ball valves; D-H Bioprosthetic valve replacements: (D) Stented porcine valve (E) Stented bovine valve (F) Stentless porcine valve (G) and (H) Transcatheter bioprosthesis.

3.2 Bioprosthetic valves

Bioprosthetic heart valves (BHV) **(Fig. 9.D-H)** are an alternative to MHV and can be obtained from auto-/allografts (human origin) and xenografts (animal-origin) [58, 61]. They are manufactured either in a stented configuration, which contains a synthetic sewing ring and struts to support the leaflets **(Fig. 9.D-E)**, or in a stentless configuration that includes the entire root **(Fig. 9.F)** [70]. Recently, BHV can also be implanted percutaneously via transcatheter aortic valve implantation to avoid the high surgical risk **(Fig.9.G-H)**. This minimal invasive technique is suitable for patients who are inoperable due to their age, left ventricular dysfunction, or other health conditions [71].

3.2.1 Homografts (Allo- and Autografts)

Homografts can be derived from human donor/cadaver tissue (allografts) or from autologous tissue (autografts). Donor heart valves are cryopreserved in liquid nitrogen before implantation and the quality of valvular tissue depends on the details of freezing and thawing protocols, the interval from death to harvest, and donor age [72]. They are implanted without a stent directly into the aortic root [73].

The first AV allografts were implanted in the descending aorta to ameliorate native AV insufficiency, in 1956 [74], but the first orthotopic use of a homograft for replacement of an AV was reported in 1962 by Donald Ross [75]. Allografts have good hemodynamics, a low incidence of thromboembolic complications and do not require any anti-coagulation [73]. However, they are unlikely to grow, remodel, or exhibit active metabolic functions and their availability is limited as suitable valves can only be prelevated from organ donors whose hearts were not accepted, or recipients of heart transplantations [76, 77].

The most common autograft is the “Ross procedure”, first performed in 1967, and mainly developed for children with diseased aortic valves to provide a hemodynamically superior and potentially viable valve that might grow with the somatic growth of children. In general, this involves the PV being grafted into the aortic site and a homograft implanted in the pulmonary site [78]. Ten-year survival for this procedure has been reported as high as 96%, with up to 75% ten-year freedom from re-operation [79]. Clinical studies have demonstrated that the Ross procedure is superior to homograft AV in adults [80], and that the growth of the pulmonary autograft in children is parallel to somatic growth [81]. However, subsequent aortic root dilation and AR are two of the known repercussions, and the fact that this now creates a two-valve problem has led some to question the utility of the procedure for some patients [82].

The long-term success of allografts is limited by progressive degeneration, and they have relatively low durability (approximately 50-90% valve survival rate at 10-15 years). The mode of failure of these valves when implanted in the left ventricle outflow tract is most frequently incompetence caused by leaflet rupture. In contrast, right sided valves in children are usually subjected to stenosis as a result of somatic growth, with or without calcification [83, 84].

3.2.2 Heterografts (Xenografts)

Heterografts can be obtained from porcine aortic valves (**p**AV) or bovine pericardium (**b**PER) [61]. Freeze-dried pig aortic valves were transplanted for the first time in 1965 into the descending aorta of dogs. Although no animal survived for more than 8 months, the heterologous valves were in good condition in all specimens [85]. In 1964, the same research group had already transplanted a

heterologous AV in a very ill patient. This patient died twenty-four hours later from causes unrelated to the heterograft [86]. These heterografts were all non-stented valves. The first stented valves were developed in 1967 and consisted of heterologous AV reinforced by a Teflon ring [87].

Due to the disastrous results of patients survival rate with these freeze dried pig valves, Carpentier et al. advocated the use of glutaraldehyde (GA) for chemical crosslinking treatment of animal tissue [88]. Cross-species implantation is prone to immune rejection and rapid tissue degeneration. GA treatment devitalizes and sterilizes tissue and reduces tissue antigenicity. This pretreatment is also aimed to fix the tissues in order to avoid autolysis and to improve mechanical stability [58, 89, 90].

Since 1971, GA-crosslinked pericardial BHV are manufactured. They contain leaflets composed of the serosa and fibrosa **(Fig.10)** of GA-treated PER attached to a frame **(Fig.9E).** Because pericardial valves lack the anatomical constraints imposed by porcine valves, they can be fabricated in any desired size and shape [91].

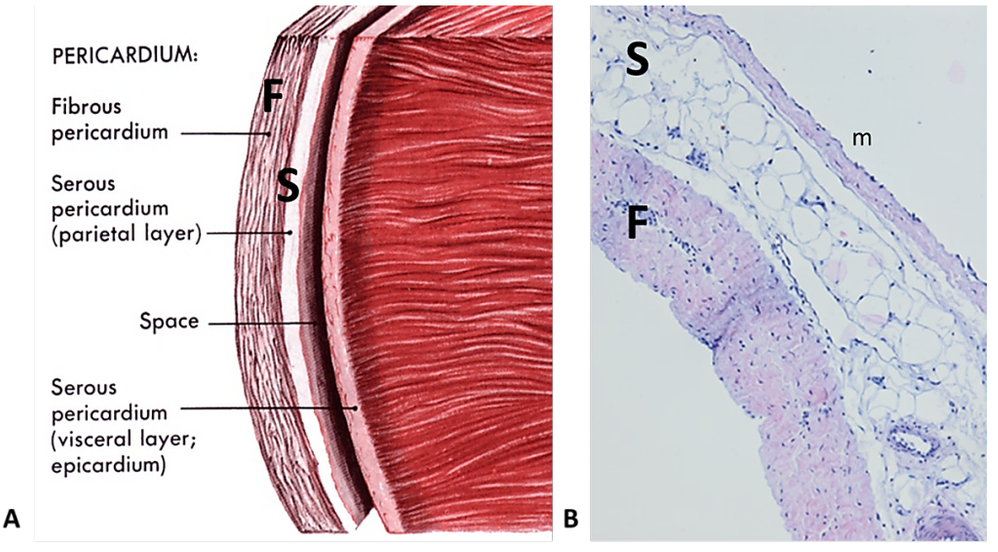

Fig.10: Macro and microstructure of pericardium

A: Schematic overview of the macrostructure of pericardium. Pericardium consists of two layers; the fibrous pericardium (= F: fibrosa) and the serous pericardium. The latter one includes two distinct layers; a parietal (= S: serosa) and a visceral layer (epicardium) (adapted from [92]). **B:** Overview of the microstructure of native pericardium (HE staining). Pericardial fibroblasts are the major cell type of the pericardium and are responsible for the production of collagen I and III, GAG and elastin fibers [93, 94]. These fibroblasts are predominantly present in the fibrosa and to a lesser extent also in the serosa. The serosa mainly contains fat cells and small blood vessels and is aligned with a mesothelium. (F: fibrosa; S: serosa; m: mesothelium)

GA-crosslinked xenografts, like allografts, show good hemodynamics, have a low incidence of thromboembolic complications and do not need any anti-coagulation, but their main advantage is their unlimited availability. Yet, they do not have the potential to grow or to remodel, are prone to (non)calcification deterioration, and their long-term success is limited (approximately 40-60% valve survival rate at 10-15 year) [95].

3.3 Choice of heart valve replacement

Choosing the most suitable prosthetic heart valve should account for the patient's values and preferences, with full disclosure of the indications for and the risks of anti-coagulant therapy and the potential need for and risk of re-operation **(Fig.11)** [96]. In general, MHV are favored in patients with less bleeding issues (no contra-indication to long-term anti-coagulation), especially in adult patients, younger than 60 years, with a long-life expectancy with the purpose to avoid open heart re-surgery [58, 61]. Also in older patients who are already taking anti-coagulation medicine (due to a mechanical prosthesis in another position or being at high risk for thromboembolism), and in patients who are at risk of accelerated BHV structural deterioration (young age, hyperparathyroidism, renal insufficiency) [97].

On the other hand, BHV are addressed to patients above 60 years old, who have shorter life expectancy and higher bleeding risk [58, 61]. If the life expectancy of the patient is less than that of a BHV, or anti-coagulation therapy is contra-indicated, or the patient is a female of childbearing age, then a BHV is also the more likely choice [97]. Furthermore, these prostheses can also be implanted in younger or pediatric patients to avoid the side effects of a life-long anti-coagulation therapy [58].

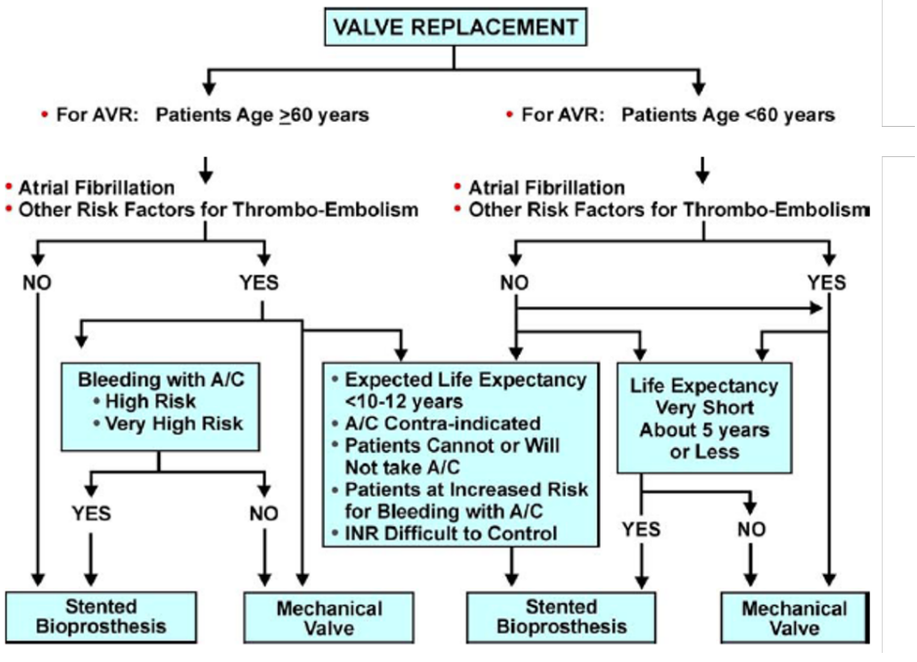

Fig.11: Choice of heart valve replacements -- a proposed algorithm (adapted from [97])
AVR: aortic valve replacement; A/C: anti-coagulation; INR: international normalized ratio

4. Heart valve tissue engineering

The “Holy Grail” of valve replacements is a non-thrombogenic and non-immunologic tissue valve which lasts the lifetime of the patient. One of the main problems of all clinically used valve substitutes is the lack of the ability to grow, repair and remodel within the patient since they are made of non-viable tissue. To overcome the limitations of these non-viable heart valve replacements, tissue engineering approaches emerged. Tissue engineered heart valves (TEHV) are most needed in the pediatric and young adult population as they outgrow valve replacements, resulting in multiple re-operations [58, 98]. Currently there are two main approaches: the top-down approach (TD-TE) and the bottom-up approach (BU-TE) [99, 100].

4.1 Different approaches for heart valve tissue engineering

4.1.1 Top-down tissue engineering (TD-TE)

In the classical top-down approach, cells are seeded onto the surface of a polymeric or decellularized scaffold and expected to recolonize the scaffold in order to generate new viable tissue **(Fig.12)**. Scaffolds can be made of biodegradable polymeric materials or decellularized tissue [99, 101, 102], and are sometimes coated with proteins, growth factors (GF) or antibodies (Ab) to enhance cell attachment [103-105]. Because of the load-bearing function of heart valves *in vivo*, any TEHV must be “pre-conditioned” to withstand mechanical loads *in vitro.* Protocols and bioreactors are being designed to improve both hemodynamics and mechanical properties [106-109]. Finally, the TEHV can be implanted, at which point it may undergo further *in situ* remodeling.

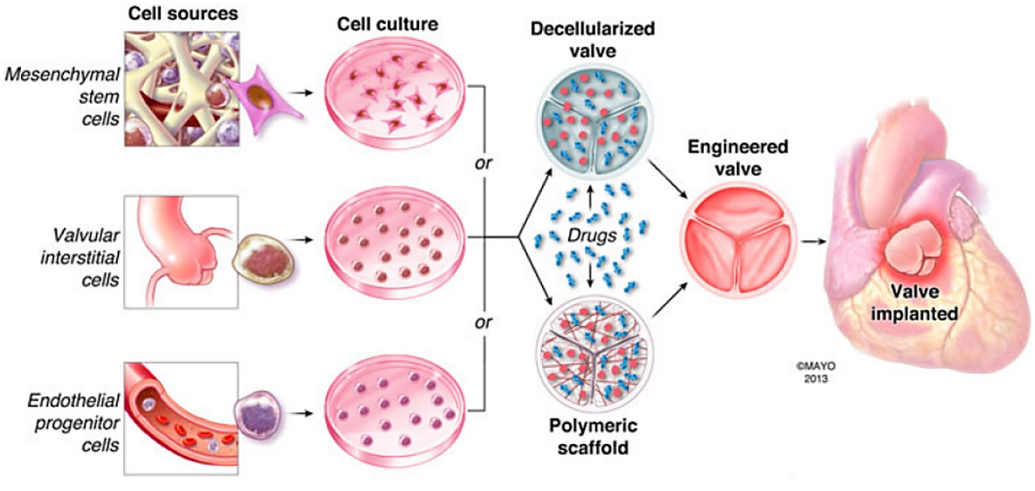

Fig.12: The top-down approach in heart valve tissue engineering (adapted from [102])

4.1.1.1 Solid synthetic and biological polymeric scaffolds

Polymeric scaffolds are made of synthetic or biological polymers and can be fabricated from a variety of techniques such as salt-leaching, electrospinning, phase separation, freeze drying, and self-assembly [101, 110]. Frequently used synthetic polymers in HVTE are the aliphatic polyesters: polyglactin, polyglycolic acid (PGA), polylactic acid (PLA), and polylactic-co-glycolic acid (PLGA), which are limited by their thickness, stiffness and non-pliability [111]; and polyhydroxyalkanoates (polyhydroxyoctanoate, poly-4-hydroxybutyrate), which possess good thermoplastic properties, are easily moldable but have a slow degradation rate [112, 113]. For this reason, composite polymers of aliphatic polyesters and polyhydroxyalkanoates have generally been favored and investigated [114]. The advantages of synthetic polymers are the minimization of infection risks, the reduction of immunogenic issues, and the possibility to tune the mechanical and chemical features, including the degradation rate which must be comparable with the rate of ECM/tissue formation [115]. However, the synthetic polymers do not easily interact with the host body due to the lack of cell recognition signals. For this reason, modifications such as adhesion peptides addition onto the synthetic scaffold, can improve the physical and chemical properties [110, 116].

Biocompatibility, low degradation rate and inflammation are some of the major drawbacks of the synthetic polymeric scaffolds. Biological scaffolds on the other hand, are naturally derived and offer many advantages. They contain natural cellular adhesion sites, inherent cell stimuli and are less likely to initiate toxic immune responses [117-119]. The main biological materials investigated for HVTE are collagen, fibrin and HA [120]. These biological components are mostly used as hydrogel scaffolds, except collagen from which also collagen sponge-scaffolds can be fabricated [121]. For this reason, these materials are discussed in more detail in **4.3 Hydrogels for heart valve tissue engineering.**

4.1.1.2 Decellularized scaffolds

ECM-based scaffolds are interesting materials for HVTE. The ECM provides mechanical support and favors attachment, migration and proliferation of cells [122]. The primary reason for using ECM as a natural biomaterial is the presence of bio-active molecules that drive tissue homeostasis and regeneration [123].

Before xenogeneic and allogeneic tissues can be used as scaffolds for HVTE, it is imperative to remove the major immunogenic component, namely the cells. Allografts are cryopreserved and undergo *in vivo* calcification mainly due to allogeneic cell debris, or can be rejected if viable cells remain within the scaffolds. Xenogeneic tissues on the other hand are currently crosslinked with GA, which render them biologically inert and inhibits immune cell penetration but at the same time, unfortunately, prevents autologous cell-infiltration [124-127]. Yet, GA treatment of xenogeneic

tissue is necessary because transplantation of unfixed tissue can result in hyper acute rejection. This hyper acute rejection is mainly due to the presence of the galactoseα1-3galactose (α-gal) epitope, which is expressed on almost all mammalian cell surfaces except for humans, apes and old-world monkeys [128].

Over the past 30 years, strategies have been developed to decellularize xeno- and allogeneic tissues, to remove the cells and in case of xenogeneic scaffolds also residual α-gal, to provide a scaffold that can promote efficient homologous cell repopulation [129]. After removal of the cellular components, an intact and natural meshwork of ECM components organized in a tissue specific architecture remains [130]. Compared to allogeneic tissues, which are scarce, xenogeneic tissues are readily available. Most widely used matrices for heart valve tissue engineering (HVTE) are decellularized bovine or porcine pericardium, porcine small intestinal submucosa (SIS) and porcine or ovine heart valves [131].

Commonly used methods to destroy cells and remove their components from porcine valves and pericardia are the non-ionic detergent, Triton X-100 (tert-octylphenylpolyoxyethylen), anionic detergents, SDS (sodium dodecyl sulfate) and SDC (sodium deoxycholate), and the enzymatic agent, trypsin [132, 133]. Ionic, non-ionic or zwitter-ionic detergents are effective in removing cellular material from tissues, since they permeabilize the cell membrane and segregate DNA from proteins. However, they can also negatively affect the native ECM structure and composition [134]. Non-ionic detergents, such as Triton X-100, are relatively mild detergents as they break lipid-lipid and lipid-protein interactions, but leave protein-protein interactions intact [135]. On the other hand, ionic detergents, such as SDC, are known to solubilize cell and nucleic membranes, but tend to denature proteins [136]. Some studies demonstrated that trypsin, a serine protease, is a useful enzyme to promote a complete tissue decellularization, since it disrupts cell-matrix interactions [137]. To enhance the action of detergents, hypo-and hypertonic buffer solutions can be incorporated into the decellularization process. Immersion in a hypotonic solution causes cells to swell and burst (osmotic lysis), and enhance the uptake of detergents. Immersion in a hypertonic solution has the opposite effect, which causes cells to dehydrate and shrink which can lead to cell death and aid detachment of cells from the matrix. Finally, following treatment with enzymes, detergents or buffers, residual nucleic acids may be left behind. Therefore, an additional nuclease enzyme digestion step is often included in the decellularization process. To satisfy the intent of decellularization Crapo et al. set minimal criteria; double-stranded DNA content needs to be below 50ng/mg ECM (dry weight), DNA fragments may have a maximum length of 200bp, and no nuclear material may be visible with DAPI or HE staining [138].

The first commercially available decellularized xenogeneic porcine valves were developed by O'Brien et al. in 1999 (SynerGraft®) [139]. The decellularization process involved cell lysis induced by incubation in water followed by nuclease digestion and a multi-day isotonic washout phase. Unfortunately, the early clinical performance of these valves in children was not successful. A fibrous overgrowth and strong inflammatory response led to catastrophic failure in three out of four cases. This response was initially attributed to a foreign-body-type reaction by the xenogeneic collagen scaffold [140]. However, two years later the same group evidenced the residual presence of α-gal epitopes in these SynerGraft valves, which possibly triggered hyper acute rejection [141]. This emphasized the need to investigate complete removal of the α-gal epitope following decellularization of xenogeneic tissues in future developments. Meanwhile, this research group also generated the first commercially available decellularized human pulmonary valves, using the same decellularization procedure (CryoValve SG®) [142]. The latest commercially available decellularized xenogeneic pulmonary valves, were developed by Dohmen et al. (Matrix P™). These valves are decellularized with 1% SDC, followed by an extensive rinsing period in normal saline solution [143]. The α-gal epitopes are entirely removed or masked after decellularization [144].

4.1.1.3 Repopulation of decellularized scaffolds

To date there is no doubt that complete recellularization and remodeling of the decellularized scaffolds is one of the key factors to limit or minimize immune based graft degeneration and structural tissue failure [145]. Ideally, autologous cells should be used, which improve biocompatibility and patients' response to the valve, as well as remodeling of the ECM in the valve leaflets. Currently, two main approaches are applied in order to obtain repopulated decellularized scaffolds. Some research groups are pre-seeding scaffold constructs with cells *in vitro* **(Table S1)**, while others rely on circulating cells to repopulate the scaffold *in vivo* **(Table S2). Table S1 and S2** are supplementary tables which give an extensive and chronological overview of studies that applied one or the other approach, including information about scaffold origin, decellularization agent, origin of cell source and the cultivation method for the *in vitro* approach, results of decellularization and *in vitro* or *in vivo* outcome of tissue recellularization. In summary these tables show that the *in vivo* repopulation is a slow and often incomplete process, but also that *in vitro* repopulation of tissues has not yet been standardized. Whether or not tissues need to be pre-seeded and which obstacles still need to be overcome will be discussed in **Chapter IV: Part A**.

4.1.1.4 Animal models

In the past, dogs, pigs, sheep, baboons, kangaroos and goats have all been used for HV research, but not all of them are favorable models due to ethics, size, physiologic complications or husbandry. Rodents are also useful as inexpensive interim models prior to initiating large animal studies but are

not suitable for orthotopic valve replacements [146]. Currently, sheep are most frequently used as a model for *in vivo* HV replacement studies, followed by pigs [147].

Swine can be used as a CVD model, there are well documented advantages and human similarities [148]. They are an excellent model for capturing valve-related thrombosis and blood-material interactions, especially for MHV [149, 150]. In BHV, the primary failure is due to calcification, which is enhanced in children. It is known that BHV do calcify in the pig model, however, the degradation rates are found to be slower than in other species [151, 152]. In addition, the usefulness of this model is overshadowed by the difficulties in surgical husbandry and somatic growth, cardiopulmonary bypass is poorly tolerated, and difficulties in maintaining anti-coagulation can lead to increased hemorrhagic complications [153-155].

Sheep are currently accepted as the gold standard for valve replacement (recommended by the Food and Drug Administration). They are the classic model for mimicking the pattern of BHV wall and leaflet calcification. In addition, the calcification rate of sheep is age-related [156]. Sheep also have similar heart rate, blood pressure, intracardiac pressure, and cardiac output to healthy young humans, can tolerate anesthesia and cardiopulmonary bypass well, and present no major difficulties in post-operative management [156, 157]. Because the risks associated with TEHV are likely to be similar to those of BHV, and different from MHV, the sheep is likely a very appropriate model for the assessment of preclinical performance and safety of TEHV.

Old World Monkey species, like baboons, are genetically more similar to humans. As previously described (in 4..1.1.2 Decellularized scaffolds), just like humans, they possess natural antibodies against the alpha-gal epitope. Such a non-human primate model could be a significant preclinical tool and a valuable alternative to the swine or pig model regarding xenograft reactions. Yet so far, only few research groups have already used this non-human primate model for valve replacements studies [158-162].

4.1.2 Bottom-up tissue engineering (BU-TE)

Due to the restriction of TD-TE to control the cell density, the diffusion of nutrients, and sometimes vascularization of tissue constructs, a bottom-up approach is proposed in tissue engineering. BU-TE aims to create biomimetic tissues by generating native microstructural functional tissue building blocks and assembling (random, directed or magnetic assembling, or by stacking) these modular units to engineer larger tissue constructs from the bottom up **(Fig.13)** [99, 100].

Recently, three-dimensional (3D) cell culture has gained interest in tissue engineering due to the fact that it overcomes the limitations of the conventional two-dimensional (2D) cell culture conditions

[163]. 3D cell culture systems mimic more closely the actual *in vivo* microenvironment. Moreover, they allow better cell-to-cell and cell-to-matrix interactions which are important for cell differentiation, proliferation and cellular functions, and which also stimulate cells to produce ECM components and to organize into microtissue-like structures *in vitro* [164, 165]. Currently, a wide variety of techniques exist to culture cells into 3D structures. These techniques can be grouped into two main categories; completely cell driven (without the use of a biomaterial), or by suspending/encapsulating cells in a biomaterial (such as hydrogels) [166, 167]. One of the most commonly used cell driven approaches currently available are the micromass cultures (homo-/heterotypic aggregates) [165].

The autonomous self-assembly relies on the physical process of embryonic organ development, where cells are the fundamental drivers of histogenesis. Early cellular components of a developing tissue create their own ECM, the proper cell signaling, and independent arrangement and patterning to yield the required biological functions and micro-architecture [168, 169].

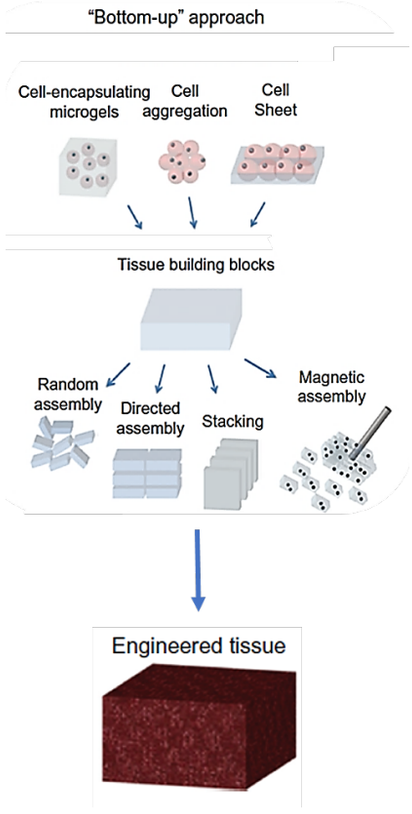

Fig.13: The bottom-up approach in tissue engineering (adapted from [100])
Engineered tissue constructs are biofabricated by combining microstructural functional tissue building blocks by random, directed or magnetic assembly, or by layer-by-layer stacking.

Self-assembled cell aggregates can be created by various scaffold-free techniques: pellet/spinner culture, hanging drop, liquid overlay, rotating wall vessel, external force, cells sheets or microfluidics. Unfortunately, all these techniques have their own limitations such as poor size control, high shear stresses, low yield, etc. [170]. However, a recently developed high throughput technique uses agarose-molded non-adhesive microwells to guide the spontaneous self-assembly of cells into 3D aggregates with predefined dimensions in order to produce high-quality tissue fragments [171]. This technique rapidly generates size and shape controlled aggregates in a low shear force environment.

4.2 Cells for heart valve tissue engineering

Cells from different animal and human sources have been used for HVTE research (**Table 1**). Cells from xenogeneic sources used in human tissue constructs pose risks (immune response, disease transfer). However, analogous cell types from animal and human sources often show almost identical phenotypes, making animal cells appropriate for *in vitro* and preclinical *in vivo* animal studies. In addition, they are readily available, less expensive, and not subjected to the same level of safety and ethical regulations compared to human cells [102].

Because VIC and VEC are not easily accessible, HVTE initially focused on the isolation of cells harvested from vascular donor tissues such as peripheral arteries and veins, from which EC and MFb-like cells could be isolated [60, 172]. Isolation of these cells is technically simple and these cells demonstrated substantial tissue formation *in vitro* [173]. However, cell harvesting prior to seeding required the sacrifice of intact vascular donor tissue. To circumvent surgical interventions, different (stem) cells are proposed as a suitable cell source for HVTE.

4.2.1 Endothelial progenitor cells

Endothelial progenitor cells (EPC) can be an alternative for the adult EC currently isolated from donor vessels. EPC were first discovered in human peripheral blood by Asahara et al., and were isolated based on $CD34^+$ and Flk-1 $(KDR/CD309)^+$ expression. The fraction of cells which attached in plated cultures, differentiated *in vitro* into EC. To confirm the EC-like phenotype, mRNA expression of CD31, endothelial nitric oxide synthase (eNOS), and Flk-1 was documented [174]. EPC are not only found in peripheral blood, they can also be isolated from other blood sources such as bone marrow (BM) [175], amniotic fluid [176, 177], or umbilical cord [178].

4.2.2 Mesenchymal stem cells

Mesenchymal stem cells (MSC) have shown considerable promise for HVTE and offer some advantages for autologous clinical employment; they are easily accessible and easy to isolate from

patients, can be culture-expanded to a large number in a matter of days, and have a minimal risk of immunogenicity [179]. But most important, they possess a multilineage differential potential (adipo-, chondro-, osteo-lineage), and it has been shown that they can be converted into EC, (myo)fibroblast (Fb/MFb), and smooth muscle cells (SMC) [180-182].

Previous studies have reported that MSC share many characteristics of VIC, are able to produce collagen in response to cyclic stretch and to yield heart valve ECM components *in vitro* [183-186]. The role of GF in MSC proliferation and differentiation has extensively been investigated over the past years. Some research groups strive to use GF which do not influence the differentiation potential of MSC, whilst others focus on the differentiation of MSC into a VIC-like phenotype. TGF-β1 is an important inducer of MFb differentiation of VIC (qVIC to aVIC), while fibroblast growth factor (FGF) enhances re-differentiation to a more Fb-like phenotype (aVIC to qVIC) [187]. Similar phenotype conversions of mesenchymal stem cells were demonstrated when TGF-β1 or FGF was supplemented to the stem cell cultures [180]. Aside from GF, it is known that also organic molecules such as β-mercapto-ethanol, retinoic acid, or ascorbic acid can play a role in the differentiation of MSC towards a MFb-like phenotype, by increasing α-SMA expression [50]. The anti-oxidant ascorbic acid and its derivative ascorbic acid-2-phosphate (AA) can also stimulate MSC proliferation and collagen synthesis, while preserving their differentiation potency [188].

MSC can be obtained from different sources: amniotic fluid [189], chorionic villi [190], umbilical cord blood [191], mucoid fetal mesenchymal tissue (Wharton's jelly) [192], periosteum [193], dental pulpa/follicle or periodontal ligament [194-196], maxillary sinus membrane [197], skin [198], synovial membrane [199] and many more. However, they are primarily being isolated from BM and adipose tissue.

4.2.2.1 Bone marrow derived mesenchymal stem cells

Apart from stem and progenitor cells of the hematopoietic lineage, the BM is also known to be a source of stem cells from non-hematopoietic origin. This subpopulation of BM cells was first identified by the pathologist Cohnheim in 1867 [200]. He hypothesized that cells with a Fb-like morphology migrate to the sites of injury and help to regenerate damaged tissue. However, it was only 100y later that Friedenstein et al. isolated, cultured and differentiated these cells, which opened a new field of stem cell research [201]. These non-hematopoietic stem cells are multipotent and referred to as MSC because of their ability to differentiate into different phenotypes of the mesoderm germ layer, or as marrow stromal cells as they appear to arise from the complex array of supporting structures found in the marrow stroma [202]. In 2006, the International Society of Cellular Therapy proposed three criteria to identify MSC: 1) plastic-adherence when maintained in

standard culture conditions; 2) expression of CD105, CD73 and CD90, and lack of expression of CD45, CD34, CD14 or CD11b, CD79a or CD19 and HLA-DR surface molecules; 3) *in vitro* trilineage differentiation potential into osteoblasts, adipocytes and chondroblasts [203].

BM-MSC are easily isolated from BM aspirates, and less sensitive to microbiological contamination compared to other tissue derived MSC [204]. However, a bone marrow harvest is a painful procedure with possible donor site morbidity as a result, and the abundance of MSC among other BM cells is estimated to be only 0.01%-0.001% [201, 205].

It is worth mentioning that some research groups not only use the adherent fraction of BM cells, represented by the MSC, but sometimes the total population of (unsorted) BM mononuclear cells (MNC) is being investigated as a potential cell source for HVTE [160, 206].

4.2.2.2 Adipose derived mesenchymal stem cells

Fat tissue is an attractive source for MSC isolation because it is easily accessible with minimal invasive procedures and large amount of tissue fragments can be obtained, mostly from liposuction (lipoaspirate) or subcutaneous fat. Compared to bone marrow aspirates, lipoaspirate contains larger quantities of MSC. 3% of total isolated cells from fat tissue are estimated to be adipose derived mesenchymal stem cells (ADSC) [207, 208]. In addition to a higher yield, ADSC are significantly more present in elderly patients (>60y). This is in contrast to the amount of BM-MSC from BM aspirates which has a negative correlation with patient's age [209].

Like BM-MSC, ADSC are positive for the classical MSC markers: CD73, CD90 and CD105 [209-211], but they also express CD13, CD29 and CD44 [212-215], and in the early passages CD34 [216, 217]. On the other hand, they are CD14, CD45 and CD31 negative [212, 218]. The *in vitro* trilineage differentiation potential of ADSC has also been shown by cultivating cells in osteogenic, chondrogenic or adipogenic induction media [219].

4.3 Soft hydrogels for heart valve tissue engineering

The last ten years, biocompatible hydrogels are gaining interest in the field of HVTE. They are not only used to generate porous scaffolds for TD-TE, but also as cell carriers/bio-ink for bioprinting applications in BU-TE.

Hydrogels are biocompatible materials with a hydrophilic character and a 3D macromolecular polymeric network, that can be crosslinked in order to form stable polymeric matrices in various shapes and sizes. Hydrogels provide a porous and hydrated environment, similar to soft tissues, which allows the exchange of oxygen, nutrients, water soluble metabolites and cellular waste [220].

To date, hydrogels from both synthetic and natural polymers are explored for HVTE applications. Synthetic hydrogels such as polyethylene glycol (PEG) ease the user to control the mechanical, physical and chemical properties [221-223]. In some cases, these hydrogels are modified with peptides in order to enhance the biological function of the synthetic hydrogel and to facilitate the interaction with cells [224]. In contrast to synthetic hydrogels, natural hydrogels such as collagen [225], gelatin (Gel) [226], alginate and HA [227, 228], show adequate bioactivity, support cellular functions and have similar features to the natural ECM. However, natural hydrogels often show poor mechanical durability [229, 230]. Recently, not only pure hydrogels, but also hybrid or composite gels such as collagen/chondroitin sulphate [225], Gel/Alginate (Alg) [231], HA/Gel [48] and PEG/Alg [232] have gained interest. By combining different natural and/or synthetical materials, hydrogels with improved bioactivity as well as mechanical properties can be generated [233].

Hydrogels can be crosslinked by exposing polymer solutions to chemical stimuli or by physical processes. The most commonly used hydrogels in HVTE (PEG, gelatin and HA, **Table 3**) are chemically crosslinked by generating covalent bonds between the polymer chains. First, photo-crosslinkable functional end groups are introduced to the polymers. Secondly, a photoinitiator (PI) is added, which generates free radicals when irradiated with ultra violet (UV) light, for the polymerization of the functional end groups [226, 227, 234, 235] **(Fig.14).**

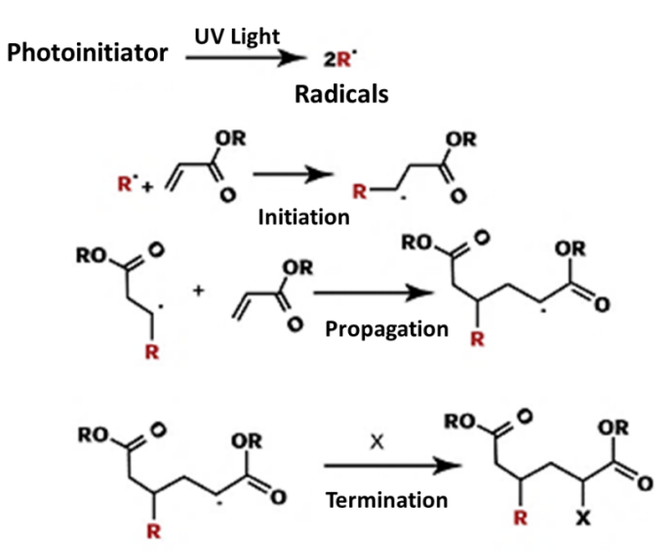

Fig.14: Free radical photo-crosslinking mechanism of polymers

Photocurable materials that form through the free-radical mechanism undergo chain-growth polymerization, which includes three basic steps: initiation, chain propagation, and chain termination. **R•** represents the radical that forms upon interaction with radiation during initiation. The active monomer that is formed is then propagated to create growing polymeric chain radicals. The propagation step involves reactions of the chain radicals with reactive double bonds of prepolymers or oligomers. The termination reaction usually proceeds through combination, in which two chain radicals are joined together (Retrieved from: http://www.pcimag.com/articles/85843-the-use-of-specialty-acrylic-esters-in-cure-in-place-coating-technology)

One of the challenges in the use of hydrogels is to obtain a good balance between scaffold degradation and newly formed ECM, which is important for creating and maintaining sufficient mechanical properties of the cell-seeded/cell-encapsulated constructs. A rapid degradation might impair the integrity and mechanical properties of constructs, whereas a slow degradation rate might impede tissue regeneration [236]. Another crucial factor in the determination of cell fate and physiological function, is the regulation of the interaction between cells and their local environment. The ideal hydrogel should provide an informative microenvironment, mimicking the physiological niche and direct cell behavior (e.g. proliferation, differentiation, morphology, ECM production, etc.) without inducing pathological effects [237]. This will be important for VIC, as it is already known that aVIC and obVIC conversion is highly dependent on the interaction between VIC and ECM components/material stiffness [238].

4.3.1 PEG-hydrogels

PEG is also known as polyethylene oxide or polyoxyethylene. It is a hydrophilic molecule with either linear or branched structures, and the basic structure is commonly expressed as $H-(O-CH_2-CH_2)_n-OH$ **(Fig.15.A).**

PEG hydrogels are of great interest for TE applications because PEG is biocompatible and non-immunogenic and has been approved for internal use by the Food and Drug Administration. The structure, mechanical behavior, and degradability of PEG hydrogels can be tuned by controlling chemistry and processing conditions [239, 240]. PEG hydrogels exhibit a wide range of elastic moduli (EM), similar to various soft tissues and have already been used to study the effect of substrate modulus on VIC behavior [241]. They are also bioinert primarily due to their non-adhesive characteristics. However, PEG hydrogels can be modified to be more bio-active and/or biodegradable by incorporation of proteins [242], peptides [224] and polysaccharides [243] into the polymer network.

To be photo-crosslinkable, the end groups of PEG can be replaced by other functional groups, such as acrylates [244]. PEG diacrylate (PEGDA) is synthesized by reaction of PEG with acryloyl chloride **(Fig.15.A).** PEG hydrogels can then be generated by crosslinking PEGDA solutions with UV light in the presence of a PI such as Irgacure 2959 (Irg, peak absorbance 276nm) [224, 245], or with visible light in the presence of a PI system composed of the photosensitizer eosin Y (peak absorbance 510nm), initiator triethanolamine (TEA) and catalyst 1-vinyl-2-pyrrolidinone (NVP) [221].

4.3.2 HA-hydrogels

HA, also called hyaluronan, is an anionic, non-sulfated GAG. HA is a soluble, linear polysaccharide that consists of alternating units of a repeating disaccharide, β-1,4-D-glucuronic acid-β-1,3-*N*-acetyl-D-glucosamine **(Fig.15.B)** [246].

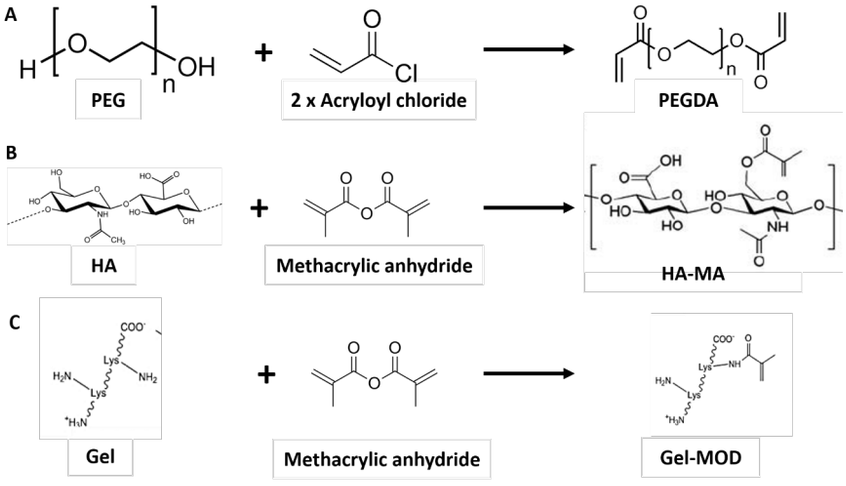

Fig.15: Chemical modification mechanisms of the most commonly used hydrogels in HVTE

HA is a component of the cardiac jelly during heart development, and comprises 55% of the total GAG content in valve leaflets, providing compressive resistance in the cardiac cycle and playing an essential role in valvular cell-matrix interactions [247]. Therefore, it may have a substantial role in valvular cellular behavior when used in HVTE [228]. Furthermore, HA hydrogels are non-immunogenic, non-thrombogenic, hydrophilic and can be rapidly degraded with hyaluronidase. HA can be modified to alter hydrogel properties related to hydrophobicity, biological activity and degradability [248-250].

To be photo-crosslinkable, the hydroxyl group in the N-acetyl glucosamine sugar can be chemically modified with methacrylic anhydride, resulting in methacrylated HA (HA-MA) **(Fig.15.B).** HA hydrogels can then be generated by crosslinking HA-MA solutions with UV light in the presence of a PI such as Irg [48, 235, 251].

4.3.3 Gel-hydrogels

Collagen is the principal structural component of the aortic valve leaflets and comprises 60% of the dry weight [8]. Its use has the potential to maintain distinct valvular mechanical properties and facilitate the interactions between valvular interstitial cells and the ECM. Collagen typically has low antigenicity *in vivo* [252, 253]. Gelatin is the product of thermal denaturation or disintegration of the triple-helix structure of natural insoluble collagen type I, from porcine or bovine skin (respectively

Type A or B), into single-strand molecules [252]. Gelatin can form a solution in water above the melting point (Tm = ~ 35°C) and undergoes a thermo-reversible gelation at temperatures lower than the glass transition temperature (Tg = ~ 28°C). In order to form crosslinked Gel hydrogels, methacrylated gelatin (Gel-MOD) is synthesized by the reaction of methacrylic anhydride with the amide groups of gelatin (**Fig.15.C)**. Gel-MOD solutions can then be crosslinked with UV light in the presence of a PI such as Irg or VA-086 (VA, peak absorbance 365nm) [254, 255].

4.4 3D (bio)printing in heart valve tissue engineering

3D printing, also called additive manufacturing technology, is one of the rapid manufacturing techniques in both approaches of TE and has the potential to improve the clinical outcome of TEHV by allowing to better match patient-specific geometries, and spatial heterogeneity of the mechanical properties and cell types of the HV [256]. 3D printing can be used to manufacture molds and scaffolds for TD-TE **(Fig.16.A-C)** [257, 258]**.** On the other hand, 3D *bio*printing relays on the use of hydrogel encapsulated cells or aggregates as a bio-ink for the directed assembly of these microscale tissue building blocks in BU-TE **(Fig.16.D-E)** [231, 234, 259]**.**

The basic work flow of most 3D printing approaches uses magnetic resonance imaging (MRI) and computer tomography (CT) as templates, which yield the necessary information of the geometry of the heart valve, that is transformed into a digital 3D model by specific software. The 3D computer model is then transformed into a digital 3D printing model that considers both machine- and material dependent aspects, and a (bio)printed TEHV can be fabricated [257, 260].

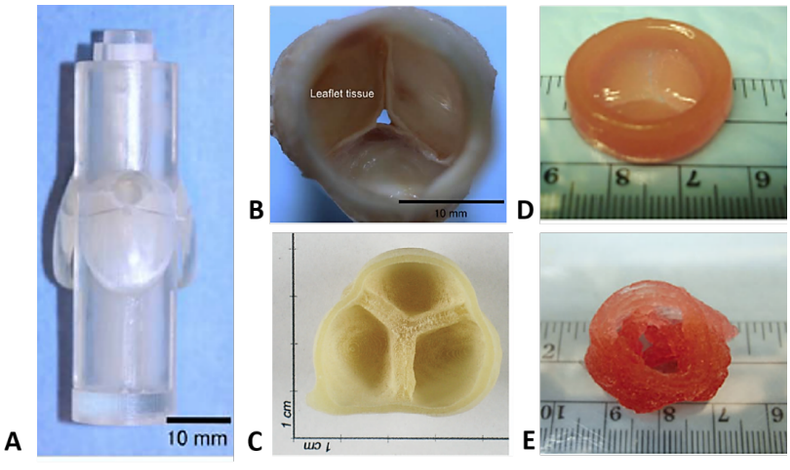

Fig.16: 3D (bio)printed tissue engineered heart valves

A) 3D printed plastic mold for the Biovalve VII, before implantation; **B)** Biovalve VII generated after 1 month of subcutaneous implantation of a 3D printed plastic mold **(A)** in goats (adapted from [258]); **C)** 3D printed HV scaffold (adapted from [257]); **D)** 3D bioprinted HV conduit, made by bioprinting of hybrid hydrogel (HA-MA/Gel-MOD) encapsulated **h**VIC (adapted from [234]); **E)** 3D bioprinted HV conduit, made by bioprinting of hybrid hydrogel (Alg/Gel) encapsulated hSMC for the aortic root structure, and encapsulated **p**VIC for the valve leaflets (adapted from [231])

Currently there are three basic types of 3D bioprinting techniques available; inkjet printing, micro-extrusion bioprinting, and laser-assisted bioprinting **(Fig.17)** [169, 261-263].

Inkjet printers, also known as drop-on-demand printers, are the most commonly used type of printers for biological and non-biological applications. To produce the bio-ink droplets, inkjet bioprinting can be done either by a thermal method or with a piezoelectric actuator **(Fig.17.B).** Thermal printers function by electrically heating the print head to produce pulses of pressure that force droplets out of the nozzle. The local heating generates a bubble in the ink reservoir and ejects a small droplet (200-300°C for ~2µs results in an overall temperature increase of 4-10°C [264]) [259]. Piezoelectric printers contain a piezoelectric crystal, which can respond to an applied pressure, inducing a rapid change in shape and creates an acoustic wave inside the print head. The acoustic wave divides the liquid in the print head into droplets at regular intervals [262].

Micro-extrusion printers are the most common and affordable printers for non-biological applications. They usually consist of a temperature controlled biomaterial dispensing system. Rather than liquid droplets, micro-extrusion yields continuous extrusion of materials by pneumatic or mechanical (piston or screw) dispensing systems **(Fig.17.C)** [265].

Laser-assisted bioprinters use the principles of laser-induced forward transfer [266]. It consists of a pulsed laser beam with a focus system, a 'ribbon' that has a donor transport support (typically made from glass) covered with a laser-energy-absorbing layer (e.g. gold or titanium), and a layer of biological material containing cells. By applying focused laser pulses on the absorbing layer of the ribbon, a high-pressure bubble is generated that forces cell-containing materials towards a collector substrate **(Fig.17.A)** [259].

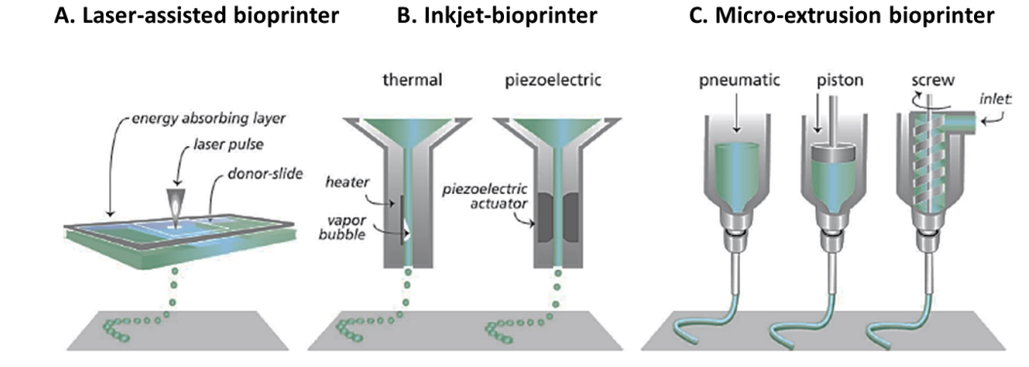

Fig.17: Basic 3D (bio)printing strategies (adapted from [263])

CHAPTER II

Aim and outline of the thesis

AIM

One of the main problems of all clinically used valve replacements is the lack of the ability to grow, repair and remodel within the patient since they are made of non-viable tissue. The overall aim of this thesis was to develop bio-active cardiac tissues, with the long term goal of generating a bio-active TEHV, which could potentially overcome the limitations of the currently available non-viable heart valve substitutes.

Part A of this thesis focuses on the generation of bio-active xenogeneic cardiac tissues (a top-down approach) and is divided into two sections. As it is known that xenogeneic cells can evoke an immunologic response post-transplantation, it is import to remove all cellular components before using xenogeneic tissues as a scaffold material. For this reason, the aim in the **first section** was to generate completely cell free porcine cardiac tissues (heart valve leaflets and pericardia). The efficacy of cell removal of different decellularization protocols and their impact on the cardiac tissues was evaluated, and the best protocol was selected.
The aim in the **second section** was to repopulate these decellularized tissues in order to obtain bio-active tissue. A static two-stage seeding protocol was used. First, the interstitium was repopulated with valvular interstitial cells or stem cells. Secondly, endothelial cells were used to generate an endothelium layer.

Part B of this thesis focuses on the generation of bio-active valvular tissues from the bottom-up and is divided into two sections. To tissue engineer a large modular tissue from the bottom-up, microscale building blocks are needed. For this reason, the aim in the **first section** was to generate microtissues from valvular interstitial cells. A scaffold-free high throughput microwell system was used, which rapidly generated microtissues in a low shear force environment.
Because the next step is to assemble these microtissues into larger tissue constructs by 3D bioprinting, a cell friendly and printable material was needed. Therefore, in the **second section**, modified gelatin hydrogels were evaluated as a microtissues-carrier material/bio-ink for future bioprinting applications.

OUTLINE

The experimental work is described in **Chapter III** and is divided in the following parts and sections:

PART A: Generation of bio-active porcine cardiac tissues from the top down

- **Section I: Impact of detergent-based decellularization methods on porcine tissues for heart valve engineering**

  Roosens A, Somers P, De Somer F, Carriel V, Van Nooten G, Cornelissen R

  (Published: Annals of Biomedical Engineering. 2016;44(9):2827-39)

- **Section II: Complete static repopulation of decellularized porcine tissues for heart valve engineering – an *in vitro* study**

  Roosens A, Asadian M, De Geyter N, Somers P, Cornelissen R

  (In press: Cells Tissues Organs)

PART B: Generation of bio-active valvular tissues from the bottom up

- **Section I: Scaffold-free high throughput generation of quiescent valvular microtissues**

  Roosens A, Puype I, Cornelissen R

  (Published: Journal of Molecular and Cellular Cardiology. 2017;106:45-54)

- **Section II: Impact of modified gelatin on valvular microtissues**

  Roosens A, Handoyo Y, Declercq H, Cornelissen R

  (Submitted: Journal of Tissue Engineering and Regenerative Medicine, June 2017)

CHAPTER III

Experimental work

PART A: Generation of bio-active porcine cardiac tissues from the top down

PART B: Generation of bio-active valvular tissues from the bottom up

PART

A

SECTION I

Based on:

Impact of detergent-based decellularization methods on porcine tissues for heart valve engineering

Roosens A, Somers P, De Somer F, Carriel V, Van Nooten G, Cornelissen R

(Annals of Biomedical Engineering. 2016;44(9):2827-39)

ABSTRACT

To date an optimal decellularization protocol of heart valve leaflets (HVL) and pericardia (PER) with an adequate preservation of the extracellular matrix (ECM) is still lacking. This study compares a four-day Triton X-100-based protocol with faster SDC-based protocols for the decellularization of cardiac tissues. Decellularized and non-treated HVL and PER were processed for histological, biochemical and mechanical analysis to determine the effect of these agents on the structure, ECM components, and biomechanical properties. Tissues treated with SDC-based protocols still showed nuclear material, whereas tissues treated with Triton X-100 1%+ENZ±TRYP were completely cell free. For both decellularized tissues, an almost complete washout of glycosaminoglycans, a reduction of soluble collagen and an alteration of the surface ultrastructure was observed. Interestingly, only the elastic fibers of pericardial tissue were affected and this tissue had a decreased maximum load. This study showed that both detergents had a similar impact on the ECM. However, Triton X-100 1% +DNase/RNase (ENZ) ± Trypsin (TRYP) is the only protocol that generated completely cell free bioscaffolds. Also, our study clearly demonstrated that the decellularization agents have more impact on pericardial tissues than on heart valve leaflets. Thus, for the purpose of tissue engineering of heart valves, it is advisable to use valvular rather than pericardial matrices.

INTRODUCTION

Valvular heart diseases represent a major healthcare issue causing significant morbidity and mortality worldwide [50]. The age-adjusted prevalence of clinically diagnosed valvular heart disease is 1.8% in the United States, but the overall prevalence of heart diseases in the Western World is estimated to be 2.5% [50, 53, 267]. To date, dysfunctional heart valves are replaced by mechanical or biological prostheses [58]. In 2003, 290 000 patients required heart valve replacement, this number is estimated to triple over 850 000 by 2050 [60].

Currently there are two basic types of heart valve replacement: mechanical and bioprosthetic heart valves. Unfortunately, both types have several disadvantages. Mechanical valves are made of artificial biomaterials, therefore, patients with mechanical heart valves require a life-long anti-coagulation treatment due to the substantial risk of thromboembolisms [58, 268]. On the other hand, most bioprosthetic heart valves are made from porcine heart valves or bovine pericardium that has been crosslinked with glutaraldehyde (GA). These bioprosthetic heart valves have better hemodynamic characteristics, require no need for long-term anti-thrombotic treatment, but suffer from premature degeneration and calcification [58, 269]. One of the main problems of all clinically used valve substitutes is the lack of the ability to grow and to remodel within the patient since they are made of non-viable tissue. To overcome the limitations of these non-viable heart valve replacements, tissue engineering approaches emerged to create cell repopulated decellularized scaffolds [270]. Tissue engineered heart valves (TEHV) have the potential to grow and allow cell infiltration. In addition, they are less prone to calcification and less thrombogenic [271].

TEHV are most needed in the pediatric and young adult population as they outgrow valve replacements, resulting in multiple re-operations [98]. Moreover, in this population the use of bioprosthetic valves is complicated by early tissue failure, associated with an immune response, followed by accelerated degeneration [272]. In addition, they are susceptible to rapid calcification related to the accelerated calcium metabolism of children and to the glutaraldehyde treatment of the valves [273].

ECM-based scaffolds derived from decellularized xenogeneic tissue are interesting materials for heart valve tissue engineering. The ECM provides mechanical support and favors attachment, migration and proliferation of cells [122]. The primary reason for using ECM as a natural biomaterial is the presence of bio-active molecules that drive tissue homeostasis and regeneration [123]. The main goal of decellularization strategies is to remove all cellular and nuclear material to prevent immune response while preserving the native ultrastructure and essential ECM components. After

removal of the cellular components, an intact and natural meshwork of ECM components, organized in a tissue specific architecture should remain [130]. Most widely used matrices for heart valve tissue engineering are decellularized bovine or porcine pericardium, porcine small intestinal submucosa and porcine or ovine heart valves [131].

Complete decellularization of tissues remains crucial as cellular material within treated tissue triggers the calcification process and evokes an adverse immune response post-implantation [94]. However, a completely cell free scaffold can still elicit a foreign body type inflammatory response [140, 274]. For this reason, some groups are crosslinking acellular matrices to make them biologically more inert [275]. Whilst others are investigating the effect of *in vitro* cell seeding of decellularized matrices on inflammation and thrombocyte activation [276].

Various methods have been used to decellularize tissues, including physical, chemical and enzymatic methods [133]. Commonly used methods to destroy cells and remove their components from porcine valves and pericardia are described in **Chapter I; 4.1.1.2.** However, a reliable standardized protocol has not yet been established and more research should be performed to investigate the preservation of the structural components of the ECM, since is known that the decellularization process can induce some alterations in the mechanical and structural characteristics of the ECM [98, 270, 277-280].

The aim of this study was to thoroughly evaluate the efficacy of two detergent-based decellularization methods and their effect on the structural ECM components of heart valve leaflets (HVL) and pericardium (PER), in order to generate a standardized protocol for the decellularization of porcine tissues for heart valve engineering. Cardiac tissues were decellularized using Triton X-100 1% +DNase/RNase (ENZ) ± Trypsin (TRYP), a protocol optimized in our lab, and compared to different and faster SDC-based decellularization protocols [271, 281-283].

METHODS

Tissue decellularization and experimental groups

All porcine aortic valves and pericardia were obtained under clean conditions from a local slaughterhouse (Ruyckaert M NV, Eeklo, Belgium), transferred to the laboratory and immediately processed. Aortic valves and pericardia were dissected and placed in Hanks buffer saline solution (HBSS) medium supplemented with a cocktail of antibiotics (100µg/ml streptomycin, 100U/ml penicillin, Gibco, Life Technologies) and 2.5µg/ml fungizone (Invitrogen, Life Technologies). Once the PER and HVL were properly dissected and cleaned, they were randomly assigned to the different experimental groups as described in **Table 1**.

Light/Fluorescence Microscopy

Samples of native and decellularized PER/HVL (n=9 each group) were fixed in 10% formalin (Merck, Darmstadt, Germany), dehydrated and embedded in paraffin. Five-micron-thick sections were cut and stained with Hematoxylin/Eosin (HE) for the histological evaluation. The ECM was assessed by several histochemical methods. Alcian blue, Orcein and Picrosirius Red stainings were performed as previously described to determine GAG, elastin and fibrillar collagens respectively [284]. Finally, 4',6-diamidino-2-phenylindole (DAPI) was used for the identification of cell nuclei with fluorescent microscopy.

Scanning Electron Microscopy

Samples of native and decellularized PER/HVL were first fixed in 2.5% of glutaraldehyde in 0.05M cacodylate buffer (pH 7.2) at 4°C during 6 hours and then washed three times in 0.05M cacodylate buffer (pH 7.2) at 4°C. Next, the samples were dehydrated in increasing concentrations of ethanol (50%, 70%, 85% and 100%), and completely dried by using hexamethyldisilazane (HMDS). Once dried, samples were cut in half, positioned and covered with gold and analyzed with a scanning electron microscope FEI Quanta 200 using the high vacuum mode.

Table 1: Protocols used for the decellularization of PER and HVL

		PER	HVL
Native tissue	Native PER/HVL were stored in HBSS medium at 4°C and used as a control group (without decellularization)	**Group 1**	**Group 6**
TRITON X-100 1%+ENZ+TRYP	PER/HVL were placed in a 5mM Tris buffer (pH=8) for 24h at 4°C. Next, they were transferred to a new 5mM Tris buffer (pH=8) with Triton X-100 (1%) (Biorad, Eke, Belgium) for 24h at 4°C. Subsequently, they were washed twice with HBSS (15min, 4°C) and transferred to HBSS medium supplemented with 100mg/L DNase, 20mg/L RNase (Sigma Aldrich, Bornem, Belgium) and trypsin (100mg/L) (2x 45min,37°C). Then they were placed in a new 5mM Tris-buffer (pH=8) + Triton X-100 (1%) for 24h, 4°C. Afterwards they were washed several times with HBSS medium, 4°C	**Group 2**	**Group 7**
TRITON X-100 1%+ENZ	The same as TRITON X-100 1% +ENZ +TRYP decellularization but without trypsin treatment	**Group 3**	**Left out**
SDC 1%+ENZ (24h)	PER/HVL were placed in a PBS solution with 1% SDC (Sigma Aldrich) and supplemented with 100mg/L DNase, 20mg/L RNase for 24h at 37°C.	**Group 4**	**Group 8**
SDC 1% (48h)	PER/HVL were placed in a PBS solutions with 1% SDC without enzymes for 48h at 37°C	**Group 5**	**Left out**
SDC 2% (48h)	HVL were placed in a PBS solutions with 2% SDC without enzymes for 48h at 37°C		**Group 9**

Quantitative biochemical analysis

Biochemical analysis was performed to analyze cellular and extracellular components of native and decellularized PER/HVL (n=9). Following tissue extraction soluble collagens (acetic acid-pepsin extraction), elastin (oxalic acid extraction) and N- and O-sulfated GAG (papain extraction) were quantified using SIRCOL, FASTIN and BLYSCAN assays respectively. In addition, these biochemical analyses were performed following the manufacture recommendations (Biocolor, Belfast, Northern Ireland). The samples were normalized according to equivalent dry weight for DNA, GAG and elastin content or wet weight for collagen content. Total DNA was isolated (QIAamp DNA Mini Kit, Qiagen, Venlo, The Netherlands) and quantified by spectroscopy NanoDrop 1000 (Isogen, Temse, Belgium).

Gel electrophoresis

DNA fragments were separated via 1% agarose gel electrophoresis. Gels were prepared by dissolving agarose in a 0.5x Tris Borate EDTA (TBE)-buffer. To load the samples, DNA was mixed with 6x loading dye (Fermentas, Thermo Scientific Life Sciences, Germany) and a 100bp DNA ladder (Fermentas) was used. DNA was detected using UV light after placing the gel for 30 minutes in an ethidiumbromide-solution (Merck Millipore Calbiochem, Belgium).

Mechanical testing

A flexural indentation test was performed as previously described [285]. A Loyd LF Plus Universal material tester (Analis NV, Suarleé, Belgium) with a 10 newton (N) load cell in combination with the build in “Compress” test program and Nexygen^{TM} MT software was used for the analysis. PER/HVL

(n=9) were placed over a 6.1-mm hole between two metal plates. Subsequently, a ball probe with a diameter of 4.45mm indented the tissue through the hole at a speed of 25mm/min. A lower force limit of 0.1N was set as the zero-indentation point for the tissues. Displacement of the ball-probe was recalculated to depth of indentation for the tissue based on these values.

The tissues were loaded with the ball probe for five times, by applying a preload of 0.1N. Subsequently the test starts and the ball probe is further depressed into the leaflet until breakage (Static rupture test) or until a maximum load of 6N is achieved (Quasi-static indentation cycle test).

Four tissue properties are derived from these tests:

1) Extension at break (mm) (EXT): the depth of indentation by the probe at the moment of rupture (defined as a sudden decrease in load with 50%); 2) Maximum load (N) (ML): the maximum load which can be applied to the cusp prior to rupture; 3) Work To Maximum Load (mJ) (WTML): ML x EXT; 4) Stiffness parameter (N/mm) (ST): the slope of the linear section of the indentation–load curve between 2.5 and 5.8N.

Statistical analysis

For each test, three independent experiments were performed in triplicate, giving a total of 9 biological relevant values (n=9). Each time, fresh HVL/PER were isolated and decellularized. Descriptive statistics are reported as the mean with the standard deviation between brackets. The Shapiro-Wilk test was used to determine normality of the variables and the Levene's test to determine homogeneity of variances. Significant differences between PER/HVL were estimated by analysis of variance. All the variables were parametric data and were analyzed with a one-way ANOVA test followed by a post-hoc Tukey's (equal variances) or a Welch F test followed by a post-hoc Dunnett's T3 (unequal variances) using the commercially available software package SPSS for windows, version 23.0 (SPSS GmbH Software, München, Germany). In this study, $p<0.05$ was considered statistically significant.

RESULTS

Histology

Histology of decellularized porcine PER

HE staining of the different decellularized pericardia showed no remaining nuclear material in any of the experimental groups **(Fig.1.2-5).** Alcian Blue staining clearly showed that there was a major loss of GAG, which are normally present throughout the entire fibrous pericardium, in all decellularized PER except in PER decellularized with Triton X-100 1%+ENZ (group 3). All decellularized PER, except SDC 1% (48h) decellularized PER (group 5) showed a positive, but less intense Picrosirius staining and an increase of the interfibrillar spaces of the collagen bundles compared with native PER, which showed intense stained dens collagen fibers. On the other hand, Orcein staining did not show a distortion of the interspersed scant short elastic fibers in any of the experimental groups. In contrast to the HE staining, DAPI staining revealed the presence of DNA fragments in all the SDC treated tissues (group 4-5). Moreover, gel electrophoresis showed DNA fragments of >1000bp in these groups, whereas Triton X-100 1%+ENZ±TRYP treated tissues (group 2-3) did not show any DNA fragments (data not shown).

Histology of decellularized porcine HVL

HE staining of the decellularized HVL revealed an effective elimination of cells when Triton X-100 1%+ENZ+TRYP was used (group 7, **Fig.2.7**). HVL that were treated with the same protocol from group 7 but without the trypsin treatment or decellularized with SDC 1% (48h) still showed nuclear material (data not shown). For this reason, these decellularized tissues were not further analyzed and left out of this study. In an attempt to optimize the SDC protocol, enzymes were added or SDC concentration was increased (SDC 1%+ENZ (24h) (group 8) and SDC 2% (48h) (group 9)). Again, the HE staining did reveal some nuclear material **(Fig.2.8-9).** This result was confirmed by DAPI staining, and gel electrophoresis revealed DNA fragments of >1000bp in these groups, whereas tissues decellularized with Triton X-100 1%+ENZ+TRYP (group 7) did not show any DNA fragments (data not shown). Alcian Blue staining revealed a complete washout of GAG of Triton X-100 1%+ENZ+TRYP and SDC 1%+ENZ (24h) treated HVL (group 7 and 8), and a major loss in the SDC 2% (48h) treated HVL (group 9) compared to native tissue. Orcein staining showed the presence of elastic fibers, which were properly organized and distributed throughout the lamina ventricularis (LV) in all experimental groups. On the other hand, Picrosirius Red staining showed a decrease in intensity of the collagen staining of all decellularized HVL in comparison with native HVL. In addition, an increase of interfibrillar spaces of the collagen bundles was observed in the lamina spongiosa (LS), especially in the LF of the Triton X-100 1%+ENZ+TRYP and SDC 1%+ENZ (24h) decellularized HVL (group 7 and 8).

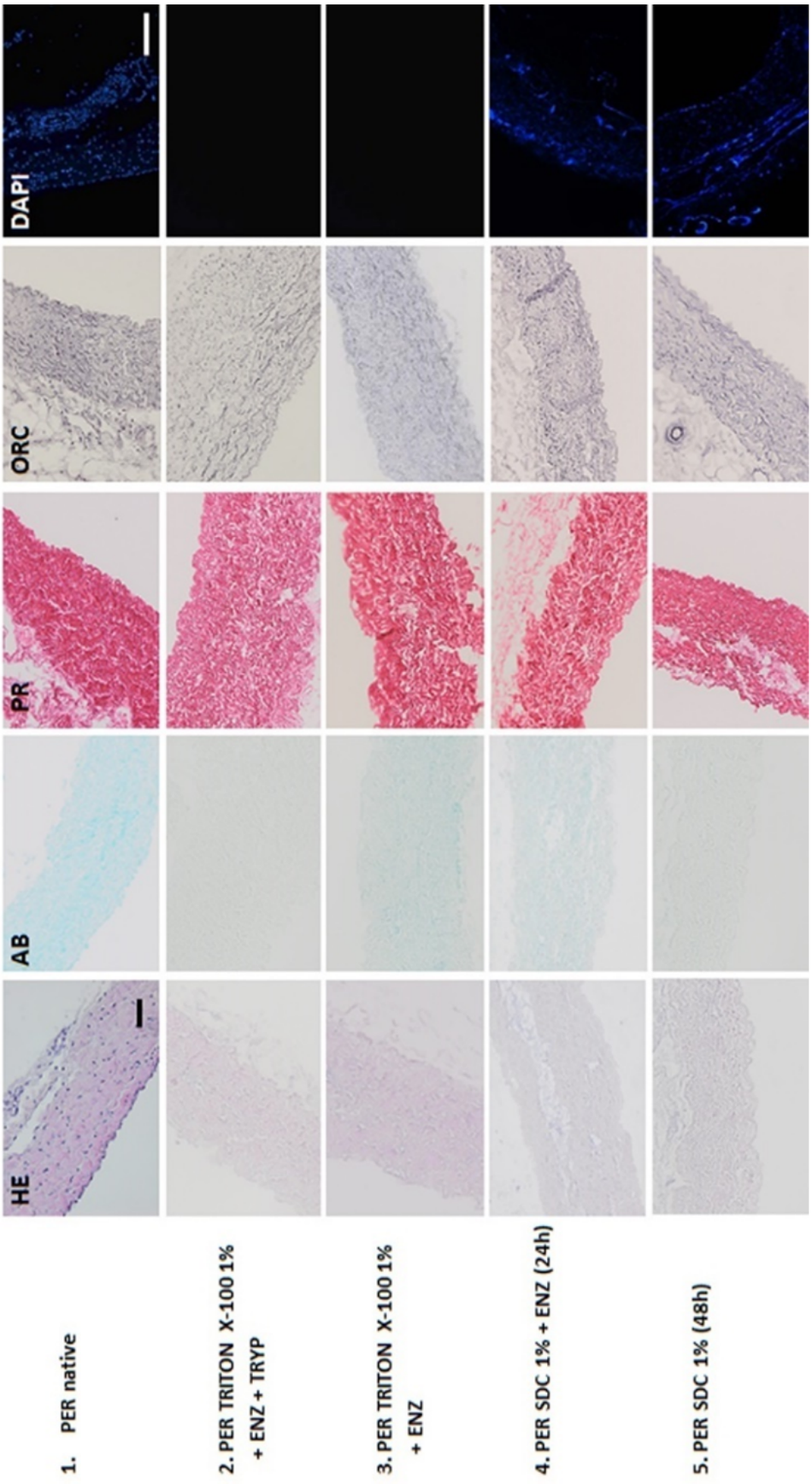

Fig.1: Light and fluorescent microsopy of (1) native and (2-5) decellularized pericardia (PER). HE; Hematoxylin Eosin staining; AB: Alcian Blue staining; ORC: Orcein staining; PR: Picrosirius Red staining and DAPI: DAPI staining. Decellularized PER showed no remaining nuclear material (HE), an almost complete washout of GAG (AB), less intense Picrosirius staining (PR) and no distortion or fragmentation of elastic fibers (ORC) for all treatment protocols. DAPI staining revealed nuclear material in group 4-5 (DAPI). (Original magnification: (HE,AB,PR,ORC) 20x, scalebar 100µm; (DAPI) 10x, scalebar 200µm)

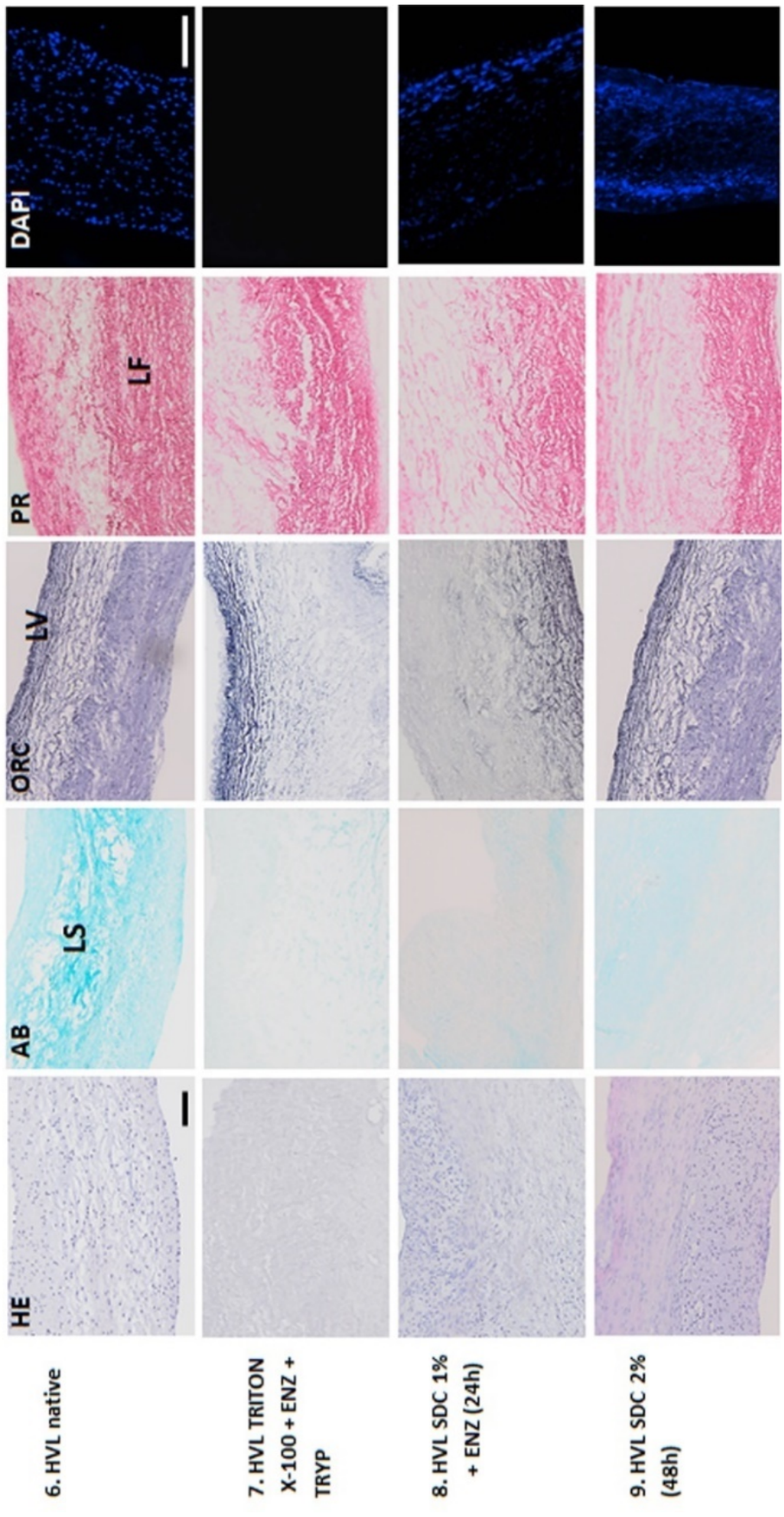

Fig.2: Light and fluorescent microsopy of (6) native and (7-9) decellularized heart valve leaflets (HVL). HE; Hematoxylin Eosin staining; AB: Alcian Blue staining; ORC: Orcein staining; PR: Picrosirius Red staining and DAPI: DAPI staining. Decellularized HVL showed only in group 7 no remaining nuclear material (HE), an almost complete washout of GAG (AB), no distortion of elastic fibers (ORC) and less intense picrosirius sta ining (PR) for all treatment protcols. DAPI staining revealed nuclear material in group 8 and 9 (DAPI). LS= lamina spongiosa; LV= lamina ventricularis; LF= lamina fibrosa (Original magnification: (HE,AB,PR,ORC) 20x, scalebar 100µm; (DAPI) 10x, scalebar 200µm)

Quantitative biochemical analysis

Quantitative biochemical tissue analysis data is summarized in **Table 2.** All samples are shown according to equivalent dry or wet weight in milligrams.

Table 2: Absolute and relative biochemical quantification of soluble collagen, GAG, elastin and DNA content of native and decellularized PER and HVL.

		Collagen µg/mg		*GAG µg/mg*		*Elastin µg/mg*		*DNA ng/mg*	
		Mean (SD)	*%*	*Mean (SD)*	*%*	*Mean (SD)*	*%*	*Mean (SD)*	*%*
1	PER native	4.43 (1.79)	100.00	4.04 (0.99)	100.00	24.82 (2.46)	100.00	920.45 (118.88)	100.00
2	PER TRITON X-100 1%+ENZ+TRYP	2.89 (1.27)	65.17	1.01 (0.59)	24.88	10.10 (3.84)	40.70	113.42 (27.96)	12.32
3	PER TRITON X-100 1%+ENZ	3.79 (0.59)	85.55	1.61 (0.18)	39.75	15.47 (0.89)	62.33	146.86 (174.88)	15.96
4	PER SDC 1%+ENZ (24h)	3.83 (0.86)	86.49	0.69 (0.09)	17.15	11.44 (3.25)	46.10	325.22 (113.72)	35.33
5	PER SDC 1% (48h)	3.39 (0.28)	76.51	1.27 (0.52)	31.41	17.70 (2.05)	71.33	296.60 (322.94)	32.22
6	HVL native	4.16 (0.98)	100.00	11.32 (2.87)	100.00	20.05 (4.63)	100.00	3245.38 (688.26)	100.00
7	HVL TRITON X-100 1%+ENZ+TRYP	3.01 (0.81)	72.23	1.78 (0.67)	15.75	22.85 (2.85)	113.96	201.06 (169.22)	6.20
8	HVL SDC 1%+ENZ (24h)	2.76 (0.49)	66.27	2.24 (0.68)	19.78	17.70 (2.30)	88.26	903.67 (447.36)	27.84
9	HVL SDC 2% (48h)	2.79 (0.76)	66.96	4.99 (1.85)	44.09	19.97 (2.88)	99.59	1105.61 (635.46)	34.07

Native and decellularized porcine PER

Figure 3 showed a statistically significant difference between DNA content of native PER compared with all decellularized PER ($p<0.01$). Interestingly, tissues treated with SDC 1%+ENZ (24h) or SDC 1% (48h) (group 4-5) still had a relatively high DNA content of more than 30%, whereas DNA content of tissue treated with Triton X-100 1%+ENZ±TRYP (group 2-3) was lower than 16%. However, there was no statistically significant difference observed between these groups **(Fig.3D).** A small, but not statistically significant, amount of soluble collagen was lost during all decellularization protocols **(Fig.3A).** On the other hand, the amount of elastin decreased statistically significant in all the decellularized pericardia ($p<0.01$) compared with native pericardium. Interestingly, PER treated with SDC 1% (48h) (group 5) had a significantly higher elastin content after decellularization compared with PER decellularized with Triton X-100 1%+ENZ+TRYP (group 2) or SDC 1%+ENZ (24h) (group 4) **(Fig.3C).** Also, GAG content of all decellularized PER was significantly different from that in native tissues ($p<0.01$), but no statistically significant difference was observed between the decellularized groups **(Fig.3B).**

Native and decellularized porcine HVL

The DNA content of decellularized HVL decreased significantly in all three decellularization protocols (group 7-9) compared with native HVL (group 6, $p<0.01$). The reduction was most pronounced in the Triton X-100 1%+ENZ+TRYP treated tissues (group 7), with only 6.2% of residual DNA left after decellularization, whereas tissues treated with SDC 1%+ENZ (24h) (group 8) and SDC 2% (48h) (group 9) still had a relatively high DNA content of respectively 27.84% and 34.07%. This difference was statistically significant between group 7 and 9 ($p<0.05$, **Fig.3D**).

A small amount of soluble collagen was lost during all decellularization processes, which was statistically significant in the SDC 1%+ENZ (24h) (group 8) and SDC 2% (48h) (group 9) decellularized HVL ($p<0.05$, **Fig.3A**). In contrast with pericardial tissue, the elastin content of the decellularized HVL was not significantly reduced (group 7-9), but showed similar values compared to the native HVL (group 6, **Fig.3C**). Total GAG content of all decellularized tissues (group 7-9) was significantly different from that of native tissues (group 6, $p<0.01$). GAG were best preserved in tissues treated with SDC 2% (48h) (group 9, **Fig.3B**).

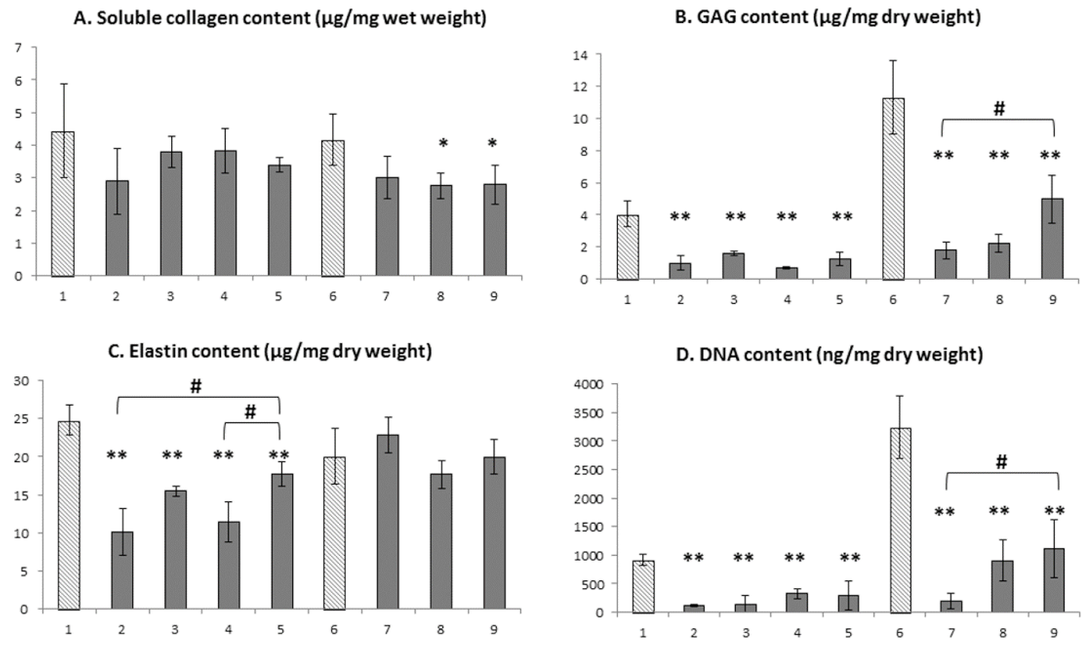

Fig.3: Quantitative biochemical analysis of soluble collagen, GAG, elastin and DNA content of native and decellularized PER/HVL. A small amount of soluble collagen and a significant amount of GAG was lost during the decellularization process of both PER and HVL. Elastin content was only significantly reduced in decellularized PER. Total DNA content decreased significantly in all the decellularized tissues. Error bars equal 95% Confidence Interval. Statistically significant differences are determined with a one-way ANOVA test followed by a post-hoc Tukey's (Collagen, DNA and GAG content) or a Welch F test followed by a post-hoc Dunnett's T3 (Elastin content). *p<0.05; **p<0.01 indicate a statistically significant difference between native and decellularized tissues. #p<0.05 indicates a statistically significant difference between different decellularization groups. [Groups: 1=PER native; 2=PER TRITON X-100 1%+ENZ+TRYP; 3=PER TRITON X-100 1%+ENZ; 4=PER SDC 1%+ENZ (24h); 5=PER SDC 1% (48h); 6=HVL native; 7=HVL TRITON X-100 1%+ENZ+TRYP; 8=HVL SDC 1%+ENZ (24h); 9=HVL SDC 2% (48h)]

Scanning electron microscopy

Figure 4 shows the surface morphology of native and decellularized PER. The serosa and fibrosa of native pericardial tissue showed a cobblestone-like microstructure **(Fig.4.1).** SEM revealed that the decellularization procedures had little effect on the serosa surface of decellularized pericardia **(Fig.4A,B).** On the other hand, the fibrosa surface of decellularized pericardia showed a loose network composed of randomly oriented fibers and large pores **(Fig.4D).** However, the cobblestone-like morphology of the surface was preserved in PER decellularized with Triton X-100 1%+ENZ±TRYP (group 2 and 3, **Fig.4C**).

These findings also applied for HVL. The surface of the LF of native HVL showed a wavy pattern, whereas the LV had a smooth surface **(Fig.5.6).** SEM revealed that the decellularization procedures had little effect on the surface of the LF of decellularized heart valve leaflets **(Fig.5A,B).** However, the LV from decellularized HVL displayed a loose network composed of randomly oriented fibers and large pores **(Fig.5D).**

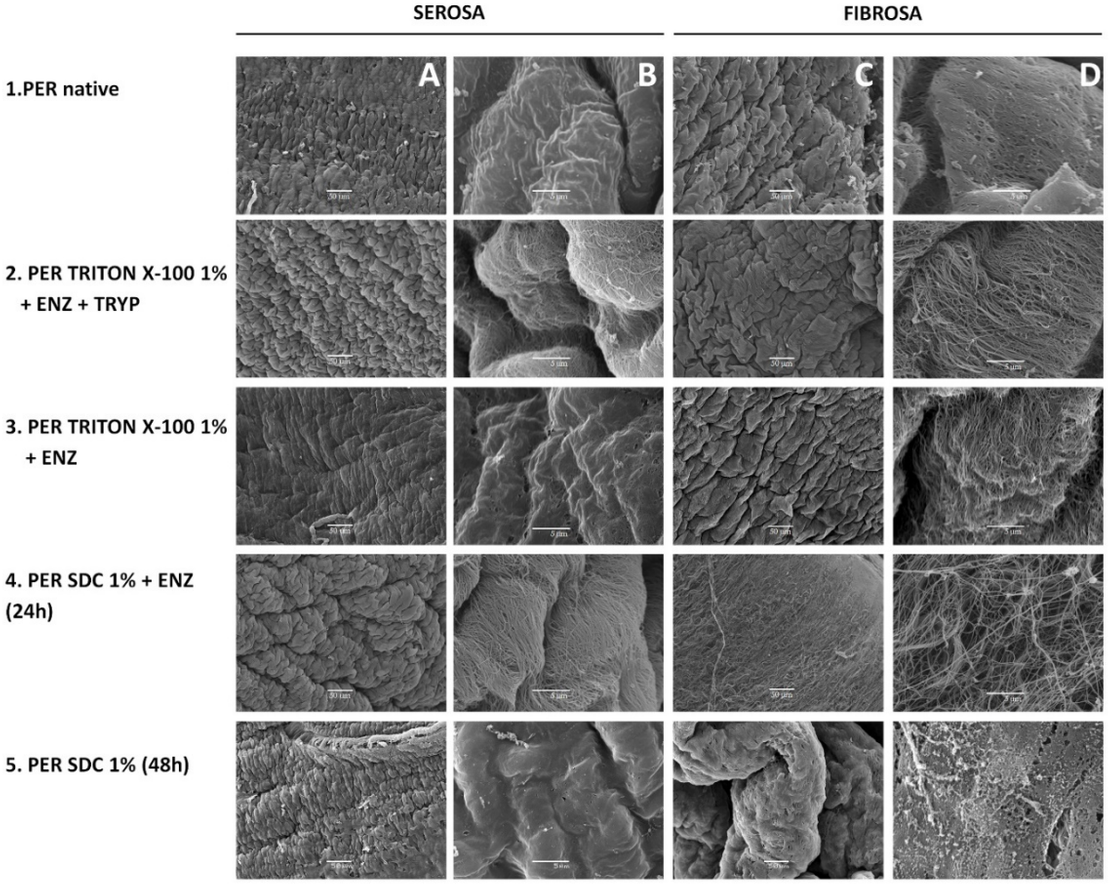

Fig.4: Scanning electron microscopy of the (A,B) serosa and (C,D) fibrosa surface of (1) native and (2-5) decellularized pericardial tissue. The surface of native PER showed a cobblestone-like microstructure, which is preserved in decellularized PER from group 2 and 4. The serosa surface of decellularized PER was little affected whearas the fibrosa surface of decellularized PER showed a loose network composed of randomly oriented fibers and large pores. (Original magnification: (A,C) 300x, scalebar 50µm; (B,D) 4500x, scalebar 5µm)

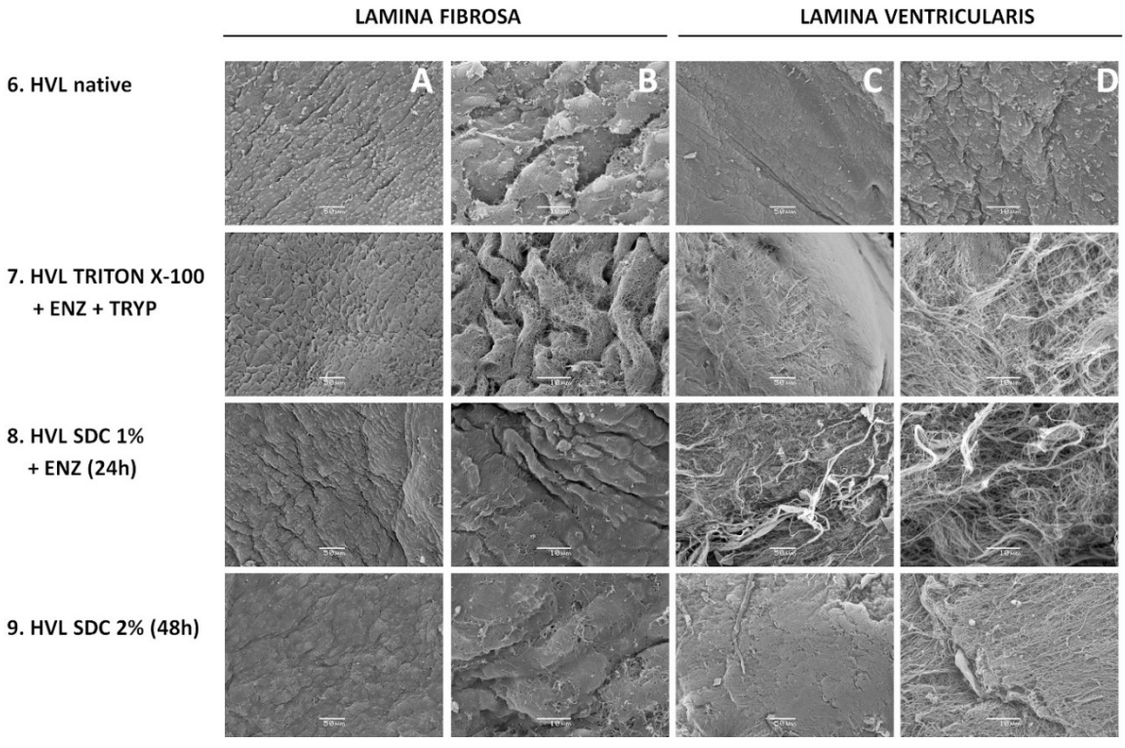

Fig.5: Scanning electron microscopy of (A,B) the lamina fibrosa and (C,D) lamina ventricularis surface of (6) native and (7-9) decellularized heart valve leaflets. The surface of the lamina fibrosa of native HVL showed a wavy pattern, which is preserved in all decellularized leaflets. The lamina ventricularis of native HVL had a smooth surface, which is destroyed after decellularization and decellularized HVL displayed a loose network of randomly oriented fibers and large pores. (Original magnification: (A,C) 300x; scalebar 50µm, (B,D) 4500x; scalebar 5µm)

Biomechanical analysis

A static rupture test and a quasi-static indentation cycle test were performed to determine the stiffness and work to maximum load of the (non-) decellularized PER and HVL. The calculated extension (EXT), maximum load (ML) and stiffness (ST) mean values are given in **Table 3**. In **Figure 6** it is shown that none of the decellularized PER showed a statistically significant difference in stiffness compared to native PER. However, the work to maximum load (WTML) was significantly reduced in PER treated with SDC 1%+ENZ (24h) (group 4) compared with native PER and PER decellularized with Triton X-100 1%+ENZ+TRYP (group 1 and 2). Only Triton X-100 1%+ENZ+TRYP treated (group 2) PER showed a WTML similar to that of native PER (group 1). On the other hand, decellularized HVL did show a significant increase in stiffness in the Triton X-100 1%+ENZ+TRYP (group 7) and the SDC 1%+ENZ (24h) (group 8) treated HVL. However, this increase in stiffness did not affect the work to maximum load.

Table 3: Results of the static rupture and quasi-static indentation cycle test for PER and HVL

		EXT (mm)	ML (N)	ST (N/mm)	WTML (mJ)
1	PER native	8.58 (3.50)	36.18 (9.31)	11.06 (1.42)	325.99 (160.94)
2	PER TRITON X-100 1%+ENZ+TRYP	8.71 (2.33)	35.68 (9.68)	9.21 (1.33)	315.68 (116.62)
3	PER TRITON X-100 1%+ENZ	6.84 (1.90)	34.83 (6.25)	9.10 (2.38)	238.80 (77.76)
4	PER SDC 1%+ENZ (24h)	4.73 (1.00)	28.36 (8.07)	10.85 (0.72)	139.79 (63.31)
5	PER SDC 1% (48h)	3.81 (1.15)	37.46 (9.72)	9.68 (1.02)	150.31 (69.55)
6	HVL native	4.00 (0.74)	14.78 (2.29)	9.17 (0.81)	58.72 (10.69)
7	HVL TRITON X-100 1%+ENZ+TRYP	3.60 (1.41)	16.32 (6.83)	10.98 (0.66)	58.86 (30.67)
8	HVL SDC 1%+ENZ (24h)	3.56 (1.12)	14.79 (2.27)	11.49 (0.82)	54.00 (21.50)
9	HVL SDC 2% (48h)	3.89 (0.52)	16.79 (2.82)	10.02 (0.70)	65.85 (14.48)

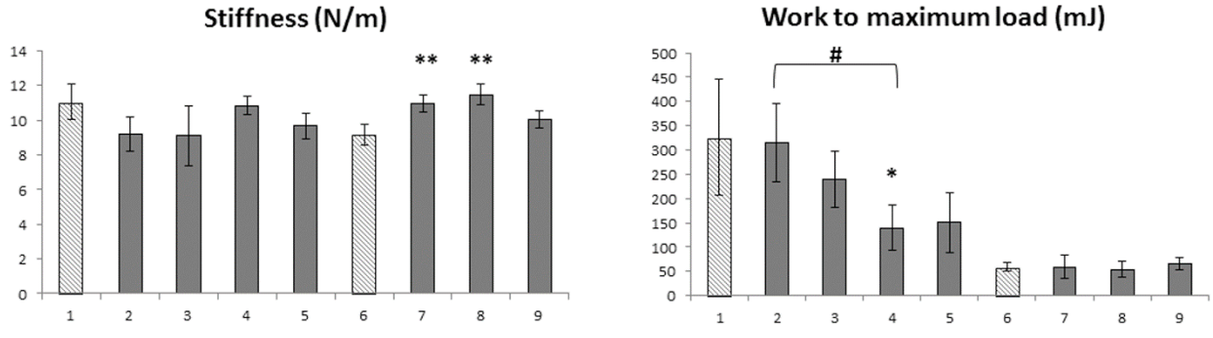

Fig.6: Stiffness and work to maximum load of native and decellularized PER/HVL. After decellularization, the stiffness of heart valve leaflets increased significantly and pericardia had a reduced work to maximum load. Error bars equal 95% Confidence Interval; Statistically significant differences are determined with a Welch F test followed by a post-hoc Dunnett's T3. *p<0.05; **p<0.01 indicate a statistically significant difference between native and decellularized tissues. #p<0.05 indicates a statistically significant difference between different decellularization groups. [Groups: 1=PER native; 2=PER TRITON X-100 1%+ENZ+TRYP; 3=PER TRITON X-100 1%+ENZ; 4=PER SDC 1%+ENZ (24h); 5=PER SDC 1% (48h); 6=HVL native; 7=HVL TRITON X-100 1%+ENZ+TRYP; 8=HVL SDC 1%+ENZ (24h); 9=HVL SDC 2% (48h)]

DISCUSSION

Xenogeneic heart valves or pericardial tissues need to be completely cell free before they can be used as scaffolds for heart valve tissue engineering, as it is known that the immunogenicity of these scaffolds is mainly due to its cell components. Also, cellular material within treated tissues has been found to lead to calcification and dysfunction of artificial heart valves [94, 140].

None of the currently used decellularization techniques are capable of removing 100% of cellular material. Therefore, Crapo et al. set minimal criteria to satisfy the intent of decellularization; double-stranded DNA content needs to be below 50ng/mg ECM (dry weight), DNA fragments may have a maximum length of 200bp, and no nuclear material may be visible with DAPI or HE staining [138].

Different research groups have reported SDC or Triton X-100 as effective detergents to remove cells from tissues [98, 271, 277-279, 283, 286-289]. However, none of these groups investigated whether the bioscaffolds met the three minimal criteria [138]. In this study Triton X-100 1%+ENZ±TRYP, a protocol optimized in our lab, was validated and compared to different and faster protocols with SDC. Some studies have shown that SDC is capable of removing cells from heart valves without affecting the ECM [289-291].

As observed by DAPI, HE staining and gel electrophoresis, it is shown that Triton X-100 1%+ENZ±TRYP (group 2, 3 and 7) is the most efficient protocol to remove nuclear material from porcine pericardium and heart valves. However, the amount of total DNA is slightly higher than the suggested limit of 50ng/mg. SDC treatment (without enzymes) has previously been reported to generate cell free HVL based on HE staining alone [281, 289]. In this study, HVL that were decellularized with SDC protocols, did not fulfill any of the three criteria. Even if enzymes were added to the protocol or incubation time was increased, the three criteria were never fulfilled (group 8-9). Interestingly, HE staining of SDC decellularized PER (group 4-5) did not show any nuclei. However, when further analyzed, they did not meet the three criteria.

Because it is known that detergents can alter the ECM structure, histological staining and quantitative biochemical analysis were performed. Collagens constitute the main structural elements of the ECM and are indispensable for the preservation of the mechanical strength of tissues. In this study, histological staining showed minor changes in the collagen organization of both decellularized tissues, when compared with native tissues. This is consistent with findings of other groups [98, 292]. By contrast, some groups claim that tissue structure is preserved when using SDC or Triton X-100 [271, 277, 286, 287]. Quantitative biochemical analysis was used in this study to confirm the histological findings. It has previously been shown that decellularization with SDC 2% can cause a loss of soluble collagen in porcine lung tissue [293]. In this study, HVL decellularized with SDC-protocols

(SDC 1%+ENZ (24h) and SDC 2% (48h)) also showed a significant reduction of soluble collagen. However, soluble collagens were preserved in HVL decellularized with Triton X-100 1%+ENZ+TRYP. Interestingly, regardless of the used decellularization protocols (Triton X-100 or SDC-based), PER were less prone to soluble collagen deterioration.

Not only collagen, also the elastic fiber architecture plays an import role in the mechanical properties of tissues. Some groups showed that decellularization with Triton X-100 did not change the elastin distribution in HVL [98, 277]. For pericardial tissue, Dong et al. found that SDC treatment could disrupt elastic fibers, whereas Yang et al. showed that elastic fibers were preserved with Triton X-100 treatment [286, 288]. In our study, histological staining and quantitative analysis showed preservation of elastic fibers in decellularized HVL. By contrast, quantitative analysis revealed a significant decrease of elastin content of decellularized PER. The reason why detergents have more impact on elastin of pericardial tissues could be explained by the different levels of organization and assembly of these elements in the stroma. Elastic fibers with low levels of organization could be more susceptible to degradation or solubilization by the decellularization agents.

Another major component of the ECM are the GAG, which are found throughout the entire parietal PER and predominantly in the spongiosa layer of the HVL. Some groups claim that SDC does not influence the GAG network [271, 283]. By contrast, this study and other authors demonstrated a significant loss of GAG after decellularization of valvular and pericardial tissues with SDC or Triton X-100[98, 278, 288].

It is known that the alteration of collagen, elastic fibers and the removal of GAG leads to changes in mechanical properties and could contribute to tissue degeneration and failure of biological valves. Lee et al. showed that elastin impairment could distend the valve leaflets, reduce their extensibility and increase their stiffness [294]. Our study showed that detergent treatment did not alter the elastic fibers of the HVL. Nevertheless, a small reduction of extensibility and a significant increase in stiffness were observed which is probably due to the alteration of collagen bundles and the washout of GAG. On the other hand, pericardial tissue did show a significant reduction of elastin content after decellularization, and a reduction of extensibility of the tissue. Although stiffness was not significantly affected, decellularized pericardial tissue was more brittle and had a decreased maximum load.

Histochemical staining and biochemical assays are useful tools for the specific evaluation of different ECM molecules, but they do not allow the observation of the 3D structure of the ECM with high accuracy. In order to analyze tissue surface ultrastructure, a SEM analysis was performed. In literature, a consensus is lacking about the effect of detergent-based decellularization of PER and

HVL on the surface level. Some groups state that SDC and Triton X-100 do not alter the surface ultrastructure of tissues [278, 287, 288], whereas others showed that after decellularization with trypsin or Triton X-100, the LF and LV from HVL displayed a looser ECM network and the matrix of bovine PER became loose, deranged and partially broken [279, 286]. In this study, it is shown that Triton X-100 and trypsin as well as SDC altered the surface ultrastructure of decellularized HVL and PER, resulting in an irregular mesh of ECM fibers with small or large pore sizes.

CONCLUSION

In this study, the combination of histological, quantitative biochemical and mechanical tests were used to compare a four-day Triton X-100 based protocol with faster SDC based protocols for the decellularization of heart valve leaflets and pericardium. It is clear that SDC decellularized tissues did not show better preservation of structural ECM components than Triton X-100 decellularized tissues, although this has been suggested in literature. Both detergents had a similar impact on the ECM. This study has also shown that it is of great importance to accurately evaluate the three minimal criteria for acellularity of decellularized scaffolds. Based on these criteria, Triton X-100 1%+ENZ±TRYP is the only protocol that generated completely cell free bioscaffolds. Also, our study demonstrated that the decellularization agents have more impact on pericardial tissue than on heart valve leaflets. Thus, for the purpose of tissue engineering of heart valves, it is advisable to use valvular rather than pericardial matrices. However, acellular pericardial matrices could be useful as cardiovascular patches, patches for cell delivery or other tissue engineering applications [295-297].

PART

A

SECTION II

Based on:

Complete static repopulation of decellularized porcine tissues for heart valve engineering – an *in vitro* study

Roosens A, Asadian M, De Geyter N, Somers P, Cornelissen R

(In press: Cells Tissues Organs)

ABSTRACT

To date, a completely *in vitro* repopulated (bio-active) tissue engineered heart valve (TEHV) has not yet been developed. This study focused on sequentially seeding two cell populations onto porcine decellularized heart valve leaflets (HVL) and pericardia (PER) to obtain fully repopulated tissues. For the repopulation of the interstitium, porcine valvular interstitial cells (VIC) and bone marrow or adipose derived stem cells (BM-MSC and ADSC respectively) were used. In parallel, ascorbic acid 2-phosphate (AA) was supplemented to the stem cell medium and its effect on recolonization was investigated. Subsequently and in order to obtain an endothelial surface layer similar to those in native heart valve leaflets, endothelial cells were seeded onto the scaffolds. It was shown that VIC efficiently recolonized HVL and partially also PER. On the other hand, stem cells only demonstrated limited or no subsurface cell infiltration of HVL and PER. Interestingly, the addition of AA increased the migratory capacity of both stem cell population. Yet, this was more pronounced for BM-MSC and recolonization of HVL appeared to be more efficient than PER tissue. VEC were demonstrated to generate a new endothelial layer onto HVL and PER. However, SEM revealed that these endothelial cells were not allowed to fully spread onto PER. This study provided a proof of concept for the future generation of a bio-active TEHV by showing that bio-active HVL can be generated *in vitro* within 14 days, by completely repopulating the interstitium with BM-MSC or VIC and subsequently generating an entirely new endothelium.

INTRODUCTION

The prevalence of heart valve diseases increases with age and is affecting more than five million people in the United States [267]. Heart valve replacements by mechanical or bioprosthetic heart valves remain mandatory for end-stage valvulopathy. Unfortunately, one of the main problems of all clinically used valve substitutes is the inability to grow, repair or remodel within the patient since they are made of non-viable material, which is especially needed in the pediatric and young adult population as they outgrow valve replacements, resulting in multiple re-operations [98]. To overcome the shortcomings of current treatment options, heart valve tissue engineering (HVTE) emerged, which focusses on the *in vitro* biofabrication of functional, living heart valve replacements. One approach of HVTE is to create autologous cell repopulated decellularized scaffolds [270].

ECM-based scaffolds derived from decellularized tissue are interesting materials for HVTE. The ECM contains bio-active molecules that drive tissue homeostasis and regeneration, it provides mechanical support and favors attachment, migration and proliferation of cells [123]. Tissues used for HVTE can either be from human (allogeneic) or animal (xenogeneic) origin. Over the past 25 years, the availability of valve allografts was a major problem as suitable valves can only be prelevated from organ donors whose hearts were not accepted, or recipients of heart transplants [76]. On the other hand, xenogeneic tissues (bovine or porcine pericardium, porcine small intestinal submucosa and porcine or ovine heart valves) are readily available [131].

Decellularization is the process used in biomedical engineering to remove all cells and cellular components from a tissue, while retaining the extracellular matrix (ECM) structure and proteins, and providing a biomechanically sufficient scaffold that allows efficient reseeding [298]. Complete decellularization of tissues remains crucial to minimize or to avoid an adverse immunologic response to foreign cellular antigens, which can trigger the calcification process and can evoke an adverse immune response post-implantation [94]. Unfortunately, a completely cell free xenogeneic scaffold sometimes can still elicit a foreign body type inflammatory response [140, 274]. Another problem of xenogeneic decellularized tissue is their highly thrombogenic surface, however, seeding the scaffold with endothelial cells can effectively abolish platelet adhesion and activation [299]. To date there is no doubt that complete recellularization and remodeling of the decellularized scaffolds is one of the key factors to limit or minimize immune based graft degeneration and structural tissue failure [145].

It is important to select suitable cell types for an appropriate and complete *in vitro* cell recolonization of decellularized tissues under static or dynamic culture conditions. Ideally, valvular interstitial cells (VIC) or VIC-like cells should be present throughout the entire interstitium and tissues should also display an endothelial covering. To achieve this result, researchers are using myofibroblasts (MFb)

[173, 300], fibroblasts (Fb) [301], endothelial (progenitor) cells (EC), or mesenchymal stem cells (MSC) [105, 302]. Among all these cells, MSC offer some advantages for autologous clinical employment; they are easily accessible and easy to isolate from patients, can be culture-expanded to a large number in a matter of days, have a minimal risk of immunogenicity [179], and they phenotypically resemble to valve cells [183-185]. But most important, they possess a multilineage differential potential (adipo-, chondro-, osteo-lineage), and it has been shown that they can be converted into EC, Fb/MFb, and smooth muscle cells (SMC) [180, 181]. Only few studies have focused on sequentially seeding two cell populations onto acellular matrices to obtain completely repopulated tissues [173, 300, 303]. Most research has been done on the acquirement of a stable endothelial covering of decellularized tissues or on only the recellularization of the interstitium.

We have previously shown that Triton X-100 in combination with Trypsin and nucleases is effective to obtain completely cell free porcine heart valve leaflets (HVL) and pericardia (PER) while preserving the main ECM components [304]. The aim of this study was to statically repopulate these decellularized tissues *in vitro* to generate viable tissues within 2 weeks. For the repopulation of the interstitium of both tissues, VIC and MSC (bone marrow or adipose derived) were used, and their repopulation capacity was compared. In parallel, ascorbic acid 2-phosphate (AA) was supplemented to the stem cell medium and its effect on MSC recolonization was investigated. Subsequently and in order to obtain an endothelial surface layer similar to those in native heart valve leaflets, VEC were seeded onto the scaffolds.

METHODS

Cell isolation

Valvular interstitial/endothelial cells (VIC/VEC)

Porcine aortic valve leaflets were dissected and VEC were isolated by mechanically removing the endothelial layer of the HVL with a cell scraper after incubating them at 37°C for 30 minutes in Dulbecco's Modified Eagle Medium (DMEM, Life Technologies) supplemented with 0.1% collagenase type 1 and 0.12% dispase (Sigma). The cell-solution was filtered with a 70µm cell strainer, and centrifuged. Cells were cultivated in complete DMEM (cDMEM: DMEM supplemented with 10% v/v FCS (Life Technologies), 100U/ml penicillin and 100µg/ml streptomycin (Life Technologies)) supplemented with 1% v/v non-essential amino acids 100x (Life Technologies), 50µg/ml endothelial cell growth supplement (Sigma), 1mM sodium pyruvate (Life Technologies), 10U/ml heparin (Sigma) in a humidified 5% CO_2-containing atmosphere at 37°C. Next, VIC were isolated by mincing the leaflets and incubating them at 37°C for 4 hours in DMEM supplemented with 0.1% collagenase type 1. Afterwards the cell-solution was filtered with a 70µm cell strainer, and centrifuged. Cells were cultivated in cDMEM in a humidified 5% CO_2-containing atmosphere at 37°C. Cells used for the experiments were between the second and fourth passage.

Bone marrow stem cells (BM-MSC)

BM-MSC were isolated from porcine bone marrow aspirate (obtained from the Experimental Surgery Department, Ghent University Hospital). Mononuclear cells from BM-aspirates were isolated with Lymphoprep (Stemcell technologies) by gradient centrifugation at a density of 1.077g/ml, washed two times with PBS, and seeded in a T175 flask filled with cDMEM. After 24 h incubation, non-adherent cells were discarded, whereas adherent cells were washed twice and fresh cDMEM was added. At passage 3, cells were divided into two groups. Group 1 was further cultivated in the presence of cDMEM, whereas 250µM ascorbic acid 2-phosphate (Sigma) was added to the medium of group 2. Cells used for the experiments were between the second and fourth passage.

Adipose tissue derived stem cells (ADSC)

Adipose derived stem cells (ADSC) were isolated from porcine subcutaneous fat tissue (obtained from the Experimental Surgery Department, Ghent University Hospital). Tissue was washed with PBS, minced into mm pieces and incubated at 37°C for 2 hours in DMEM supplemented with 0.1% collagenase type 1. The cell-solution was filtered with a 70µm cell strainer, and centrifuged. Cells were cultivated in cDMEM. At passage 3, cells were divided into two groups. Group 1 was further

cultivated in cDMEM, whereas 250µM ascorbic acid 2-phosphate was added to the cDMEM of group 2. Cells used for the experiments were between the second and fourth passage.

Multilineage differentiation of stem cells

For adipogenic and osteogenic differentiation, $4*10^4$ cells were seeded onto thermanox coverslips in 24 well plates. After 1 day, cDMEM was replaced with differentiation medium. Adipogenic differentiation was induced for 14 days in the presence of cDMEM supplemented with 1µM dexamethasone, 200µM indomethacin, 10µg/mL insulin, 0.5mM 3-Isobutyl-1-methylxanthine (all from Sigma). Osteogenic differentiation was induced for 14 days in the presence of cDMEM supplemented with 10mM β-glycerophosphate, 100µM ascorbic acid 2-phosphate, 100nM dexamethasone (all from Sigma). To evaluate the presence of neutral lipids or calcium deposition cells were stained with Oil Red O or Von Kossa respectively. For chondrogenic differentiation, a three- dimensional pellet culture system was used. Pellets were formed by centrifugation of $1*10^6$ cells in 2ml Eppendorf micro centrifuge tubes. All tubes were maintained in an incubator at 37°C with a humidified atmosphere of 5% CO2. After 1 day, cDMEM medium was replaced with STEMPro Chondrogenesis Differentiation Medium (Invitrogen) and carefully refreshed every third day for 21 days. Sections of these pellet were stained with Alcian Blue to evaluate the presence of proteoglycans and with Hematoxylin/Eosin (HE) for the overall morphology. All differentiation experiments were carried out in triplicate.

Gene expression analysis (RT-qPCR)

Total RNA (n = 3) was isolated from ADSC and BM-MSC from group 1 and 2 using a lysis buffer (RLT buffer, Qiagen). The concentration and purity of the isolated RNA was determined by a NanoDrop. To convert RNA into cDNA, the High Capacity cDNA Reverse Transcription Kit (Life Technologies) was used according to the manufacturer's protocol. A 7500 Fast Real-Time PCR system (Applied Biosystems) and a SYBR Green PCR kit (Life Technologies) were used according to the manufacturer's instructions and protocols. Primer details are listed in **Table 1.**

Stability of six reference genes was determined and the two most stable reference genes (ADSC: ActB and HPRT1, BM-MSC: ActB and EEF1A1) were selected via geNORM (qbase$^+$ software, Biogazelle). Gene expression analysis was normalized to the geometric mean of these reference genes.

The relative gene fold changes were determined by the $2^{-\Delta\Delta Ct}$ method. For comparative gene expression analysis, gene expression of cells cultivated in cDMEM (group 1) were compared to cells cultivated in cDMEM supplemented with 250µM ascorbic acid 2-phosphate (group 2).

Table 1: Primers for porcine BM-MSC and ADSC

Gene Description	Gene Symbol	Accession Number	Forward Primer 5' → 3'	Reverse Primer 3' → 5'	Amplicon Length (bp)	Primer Efficiency (%)
Eukaryotic translation elongation factor 1 alpha 1	EEF1A1	NM_001097418.2	CAACATGCTGGAGCCAAGTG	AGTGTGGTTCCACTGGCATT	87	94.2
Actin beta	ACTB	XM_003357928.2	GCGTAGCATTTGCTGCATGA	GTTTCAGGAGGCTGGCATGA	82	94.2
Hypoxanthine phosphoribosyl transferase 1	HPRT1	NM_001032376.2	GGGAGGCCATCACATCGTAG	CGCCCGTTGACTGGTCATTA	167	89.9
Alpha smooth muscle actin	α-SMA ACTA2	NM_001164650.1	GGACCCTGTGAAGCACCAG	GTCACCCACGTAGCTGTCTT	198	98.9
Vimentin	VIM	XM_005668106.1	TCTGGAATCCCTCCCTCTGG	TCGCTGCACAGAGTACATGC	146	93.8
Integrin subunit beta 1	CD29 ITGB1	NM_213968.1	GAATGCCAAATGGGACACGG	GCCCTGAAGCTACCTCACTG	155	91.8
Ecto-5'-nucleotidase	CD73 NT5E	XM_001927095.2	GACACCCGGATGAGATGTCC	AGCCAGGTTCTCCCAGGTTA	116	93.9
Cluster of Differentiation 90	CD90 Thy-1	NM_001146129.1	CATTGGCATCGCTCTCTTGC	TGGGCAGGTTGGTGGTATTC	131	95.4
Endoglin	CD105 ENG	NM_214031.1	CCATCTGGACTGGCACAACT	GTCTCTGTGTGGCGGTTACA	102	93.4
Alpha-1 type I collagen	COL1A1	XM_005668927.1	AGACATCCCACCAGTCACCT	TCACGTCATCGCACAACACA	122	96.9
Alpha-1 type II collagen	COL2A1	XM_001925959.5	GATGTTGGTGAGAAAGGCCC	GTCCAGTCTCTCCACGTTCA	181	91.0
Alpha-1 type III collagen	COL3A1	NM_001243297.1	GCTCCCATCTTGGTCAGTCC	ATGGGATCTCAGGGTTGGGA	147	94.5

Decellularization of heart valve leaflets and pericardium

All porcine aortic valves and pericardia (PER) were obtained under clean conditions from a local slaughterhouse (Ruyckaert M NV, Eeklo, Belgium), transferred to the laboratory and immediately processed. Tissues were decellularized with Triton X-100 and a combination of enzymes as previously described [304].

Static repopulation of heart valve leaflets and pericardium

Mono-cultures; a) A concentration of $2*10^5$ VEC /cm² was seeded onto the lamina ventricularis (LV) of decellularized HVL or onto the fibrous layer of PER (fibrosa) and maintained in a static culture for 3 days. Subsequently $2*10^5$ VEC /cm² were seeded onto the lamina fibrosa (LF) of HVL or onto the parietal layer of serous PER (serosa) for another 3 days. b) A concentration of $1*10^6$ VIC/ADSC/BM-MSC/cm² was seeded onto the LV of decellularized HVL or onto the fibrous layer of PER and statically cultivated for 14 days.

Co-cultures; A concentration of $1*10^6$ VIC/ADSC/BM-MSC/cm² was seeded onto LV of decellularized HVL or onto the fibrous layer of PER and statically cultivated for 7 days. Next, a concentration of $2*10^5$ VEC /cm² was seeded onto the LV of decellularized HVL or onto the fibrous layer of PER (fibrosa) and maintained in a static culture for 3 days. Subsequently $2*10^5$ VEC /cm² were seeded onto the LF of HVL or onto the parietal layer of serous PER (serosa) for another 3 days.

Table 2: Experimental set up of the static repopulation of heart valve leaflets and pericardium

		D0	D4	D7	D11	D14
HVL	Mono-culture VEC	LV: $2*10^5$ cells/cm²	LF: $2*10^5$ cells/cm²	fixation		
	Mono-culture VIC/ADSC/BM-MSC	LV: $1*10^6$ cells/cm²				fixation
	Co-culture VIC/ADSC/BM-MSC and VEC	LV: $1*10^6$ cells/cm²		LV: $2*10^5$ cells/cm²	LF: $2*10^5$ cells/cm²	fixation
PER	Mono-culture VEC	F: $2*10^5$ cells/cm²	S: $2*10^5$ cells/cm²	fixation		
	Mono-culture VIC/ADSC/BM-MSC	F: $1*10^6$ cells/cm²				fixation
	Co-culture VIC/ADSC/BM-MSC and VEC	F: $1*10^6$ cells/cm²		F: $2*10^5$ cells/cm²	S: $2*10^5$ cells/cm²	fixation

LV = lamina ventricularis; LF = lamina fibrosa; F = fibrosa; S = serosa

Histology of heart valve leaflets and pericardium

HVL and PER were fixed (4% paraformaldehyde, Merck, Darmstadt, Germany), dehydrated and embedded in paraffin. Five-micron-thick sections were cut and stained with Hematoxylin/Eosin for histological evaluation. An immunohistochemical anti Pecam-1 (CD31) staining for endothelial cells was performed: sections were subjected to heat-induced antigen retrieval (citric acid buffer, pH=6), endogenous peroxidase was quenched using 3% v/v H_20_2 for 10min, and a 30min treatment with blocking reagent (5% v/v normal swine serum (Dako), 1% w/v BSA (Roche), 0.2% v/v Tween 20 (VWR) in PBS) was performed. The sections were incubated with the primary antibody (polyclonal rabbit anti- CD31 (Santa Cruz, SC1506R), dilution 1:500) for 2h and subsequently with the secondary antibody (goat anti-rabbit (Dako, E0432), dilution 1:200) for 30 min. A 3,3-diaminobenzidine tetrahydrochloride substrate (Sigma) was used to visualize the horse radish peroxidase coupled secondary antibody. Sections were counterstained with hematoxylin, mounted and visualized under the microscope.

Scanning electron microscopy

Samples of native and decellularized PER/HVL were first fixed in 2.5% of glutaraldehyde in 0.05M cacodylate buffer (pH 7.2) at 4°C during 6 hours and then washed three times in 0.05M cacodylate buffer (pH 7.2) at 4°C. Next, the samples were dehydrated in increasing concentrations of ethanol (50%, 70%, 85% and 100%), and completely dried by using hexamethyldisilazane (HMDS). Once dried, samples were positioned, covered with gold and analyzed with a scanning electron microscope JEOL JSM-6010 PLUS/LV using the high vacuum mode.

Statistical analysis

The Shapiro-Wilk test was used to determine normality of the variables. All the variables were parametric data and were analyzed with a student t-test using the commercially available software package SPSS for windows, version 23.0 (SPSS GmbH Software, München, Germany). Descriptive statistics are reported as the mean with the standard deviation between brackets and $p<0.05$ was considered statistically significant.

RESULTS

In vitro trilineage differentiation of BM-MSC and ADSC

When cultured in an osteogenic medium, spindle shaped BM-MSC and ADSC adopted a more elongated phenotype and a mineralization of the ECM of both stem cell populations occurred. Deposited calcium phosphate of the mineralized nodules was confirmed by highly positive von Kossa staining at day 21 **(Fig.1.A).** Morphologic changes and the formation of vacuoles was observed at two weeks after adipogenesis induction. The adipocytes were rounded and filled with neutral lipid droplets that accumulated and fused to form vacuoles which could be stained by Oil Red O **(Fig.1.B).** In all pellet cultures, independent of the presence of a chondrogenic medium, compaction of the pellets into single aggregates was observed after 24h. The chondrogenic differentiation potential was evaluated after 28 days. HE-stained sections showed that the periphery of each pellet consisted of rounded, enlarged cells, which were similar to chondrocytes **(Fig.1.C).** The cartilaginous nature of the pellets was verified by Alcian blue staining of cartilage proteoglycans, demonstrating secretion of the ECM of chondrocytes **(Fig.1.D).** Adipogenic, osteogenic, and chondrogenic differentiation was not observed in the control groups. All results were representative of three independent experiments.

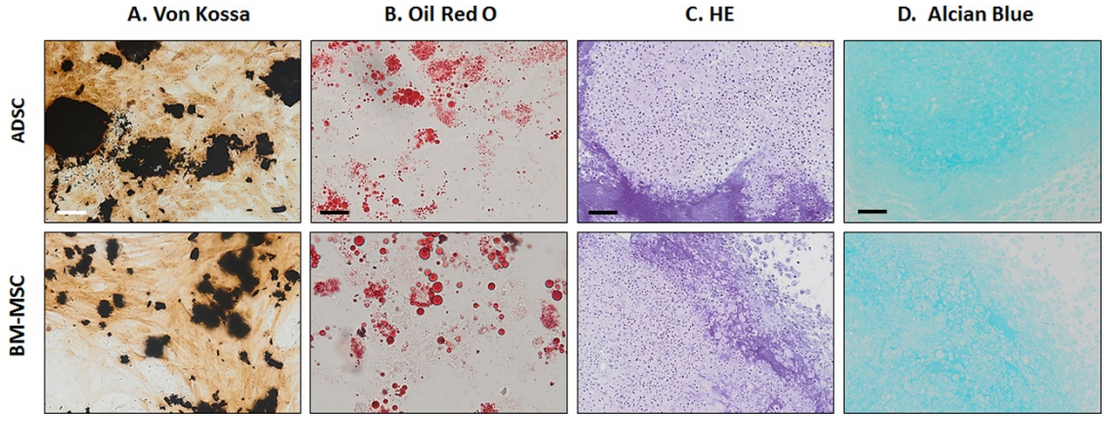

Fig.1: Trilineage differentiation of multipotent porcine stem cells (BM-MSC and ADSC). (A) Osteogenic differentiation was evaluated by von Kossa staining at day 21 (Scale bar = 50µm, original magnification x20). (B) Adipogenic differentiation potential was shown by Oil Red O staining at day 14 (Scale bar = 20µm, original magnification x40). (C) Chondrogenic differentiation was visualized by HE staining and (D) by Alcian blue staining at day 28 (Scale bar 100µm, original magnification x10). Representative images of n = 3 independent experiments.

Influence of AA on mRNA expression of BM-MSC and ADSC

When culture medium was supplemented with AA, α-SMA mRNA levels were significantly upregulated in BM-MSC (p=0.006) as well as in ADSC (p=0.037). Also, collagen type I (only BM-MSC) and to a lesser extent collagen type III expression levels increased. Yet, this was only significant for collagen type I in BM-MSC (p=0.042). No differences in vimentin and the stem cell markers: CD29/73/90/105 mRNA levels were observed between stem cells cultured in or without the presence of AA.

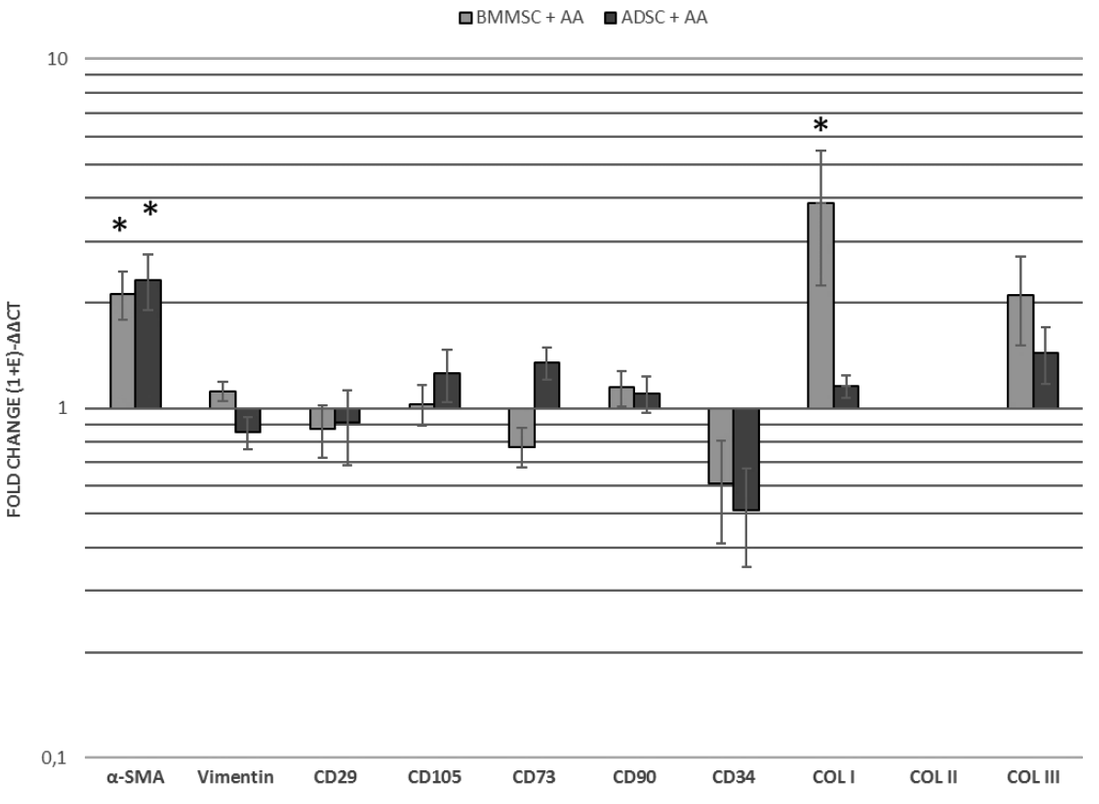

Fig.2: Gene expression analysis (fold change) of porcine BM-MSC and ADSC cultivated in the presence of AA compared with BM-MSC and ADSC cultivated in standard culture medium. Data is presented as mean and error bars indicate the 95% confidence interval. Statistically significant differences compared to standard cultured cells are marked with *p<0.05. Gene expression values are normalized to the geometric mean of two stable reference genes (EEF1A1/ActB (BM-MSC) or HPRT1/ActB (ADSC)). A Student t-test was used for the statistical analysis between the two culture methods, n = 3. AA; ascorbic acid 2-phosphate.

Decellularization of HVL and PER

HVL and PER were decellularized with Triton X-100 and extensively analyzed previously by our group [304]. In this study, a HE staining was used to verify the effective elimination of native cells. In native HVL/PER, darkly purple stained nuclei are present on the matrix surface and interstitium of both tissues. After decellularization, no remaining nuclear material could be detected by HE staining of the tissues **(Fig.3),** and SEM showed removal of the endothelial surface of the lamina fibrosa and ventricularis of HVL **(Fig.4)** and the fibrous PER **(Fig.5).**

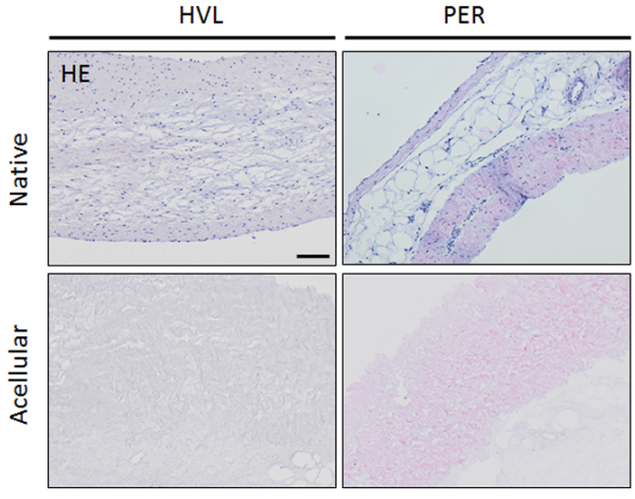

Fig.3: Light microscopy of native and acellular heart valve leaflets (HVL) and pericardia (PER). HE; Hematoxylin/Eosin. Representative images of n = 3 independent experiments. Scale bar 100µm, and original magnification x10.

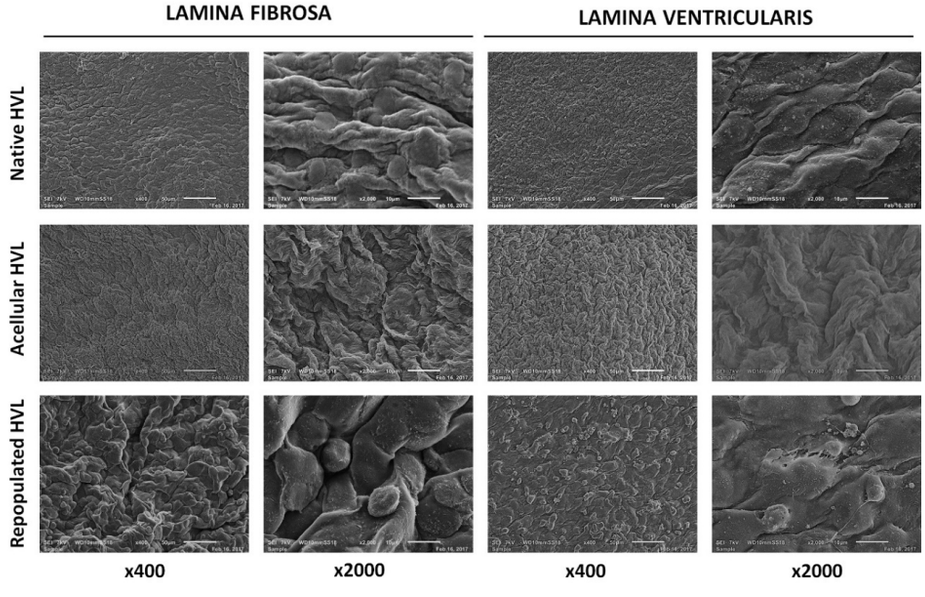

Fig.4: Scanning electron microscopy of native, acellular and VEC repopulated heart valve leaflets (HVL). Scale bar 50µm (x400), and 10 µm (x2000).

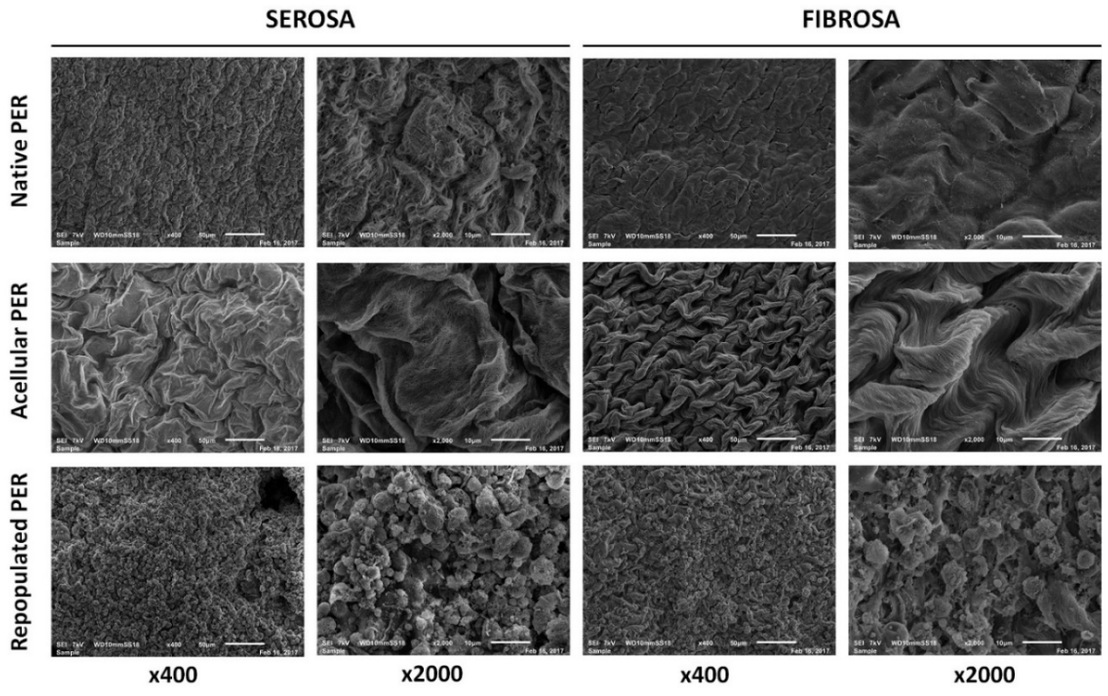

Fig.5: Scanning electron microscopy of native, acellular and VEC repopulated pericardia (PER) Scale bar 50µm (x400), and 10 µm (x2000).

Static repopulation of HVL and PER

Repopulation of HVL/PER with VIC and VEC

The histology of VIC and VEC repopulated HVL and PER after a 7 or 14-day culture period is shown in **Figure 6**. After 14 days, HVL were completely repopulated with VIC, which showed a normal mesenchymal fibroblast-like morphology, with a fully spread shape, and were distributed uniformly throughout the interstitium at approximately the same density as native HVL. VIC also seemed to migrate well throughout the fibrosa of PER. However, no cells were seen in the serosa layer. In parallel, tissues were seeded on both sides with VEC for 7 days. Endothelial cells adhered to the surface of both tissues and formed a thin confluent layer. An anti-CD31 staining was performed, to confirm the endothelial origin of these cells. To obtain repopulated tissues with VIC and VEC, 14-day co-culture repopulation experiments were performed. After 7 days of repopulation with VIC, VEC were seeded onto the surface of both tissues for another 7-days culture. The HE staining of the co-culture experiments showed repopulation of the interstitium (complete in HVL, only the serosa of PER), and a confluent layer of cells at the surface. A positive CD31 staining confirmed that the surface layer consisted of endothelial cells.

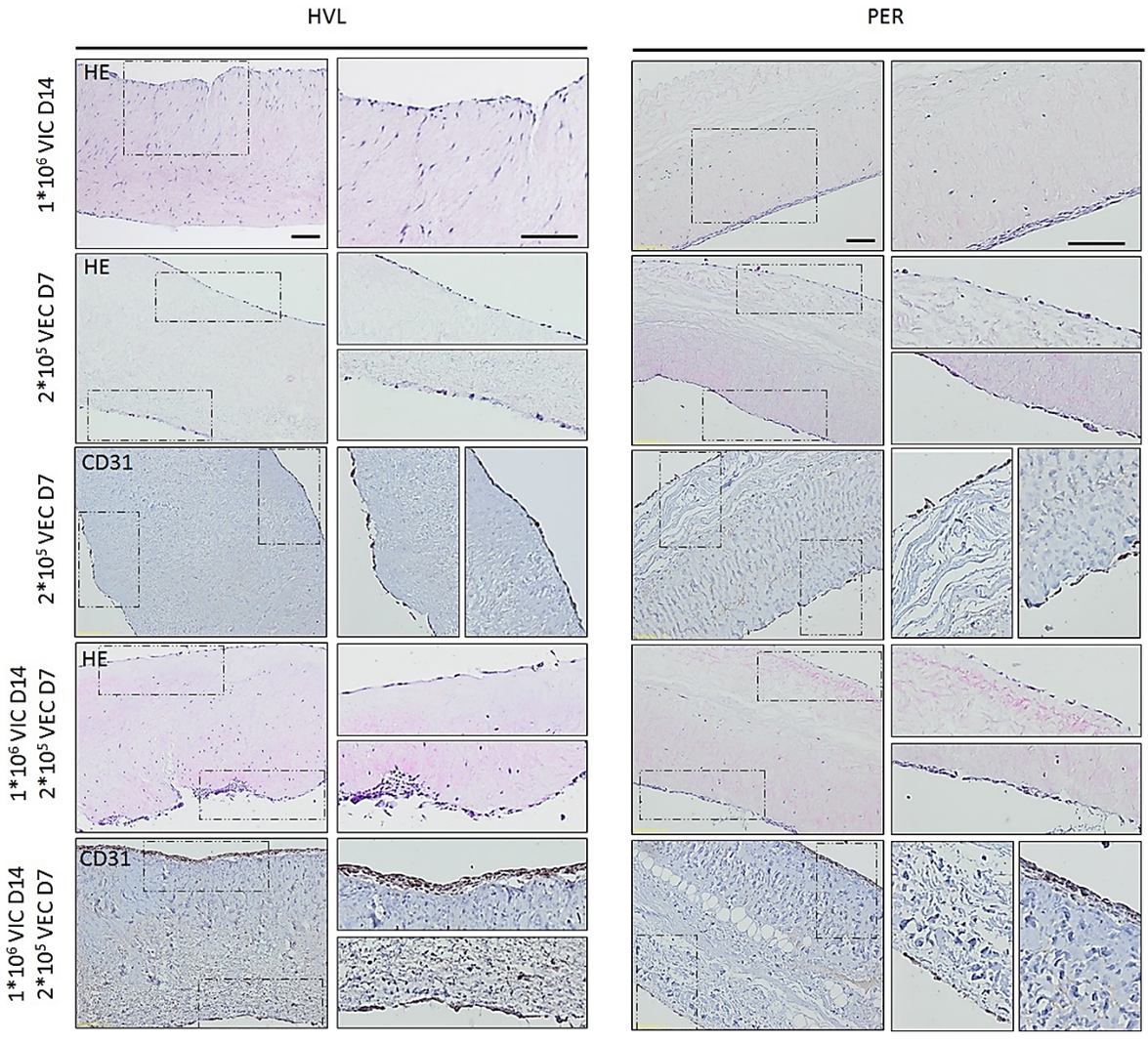

Fig.6: Static repopulation of heart valve leaflets (HVL) and pericardia (PER) with valvular interstitial cells (VIC) and valvular endothelial cells (VEC). HE; Hematoxylin/Eosin. Representative images of n = 3 independent experiments. Scale bar 100µm, original magnification x10 (insert x40, scalebar 200µm).

Repopulation of HVL and PER with BM-MSC/ADSC ± AA and VEC

The histology of stem cell ± VEC repopulated HVL after a 14-day culture period is shown in **Figure 7.** When stem cells, cultured in standard culture medium (-AA), were seeded onto the ventricularis layer of HVL, no (ADSC) or little (BM-MSC) cell ingrowth could be detected and ADSC seemed to not attach well to the surface. Supplementation of AA to stem cell cultures prior to seeding, greatly increased repopulation capacity. ADSC did attach to the leaflets and a small number of cells migrated superficially. Interestingly, after 14 days, BM-MSC repopulated the entire leaflet, showed a normal mesenchymal fibroblast-like morphology, and were distributed uniformly throughout the interstitium. To obtain repopulated HVL with stem cells and VEC, 14-day co-culture repopulation experiments were performed. After 7 days of repopulation with stem cells, VEC were seeded onto

the surface of HVL for another 7-days culture. The HE staining of the co-culture experiments showed repopulation of the interstitium (complete with BM-MSC, only superficially with ADSC), and a thin confluent layer of cells at the surface. A positive CD31 staining confirmed that the surface layer consisted of endothelial cells.

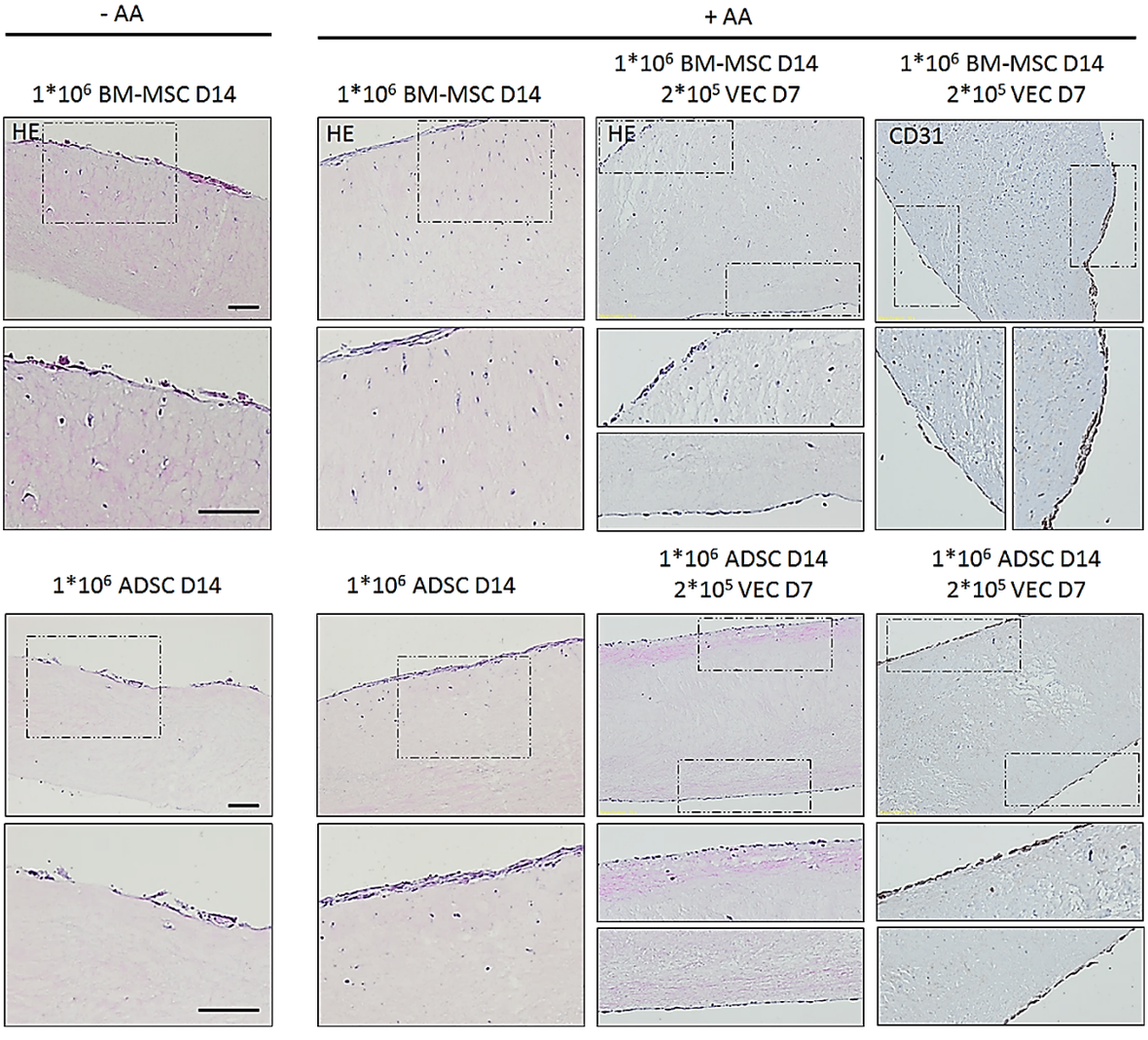

Fig.7: Static repopulation of heart valve leaflets (HVL) with BM-MSC (upper part) or ADSC (lower part) ± AA and valvular endothelial cells (VEC). HE; Hematoxylin/Eosin. Representative images of n = 3 independent experiments. Scale bar 100µm, original magnification x10 (insert x40, scalebar 200µm).

The histology of stem cell ± VEC repopulated PER after a 14-day culture period is shown in **Figure 8.** When stem cells, cultured in standard culture medium (-AA), were seeded onto the fibrosa layer of PER, no cell ingrowth and only little cell attachment could be detected. Supplementation of AA to stem cell cultures prior to seeding, lightly increased repopulation capacity. Stem cells did attach to the leaflets and a small number of cells migrated superficially (ADSC) or scattered throughout the fibrosa (BM-MSC). To obtain repopulated PER with stem cells and VEC, 14-day co-culture repopulation experiments were performed. After 7 days of repopulation with stem cells, VEC were

seeded onto the surface of PER for another 7-days culture. The HE staining of the co-culture experiments showed scarcely repopulation of the interstitium (scattered repopulation with BM-MSC, only superficially with ADSC), and a thin confluent layer of cells at the surface. A positive CD31 staining confirmed that the surface layer consisted of endothelial cells.

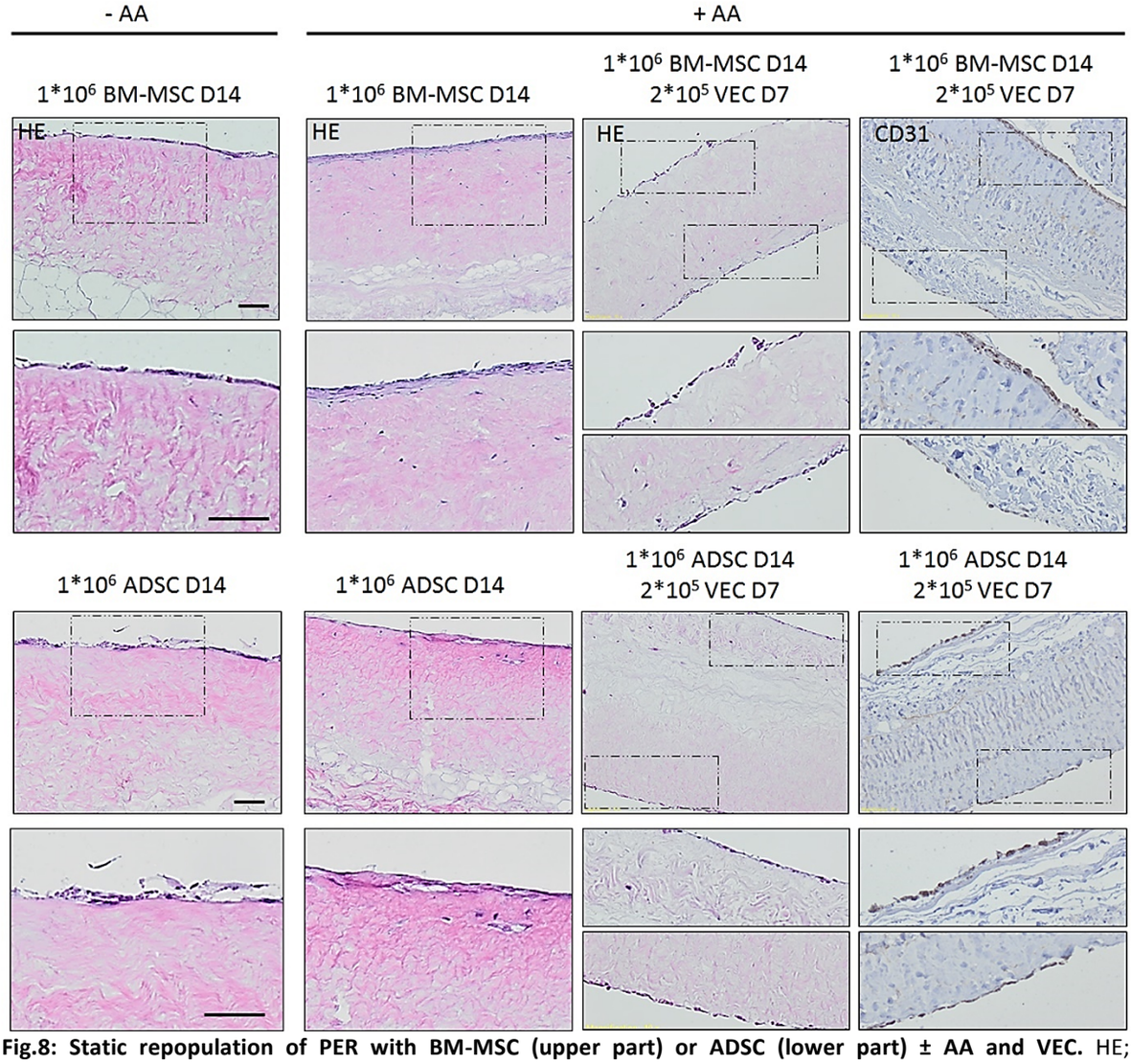

Fig.8: Static repopulation of PER with BM-MSC (upper part) or ADSC (lower part) ± AA and VEC. HE; Hematoxylin/Eosin. Representative images of n = 3 independent experiments. Scale bar 100µm, and original magnification x10 (insert x40, scalebar 200µm).

SEM of VEC repopulated HVL and PER

VEC were seeded on both sides of HVL and PER, after 7 days SEM was performed. Endothelial cells were able to attach, spread and to form a confluent monolayer onto the LF and the LV of HVL. After 7 days, the surface morphology of reseeded leaflets was comparable to the endothelium of native leaflets **(Fig.4).** In contrast, seeding of VEC onto the fibrosa or serosa of PER resulted in isolated, rounded VEC that did not spread on the surface nor formed a confluent monolayer **(Fig.5).**

DISCUSSION

Tissue-engineered constructs from allogeneic or xenogeneic decellularized valve scaffolds covered with autologous cells are considered as potential valve replacements. Given the paucity of organ donations, it will be imperative to rely on the readily available animal organs to create new valve alternatives. Two main approaches are applied in order to obtain repopulated decellularized scaffolds (1) by *in vitro* cell seeding, and (2) by *in vivo* repopulation through circulating cells without prior *in vitro* cell seeding. Steinhoff et al. was the first group to suggest that decellularized matrices seeded with autologous cells could yield viable valves. Unseeded control valves, implanted in sheep for up to 3 months, showed partial degeneration and no interstitial tissue reconstitution, whereas the *in vitro* seeded counterparts, although not completely repopulated *in vitro*, showed partial restitution of the endothelium, interstitial cell population, and matrix synthesis [305]. To date, only few studies have focused on sequentially seeding two cell populations onto acellular matrices to obtain completely (interstitium and surface) repopulated tissues [173, 300]. So far, only Schenke-Layland et al. succeeded in the complete repopulation of decellularized HVL, by using a dynamic culture system (bioreactor), and Fb and EC as a cell source [173].

Our study used a two-stage seeding protocol (first MSC or VIC, followed by VEC) to investigate the complete *in vitro* repopulation potential of decellularized porcine tissues (aortic HVL and PER). The first stage involved the repopulation of the interstitium of Triton X-100 decellularized porcine tissues with VIC or MSC (bone marrow or adipose derived). VIC are the most prevalent cell type in the heart valves. By using this native cell type, complete repopulation of the interstitium of heart valve leaflets and the fibrosa of PER was established. Moreover, VIC were distributed uniformly throughout the interstitium at approximately the same density as interstitial cells in native tissue **(Fig.6).** However, a surrogate cell source for VIC is needed as autologous VIC are not easy to isolate and may not yield an adequate cell population for clinical use, depending on the age and medical condition of the donor.

MSC have shown considerable promise for HVTE, as they phenotypically resemble to valve cells. Previous studies have reported that MSC share many characteristics of VIC, are able to produce collagen in response to cyclic stretch and to produce heart valve ECM components *in vitro* [183-186]. Only few studies have investigated the feasibility of repopulating the interstitium of decellularized tissues with MSC [103, 105, 302, 306-308]. Most of these studies failed to accomplish complete recellularization, as very few MSC invaded the tissues [103, 308] or only a subsurface population of cells was present [307]. To our knowledge, Kajbafzadeh and Iop et al. are the only two groups that succeeded in the complete repopulation of the interstitium with MSC [105, 302]. Kajbafzadeh et al. seeded ovine BM-MSC onto ovine aortic valves in a dynamic bioreactor system and implanted them

in the descending thoracic aorta in a sheep model. Complete recellularization was established 19 months post-implantation, however, no data was shown concerning the efficacy of the *in vitro* repopulation of the aortic valve conduits [302]. In the other study, Iop et al. statically seeded human BM-MSC onto the lamina fibrosa or ventricularis of porcine and human pulmonary valve leaflets for 30 days, and showed that the 2 valve layers behaved differently regarding BM-MSC repopulation potential, with a higher degree of spreading when cells were seeded onto the lamina ventricularis. However, it should be noted that these decellularized valve leaflets were pre-coated with FBS and fibronectin, to enhance cell attachment [105].

In this study, porcine ADSC and BM-MSC were seeded onto the lamina ventricularis of decellularized porcine HVL or onto the fibrous PER without pre-coating. In parallel, ascorbic acid 2-phosphate (AA) was supplemented to the stem cell medium to investigate its effect on MSC recolonization. AA has been reported to upregulate collagen I and III synthesis [309], and to stimulate proliferation of MSC [188]. In addition, AA is an anti-oxidant and can protect cells against oxidative stress-induced cell damage [310-312].

After 14 days, only little cell attachment and no cell ingrowth of both stem cell populations could be detected in decellularized PER. However, a small population of BM-MSC attached and migrated through decellularized HVL. Interestingly, when AA was supplemented to the stem cell culture medium before and during the static reseeding, there was a remarkable increase in migratory capacity of both stem cell populations, especially in the BM-MSC which repopulated the complete interstitium of HVL within 14 days **(Fig.7-8).** We want to acknowledge that the exact mechanism by which AA stimulated MSC migration in decellularized HVL/PER remains unknown and needs to be further investigated. Yet, we have demonstrated that AA not only upregulated collagen but also α-SMA expression **(Fig.2).** Since α-SMA expression is normally largely restricted to SMC, pericytes, MFb [313], it is hypothesized that it is possible that AA stimulated MSC towards another, potentially more migratory, cell type.

Recently, some researchers are investigating the *in vivo* recellularization capacity by implanting non-recellularized acellular scaffolds into animal models and humans [151, 314-316]. However, incomplete repopulation of the interstitium, even 2-6 months [151, 314, 315] or 20 months [316] post-implantation, still remains a problem. The spontaneous *in vivo* re-endothelialization in these studies, has also often been shown to be incomplete [151, 315, 317]. This raises the question for the need of a prior *in vitro* re-endothelization. It is known that a valve endothelium is important for the maintenance of a lifelong valve integrity and function. Healthy endothelial cells express antiplatelet and anti-coagulant agents that prevent platelet aggregation and fibrin formation, respectively [318].

Disruption of the valve endothelium is commonly observed in malfunctioning valves and is associated with pathological processes that promote sclerosis and calcification [319].

In the second stage of this study, VEC were seeded onto the surfaces of decellularized HVL and PER in order to obtain newly formed endothelium. Previous studies have already revealed the superior cellular adhesive properties of endothelial cells on acellular HVL leading to a confluent monolayer [292]. However, to our knowledge this is the first time that endothelial cells were seeded onto decellularized porcine PER. By histological staining **(Fig.6)** we were able to demonstrate a confluent monolayer of VEC on HVL as well as on PER after 7 days. Ultrastructure analysis by SEM showed that the surface of the reseeded leaflets was comparable to the endothelium of native leaflets **(Fig.4).** However, SEM also revealed that decellularized PER only allow VEC to attach to the surface but not to spread **(Fig.5).**

CONCLUSION

The suitability of BM-MSC, once cultivated in the presence of AA, as an efficient cell source for the complete repopulation of the interstitium of Triton X-100 non-coated decellularized heart valve tissue was demonstrated *in vitro*. Compared with ADSC, BM-MSC showed greater migratory potential and recolonized HVL more efficient than PER tissue. This study also showed that within 14 days, not only the interstitium of HVL can be recolonized but it is also possible to co-culture endothelial cells on the surface to obtain a continuous endothelium layer.

ACKNOWLEDGMENTS

The authors would like to thank the technical staff for their help with the (immuno)histological stainings (Leen Pieters) and RT-qPCR (Greet De Smet).

PART

B

SECTION I

Based on:

Scaffold-free high throughput generation of quiescent valvular microtissues

Roosens A, Puype I, Cornelissen R

(Journal of Molecular and Cellular Cardiology, 2017;106:45-54)

ABSTRACT

AIMS: The major challenge of working with valvular interstitial cells *in vitro* is the preservation or recovery of their native quiescent state. In this study, a biomimetic approach is used which aims to engineer small volume, high-quality valvular microtissues, having a potential in regenerative medicine and as a relevant 3D *in vitro* model to provide insights into valve (patho)biology.

METHODS AND RESULTS: To form micro-aggregates, porcine valvular interstitial cells were seeded in agarose microwells and cultured in medium supplemented with 250µM Ascorbic Acid 2-phosphate for 22 days. Histology showed viable aggregates with normal nuclei and without any signs of calcification. Aggregates stained strongly for GAG and collagen I and reticular fibers were present. ECM formation was quantified and showed a significant increase of GAG, elastin and Col I during aggregate culture. Cultivation of VIC in aggregates also promoted mRNA expression of Col I/III/V, elastin, hyaluronan, biglycan, decorin, versican, MMP-1/2/3/9 and TIMP-2 compared to monolayer cultured VIC. Phenotype analysis of aggregates showed a significant decrease in α-SMA expression, and an increase in FSP-1 expression at any time point. Furthermore, VIC aggregates did not show a significant difference in OCN, Egr-1, Sox9 or Runx2 expression.

CONCLUSION: In this study, high-quality valvular interstitial cell aggregates were generated that are able to produce their own ECM, resembling the native valve composition. The applied and completely cell driven 3D approach overcomes the problems of VIC activation in 2D, by downregulating α-SMA expression and stimulating a homeostatic quiescent VIC state.

INTRODUCTION

Scaffold-free, self-assembled high-quality valvular microtissues, that mimic the function and architecture of *in vivo* tissues are promising for the biofabrication of tissue engineered heart valves. Microtissues can be used for bottom-up tissue engineering, which aims to create biomimetic tissues by mimicking native microstructural functional tissue blocks and using these modular units as building blocks to engineer larger tissue constructs [99, 100]. Besides their use in regenerative medicine, the strategy proposed to create microtissues might be an important step towards a relevant 3D *in vitro* model of the heart valve to provide important insights into valve (patho)biology, for toxicology testing and drug discovery [170].

As a rule, tissue engineering requires the generation of living functional tissue whose cellular components assume a homeostatic functional state. Valvular interstitial cells (VIC) are the most abundant cell type in heart valve leaflets and are responsible for ECM synthesis, repair and remodeling [14]. In normal heart valve tissue, although the leaflets are constantly deformed and under stress, the majority of VIC are in a quiescent state (qVIC) and have a fibroblast-like phenotype, low proliferation capacity and minimal activity [33, 34]. VIC remain in this quiescent state in the absence of disease throughout life to maintain extracellular matrix (ECM) homeostasis [36-38]. Some studies suggest that qVIC can become activated (aVIC) during valve injury or under pathological conditions. These aVIC are more contractile, have a higher proliferation rate and upregulate the myofibroblast marker alpha smooth muscle actin (α-SMA) [33, 37]. Reversal of this activated state leads to a decrease in α-SMA expression and an increase of fibroblast-specific protein 1 (FSP-1 or also known as S100A4) [44]. VIC can also differentiate towards a more osteoblast-like phenotype (obVIC), which are thought to be responsible for valve calcification. There is evidence that in calcified valves the levels of calcification-associated proteins such as osteopontin and osteocalcin (OCN) [45], as well as the expression of the transcription factors: Sox9 [46, 47], runt related transcription factor 2 (Runx2 or also known as Cbfa1) [45-47] and early growth response 1 (Egr-1) [320] are elevated. These markers provide a useful tool to determine how VIC phenotype responds in different cell cultures, treatments or environments. To date, it is still unclear whether these obVIC arise from qVIC or aVIC [1, 14, 48].

One of the main problems of working with VIC is the control of their activated/quiescent state. Culture of cells in a 2D environment often results in the loss of cellular differentiation or loss of cell function. It is known that when VIC are cultured in 2D, on cell culture plastics or seeded on synthetic/biological scaffolds to provide a substrate allowing cell migration and repopulation of the scaffold, they become activated (aVIC) [321-323]. Finding the optimal culture conditions in which VIC

could preserve or regain their native, fibroblast-like quiescent phenotype while promoting VIC-mediated ECM production, could be promising for the development of a tissue engineered living valve substitute.

Recently, three-dimensional (3D) cell culture has gained interest in tissue engineering due to the fact that it overcomes the limitations of the conventional two-dimensional (2D) cell culture conditions and a wide variety of techniques exist to culture cells into 3D structures [163]. One of the most commonly used cell driven approaches currently available are the micromass cultures (homo-/heterotypic aggregates) [165] **(See Chapter I; 4.1.2).**

The aim of this study was to use a agarose-molded non-adhesive microwells to guide the spontaneous self-assembly of valvular interstitial cells into 3D aggregates/microtissues with predefined dimensions in order to produce high-quality tissue fragments [324]. This completely cell driven, high throughput technique can rapidly generate size and shape controlled microtissues in a low shear force environment. It was hypothesized that this microtissue culture, which mimics more closely the actual *in vivo* microenvironment, can drive VIC to a functional homeostatic quiescent state.

METHODS

Isolation and cell culture of valvular interstitial cells

Porcine hearts were obtained under clean conditions from a local slaughterhouse (Ruyckaert M NV, Eeklo, Belgium), transferred to the laboratory and immediately processed. Aortic valve leaflets were dissected and washed in Hanks Balanced Salt Solution (HBSS, Life Technologies) supplemented with a cocktail of antibiotics (100 µg/ml streptomycin, 100 U/ml penicillin, Life Technologies) and 2.5µg/l fungizone (Life Technologies). Before VIC could be isolated, the endothelial layer was mechanically removed from the surface of the leaflets with a cell scraper after incubating them at 37°C for 30 minutes in Dulbecco's Modified Eagle Medium (DMEM, Life Technologies) supplemented with 0.1% collagenase type I and 0.12% dispase (Sigma). Next, VIC were isolated by incubating the leaflets at 37°C for 4 hours in DMEM supplemented with 0.1% collagenase type I. Afterwards the cell-solution was filtered with a 70µm cell strainer, and centrifuged. Cells were cultivated in standard culture medium: DMEM (supplemented with 10% v/v FCS (Life Technologies), 100U/ml penicillin and 100µg/ml streptomycin) in a humidified 5% CO_2-containing atmosphere at 37°C until passage 4 (P4). In parallel, cells at P4 were also cultured in standard culture medium supplemented with 250µM AA (Sigma). Cells where used when approximately 90% confluency was reached.

Agarose microwell synthesis and micro-aggregate formation

To produce the non-adherent agarose microwells, sterilized powder Ultrapure Agarose (Life Technologies) was dissolved (3% w/v) in PBS and heated until boiling point. The liquid agarose solution was added to a tailor-made, negative polydimethylsiloxane (PDMS) mold and left to solidify at RT. After cooling, the gels were separated from the molds and subsequently transferred into 12 well culture plates as previously described [324]. Micro-aggregates were generated by seeding $1x10^6$ VIC (P4) into the microwells. Every micro-aggregate, formed in one pore of the microchip (pore diameter=400µm), contained approximately 629 cells. Aggregates were cultivated in standard culture medium or standard culture medium supplemented with 250µM AA (Sigma). Medium was replenished 24h after seeding and hereafter, every three days. Micro-aggregates were harvested at different time points, as indicated in the results section. Aggregate diameter, perimeter (p) and aggregate area (A) were determined using Xcellence image software. Circularity was calculated using the formula $f_{circ} = (4\pi A)/p^2$.

Histological and immunohistochemical analysis

Aggregates were fixed (4% paraformaldehyde, Merck, Darmstadt, Germany), dehydrated and embedded in paraffin. Five-micron-thick sections were cut and stained with Hematoxylin/Eosin (HE) for histological evaluation. The ECM was assessed by (immuno-)histochemical methods; Alcian Blue

(for acid glycosaminoglycans (GAG)), silver staining (reticular fibers) and collagen I staining. For collagen I staining, sections were subjected to an enzymatic digestion with pepsin for 10min at 37°C (Dako, 4mg/ml in 0.2N HCL). Endogenous peroxidase was quenched using 3% v/v H_20_2 for 10min, and a 30min treatment with blocking reagent (5% v/v normal rabbit serum (Dako), 1% w/v BSA (Roche), 0.2% v/v Tween 20 (VWR) in PBS) was performed. The samples were incubated with the primary antibody (monoclonal mouse anti-collagen I (Abcam, 6308), dilution 1:100) for 2h and subsequently with the secondary antibody (rabbit anti-mouse (Dako, P0397), dilution 1:200) for 30 min. A 3,3-diaminobenzidine tetrahydrochloride substrate (Sigma) was used to visualize the horse radish peroxidase coupled secondary antibody. Sections were counterstained with hematoxylin, mounted and visualized under the microscope.

Micro-aggregate viability (Live/dead fluorescence staining)

To assess the cell viability, micro-aggregates were collected and washed twice with PBS and incubated for 10min with 2µg/ml calcein-AM (AnaSpec) and 2µg/ml propidium iodide (Sigma). Cell viability was evaluated by determining the ratio of green (live) versus red (dead) cells using an inverted fluorescence microscope (Olympus IX81) equipped with Xcellence software (Olympus).

Gene expression analysis (RT-qPCR)

Total RNA (n=3) was isolated from VIC aggregates using a lysis buffer (RLT buffer, Qiagen). The concentration and purity of the isolated RNA was determined by a NanoDrop. To convert RNA into cDNA, the High Capacity cDNA Reverse Transcription Kit (Life Technologies) was used according to the manufacturer's protocol. A 7500 Fast Real-Time PCR system (Applied Biosystems) and a SYBR Green PCR kit (Life Technologies) were used according to the manufacturer's instructions and protocols. Primer details are listed in **Table 1.**

Stability of six reference genes was determined and the two most stable reference genes (EEF1A1 and HPRT) were selected via geNORM (qbase$^+$ software, Biogazelle). Gene expression analysis was normalized to the geometric mean of these reference genes.

The relative gene fold changes were determined by the $2^{-\Delta\Delta Ct}$ method. For comparative gene expression analysis, gene expression of aggregate cultured VIC P4 (+AA), and monolayer cultured VIC P4 (+AA) were compared to expression levels of standard monolayer cultured VIC P4 (-AA).

Table 1: Primer sequences for porcine valvular interstitial cells (VIC)

Gene Description	Gene Symbol	Accession Number	Forward Primer 5′ ➔ 3′	Reverse Primer 3′ ➔ 5′	Amplicon Length (bp)	Primer Efficiency (%)
Eukaryotic translation elongation factor 1 alpha 1	EEF1A1	NM_001097418.2	CAACATGCTGGAGCCAAGTG	AGTGTGGTTCCACTGGCATT	87	94.2
Hypoxanthine phosphoribosyltransferase 1	HPRT1	NM_001032376.2	GGGAGGCCATCACATCGTAG	CGCCCGTTGACTGGTCATTA	167	89.6
Actin, alpha 2, smooth muscle	α-SMA	NM_001164650.1	GGACCCTGTGAAGCACCAG	GTCACCCACGTAGCTGTCTT	198	98.9
Vimentin	VIM	XM_005668106.1	TCTGGAATCCCTCCCTCTGG	TCGCTGCACAGAGTACATGC	146	93.8
Fibroblast specific protein, S100A4	FSP-1	JN122624.1	TACTCAGGCAAGGAGGGTGA	TGGAAAGCAGCTTCATCCGT	113	94.3
Osteocalcin, bone gamma carboxylglutamic acid containing protein	OCN	AY150038.1	TACCCAGATCCTCTGGAGCC	TGCCATAGAAGCGCCGATAG	109	110.4
Early growth response protein 1	Egr-1	AJ238156.1	CTATCAAGGCCTTTGCCACG	AGCTCATCTGAGCGGGAGA	193	104.4
SRY-box 9	Sox9	NM_213843.1	CATCTCTCCCAACGCCATCT	TCTCGCTTCAGGTCAGCCTT	174	94.6
Runt-related transcription factor 2	Runx2	XM_013977989	CAACTTCCTGTGCTCTGTGCT	GAGAACCAGGGTTGAGGTGAT	90	93.7
Collagen alpha-1(I) chain	COL1A1	XM_005668927.1	AGACATCCCACCAGTCACCT	TCACGTCATCGCACAACACA	122	96.9
Collagen type III alpha 1 chain	COL3A1	NM_001243297.1	GCTCCCATCTTGGTCAGTCC	ATGGGATCTCAGGGTTGGGA	147	94.5
Collagen, type V, alpha 1	COL5A1	NM_001014971.1	GCTCAGCGTCCACAAGAAGA	GTGGTCCGAGACAAAGAGCA	184	91.4
Elastin	ELN	XM_003354509.3	CCCACACATCGAAACCCTCA	CACAAGAGCAAGGGGGCTAA	155	94
Hyaluronan and proteoglycan link protein 1	HAPLN1	NM_001004028.1	GTGATTGCCTCCTTCGACCA	TGCACAGACCCATCACTGAG	89	94.4
Biglycan	BGN	XM_003135475.3	TCACTGGCATCCCCAAAGAC	AGGGTGGGCAGAAAACTCAG	178	97.4
Decorin	DCN	NM_213920.1	CCTGCAAACTCTTGCTTGGG	TAATCCGGGGATTTGCCACA	81	94.6
Versican	VCAN	NM_001206429.1	AACCAGACAGGCTTCCCTTC	AAGTGGGTGAGGCAGTTTCT	124	92.7
Matrix metallopeptidase 1	MMP-1	NM_001166229.1	GGCCATCTATGGACCTTCCG	TGTGCGCATGTAGAACCTGT	145	101.5
Matrix metallopeptidase 2	MMP-2	NM_214192.1	CGATGGCTTCCTCTGGTGTT	AGCTGTTGTAGGATGTGCCC	155	94
Matrix metallopeptidase 3	MMP-3	NM_001166308.1	CACTTACAGACCTGGCTCGG	AGATTCTGTGGGCTCAACGG	113	89.3
Matrix metallopeptidase 9	MMP-9	NM_001038004.1	ACTTCGGAAACGCAAAAGGC	AAGAGTCTCTCGCTAGGGCA	169	110.9
Metallopeptidase inhibitor 1	TIMP-1	NM_213857.1	CACCTGCAGTTTTGTGGCTC	GGGATGGATGTGCAGGGAAA	117	89.5
Metallopeptidase inhibitor 2	TIMP-2	NM_001145985.1	CTCCGGGAACGACATCTACG	GCCTTTCCTGCGATGAGGTA	180	93

Biochemical analysis

Biochemical analysis was performed to analyze the ECM formation of VIC aggregates per microwell (n=6). Following tissue extraction, elastin (oxalic acid extraction), N- and O-sulfated GAG (papain extraction), hydroxyproline (HCL hydrolysis) were quantified using FASTIN (Biocolor), BLYSCAN (Biocolor), and Hydroxyproline Assay kit (Sigma) respectively, following the manufacturer's recommendations. Hydroxyproline content was converted to collagen content with a factor of 7.25 [325].

Statistical analysis

The Shapiro-Wilk test was used to determine normality of the variables. All the variables were parametric data and were analyzed with a one-way ANOVA test followed by a post-hoc Tukey's using the commercially available software package SPSS for windows, version 23.0 (SPSS GmbH Software, München, Germany). Descriptive statistics are reported as the mean with the standard deviation between brackets and $p<0.05$ was considered statistically significant.

RESULTS

Monolayer expansion and mRNA expression profile of 2D passaged VIC

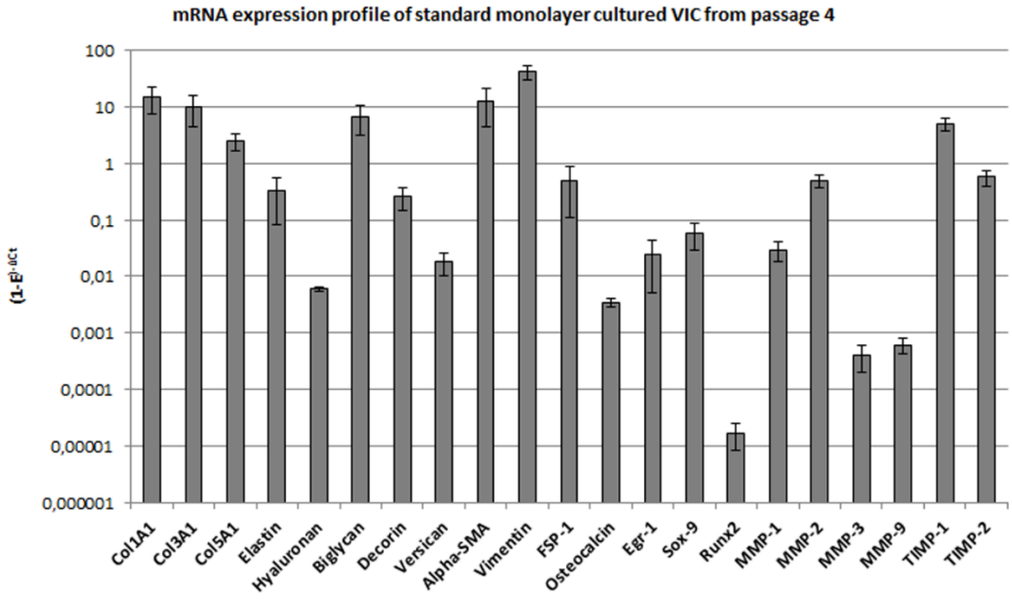

Fig.1: mRNA expression profile of monolayer cultured VIC at passage 4. Relative expression levels of ECM molecules, phenotype markers, and MMP/TIMP of standard monolayer cultured VIC at passage 4 (n=3). Data is presented as mean and error bars indicate the 95% confidence interval. Gene expression values are normalized to the geometric mean of two stable reference genes (EEF1A1 and HPRT).

During monolayer expansion, a change in VIC morphology could be observed. Primary cells were very small and polygonal in shape. Upon sub-culturing (until P4), VIC became larger, more elongated and adopted a fibroblast-like shape (data not shown).

mRNA expression analysis of monolayer cultured VIC at passage 4 showed a high expression of the following ECM molecules: collagen I/III/V, elastin, biglycan, decorin and versican (C_t values <25). VIC also showed high expression of MMP-2, TIMP-1/2 (C_t values <23) and lower expression of MMP-1/3/9 (C_t values between 27-32). In addition, the expression of specific phenotype markers was investigated. A high expression of α-SMA, vimentin and FSP-1 (C_t values <21), a lower expression of OCN, Egr-1, and Sox9 (C_t values between 25-28) and an almost undetectable expression of Runx2 (C_t values >35) was determined **(Fig.1).**

250µM of AA was supplemented to VIC at P4 and morphology and mRNA expression levels were examined. Addition of AA did not influence cell morphology, VIC still showed a fibroblast-like shape (data not shown). Interestingly, a significant increase of collagen I, elastin, biglycan, α-SMA, vimentin, Egr-1 and Runx2 was observed. Collagen III/V, HA, decorin, versican, FSP-1 and OCN also increased. Yet, the increase was not significant. Sox9 levels slightly decreased and MMP-9 levels remained unchanged **(Fig.2).**

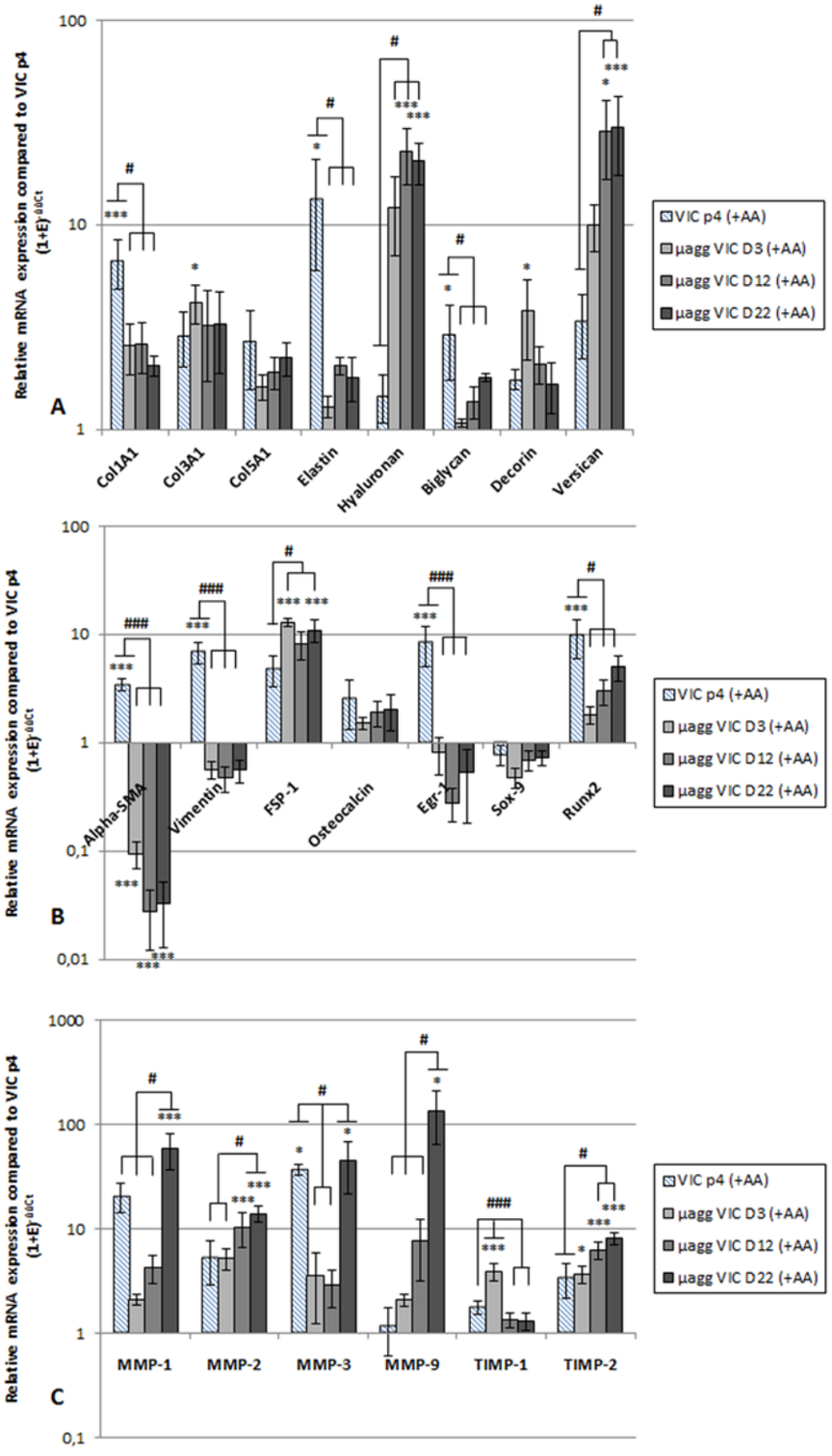

Fig.2: mRNA expression profile of 2D and 3D cultured VIC (+AA) compared to standard monolayer cultured VIC (-AA). Relative expression levels of (A) ECM molecules (B) phenotype markers (C) MMP/TIMP of aggregate cultured VIC (+AA) from D3, 12 and 22, and monolayer cultured VIC at passage 4 (+AA) *compared to standard monolayer cultured VIC at passage 4 (value = 1)*. Data is presented as mean and error bars indicate the 95% confidence interval. Statistically significant differences are marked with *p<0.05 or ***p<0.001 compared to standard monolayer cultured VIC at passage 4, and $^{\#}$p<0.05, $^{\#\#\#}$p<0.001 for significant differences between groups, n=3. Gene expression values are normalized to the geometric mean of two stable reference genes (EEF1A1 and HPRT). A one-way ANOVA test followed by a post-hoc Tukey's was used for the statistical analysis.

VIC micro-aggregates

Impact of AA on micro-aggregate formation

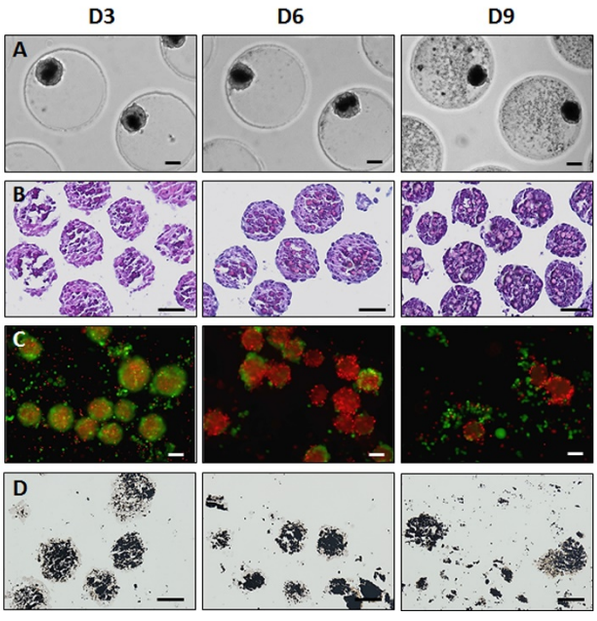

Fig.3: Formation of VIC micro-aggregates in agarose microwells without AA supplementation. (A) Light microscopy, (B) HE staining, (C) Live/Dead staining, (D) Von Kossa staining. Representative images of n=3 independent experiments. Scale bar = 100µm, magnification x10 (A, C), x20 (B, D).

In a first attempt to form micro-aggregates, VIC were seeded in microwells in standard culture medium. After 1 hour, cells were concentrated at the bottom of the microwells and aggregation started within several hours. Spherical, uniform aggregates were formed within 24h. However, degeneration of the newly formed aggregates was rapidly observed. After 3 days, aggregates showed dense central regions, which increased over time **(Fig.3A).** HE staining showed non-viable cells with abnormal nuclei and many deeply basophilic, irregular and granular clumps which could indicate Ca-salts **(Fig.3B).** Aggregates did not remain viable after a culture period of 9 days, which was shown with a live/dead staining **(Fig.3C).** Mineralization of aggregates was confirmed with a Von Kossa staining on all time points **(Fig.3D).**

In order to improve aggregate culture conditions, 250µM AA was supplemented to the culture medium when aggregates were formed (after 24h). After 3 days, aggregates showed again dense central regions. Yet, these regions were smaller than observed without the supplementation of AA **(Fig 4A).** HE staining showed viable cells with normal nuclei and only a small amount of deeply basophilic, granular clumps **(Fig.4B).** Aggregates remained viable during a culture period of 9 days, which was shown with a live/dead staining **(Fig.4C).** Von Kossa staining was also performed, showing only small areas of mineralization **(Fig.4D).**

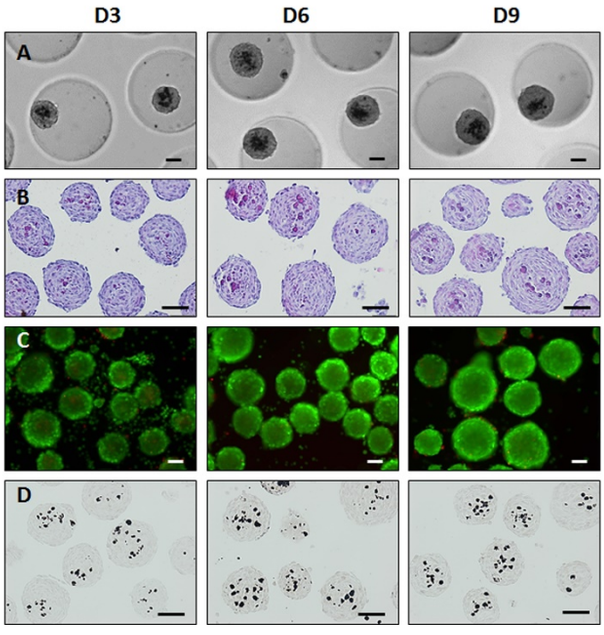

Fig.4: Formation of VIC micro-aggregates in agarose microwells with AA supplementation (from day 1). (A) Light microscopy, (B) HE staining, (C) Live/Dead staining, (D) Von Kossa staining. Representative images of n=3 independent experiments. Scale bar = 100µm, magnification x10 (A, C), x20 (B, D).

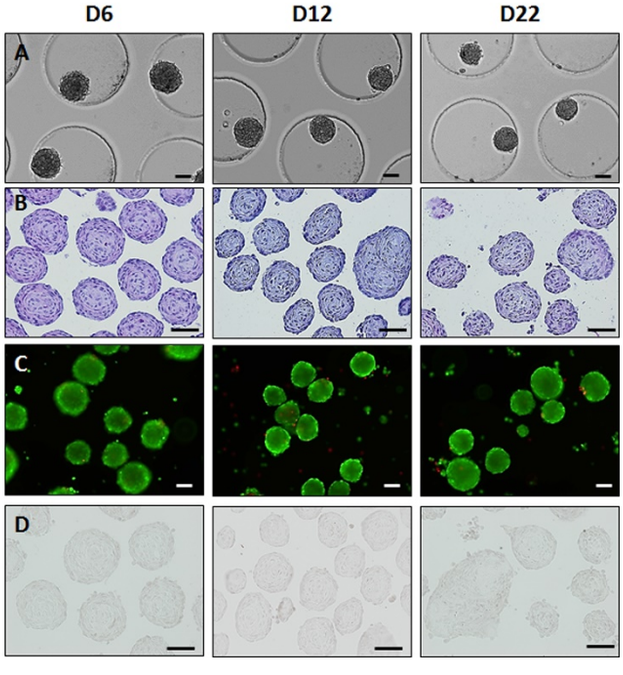

Fig.5: Formation of VIC micro-aggregates in agarose microwells with AA supplementation (from day 0). (A) Light microscopy, (B) HE staining, (C) Live/Dead staining, (D) Von Kossa staining. Representative images of n=3 independent experiments. Scale bar = 100µm, magnification x10 (A, C), x20 (B, D).

When 250µM AA was supplemented to the aggregate cultures from day 0, no dense central regions where observed **(Fig.5A)**. HE staining showed viable cells with normal nuclei and no basophilic, granular clumps throughout the complete culture period **(Fig.5B)**. Aggregates remained viable during a culture period of up to 22 days **(Fig.5C)**, and no mineralization of aggregates could be detected with Von Kossa staining **(Fig.5D).** At any time point during culture, aggregates maintained their circularity (88.81% (SD: 0.81, day 3) to 88.64 (SD: 1.1, day 22)) and no disintegration was observed **(Fig.6B)**. Over time, aggregate diameter reduced from 149.6 µm (SD: 18.1, day 3) to 114.6 µm (SD: 14.4, day 22) **(Fig.6A)**.

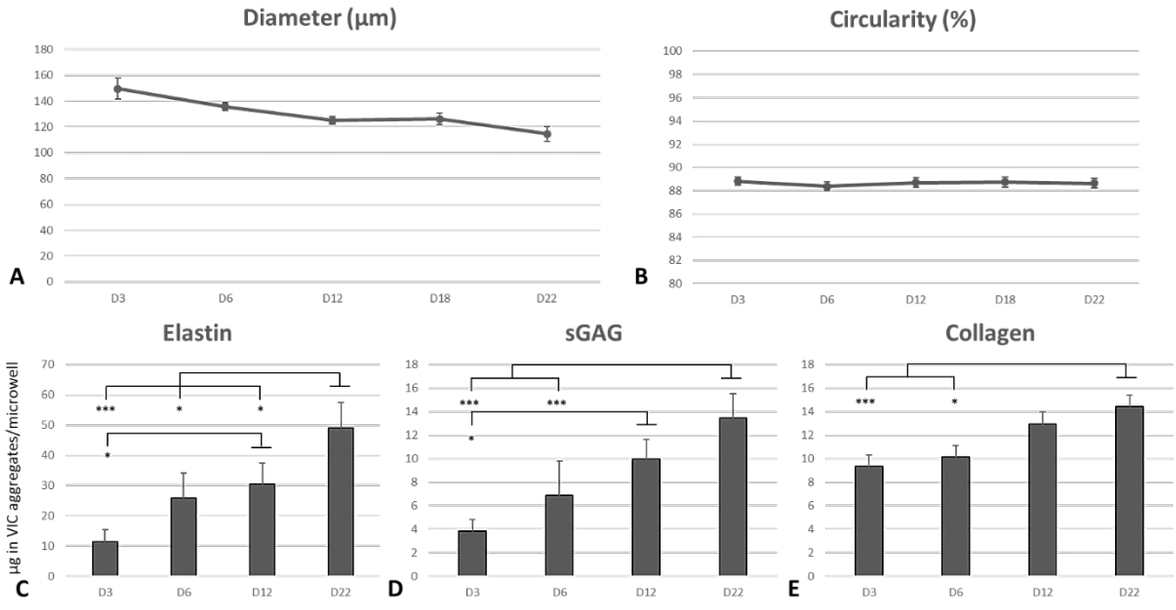

Fig.6: Diameter/circularity and biochemical quantification of elastin, sGAG and collagen content of VIC micro-aggregates (+AA) during 3D microwell culture. (A-B) Diameter and circularity of VIC microaggregates (+AA). Representative data of n=3 independent experiments. Error bars indicate the 95% confidence interval. (C) Elastin content, (D) sGAG content and (E) Collagen content of VIC microaggregates (+AA). Data is presented as mean and error bars indicate the 95% confidence interval. Statistically significant differences between groups are indicated with *p<0.05 or ***p<0.001, n=6. A one-way ANOVA test followed by a post-hoc Tukey's was used for the statistical analysis.

VIC phenotype in micro-aggregates

Fig.2B shows that when VIC are cultured in aggregates there is a statistically significant decrease in α-SMA expression, and a slight, but not significant, decrease in vimentin expression compared to standard monolayer cultured VIC at any time point. FSP-1 expression, on the other hand, is significantly increased in VIC aggregates. Furthermore, VIC aggregates did not show a significant difference in OCN, Egr-1, Sox9 or Runx2 expression compared to monolayer cultured VIC.

ECM production in micro-aggregates

To visualize collagen I formation, an IHC staining was performed **(Fig.7A)**. Collagen I was present throughout the matrix of the aggregates from day 3. From day 6, collagen I was aligned in small fibrils, which could be detected especially at the periphery of the aggregates. By day 22, collagen I fibrils could be observed in the entire matrix. An Alcian Blue staining was used to stain acidic polysaccharides such as GAG **(Fig.7B).** Only a small amount of GAG was observed in aggregates at day 6, but the GAG production increased remarkable by day 22. To investigate the presence of reticular fibers, a silver staining was performed **(Fig.7C)**. Reticular fibers were present from day 3 and were circumferentially aligned at the periphery of the aggregates. No increase or reorganization of these fibers could be observed by day 22.

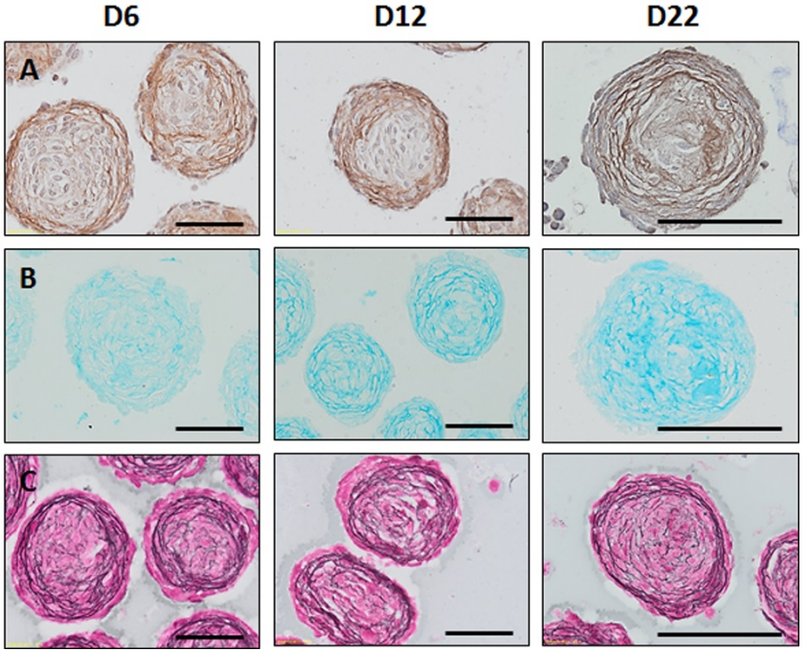

Fig.7: (Immuno)-histological stainings for ECM components in VIC micro-aggregates (+AA) during 3D microwell culture. (A) Collagen I staining, (B) Alcian Blue staining, (C) Silver staining. Representative images of n=3 independent experiments. Scale bar = 100µm, magnification x20 (D6, 12), x40 (D22).

To investigate mRNA expression of ECM molecules and MMP/TIMPs, RT-qPCR was performed. Expression levels in VIC aggregates were compared to expression levels in standard monolayer cultured VIC **(Fig.2).** Cultivation of VIC in aggregates promoted mRNA expression of collagen I/III/V, elastin, hyaluronan, biglycan, decorin and versican. However, only the increase of collagen III (day 3), HA (day 12 and 22), decorin (day 3) and versican (day 12, 22) was statistically significant **(Fig.2A)**.

Cultivation of VIC in aggregates also promoted mRNA expression of MMP/TIMPs. At day 22, expression of MMP-1/2/3/9 and TIMP-2 was statistically higher than in monolayer cultured VIC. TIMP-1 expression peaked significantly at day 3 ($p<0.001$), but decreased by day 12 and remained stable thereafter **(Fig.2C).**

Elastin, GAG and collagen content of VIC aggregates were quantified at different time points. **Fig.6A-C** shows that elastin, GAG and collagen content of VIC aggregates increased gradually and there was a statistically significant difference between day 3 and day 22. The amount of elastin per microwell increased from 11.35µg (SD: 4.01) to 49.1µg (SD: 8.41), GAG content increased from 3.85µg (SD: 0.99) to 13.4µg (SD: 2.07) and the amount of collagen increased from 9.33µg (SD: 1.31) to 14.43µg (SD: 2.32).

DISCUSSION

The major challenge of working with VIC in tissue engineering is the preservation or recovery of their native quiescent state, because VIC phenotype changes could cause progression towards diseases [14]. It is known that when cells are seeded onto synthetic/biological scaffolds, allowing cell migration and repopulation of the scaffold, cells can become activated [326]. In this study we used an alternative, biomimetic approach which aims to engineer small volume, high-quality valvular microtissues that can be used as building blocks for the biofabrication of heart valve tissue. We hypothesized that the 3D culture of VIC as aggregates, which mimics more closely the actual *in vivo* microenvironment, can stimulate VIC to a functional homeostatic quiescent state. Although not the main focus of this study, we also discuss that the biofabricated microtissues might have a potential as a relevant 3D *in vitro* model to study valve (patho)biology.

Before micro-aggregates can be generated, VIC need to be expanded. This study, as well as others, have shown that the cultivation of VIC onto 2D rigid polystyrene substrates, leads to an activated VIC phenotype which is shown by the expression of α-SMA in primary cultures [322, 323]. To date, there is still some discrepancy whether or not α-SMA levels increase [322], decrease [187] or remain relatively unchanged when passage number increases [327]. Recently, Xu et al. showed that confluent VIC monolayers express lower α-SMA levels compared to sub-confluent cultures [328]. For this reason, and to exclude variation between different passages, all experiments in this study were performed with VIC originating from the same passage (P4) when confluency was reached.

In this study, we generated a large number of viable, uniform, and small aggregates from VIC, in an efficient and highly controllable manner using agarose microwells. When VIC aggregates were formed in standard culture medium, there was a rapid degeneration and calcification of the aggregates.

In an effort to optimize aggregate formation, AA was supplemented to the culture medium before aggregation started. AA, also known as vitamin C, is an essential nutrient acting as an anti-oxidant, protecting against oxidative stress-induced cell damage, and as a cofactor for post-translational processing enzymes from which some participate in collagen hydroxylation [312]. Adding AA resulted in the formation of viable, high-quality aggregates without any signs of degeneration or calcification. The calcification process of VIC in heart valve leaflets is very complex and still not completely unraveled. To date, two hypotheses of calcification dominate current thinking: the dystrophic/apoptotic calcification theory (calcification of dead or damaged cells, a passive process) and the ossification theory (phenotype conversion to a more osteoblast-like VIC, an active process) [45, 49]. We hypothesize that it is possible that the former calcification process occurred in

aggregate cultures (when AA was omitted), as spontaneous dystrophic calcification in VIC aggregates of similar size has recently been demonstrated by Cirka et al. [329]. It should also be noted that so far, the osteogenic calcification process has only been demonstrated *in vitro* when induced by the addition of organic phosphate to culture media [330]. However, we did not further investigate this calcification process.

At present, the exact mechanism by which AA promotes aggregate formation and survival is still unclear. However, the protective and stimulating effect of AA on VIC aggregates could be partly due to protection against oxidative DNA damage through the scavenging of reactive oxygen species (ROS), as this is previously demonstrated in MCF-7 human breast cancer cells [331], corneal endothelial cells [332], and PC12 cells [333]. AA has also been reported to upregulate collagen I and III synthesis in human dermal fibroblast [334] and to stimulate the proliferation of mesenchymal stem cells while preserving their differentiation ability [188].

To ultimately produce a functional living tissue, micro-tissues should mimic the native cell phenotype and native tissue composition from which the living components produce ECM and other bio-active components (such as chemical signals, MMP/TIMPs). In this study, ECM formation of aggregates was investigated by (immuno)-histological stainings and biochemical assays (protein level) as well as RT-qPCR (mRNA level). Based on the histological findings, our data indicated that aggregates were able to produce GAG, collagen I fibrils and reticular fibers (which mainly consist of collagen III [335]), some of the main ECM components of heart valve leaflets [336]. In addition, biochemical quantification demonstrated that elastin, GAG and collagen content of VIC aggregates increased gradually over time and there was a statistically significant difference between day 3 and day 22. As for mRNA expression levels of the main ECM components of heart valve leaflets, aggregates showed upregulated expression of collagen I/III/V, elastin, hyaluronan, biglycan, decorin and versican compared to standard monolayer cultured cells. Moreover, the expression of MMP-1/2/3/9 and TIMP-1/2 was also elevated. This data clearly indicated matrix production and remodeling in VIC aggregates. Phenotype of VIC in aggregates was determined based on mRNA expression, which showed a significant decrease of α-SMA and an increase of FSP-1. Based on these findings we can state that VIC in aggregates are being stimulated to a more quiescent phenotype.

To investigate if the enhanced ECM production and phenotype switch to a quiescent state of VIC in aggregates could be due to the addition of AA or due to the 3D culture itself, ideally VIC aggregate cultures with or without the addition of AA should be compared. Unfortunately, long term viable aggregates could not be generated without the addition of AA. For this reason, we first examined the effect of AA on standard monolayer cultured VIC. To our knowledge, this is the first study that

showed that AA can significantly upregulate α-SMA in monolayer cultured VIC, which indicates stimulation of VIC activation. However, this upregulation of α-SMA expression by AA, has already been demonstrated in other cell types (e.g. stem cells and other progenitor cells) [337, 338]. In this study, AA also significantly promoted vimentin, collagen I, elastin, biglycan, Egr-1, Runx2 and MMP-3 expression of VIC. More research needs to be done to investigate the effect of AA on monolayer cultures on the long term, because this data could suggest a phenotype switch to a more osteo-/chondrogenic phenotype. AA is frequently used in osteoblast/chondrocyte culture- and differentiation medium and is known to enhance collagen I/III [334] and Runx2 production [339]. Egr-1 can regulate bone properties and is known to play a role in valve calcification [320, 340].

Secondly, we looked for differences between monolayer cultured VIC and VIC aggregates (both +AA). Interestingly, our data indicated a significant difference in expression of α-SMA, vimentin, collagen I, HA, elastin, biglycan, Egr-1, Runx2 from day 3, versican, MMP2 and TIMP2 from day 12, and MMP1/9 from day 22. We state that these differences are due to the different culture methods, especially when we noticed opposite effects (α-SMA, vimentin, Egr-1). Based on these findings, we showed that aggregate culture, even though AA needed to be supplemented to the culture medium, stimulated a quiescent VIC phenotype. In addition, we found that the molecular markers OCN, Egr-1, Sox9 and Runx2, which can play a role in the conversion of VIC to an obVIC phenotype, did not show any significant changes compared to standard 2D cultured VIC.

Because future research will be focused on the directed assembly of aggregates using bioprinting applications for the biofabrication of larger tissue constructs, aggregate uniformity and diameter is important (maximum nozzle diameter is 300µm). In this study, aggregates with a mean diameter of 150µm (day 3) were formed. This diameter did not increase over time. In contrast, the diameter decreased to approximately 110µm (day 22), which could suggest that aggregates did not proliferate. However, we cannot completely exclude this possibility since aggregates might undergo further compaction while proliferating.

This study described a completely cell driven formation of quiescent valvular microtissues by generating micro aggregates. They are currently not only used for modular engineering, but might also offer a new platform to provide insights into valve (patho)biology. In the case of toxicological/disease studies, it is important to start with native cells or tissues that simulate the *in vivo* situation. Almost all studies (mainly calcification studies) are performed, starting from 2D monolayer cultured highly α-SMA positive cells, or from aggregates which are spontaneously (with poor control of amount and size) formed when over-confluency has reached and which spontaneously calcify or whereby calcification is enhanced by TGF-β or osteogenic medium.

Recently, Cirka et al. improved the aggregate culture through controlling the size and amount of aggregates/cm² by using micro-contact patterning on tunable polyacrylamide (PA) hydrogels, resulting in the rapid formation of PA cultured aggregates. They also demonstrated spontaneous apoptosis of their aggregates within 24h, followed by dystrophic calcification [329]. Our aggregates are formed in non-adhesive microwells, which means that they are currently not attached to a substrate and can easily be collected for analysis. Spontaneous calcification can be demonstrated within 3 days (when AA was omitted), and aggregates are viable for at least 22 days, without signs of calcification (when AA was added).

We believe that these viable valvular microtissues are a good starting point for fundamental understanding of VIC (patho)biology related studies and a better alternative compared to the current existing 2D models since VIC are in a native-like quiescent state, whereas 2D cultured VIC are already activated. This model allows to investigate the influence of isolated specific biological cues on VIC phenotype. For example, by cultivating these viable aggregates, instead of single cells or aggregates which spontaneously calcify, on or by encapsulating them in a hydrogel, the influence of substrate modulus on VIC phenotype and calcification can be validated, as it is well known that substrate stiffness can influence VIC behavior [341]. Also, VIC behavior appears to be dependent on biochemical factors (such as peptide sequences [342], growth factors [187], cytokines [343], etc.) which can easily be incorporated into this model.

We want to acknowledge that the quiescent VIC aggregates are currently cultured *in vitro* under static conditions and want to point out that the performance of VIC and valvular tissue under dynamic conditions is still one of the main challenges. Dynamic conditions (bioreactor or microfluidic systems) more closely resemble the *in vivo* situation and could be favorable for the maturation of our premature microtissues by potentially stimulating matrix production. In addition, bioreactors are also used to study mechanotransduction from stresses (i.e. planar tension, flexure, and shear stress) on heart valves and VIC phenotype. Studies have revealed that these stresses can alter VIC phenotype in heart valve leaflets, by stimulating aVIC or obVIC conversion [344, 345], but so far, only one *in vitro* model system has incorporated dynamic stimulation and evaluated the effect of mechanical strain on aVIC aggregation and calcification [346].

CONCLUSION AND FUTURE PERSPECTIVES

In conclusion our findings showed that (1) agarose microwells are well suited for the large scale production of uniform, high-quality VIC aggregates, (2) supplementation of AA to the culture medium before aggregation starts is indispensable, (3) AA promotes ECM production and upregulates α-SMA in monolayer cultured cells, stimulating an active VIC state, (4) downregulation of α-SMA expression can be obtained in aggregates and is due to the 3D culture, resulting in the stimulation of a quiescent VIC phenotype, (5) VIC aggregates are able to produce their own ECM, resembling the native valve composition.

In future research, these aggregates will be used as building blocks for the biofabrication of heart valve tissue by modular tissue engineering. However, we want to highlight that scaffold-free, self-assembled 3D aggregates, that mimic the function of *in vivo* tissues might serve as important *in vitro* models.

ACKNOWLEDGEMENTS

The authors would like to thank Prof. Dr. Jan Vanfleteren for kindly providing the PDMS molds for the agarose microwells and the technical staff for their help with the (immuno-)histological stainings (Leen Pieters) and RT-qPCR (Greet De Smet).

PART

B

SECTION II

Based on:

Impact of modified gelatin on valvular microtissues

Roosens A, Handoyo Y, Declercq H, Cornelissen R

(Submitted: Journal of Tissue Engineering and Regenerative Medicine, June 2017)

ABSTRACT

A significant challenge in the field of tissue engineering is the biofabrication of large three-dimensional (3D) living tissues and organs. Multi-cellular valvular microtissues can be used as building blocks for the formation of larger-scale valvular macrotissues. Yet, for the controlled biofabrication of 3D macrotissues with predefined complex shapes, directed assembly of microtissues through bioprinting is needed. Modified gelatin is a printable hydrogel. This study aimed to investigate if modified gelatin is a suitable encapsulation material for valvular microtissues. Valvular microtissues were encapsulated in different modified gelatin hydrogels and crosslinked in the presence of a photoinitiator (Irgacure 2959 or VA-086). Hydrogel properties were determined and valvular interstitial cell functions like phenotype, proliferation, migration, mRNA expression of extracellular matrix (ECM) molecules, ECM deposition and tissue fusion were characterized by histochemical stainings and RT-qPCR. Encapsulated microtissues remained viable during the complete study duration, were able to produce heart valve related ECM components and remained in a quiescent state. However, encapsulation induced some changes in ECM formation and gene expression. Encapsulated microtissues showed lower remodeling capacity and increased expression levels of Col I/V, elastin, hyaluronan, biglycan, decorin and Sox9 compared to non-encapsulated tissues. Furthermore, this study demonstrated that proliferation, migration and tissue fusion was more pronounced in softer gels. In general, we evidenced that modified gelatin is a suitable encapsulation material for valvular microtissues and provided a proof of concept for the formation of larger valvular tissue by showing that microtissues were able to randomly assemble in soft gels and to fuse into macrotissues.

INTRODUCTION

Clinical treatment of end-stage valvulopathy still primarily relies on mechanical or bioprosthetic heart valve replacements, but none of them are ideal valve substitutes and each of them have disadvantages (e.g. life-long anti-coagulation therapy, limited durability, degeneration and/or calcification) [347]. Yet one of the main problems is that they are made of non-viable material. To overcome the shortcomings of these current treatment options, heart valve tissue engineering (HVTE) approaches have emerged, all with the same goal: to engineer a bio-active, living autologous heart valve with regeneration, remodeling and growth potential, which is especially needed for younger patients as they outgrow valve replacements, resulting in multiple reoperations [98]. The past twenty years, most research groups focused on TE a heart valve substitute by combining biological or synthetic scaffolds with cells. Although much progress has been made with this approach, a bio-active living TEHV is still not developed and alternative approaches should be explored. Such an alternative approach could be the generation of bio-active valvular tissue from the bottom-up. Bottom-up tissue engineering aims to create native microstructural functional tissue blocks, mimicking native tissues, and using these modular units as building blocks to engineer larger tissue constructs [99, 100].

The bottom-up assembly of spatially organized multicomponent tissues can be done starting from single cells, cell sheets or micro-aggregates/microtissues [348]. The main advantage of using microtissues as building blocks is that they already contain fully formed cell-cell and cell-matrix interactions. Moreover, 3D microtissues more closely resemble the *in vivo* microenvironment where cells naturally interact with their neighboring cells and ECM components [167, 349]. Recently, we showed that scaffold-free, high quality valvular microstructural functional tissue blocks can be made using agarose-molded non-adhesive microwells to guide the spontaneous self-assembly of valvular interstitial cells into 3D microtissues with predefined dimensions in a low shear force environment [350]. In addition, several studies have already demonstrated that closely placed microtissues undergo tissue fusion, a process that represents a fundamental biological and biophysical principle of developmental biology-inspired tissue engineering [351, 352]. Yet, for the controlled biofabrication of a 3D functional living valvular macrotissue with predefined complex shape, directed assembly of microtissues through bioprinting is needed.

Prior to bioprinting, microtissues need to be encapsulated in a cell friendly and printable material, functioning as a bio-ink during the printing process. This bio-ink, usually a hydrogel, should provide an informative microenvironment, mimicking the physiological niche and direct valvular interstitial cell (VIC) behavior (e.g. proliferation, differentiation, morphology, ECM production, etc.) without

inducing pathological effects [237]. VIC play an active role in the normal function of the aortic valve and determine the quantity and quality of the ECM components. The main ECM components in heart valve tissue are collagen type I/III/V, elastin and glycosaminoglycans (GAG) [13, 25]. The majority of VIC are in a quiescent state (qVIC) and have a fibroblast-like phenotype, low proliferation capacity, minimal activity and express high vimentin and low alpha smooth muscle actin (α-SMA) [33-35]. qVIC can become activated (aVIC) during valve injury and repair or under pathological conditions. These aVIC are more contractile, have a higher proliferation rate and upregulate the myofibroblast (MFb) marker α-SMA [33, 37]. VIC can also differentiate towards a more osteoblast-like phenotype (obVIC), which are thought to be responsible for valve calcification. There is evidence that in calcified valves the levels of calcification-associated proteins such as osteopontin and osteocalcin (OCN) [45], as well as the expression of chondrogenesis and osteogenesis-associated transcription factors: Sox9 [46, 47] and runt related transcription factor 2 (Runx2) [45-47] are elevated.

The past ten years, several research groups have been evaluating polyethylene glycol (PEG), hyaluronic acid (HA), gelatin as well as hybrid hydrogels as encapsulation material for valvular interstitial cells (VIC) [226, 228, 353, 354]. Yet so far, apart from one study which encapsulated large spheroids from VIC in HA and HA/Gelatin hydrogels [227] and only investigated VIC phenotype and migration, nothing is known about the encapsulation of valvular microtissues. Since our research group already successfully bioprinted gelatin encapsulated HepG2 cells and primary hepatocyte microtissues [255, 324, 355], it was assumed that gelatin could be a suitable encapsulation material for valvular microtissues as well. Gelatin is synthesized upon the partial breakdown of the natural triple-helical structure of collagen [229] and is considered a generally-regarded-as-safe material by the Food and Drug Administration [356]. However, due to the thermo-reversible characteristics of gelatin, chemical covalent crosslinking is needed in order to form solid and stable gel-constructs.

In this study, we exploited the utility of chemically modified gelatin (Gel-MOD), first introduced by Van den Bulcke et al., which has methacrylate-groups that can be crosslinked with UV irradiation in the presence of a photoinitiator [357], as a suitable encapsulation material for valvular microtissues. Two different w/v% gel-MOD hydrogels were generated and crosslinked in the presence of the photoinitiator Irgacure 2959 (Irg), which has been largely used in tissue engineering and is considered as the golden standard for Gel-MOD crosslinking, or VA-086 (VA), which has been shown to be a more cytocompatible photoinitiator [254, 255, 358]. Physical and biomechanical analysis was performed to analyze hydrogel properties (gel fraction, swelling ratio and stiffness). ECM production, matrix metalloproteinases and their inhibitors (MMP/TIMP) expression, VIC phenotype, proliferation, migration and fusion were followed as a function of time to gain better understanding of the impact of hydrogel properties on valvular microtissues. Such information is useful to select the most suitable

conditions for future bioprinting experiments and the biofabrication of larger-scale valvular macrotissues.

METHODS

Isolation and cell culture of valvular interstitial cells

Porcine hearts were obtained under clean conditions from a local slaughterhouse (Ruyckaert M NV, Eeklo, Belgium), transferred to the laboratory and immediately processed. Aortic valve leaflets were dissected and washed in Hanks Balanced Salt Solution (HBSS, Life Technologies) supplemented with a cocktail of antibiotics (100 µg/ml streptomycin, 100 U/ml penicillin, Life Technologies) and 2.5µg/l fungizone (Life Technologies). Before VIC could be isolated, the endothelial layer was mechanically removed from the surface of the leaflets with a cell scraper after incubating them at 37°C for 30 minutes in Dulbecco's Modified Eagle Medium (DMEM, Life Technologies) supplemented with 0.1% collagenase type I and 0.12% dispase (Sigma). Next, VIC were isolated by incubating the leaflets at 37°C for 4 hours in DMEM supplemented with 0.1% collagenase type I. Afterwards the cell-solution was filtered with a 70µm cell strainer, and centrifuged. Cells were cultivated in standard culture medium: DMEM (supplemented with 10% v/v FCS (Life Technologies), 100U/ml penicillin and 100µg/ml streptomycin) in a humidified 5% CO_2-containing atmosphere at 37°C until passage 4 (P4). Cells where used when approximately 90% confluency was reached.

Agarose microchip synthesis and microtissue formation

To produce the non-adherent agarose microchips, sterilized powder Ultrapure Agarose (Life Technologies) was dissolved (3% w/v) in PBS and heated until boiling point. The liquid agarose solution was added to a tailor-made, polydimethylsiloxane (PDMS) mold and left to solidify at RT. After cooling, the gels were separated from the molds and subsequently transferred into 12 well culture plates as previously described [350]. Microtissues were generated by seeding $1x10^6$ VIC (passage 4) into the microwells. Every microtissue, formed in one pore of the microchip (1590 pores, Ø400µm), contained approximately 629 cells. Microtissues were cultivated in standard culture medium supplemented with 250µM L-ascorbic acid 2-phosphate (Sigma) [350]. Medium was replenished 24h after seeding and hereafter, every three days.

Methacrylamide-modified gelatin (Gel-MOD) synthesis

Gelatin methacrylamide was prepared by reaction of Bovine type B gelatin (Rousselot) with methacrylic anhydride. After dissolution of gelatin in phosphate buffer (pH 7.8) at 50 °C, methacrylic anhydride was added while vigorously stirring. After 1 h, the reaction mixture was diluted and dialyzed for 24 h against distilled water at 40 °C. Purified gelatin methacrylamide had a degree of substitution of 61.72%, as determined by 1H NMR (Bruker AVANCE II 500 MHz). Prior to use, the freeze-dried gel-MOD building blocks were sterilized by ethylene oxide treatment (cold cycle, AZ Sint-Jan hospital, Bruges).

Equilibrium swelling experiments

An equilibrium swelling test was performed to analyze the effect of the photoinitiator concentration (PI) (2 mol% Irg or 20 mol% VA, Wako Chemicals) and Gel-MOD concentration (10 and 20 w/v%) on the crosslinking and swelling behavior of gels. Hydrogel disks (Ø = 15mm; height = 2mm) were prepared by pipetting 300µl Gel-MOD solution in each well of a 24-well plate and crosslinked for 20min with 365nm UV-A light (4mW/cm^2, UVP Inc.). After crosslinking, the disks were freeze-dried at 0.370 atm and -50°C in a Christ Alpha1-4 freeze-dryer and weighed (W_{d0}). The dried disks were then immersed in DMEM at 37°C until equilibrium swelling was reached. At this temperature, non-covalent crosslinked polymer chains will leach out from the hydrogels by diffusion. Consequently, disks were removed from the medium, gently wiped with paper and weighted again (W_{he}). Subsequent lyophilization gave the final dry weight (W_{de}). The gelfraction is calculated as the percentage of the hydrogel that is covalently incorporated into the 3D network according to **equation 1** (**Eq. 1**), while the equilibrium mass swelling ratio is calculated according to **equation 2** (**Eq. 2)** [255]. All measurements were performed in triplicate.

$$\%Gelfraction = \frac{W_{de}}{W_{d0}}.100 \quad \textbf{(Eq. 1)}$$

$$\%Swelling = \frac{W_{he} - W_{d0}}{W_{d0}}.100 \quad \textbf{(Eq. 2)}$$

Compression experiments

A TA500 texture analyzer (Lloyd Instruments) equipped with a 10N load cell was used at a rate of 5mm/min. Cross-linked hydrogel disks (Ø = 15mm; height = 2mm) were prepared by pipetting 300µl 10 or 20 w/v% Gel-MOD solution in each well of a 24-well plate and crosslinked for 20min with 365nm UV-A light (4mW/cm^2, UVP Inc.) in the presence of a 2 mol% Irg or 20 mol% VA. Hydrogel disks were compressed at room temperature over a distance of 0.5mm. The compressive modulus (kPa) was determined from the slope of the stress-strain curve. All measurements were performed in triplicate.

Encapsulation of microtissues in gel-MOD

Microtissues were collected from the microwells after three days of culture and encapsulated in 10 or 20 w/v% gel-MOD hydrogels (microtissues from 6 microchips (n = 9540)/ml Gel-MOD). Hydrogel-discs (Ø = 15mm; height = 2-3mm) were prepared by pipetting 250µl Gel-MOD solution in each well of a 48-well plate, and crosslinked for 20min with 365nm UV-A light (4mW/cm^2, UVP Inc.) in the presence of 2mol% Irg or 20mol% VA. After crosslinking, gels were transferred to a 6 well-plate. Medium was replenished 24h after encapsulation and hereafter, every three days. For the fusion

experiments, microtissues were encapsulated in 10 w/v% Gel-MOD at a high density (microtissues from 200 microchips (n = $3.18*10^5$/ml) in the presence of 20mol% VA.

Viability of microtissues (Live/dead fluorescence staining)

To assess the cell viability, gels were collected and washed twice with PBS and incubated for 10min with 2µg/ml Calcein-AM (AnaSpec) and 2µg/ml Propidium iodide (Sigma). Cell viability was evaluated by determining the ratio of green (live) versus red (dead) cells using an inverted fluorescence microscope (Olympus IX81) equipped with Xcellence software (Olympus).

Histological analysis

Gels were fixed (4% paraformaldehyde, Merck, Darmstadt, Germany), dehydrated and embedded in paraffin. Five-micron-thick sections were cut and stained with Haematoxylin/Eosin (HE). The ECM was assessed by histochemical methods; Alcian Blue (for acid glycosaminoglycans (GAG) and silver staining (reticular fibers, Collagen III [335]).

Gene expression analysis (RT-qPCR)

Four gels were incubated in 25mg/ml Collagenase Type IA (Sigma) in PBS at 37°C for approximately 1 hour or until completely dissolved. Total RNA (n=3) was isolated from microtissues using a lysis buffer (RLT buffer, Qiagen). The concentration and purity of the isolated RNA was determined by a NanoDrop1000 (Isogen). To convert RNA into cDNA, the High Capacity cDNA Reverse Transcription Kit (Life Technologies) was used according to the manufacturer's protocol. A 7500 Fast Real-Time PCR system (Applied Biosystems) and a SYBR Green PCR kit (Life Technologies) were used according to the manufacturer's instructions and protocols. Primer details are listed in Table 1.

Stability of six reference genes was determined and the two most stable reference genes (EEF1A1 and HPRT) were selected via geNORM (qbase$^+$ software, Biogazelle). Gene expression analysis was normalized to the geometric mean of these reference genes. The relative gene fold changes were determined by the $2^{-\Delta\Delta Ct}$ method. For comparative gene expression analysis, gene expression of encapsulated and non-encapsulated microtissues were compared to expression levels of standard monolayer cultured VIC P4.

Table 1. Primer sequences for porcine valvular interstitial cells (VIC)

Gene Description	Gene Symbol	Accession Number	Forward Primer 5' ➔ 3'	Reverse Primer 3' ➔ 5'	Amplicon Length (bp)	Primer Efficiency (%)
Eukaryotic translation elongation factor 1 alpha 1	EEF1A1	NM_001097418.2	CAACATGCTGGAGCCAAGTG	AGTGTGGTTCCACTGGCATT	87	94.2
Hypoxanthine phosphoribosyltransferase 1	HPRT1	NM_001032376.2	GGGAGGCCATCACATCGTAG	CGCCCGTTGACTGGTCATTA	167	89.6
Actin, alpha 2, smooth muscle	ACTA2/ α-SMA	NM_001164650.1	GGACCCTGTGAAGCACCAG	GTCACCCACGTAGCTGTCTT	198	98.9
Vimentin	VIM	XM_005668106.1	TCTGGAATCCCTCCCTCTGG	TCGCTGCACAGAGTACATGC	146	93.8
Fibroblast specific protein, S100A4	FSP-1	JN122624.1	TACTCAGGCAAGGAGGGTGA	TGGAAAGCAGCTTCATCCGT	113	94.3
Osteocalcin, bone gamma carboxylglutamic acid containing protein	BGLAP/ OCN	AY150038.1	TACCCAGATCCTCTGGAGCC	TGCCATAGAAGCGCCGATAG	109	110.4
Early growth response protein 1	Egr-1	AJ238156.1	CTATCAAGGCCTTTGCCACG	AGCTCATCTGAGCGGGAGA	193	104.4
SRY-box 9	Sox9	NM_213843.1	CATCTCTCCCAACGCCATCT	TCTCGCTTCAGGTCAGCCTT	174	94.6
Runt-related transcription factor 2	Runx2	XM_013977989	CAACTTCCTGTGCTCTGTGCT	GAGAACCAGGGTTGAGGTGAT	90	93.7
Collagen type I alpha 1 chain	COL1A1	XM_005668927.1	AGACATCCCACCAGTCACCT	TCACGTCATCGCACAACACA	122	96.9
Collagen type III alpha 1 chain	COL3A1	NM_001243297.1	GCTCCCATCTTGGTCAGTCC	ATGGGATCTCAGGGTTGGGA	147	94.5
Collagen type V alpha 1 chain	COL5A1	NM_001014971.1	GCTCAGCGTCCACAAGAAGA	GTGGTCCGAGACAAAGAGCA	184	91.4
Elastin	ELN	XM_003354509.3	CCCACACATCGAAACCCTCA	CACAAGAGCAAGGGGGCTAA	155	94
Hyaluronan	HAPLN1	NM_001004028.1	GTGATTGCCTCCTTCGACCA	TGCACAGACCCATCACTGAG	89	94.4
Biglycan	BGN	XM_003135475.3	TCACTGGCATCCCCAAAGAC	AGGGTGGGCAGAAAACTCAG	178	97.4
Decorin	DCN	NM_213920.1	CCTGCAAACTCTTGCTTGGG	TAATCCGGGGATTTGCCACA	81	94.6
Versican	VCAN	NM_001206429.1	AACCAGACAGGCTTCCCTTC	AAGTGGGTGAGGCAGTTTCT	124	92.7
Matrix metallopeptidase 1	MMP-1	NM_001166229.1	GGCCATCTATGGACCTTCCG	TGTGCGCATGTAGAACCTGT	145	101.5
Matrix metallopeptidase 2	MMP-2	NM_214192.1	CGATGGCTTCCTCTGGTGTT	AGCTGTTGTAGGATGTGCCC	155	94
Matrix metallopeptidase 3	MMP-3	NM_001166308.1	CACTTACAGACCTGGCTCGG	AGATTCTGTGGGCTCAACGG	113	89.3
Matrix metallopeptidase 9	MMP-9	NM_001038004.1	ACTTCGGAAACGCAAAAGGC	AAGAGTCTCTCGCTAGGGCA	169	110.9
Metallopeptidase inhibitor 1	TIMP-1	NM_213857.1	CACCTGCAGTTTTGTGGCTC	GGGATGGATGTGCAGGGAAA	117	89.5
Metallopeptidase inhibitor 2	TIMP-2	NM_001145985.1	CTCCGGGAACGACATCTACG	GCCTTTCCTGCGATGAGGTA	180	93
Collagen type II alpha 1 chain	COL2A1	XM_001925959.6	AGAAGTTGGACCTCCCGTGT	GGGTCCAGTCTCTCCACGTT	76	92

Statistical analysis

The Shapiro-Wilk test was used to determine normality of the variables. All the variables were parametric data and were analyzed with a one way ANOVA test followed by a post-hoc Tukey's using the commercially available software package SPSS for windows, version 24.0 (SPSS GmbH Software, München, Germany). Descriptive statistics are reported as the mean with the standard deviation between brackets and $p<0.05$ was considered statistically significant.

RESULTS

Gel-MOD properties

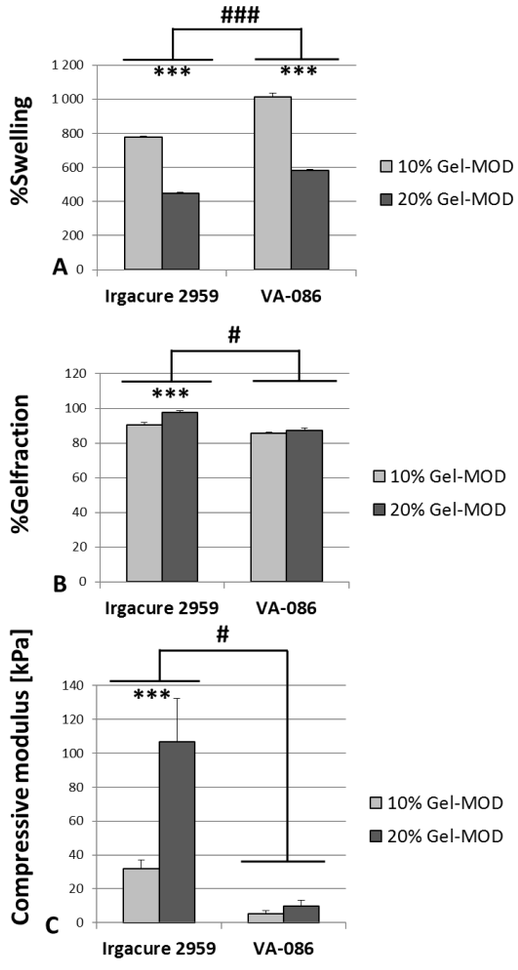

Fig.1: %Swelling (A), % gelfraction (B), and compressive modulus (C) of 10 and 20 w/v% Gel-MOD crosslinked in the presence of 2 mol% Irg or 20 mol% VA. Data is presented as mean and error bars indicate the 95% confidence interval. Statistically significant differences between 10 w/v% and 20 w/v% Gel-MOD hydrogels are marked with ***p < 0.001, and #p < 0.05, ###p < 0.001 for significant differences between Irgacure 2959 and VA-086 crosslinked hydrogels. A one-way ANOVA test followed by a post-hoc Tukey's was used for the statistical analysis, n = 3.

An equilibrium swelling test was performed to analyze the effect of photoinitiator (PI) (2 mol% Irg or 20 mol% VA) and Gel-MOD concentration (10 and 20 w/v%) on the crosslinking and swelling behavior of gels. **Fig.1A** shows that the swelling ratio of hydrogels significantly increased with decreasing Gel-MOD concentration and that VA-crosslinked hydrogels had a significantly higher swelling ratio (581.5-1081.2%) compared to Irg-crosslinked gels (446.9-778.0%). **Fig.1B** illustrates the percentage of the hydrogel that is covalently crosslinked and incorporated into the 3D structure. Irg-crosslinked gels had significantly more covalently incorporated material (90.5-97.5%) compared to VA-crosslinked gels (85.5-87.3%). In addition, a significantly higher percentage of gel fraction was observed in 20 w/v% Irg-crosslinked gels compared to 10 w/v% Gel-MOD. The stiffness of the gels is

described as compressive modulus and appeared to be dependent on the concentration of Gel-MOD, however, only a significant difference was observed between 10 and 20 w/v% Irg-crosslinked gels **(Fig.1C)**. In addition, Irg-crosslinked gels showed a significantly higher compressive modulus (31.9-106.6 kPa) compared to VA-crosslinked gels (5.0-9.6 kPa).

Gel-MOD encapsulated valvular microtissues

Overall morphology, viability and proliferation of encapsulated microtissues

Microtissues were encapsulated in 10 and 20 w/v% Gel-MOD and crosslinked with UV light irradiation in the presence of Irg or VA. The morphology, viability, and proliferation of VIC in encapsulated microtissues was evaluated up to day 14, except for the 10 w/v % VA-crosslinked hydrogels (which started to disintegrate from day 7).

A fluorescent live/dead staining showed that microtissues remained viable in all hydrogels, regardless the PI used for the photopolymerization and regardless the gel-MOD concentration **(Fig.2-3B/F)**. Furthermore, a HE staining of encapsulated microtissues showed viable cells with normal nuclei **(Fig.2-3C/G).** Interestingly, HE staining and bright field microscopy demonstrated that VIC from 10 w/v% VA-crosslinked hydrogels started to migrate out of the microtissues into the surrounding hydrogel, something that was not seen in the other hydrogels **(Fig.2A&C, black arrows).** Proliferation of VIC was shown with a Ki67 immuno-staining. In the 10 w/v% gels, $Ki67^+$ VIC were found at the periphery of the microtissues **(Fig.2D and Fig.3D),** and also some migrating cells were $Ki67^+$ at day 7 **(Fig.2D).** VIC at the outer edges from microtissues encapsulated in 20 w/v% gels were only sporadically $Ki67^+$ at day 1, and the amount of positive cells rapidly decreased over time **(Fig.2H and Fig.3H).**

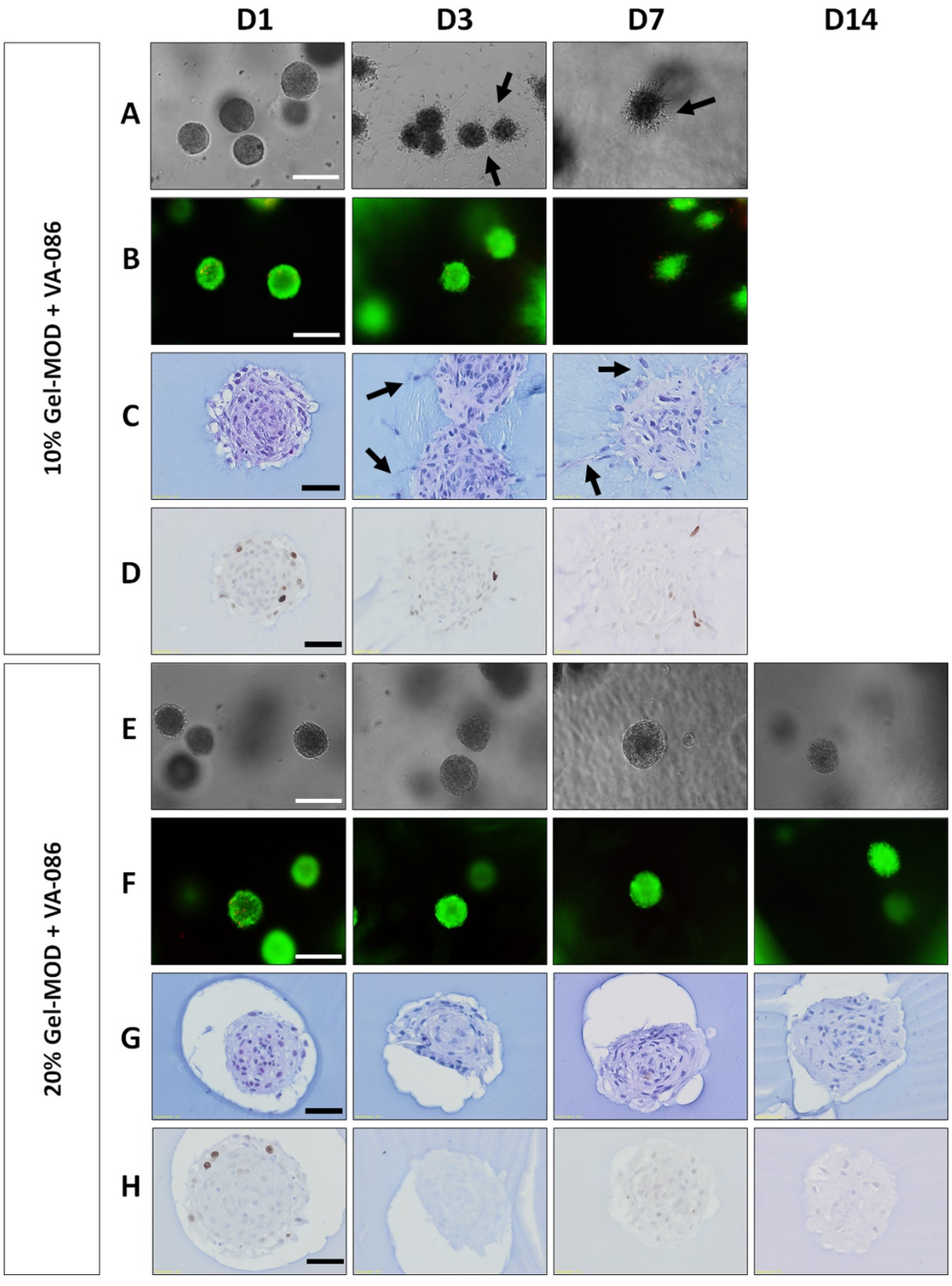

Fig.2: Morphology (A and E: bright field microscopy; C and G: HE staining), viability (B and F: Ca/Pi staining), and proliferation (D and H: Ki67 immuno-staining) of microtissues encapsulated in 10 or 20 w/v% VA-crosslinked hydrogels at day 1, 3, 7, and 14 of encapsulation. Representative images of n = 3 independent experiments. Scale bar = 200µm, magnification 10x (A, B, E, F), Scale bar = 40µm, magnification 40x (C, D, G, H). Black arrows = migrating VIC.

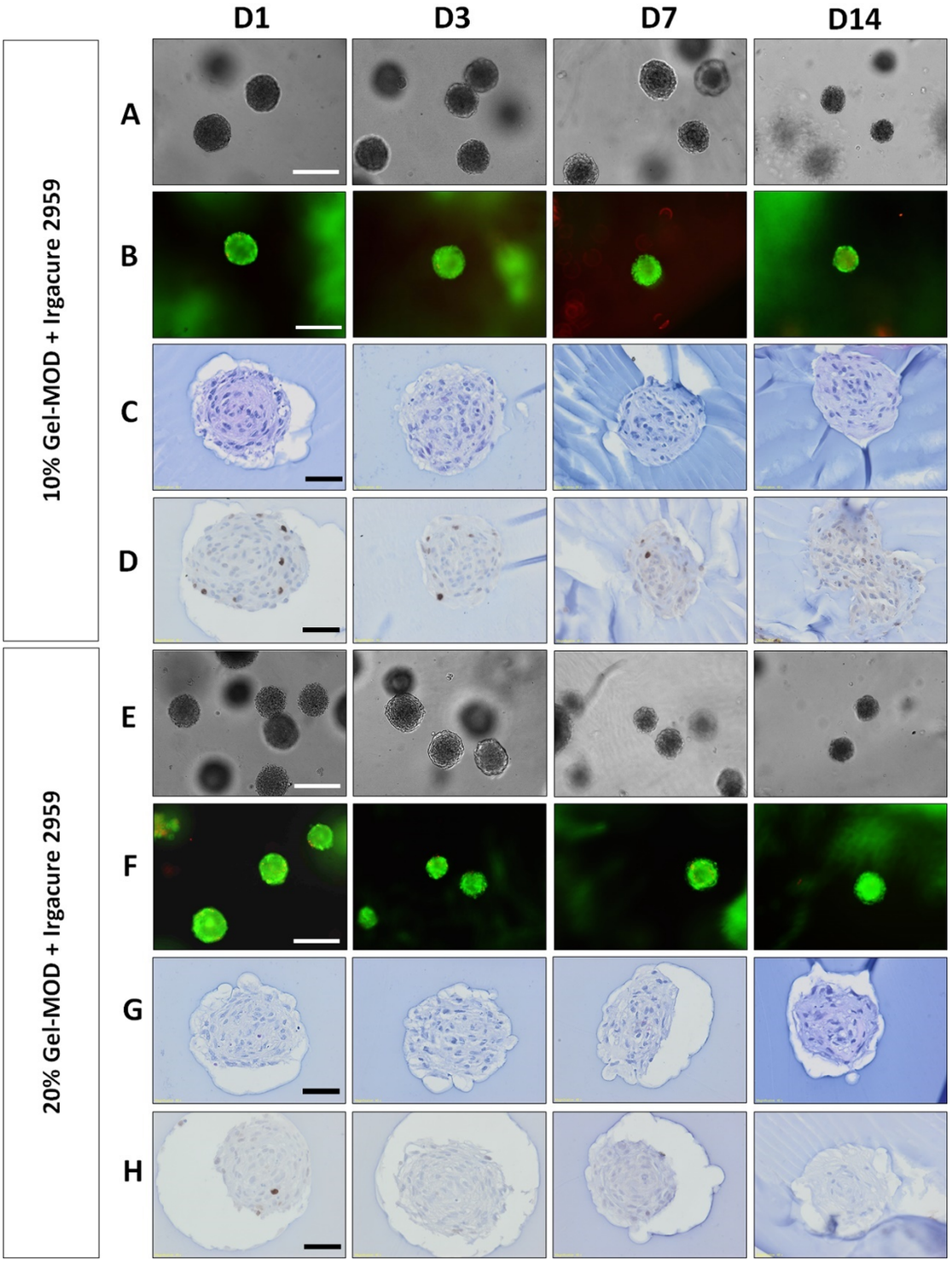

Fig.3: Morphology (A and E: bright field microscopy; C and G: HE staining), viability (B and F: Ca/Pi staining), and proliferation (D and H: Ki67 immuno-staining) of VIC microtissues encapsulated in 10 or 20 w/v% Irgacure-crosslinked hydrogels at day 1, 3, 7, and 14 of encapsulation. Representative images of n = 3 independent experiments. Scale bar = 200µm, magnification 10x (A, B, E, F), Scale bar = 40µm, magnification 40x (C, D, G, H).

ECM production of VIC in (non)-encapsulated microtissues

An Alcian Blue (AB)- and Silver staining was performed on encapsulated microtissues from all conditions, to visualize acidic polysaccharides such as GAG and reticular fibers, respectively. After one day of encapsulation, microtissues were only slightly stained with AB staining, indicating only limited presence of GAG. However, from day 3 until day 7/14, a rapid time dependent production of GAG was observed, as indicated by the increase in intensity of the AB staining of the encapsulated microtissues. This increase was more pronounced in 20 w/v% than in 10 w/v% encapsulated microtissues **(Fig.4A/C and Fig.5A/C).** On the other hand, reticular fibers were abundantly present from day 1 in encapsulated microtissues of all conditions, and a time-dependent circular fiber alignment towards the outer edge of the microtissues was noticed. Interestingly, microtissues which located close to each other appeared to fuse as indicated by the interconnection of the reticular fibers of these microtissues (black arrow) and reticular fibers seemed to attach to the surrounding hydrogel (white arrows) (except microtissues in 20 w/v% Irg-crosslinked hydrogels) **(Fig. 4B/D and Fig.5 B/D).**

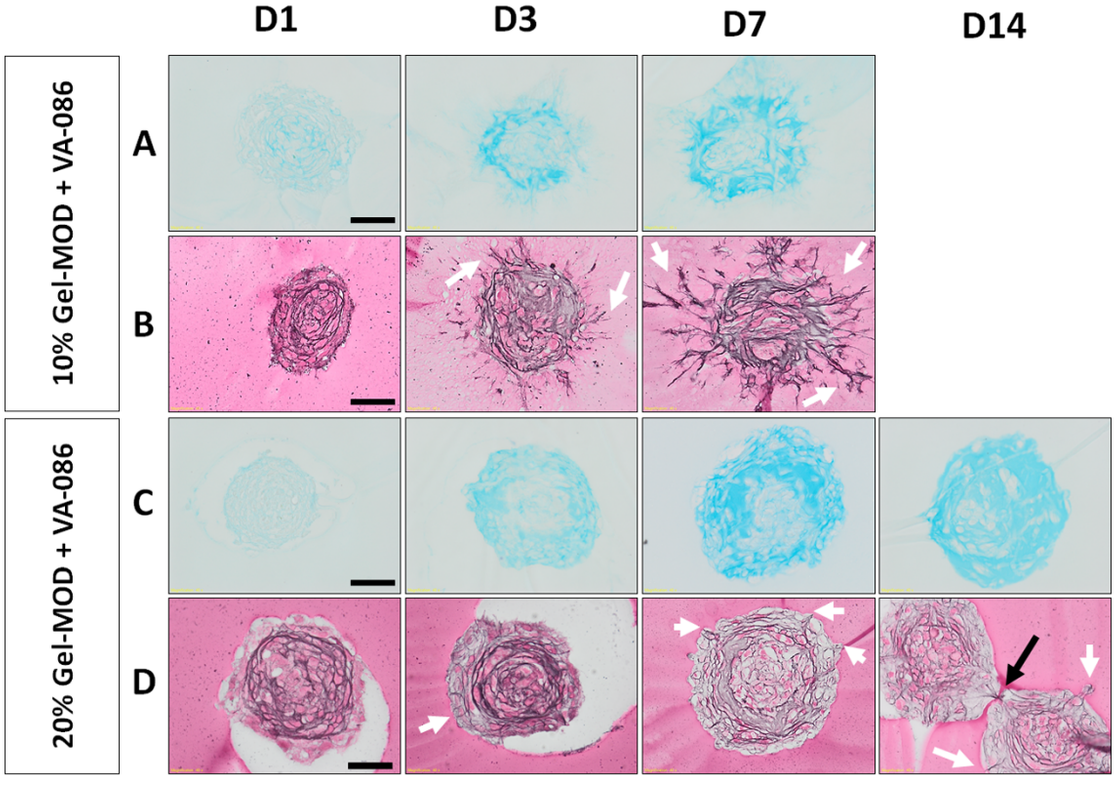

Fig.4: ECM production (A and C: Alcian Blue staining (GAG); B and D: Silver staining (reticular fibers)) of microtissues encapsulated in 10 or 20 w/v% VA-crosslinked hydrogels at day 1, 3, 7, and 14 of encapsulation. Representative images of n = 3 independent experiments. Scale bar = 40µm, magnification 40x. White arrows = contact points reticular fibers with hydrogel. Black arrow = interconnection reticular fibers of two microtissues.

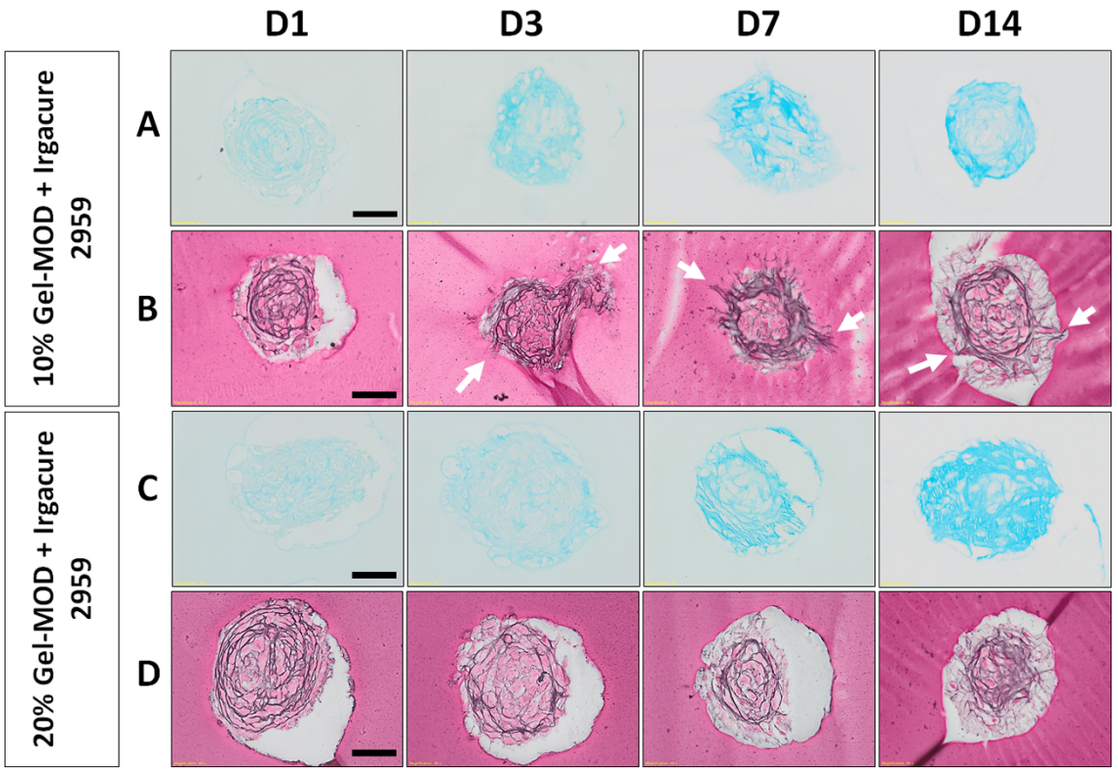

Fig.5: ECM production (A and C: Alcian Blue staining (GAG); B and D: Silver staining (reticular fibers)) of microtissues encapsulated in 10 or 20 w/v% Irgacure-crosslinked hydrogels at day 1, 3, 7, and 14 of encapsulation. Representative images of n = 3 independent experiments. Scale bar = 40µm, magnification 40x. White arrows = contact points reticular fibers with hydrogel.

Next, RT-qPCR was performed to analyze the mRNA expression levels of a broad panel of ECM components (Col I/III/V, elastin, HA, biglycan, decorin and versican), and MMP/TIMPs (MMP-1/2/3/9, TIMP-1/2) **(Fig.6A-B).** The mRNA expression levels of VIC in non-encapsulated and encapsulated microtissues (20 w/v% Irg-crosslinked hydrogels) at an early (day 7) and a late time point (day 18) were compared and shown as the fold change to standard monolayer cultured VIC.

Fig.6A shows that the mRNA expression of every investigated ECM component produced by VIC in non-encapsulated as well as encapsulated microtissues was higher compared to standard monolayer cultured VIC. Col I/III/V mRNA expression levels of VIC in encapsulated microtissues increased over time, while remaining unchanged in non-encapsulated microtissues. This increase was significant for Col I and V in encapsulated microtissues. Moreover, it was shown that Col V was significantly more expressed after 18 days in encapsulated microtissues compared to non-encapsulated microtissues. There was also a time-dependent increase noticed of elastin, non-sulfated GAG (HA), and PG (versican, biglycan, and decorin) expression in encapsulated microtissues, and after 18 days the expression levels were higher compared to non-encapsulated microtissues, except for versican. Nevertheless, this was only significant for biglycan.

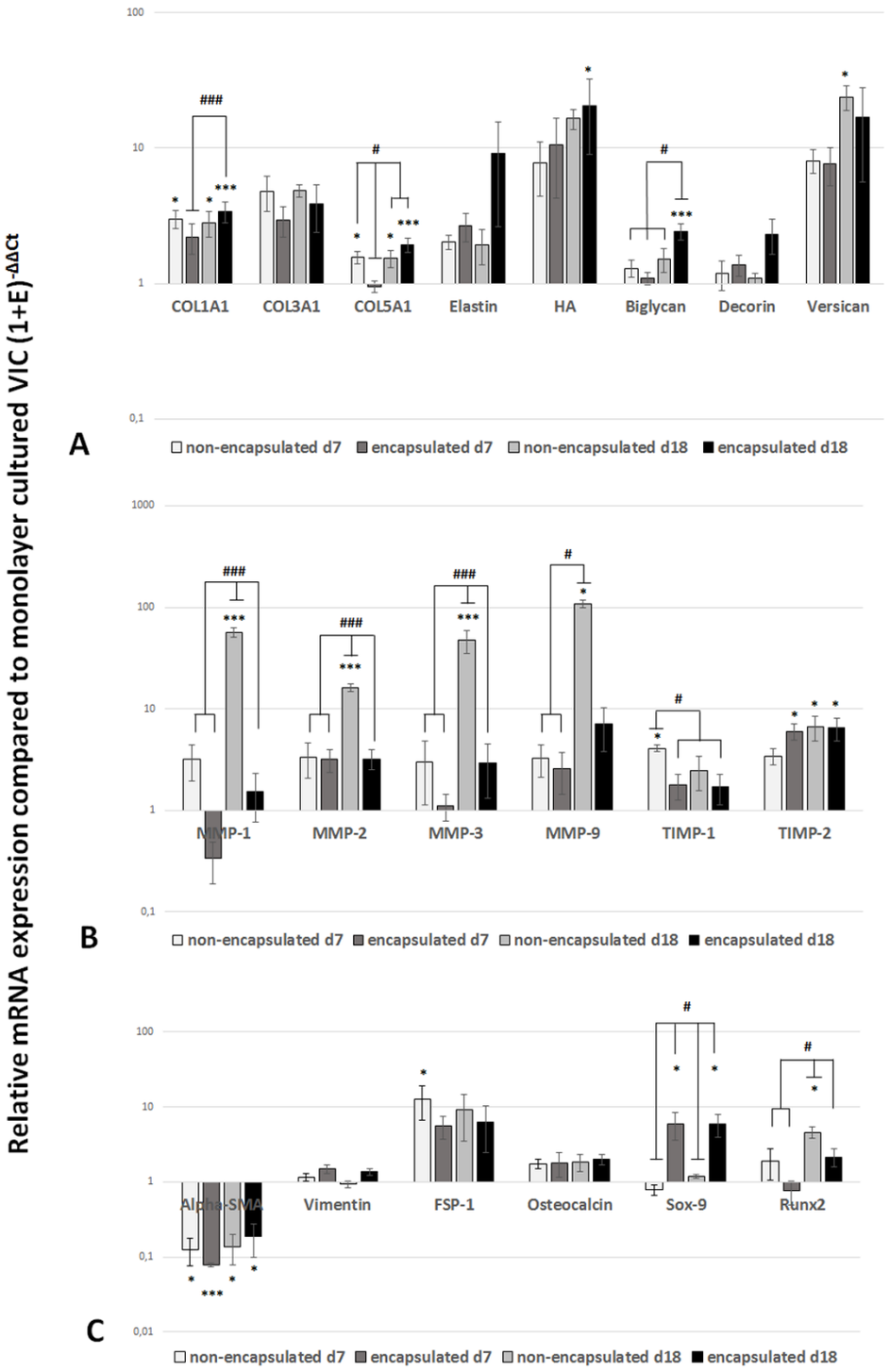

Fig.6: mRNA expression profile of VIC in non-encapsulated and encapsulated microtissues (20 w/v% Irg-crosslinked hydrogels) compared to standard monolayer cultured VIC. Microtissues were encapsulated after 3 days of culture. Relative expression levels of (A) ECM molecules, (B) MMP/TIMP, and (C) phenotype markers of VIC in (non)-encapsulated microtissues at an early time point (day 7 of microtissue culture = day 4 of encapsulation) tissues) and a late time point (day 18 of microtissue culture = day 15 of encapsulation) compared to standard monolayer cultured VIC at passage 4 (value=1). Data is presented as mean and error bars indicate the 95% confidence interval. Statistically significant differences are marked with *p < 0.05 or ***p < 0.001 compared to standard monolayer cultured VIC at passage 4, and #p < 0.05, ###p < 0.001 for significant differences between groups. Gene expression values are normalized to the geometric mean of two stable reference genes (EEF1A1 and HPRT). A one-way ANOVA test followed by a post-hoc Tukey's was used for the statistical analysis, n = 3.

Fig.6B shows that after 18 days, the mRNA expression of MMP-1/2/3/9 and TIMP-2 was significantly increased in non-encapsulated microtissues. However, when microtissues were encapsulated in gelatin, the increase of MMP-1/2/3 was significantly less pronounced and TIMP-1/2 expression levels remained stable over time.

VIC phenotype in (non)-encapsulated microtissues

Fig.6C demonstrates the expression level of several markers used to study the phenotype of VIC in (non)-encapsulated microtissues. Compared to monolayer cultured VIC, VIC in non-encapsulated as well as encapsulated microtissues expressed significantly less α-SMA, while vimentin levels were comparable, and FSP-1 and OCN expression levels were increased. α-SMA, vimentin, FSP-1 and OCN expression levels remained stable over time.

VIC in encapsulated microtissues significantly expressed more Sox9 and less Runx2 compared to non-encapsulated microtissues. HIF-α expression levels were stable in (non)-encapsulated microtissues and comparable to the expression levels of standard monolayer cultured VIC at all time points.

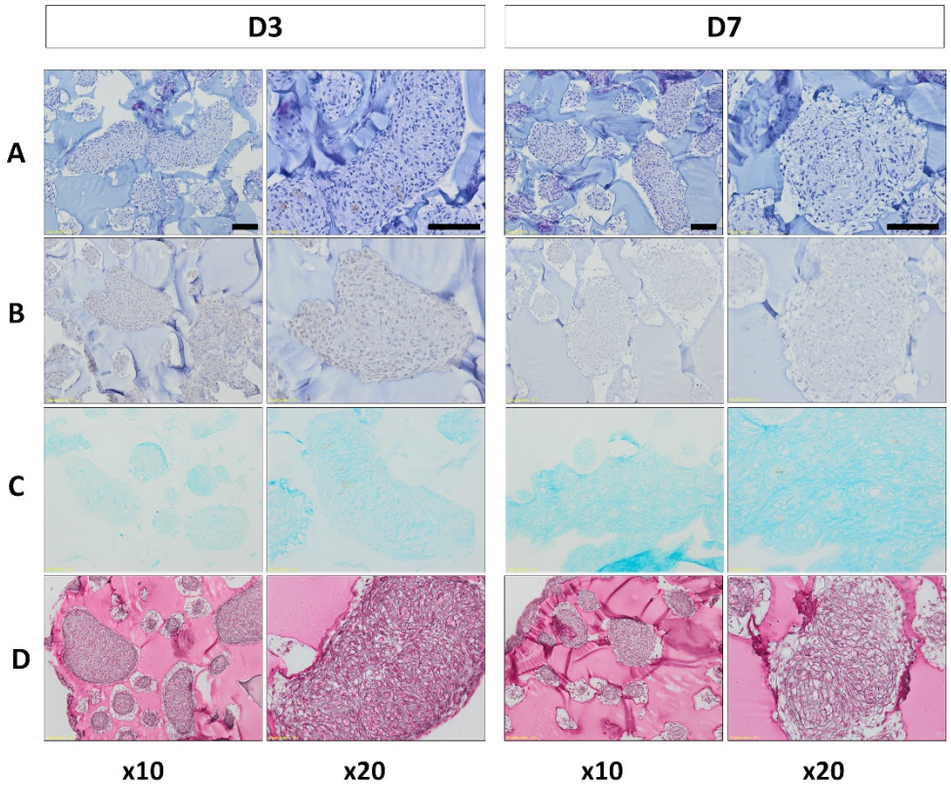

Fig.7: Morphology (A: HE staining), proliferation (B: Ki67 immuno-staining) and ECM production (C: AB (GAG) staining; D: Silver (reticulin fibers) staining) of encapsulated microtissues in 10 w/v% Gel-MOD with VA-086 PI at day 3 and 7 of encapsulation. Representative images of n = 3 independent experiments. Scale bar = 100µm, magnification 10x , Scale bar = 200µm, magnification 20x.

Towards a larger tissue: tissue fusion

A large amount of VIC microtissues were encapsulated in 10 w/v % VA-crosslinked gel-MOD and microtissues morphology, fusion, proliferation, migration, and ECM production was analyzed at day 3 and 7. **Fig.7** shows that by day 3 microtissues had already fused to form larger valvular tissues in some regions of the hydrogel. These valvular tissues had normal morphology with round nuclei at day 3 and 7, as shown by HE staining. However, in the central regions of some tissues few pycnotic nuclei were noticed at day 7 **(Fig.7A).** VIC in micro-tissues were sporadically positive for Ki67 at day 3, but proliferating $Ki67^{+}$ VIC were no longer noticed by day 7 **(Fig.7B).** Fused valvular tissues also showed a time-dependent increase of GAG **(Fig.7C)** and an early massive, but unorganized, reticular fiber production **(Fig.7D).**

DISCUSSION

3D bioprinting has the potential to biofabricate a viable tissue construct by directed assembling of micro-scale building blocks into a larger tissue construct. This study investigated whether modified gelatin is an appropriate carrier-material for valvular microtissues, to be used as a potential bio-ink for the biofabrication of a larger, macro-scale valvular tissue.

This work aimed to elucidate how microtissues respond to encapsulation in a hydrogel environment. Specifically, VIC characteristics like phenotype, proliferation, migration, mRNA expression of ECM molecules, ECM deposition and tissue fusion were characterized by histochemical stainings and RT-qPCR. Collectively, these results suggest that variation in initial physical and biomechanical hydrogel properties directly impact events that influence long term matrix deposition and tissue fusion.

Over the past ten years, gelatin and hybrid gelatin hydrogels have been investigated for the encapsulation of VIC [48, 226, 235, 354]. However, this is the first time gelatin is used for the encapsulation of valvular microtissues. Gelatin has similar properties to native collagen, such as RGD peptide sequences which are essential to stimulate cell attachment, cell migration, cell differentiation, and cell growth [226, 359]. However, due to the thermo-reversible characteristic of gelatin, crosslinking is needed to enhance the mechanical properties of the 3D construct [233] [226]. In this study, chemically modified gelatin is crosslinked with UV irradiation in the presence of Irg or VA. Irg has been largely used in tissue engineering and is non-cytotoxic in its native state, however, the photogenerated radical form of Irg can decrease cell viability [358]. It has been shown by Rouillard et al. that when the Irg concentration was raised from 0.02 to 0.03 w/v%, the viability of bovine chondrocytes reduced from >60% to <40% [358]. The optimal concentration of PI to rapidly and efficiently crosslink the gels with a short irradiation time is absolutely essential to minimize the effect of the radical agents on the cells [354]. On the other hand, both the inactive and the activated form of VA have shown to have minimal effect on the cell viability [254, 358]. In the same study, Rouillard et al. showed that VA-crosslinked hydrogels, with concentrations up to 0.3 w/v%, contained >90% viable chondrocytes [358].

Crosslinking with either Irg or VA resulted in solid hydrogel constructs and gel fraction analysis showed that 85.5-87.3% (10-20 w/v% VA-crosslinked gels) or 90.5-97.5% (10-20 w/v% Irg-crosslinked gels) of the Gel-MOD was incorporated into a 3D network. In addition, it was shown that microtissues remained viable in all gels during the complete study duration and viability was not influenced by the type of PI. Unfortunately, during the follow-up, early disintegration of VA-crosslinked gels was noticed (around day 7 or 14, for 10 or 20 w/v% gels respectively), while Irg-crosslinked gels were stable for at least 14 days. Further analysis of the hydrogels revealed that, although solid gels could be generated, the crosslinking extent was far less when VA was used,

indicated by the remarkable higher swelling ratio compared to Irg-crosslinked gels. This could explain the early degeneration since less crosslinked gels could be more susceptible to solubilization at 37°C.

Stiffness of the different hydrogels was determined and it was shown that 10 w/v% gels and VA-crosslinked gels were softer (lower compressive moduli) compared to 20 w/v% gels and Irg-crosslinked gels (higher compressive moduli). Based on the fact that stiffer hydrogels have denser networks and can delay the cell spreading process [353, 354], it was hypothesized that softer gels could be more favorable for VIC migration into the gel. As expected, migration of VIC from microtissues into the gel was most pronounced in the softest 10 w/v% VA-crosslinked gels (5.0 kPa). Although not investigated in this research, it is likely that the softer hydrogels had larger and maybe interconnected pores which can also have favored migration. This is suggested since previous studies have already visualized an increase in pore size and interconnectivity by decreasing gel-MOD concentration [353] and larger pores were noticed in gel-MOD hydrogels when crosslinked using lower Irg concentrations [226].

To ultimately produce a functional living tissue, microtissues should mimic the native cell phenotype and native tissue composition. We previously showed that microtissues were able to produce valve related ECM components while remaining in a quiescent state [350]. In this study, we showed that the Gel-MOD encapsulated valvular microtissues were still able to produce heart valve related ECM components. In addition, remodeling capacity and low α-SMA expression (indicating a quiescent VIC phenotype) were evidenced when encapsulated in Irg-crosslinked hydrogels and there were no indications of calcification. Yet, some differences were noticed between encapsulated and non-encapsulated microtissues. First, encapsulated microtissues showed lower MMP-1/2/3/9 and TIMP-1 mRNA expression levels, indicating lower remodeling capacity. Secondly, more GAG production and elevated mRNA expression levels of Col I/V, elastin, HA, biglycan and decorin were noticed, while the expression or production of the other investigated ECM components remained the same, demonstrating selective stimulation of certain ECM molecules. Thirdly, a significant increase of Sox9 mRNA expression was noticed. The transcription factor Sox9 is required for ECM organization and plays an essential role in heart valve development [360, 361]. It is also an early chondrogenic marker and required for cartilage formation [362]. However, further research is necessary to elucidate the role of Sox9 in encapsulated microtissues.

It is demonstrated that by encapsulating microtissues, changes in ECM formation and gene expression can be induced. Although so far only a limited amount of histological stainings were performed and mRNA expression was analyzed on microtissues encapsulated in the stiffest Irg-crosslinked hydrogels, we believe that ECM production and possibly also VIC phenotype could be

influenced by the hydrogel stiffness, yet this needs to be further investigated. We also want to acknowledge that it is likely that the hydrogel type (Gel-MOD), and not only the stiffness, can enhance/inhibit ECM formation as it is already shown by Duan et al. that GAG content only significantly increased in Gel-MOD/HA-MA hybrid gels compared to pure HA-MA gels [227].

As the overall goal is to generate a larger macro-scale valvular tissue, microtissues should be able to fuse in the hydrogel. For this reason, and based on the proliferation and migration capacity of VIC, which were more apparent in the soft gels, microtissues were encapsulated at a high density in 10 w/v% VA-crosslinked gels to investigate the potential fusion capacity. With this preliminary and limited experiment we provided a proof of concept as we have shown that microtissues in these hydrogels were able to fuse within 3 days and larger valvular microtissues were formed in various sizes (±150-1400µm). These valvular microtissues also showed time-dependent increase of valve-related ECM components.

CONCLUSION

We evidenced that Gel-MOD is a good encapsulation material for valvular microtissues (Ø150µm). Encapsulated microtissues remained viable during the complete study duration, showed a quiescent phenotype and were able to produce heart-valve related ECM components. In addition, a proof of concept for the formation of larger valvular tissue was provided by showing that microtissues were able to randomly assemble in Gel-MOD and to fuse into larger tissues (Ø150-1400µm). For this reason, we believe that soft microtissues-laden Gel-MOD hydrogels are suitable as a bio-ink for future biofabrication of larger-scale valvular macrotissue with predefined shapes, through directed assembly by bioprinting.

ACKNOWLEDGEMENTS

The authors would like to thank Prof. Peter Dubruel for kindly providing the modified gelatin and the technical staff for their help with the (immuno)histological stainings (Leen Pieters), RT-qPCR (Greet De Smet) and the gel-MOD analysis (Chris Vercruysse).

CHAPTER IV

General discussion

GENERAL DISCUSSION

Requirements for an ideal heart valve substitute

Valvular heart diseases represent a major healthcare issue causing significant morbidity and mortality worldwide. Clinical treatment of end-stage valvulopathy still primarily relies on heart valve replacements. In the 60s, Dwight E. Harken, an innovator in heart surgery, defined the essential characteristics of an ideal heart valve substitute in the "Ten Commandments of Satisfactory Prosthetic Aortic Valves'' [363]. From then on, researchers have added additional criteria which are summarized in **Table 1** [4, 204, 364, 365].

Table 1. The ideal properties of a heart valve replacement

Non-thrombogenic
Chemically inert and non-hemolytic
Non-obstructive (no resistance to physiological flows)
Close promptly and complete
Infection resistant
Resistant to tissue overgrowth
Durable for extended intervals
Not annoying to the patient (noise free)
Technically practical to insert
Easily and permanently inserted into an appropriate physiologic site (orthotopic)
Resistant to calcification
Lasting physical and geometrical features, and mechanical properties
Off-the-shelf availability
Potential growth with the patient
Regenerative capacity

None of the currently available mechanical or bioprosthetic valve replacements meet all the above mentioned criteria. Therefore, the last 20 years, different HVTE approaches have emerged, all with the same goal: to engineer a living autologous heart valve with regeneration and growth potential.

TE evolved from the field of biomaterials development and refers to the practice of combining cells, biologically active molecules, and/or scaffolds, into functional tissues. The goal of TE is to assemble functional constructs that restore, maintain, or improve damaged tissues or whole organs [366].

In this work, two different TE approaches were explored to generate bio-active cardiac tissues for the development of a bio-active TEHV.

A. Generation of bio-active porcine cardiac tissues from the top down

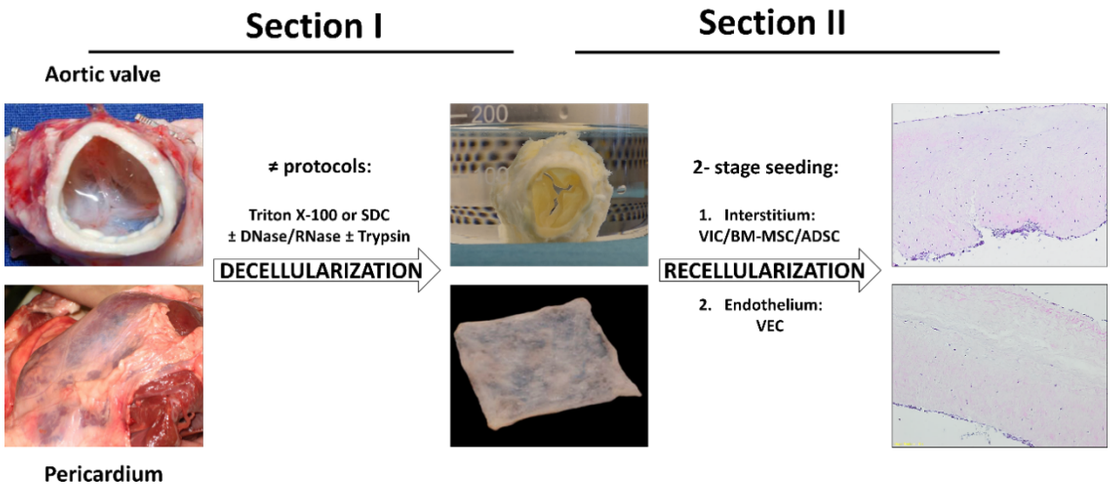

Schematic overview experimental outline Part A

The overall goal of Part A was to generate bio-active repopulated porcine cardiac tissues. To achieve this goal, a step-wise approach was followed. The first step involved the decellularization of porcine cardiac tissues (aortic HVL and PER), with different detergent based protocols, to remove all xenogeneic cellular material **(Chapter 3A, Section I**). Next, a 2-stage seeding protocol was used to completely repopulate the interstitium and generate a new endothelium **(Chapter 3A, Section II**).

Biological tissue as a starting point

For the generation of a viable TEHV, a suitable scaffold is needed. Such a scaffold should fulfill mechanical and biological integrity, provide dynamic and biochemical signals, allow cell attachment and migration, secure diffusion of vital cell nutrients and expressed factors, and allow dynamic changes of scaffold's architecture [367].

Although synthetic scaffolds are easy to produce in different sizes and shapes, are less immunogenic and are free of transmittable diseases [72], in this study we preferred the use of biological scaffolds. By using native tissue, biological stimuli and native ECM components as well as native anatomic macro-structure and micro-architecture are already present and do not need to be mimicked/rebuilt [368]. Moreover, there is no need to optimize the degradation rate as the purpose of a biological HV scaffold is to remain in the body, whereas polymeric scaffolds are dependent of scaffold repopulation, ECM formation and scaffold degradation [90, 369].

Allogeneic tissues are not unlimited available and the use of xenograft tissue as natural tissue scaffolds requires chemical, physical and/or enzymatic pretreatment aimed at preserving the tissue by enhancing the resistance to degradation, reducing the immunogenicity and sterilizing the tissue [127]. Since the conventional xenogeneic GA crosslinked tissues are not suitable for HVTE and so far none of the alternative crosslinkers (e.g. genipin [370, 371], quercitin [275] and triglycidyl amine [372]) have yet proven to extend the durability of xenogeneic tissue, nor to allow *in vitro* and/or *in*

vivo autologous repopulation, the followed strategy in this thesis was decellularization to obtain biological tissue scaffolds **(Chapter 3A, Section I)** for the generation of bio-active repopulated tissues **(Chapter 3A, Section II).**

Decellularization of biological tissues

Decellularized biological heart valve scaffolds can be made from HV or PER and possess great potential as a stand-alone valve replacement and/or as a scaffold for HVTE. **Table S1 and S2** show that most cardiac biological tissues are decellularized with detergents (SDS, SDC, and Triton X-100), sometimes in combination with enzymes. Unfortunately, decellularization efficiency is often poorly evaluated (mostly only determined by histological staining) and preservation of ECM components and mechanical integrity of scaffolds are often not investigated. We believe that it is necessary to evaluate the three minimal criteria set by Crapo et al. to satisfy the extent of acellularity (DNA content <50ng/mg, DNA fragments <200bp and no visible nuclei) and to thoroughly evaluate the effect of the decellularization agent on the ECM components since maintaining structural integrity is essential to generate a durable TEHV [138].

The first focus of Part A **(Chapter 3A, Section I)** was the generation of completely cell free porcine cardiac tissues. Porcine HVL and PER were decellularized with different protocols (Triton X-100 or SDC based protocols ±ENZ±TRYP). Cell removal (three criteria), preservation of the main ECM components (Col, GAG and elastin) as well as the mechanical properties (stiffness and WTML) of tissues were evaluated.

It was shown that decellularization of cardiac tissues with Triton X-100+ENZ+TRYP efficiently removed cellular material from porcine PER and HVL and that although SDC did reduce cellular content, the three criteria of acellularity were not fulfilled. By contrast, Dohmen et al. stated that this SDC treatment resulted in acellular porcine valves (Matrix P^{TM}), which are commercially available [271, 281, 289, 373]. Interestingly, an independent study revealed that the Matrix P scaffolds still contained cells, indicating that this SDC-based protocol is not efficient [374].

Further analysis of Triton X-100 decellularized tissue revealed that collagen and elastin, two main ECM components, were more preserved in HVL than in PER. Yet, a significant loss of GAG in both tissues was detected. This was expected since cell extraction protocols are known to remove GAG from tissue [98, 278, 288]. To date, there is still no decellularization protocol that prevents this loss. The loss of GAG, alterations of collagen and elastin and cell remnants all contribute to tissue calcification [375]. Furthermore, GAG are also known to play an important role in the morphogenesis and maintenance of various tissues through interactions with cell adhesion molecules, ECM

molecules and GF [376]. This could potentially influence repopulation efficiency of decellularized tissues.

It should also be noted that the Triton X-100 decellularized HVL in this study displayed a slight, but significant, increase in leaflet stiffness (± 20% > compared to native tissue) and that PER tissue was more brittle. Mechanical changes can facilitate valve failure through direct tearing of tissue or by accelerating calcification [127]. However, the 20% increase in stiffness of decellularized HVL is still lower than the increase in stiffness of GA treated BHV (± 50% > compared to native tissue [370]).

Decellularization of biological scaffolds = the new standard pretreatment?

One of the main questions is whether decellularization can become the new standard pretreatment of heart valve scaffolds. More specific: as a stand-alone valve, can decellularized xenografts replace the conventional GA-fixed valves and decellularized allografts the conventional cryopreserved valves? As a TEHV, can decellularized tissues be repopulated to generate a viable valve replacement? The latter question is being addressed in the next sections, the former in the following paragraphs.

As previously mentioned in the introduction, there are currently three main research groups that are performing clinical studies with decellularized allo- or xenografts **(Chapter I Section 4.1.1.2**). The first group is using the allogeneic pulmonary CryoValves^{TM} [139, 377-381] and showed that after a follow up of 2-5 years no clinical significant differences were noticed between the CryoValves and conventional pulmonary valves [380]. The second group of Cebotari et al., also with extensive experience in decellularized pulmonary allografts [382-384], recently confirmed their earlier results of reduced re-operation rates compared to cryopreserved and BHV, with a 100% freedom of explantation after ten years [383]. In addition, this is the first group that also investigated the clinical potential of decellularized aortic valves and demonstrated that, with a mean follow-up of 2 years (maximum 7.6 years), these aortic allografts can withstand systemic circulation and appear as an alternative to conventional grafts in young patients [384].

The third group of Dohmen et al. analyzed the clinical performance of decellularized pulmonary xenografts (Matrix P^{TM}). This group demonstrated that PERV-RNA was not detectable and the α-gal antigens were removed in Matrix P [144, 271]. Dohmen et al. also stated that the performance of the Matrix P was close to normal physiologic dynamics, after a follow up of two years [271] and freedom of re-operation was 84% after 3 years [385]. These short-term clinical results looked encouraging but long-term follow up data is needed. Interestingly, the Matrix P scaffolds are currently being evaluated in other independent studies and discouraging adverse results were disclosed [374, 386-388]. One study reported failure of 33 out of 93 patients and freedom of re-operation was only 60%

after 12 months [387]. The main failure sign was stenosis and there were histopathological evidences of massive inflammatory reaction and exaggerated fibrosis.

It is safe to say that as a stand-alone valve replacement, the design of decellularized allograft valves is well proven and that the acellular nature reduces the immunological response and host rejection [389]. Whether this benefit translates to greater valve longevity or better long-term function (currently 10 years for decellularized pulmonary valves [383]) remains to be demonstrated. Nevertheless, the controversial results with the Matrix P impose more caution in the application of xenogeneic-tissue scaffolds in humans and decellularized xenografts may have entered the clinic too early. A step back to preclinical evaluation in non-human primates is mandatory to verify effective biocompatibility in xeno-interactions.

To seed or not to seed before implantation?

One of the first hypotheses researchers made was that decellularized tissues have an intrinsic *in vivo* repopulation potential and that circulating host cells can invade and repopulate these tissue scaffolds, which led to the second hypothesis of *in vivo* growth potential.

Animal and clinical studies that investigated this *in vivo* repopulation potential are summarized in **Table S2** and it can be concluded that decellularized tissues have an *in vivo* repopulation potential, yet this is a slow process. The *in vivo* formation of a complete new EC monolayer on the surface of the arterial wall and valve leaflets takes approximately one year (explants from short repopulation experiments (3-9 months) revealed incomplete endothelium restoration [151, 315, 317, 390], explants from later time points (11-20 months) showed a complete newly formed endothelium [271, 316, 391, 392]). In addition, the repopulation of the interstitium of the leaflets and the aortic root is mostly incomplete, even 2 years after implantation [151, 316, 390, 392, 393].

As for the evidence of growth potential of unseeded decellularized valves, to our knowledge only two studies have addressed this issue. The first study implanted Matrix P valves (valve diameter 17mm), in juvenile sheep. After 9-11 months all sheep had doubled their weight and valve diameter increased to 27.5mm [394]. However, no comparison was made with conventional valve replacements or autografts. In contrast, a second more recent study compared the performance of decellularized aortic allografts with pulmonary autografts in the growing sheep model. After 20 months, valve diameters were increased, but autografts were still in mean 4mm larger than decellularized allografts (allografts: from 15.7 to 21.0 ± 2.4; autografts from 15.7 ± 13.4 to 25.0 ± 3.4) [316].

With cautious it can be concluded that decellularized heart valves have the potential to grow, despite their incomplete and slow repopulation *in vivo*. However, this growth is still remarkably less when compared with autografts and more research and comparison between cryopreserved allografts, decellularized xeno/allografts and autografts is mandatory.

Now the question many research groups are trying to investigate is whether prior *in vitro* seeded and completely repopulated TEHV can outperform these non-preseeded valves in terms of growth potential and potentially also longevity. It is also hypothesized that by complete repopulation of xenogeneic tissues, functionally ‘‘humanized’’ xenogeneic valves can be developed, in which an *in vivo* potential xenoreaction might be prevented by biomimetic strategies, as the one provided by masking porcine antigens with human ECM components by autologous cells [105].

***In vitro* repopulation efficiency of decellularized tissues**

Table S1 shows that the last 20 years, researchers have been exploring different decellularization protocols, different cell types, different cultivation methods and different seeding designs (homo/heterotypic experiments), which makes it almost impossible to compare the different studies and to investigate why a complete repopulated HVTE scaffold has not yet been developed.

In the second section of Part A **(Chapter 3A, section II)** we focused on the complete repopulation of Triton X-100+TRYP+ENZ decellularized porcine HVL and PER, by using a static two-stage seeding protocol.

In the first stage, the interstitium was repopulated with porcine VIC or MSC. To our knowledge only three studies have previously investigated the homotypic VIC repopulation of HVL [395, 396] and PER [397]. Although these studies proved the feasibility of cell seeding, no migration (PER) or only uncomplete (HVL) repopulation of the interstitium was noticed. In contrast, we have demonstrated that it is possible to repopulate HVL and the fibrosa of PER with VIC within 14 days, which led us believe that the decellularization process could play a role in the susceptibility of tissue to cell migration. Hof et al. recently showed that brief enzymatic digestion of decellularized HVL with trypsin positively influenced VIC migration [395]. Trypsin is one of the agents used in our decellularization protocol and not part of the standard procedures in the other studies (SDS/SDC [395], SDS+ENZ [397], Triton X-100/SDC [396]).

MSC have shown considerable promise for HVTE and have the potential to serve as a surrogate cell source for VIC in autologous clinical applications. Previous studies have shown that it is extremely difficult to repopulate decellularized tissues with MSC, in homotypic as well as heterotypic seeding experiments [103, 206, 306, 307, 398]. For this reason, researchers opted additional treatments in

order to improve the porosity of scaffolds (e.g. acetic acid treatment [306]), or to improve cell adhesion (e.g. RGD-peptide modification [306], growth factors [103], fibronectin coating [105]). So far, only porcine decellularized pulmonary HVL, coated with fibronectin have shown complete repopulation, after seeding porcine BM-MSC [105].

In this research, ADSC and BM-MSC were cultivated and seeded onto decellularized HVL and PER with and without the addition of AA. It was hypothesized that AA could enhance remodeling and repopulation of decellularized tissues. AA is an essential nutrient acting as an anti-oxidant, protecting against oxidative stress-induced cell damage [310-312]. AA has also been reported to upregulate collagen I and III in human dermal fibroblast [309], and to stimulate proliferation of MSC [188]. As expected, AA stimulated Col I (but only in BM-MSC) and to a lesser extent Col III expression. MSC cultivated and seeded in the presence of AA also showed greater repopulation potential compared to standard cultured MSC. Yet, this was more pronounced for BM-MSC and recolonization of HVL appeared to be more efficient than PER tissue.

We want to acknowledge that the exact mechanism by which AA stimulated MSC migration in decellularized HVL/PER remains unknown. One possible theory is that seeded MSC are susceptible to increased oxidative stress. By preventing oxidative induced cell death, more MSC were allowed to attach which indirectly resulted in more migration. Another possible theory is that AA stimulated MSC towards another, potentially more migratory, cell type. This differentiation could explain the increased α-SMA expression, which is normally largely restricted to SMC, pericytes and MFb [313]. Also aVIC express α-SMA and are known to stimulate cellular repair processes in the heart valves, including proliferation, migration, and matrix remodeling [14].

In the second stage, porcine VEC were used to generate a newly formed endothelium by subsequently seeding VEC onto both sides of the tissue. It should be noted that re-endothelization of decellularized tissues has already been demonstrated for porcine [98, 292], ovine [399-401] and human [402, 403] pulmonary and aortic valves in other homotypic as well as in heterotypic seeding experiments but little is known about the re-endothelization of PER tissue. After a 7-day static culture we were able to demonstrate confluent monolayers of $CD31^+$ on both tissues, however, VEC did not fully spread onto PER.

Conclusion

Based on the three minimal criteria for acellularity, we have shown that decellularization with Triton X-100+ENZ+TRYP was more effective than with SDC and resulted in cell free HVL as well as PER. However, we believe that for the generation of bio-active tissue, HVL are more suitable than PER since the decellularization procedure had less impact on HVL (GAG were lost but collagen and elastin fibers were preserved) and decellularized HVL showed greater repopulation capacity.

This study provided a proof of concept for the generation of a bio-active TEHV by showing that bio-active HVL can be generated *in vitro* within 14 days, by completely repopulating the interstitium with BM-MSC or VIC and subsequently generating a complete new endothelium.

Study limitations and future perspectives

Before Triton X-100 decellularized porcine tissues can be introduced into the clinic, α-gal removal should be investigated, since α-gal epitopes could remain exposed and reactive in cellular membrane residues entrapped between fibers of the ECM. Moreover, not only known (α-gal and MHC I) but also unknown (against which graft-specific antibodies are produced) xenoantigens could be persisted in supposedly acellular matrices. For this reason, we believe that preclinical evaluation in Old World monkeys, a discordant xenotransplantation model, is mandatory to verify effective biocompatibility of the Triton X-100 decellularized porcine tissues.

Although it was shown that HVL can be repopulated with VIC/BM-MSC and cells were distributed throughout all the three layers, quantification of the amount of cells in repopulated tissues would be desirable. Preliminary quantification has shown that the cell density in repopulated HVL is close to native cell density when HVL were repopulated with VIC (77.39%; SD:6.5), and 53.26% (SD:4.43) when BM-MSC were used. It can be interesting to investigate if increasing the initial cell seeding density to $>1*10^6/cm^2$ can positively influence cell repopulation density.

There are also some aspects of BM-MSC/VIC reseeded HVL that can be further investigated to demonstrate the suitability of these cells. First, it can be interesting to investigate the cell phenotype after recolonization. In the best case scenario, the majority of VIC are in a homeostatic quiescent state and MSC differentiate towards a more qVIC-like phenotype. Secondly, ECM production by both cell types can be investigated as it is hypothesized that VIC and MSC can remodel the ECM and could potentially also restore GAG content. Thirdly, the mechanical properties of repopulated tissue should be compared to native and decellularized tissue to rule out altered properties.

In order to repopulate a complete heart valve, not only the leaflets need to be repopulated but also the aortic root. Triton X-100 decellularization efficiency of the aortic root and repopulation with BM-MSC/SMC still needs to be investigated. In addition, we want to acknowledge that we are aware that the generation and preconditioning of a whole bio-active TEHV will require the use of a bioreactor culture system, and that reseeding of complete HV will be more complex than flat leaflet repopulation.

B. Generation of bio-active valvular tissues from the bottom up

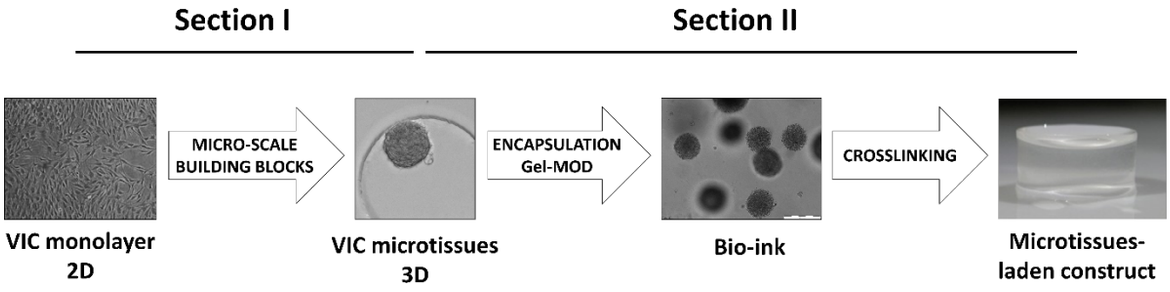

Schematic overview experimental outline Part B

The overall goal of Part B was to generate bio-active valvular tissue from the bottom-up. To achieve this goal, a step-wise approach was followed. The first step explored the possibility of generating micro-scale building blocks from VIC by generating 3D microtissues **(Chapter 3B, Section I)**. Next, gelatin was investigated as a valvular microtissues-carrier/encapsulation material, to obtain a bio-ink that can be used for the biofabrication of larger, macro-scale valvular tissue **(Chapter 3B, Section II)**.

Valvular micro-scale building blocks: criteria?

The first focus of Part B **(Chapter 3B, Section I)** was the generation of micro-scale tissue building blocks (micro-aggregates/microtissues) from VIC, with the long-term goal of using 3D bioprinting for the directed assembling of these valvular microtissues into a larger-scale valvular macrotissue [99, 100]. With this in mind it was important to use a technique that rapidly generated a large number of uniform microtissues (Ø <200µm) that do not obstruct and can easily pass through the printhead nozzle (Ø200-300µm). In addition, it was important to generate high-quality microtissues which resemble the native valve composition and contain native-like quiescent VIC that are able to produce and to remodel the ECM.

Generation of valvular microtissues: viability and the problem of calcification

The spontaneous self-assembly of VIC into 3D microtissues with predefined dimensions was explored by seeding VIC in agarose-molded non-adhesive microwells. This high throughput system has already been successfully used by other groups for the generation of homotypic and complex heterotypic micro-aggregates [171, 352, 404] and in our lab for the generation of hepatocyte [324] and fibrochondrocyte [405] micro-aggregates. Yet, this is the first time that non-adhesive, solid micro-aggregates were generated from VIC.

Before micro-aggregates can be generated, VIC need to be largely expanded. One of the main problems of working with VIC is the control of their activated/quiescent state. VIC are mechanosensitive cells and are known to have an increased myofibroblastic activity (activated state)

when cultured on stiff substrates, such as rigid polystyrene 2D culture substrates [241, 406, 407]. The transitional modulus between the quiescent and activated state in monolayer cultured VIC is approximately ≥15kPa [406]. Because 3D microtissues more closely resemble the actual *in vivo* microenvironment, it was hypothesized that VIC in these microtissues could regain their native, fibroblast-like quiescent phenotype while promoting VIC-mediated ECM production.

Unfortunately, when microtissues were formed and cultivated in standard culture medium, a rapid degeneration and calcification of the microtissues occurred. The *in vitro* calcification and nodule formation of VIC has already been shown in 2D high density monolayer cultures. When VIC reach confluency they spontaneously form multicellular non-size controllable aggregates that subsequently develop into calcified nodules [408]. The events initiating this process are still not clear. Increased cell proliferation, migration, activation, cell stress, apoptosis, and substrate modulus have all been attributed to causing nodule formation in 2D cultures, but no consensus has been reached [329, 408, 409]. In this research it was hypothesized that oxidative stress could be involved in the *in vitro* calcification of valvular microtissues. Several studies have already shown that oxidative stress is present in and contributes to calcification of the aortic valve [410-412]. In addition, oxidative stress accumulation has been associated with reduced antioxidant enzymes expression and increased DNA damage in the early stage of calcific aortic valve disease [413].

In an effort to optimize microtissue formation, AA was supplemented to the culture medium before aggregation started. AA has an anti-oxidant function and was presumed to reduce or inhibit the calcification of microtissues. Moreover, AA was also expected to stimulate ECM production of VIC, which could be favorable for microtissue formation. As hypothesized, adding AA resulted in the formation of viable, high-quality microtissues within 24h. By day 2-3 microtissues were solid and completely compacted (Ø 150 µm) and no signs of degeneration or calcification were noticed during the follow-up of 22 days. Interestingly, calcification of microtissues appeared to be a rapid occurring process, since adding AA once aggregates were formed (after 1 day) could not prevent calcification, yet, it did prevent further progression.

Towards native *in vivo*-like valvular microtissues

To ultimately produce a functional living tissue, microtissues should mimic the native cell phenotype and native tissue composition from which the living components produce ECM and other bio-active components (such as chemical signals, MMP/TIMPs).

The main ECM components produced by VIC in native HVL are GAG, elastin and collagens type I, III and V [13, 25, 336]. In this research, VIC in the generated microtissues were able to produce GAG,

elastin, collagen I fibrils, and reticular fibers (which mainly consist of collagen III [335]). In addition, biochemical quantification demonstrated that elastin, GAG and collagen content gradually increased over time. Compared to standard monolayer cultured VIC, microtissues also showed upregulated mRNA expression of collagen I/III/V, elastin, HA, biglycan, decorin and versican and the expression of MMP-1/2/3/9 and TIMP-1/2 was also elevated. This data clearly indicated matrix production of valve related ECM components and ECM remodeling in valvular microtissues**.**

It is previously mentioned that in normal valves VIC are considered to have a fibroblast-like quiescent phenotype and that 2D culture of VIC results in differentiation to a myofibroblastic activated state, which can be characterized by α-SMA expression [14]. We evidenced downregulation of this marker in the valvular microtissues indicating re-differentiation of VIC, to a more homeostatic quiescent state.

Gelatin as a bio-ink

As the final goal of the research is the controlled biofabrication of larger, macro-scale valvular tissue by bioprinting, the next step was to find a suitable printable and cell friendly bio-ink to combine with the valvular microtissues. **Table S3** shows that over the past ten years, several research groups have been evaluating PEG-, HA-, and gelatin hydrogels as encapsulation material for VIC. Although all these gels have been shown to be cell compatible, so far the group of Butcher et al. is the only one that has already applied these hydrogels for HV bioprinting purposes [231, 232, 234].

Because our research group has experience with the bioprinting of gelatin hydrogels, which have already been successfully used for the bioprinting of HepG2 cell- and primary hepatocyte aggregate-laden scaffolds [324, 355], it was assumed that gelatin could be a suitable bio-ink for the valvular microtissues as well.

Due to the thermo-reversible characteristics of gelatin, chemical covalent crosslinking is needed in order to form solid and stable gel-constructs [226, 233]. For this reason, gelatin was modified with methacrylate groups (Gel-MOD) which can be crosslinked with UV irradiation in the presence of a PI, such as Irgacure 2959 or VA-086. Irgacure has been largely used in tissue engineering and is considered as the golden standard for Gel-MOD crosslinking [254, 358]. Irgacure, in its native state, is non-cytotoxic. However, the photogenerated radical form of Irgacure can decrease cell viability and the optimal concentration of Irgacure to rapidly and efficiently crosslink the gels within a short irradiation time is absolutely essential to minimize the effect of the radical agents on the cells [354, 358]. On the other hand, both the inactive and the activated form of VA have shown to be cytocompatible and to have minimal effect on the cell viability [254, 358].

To investigate the impact of Gel-MOD on valvular microtissues, in the second section of Part B **(Chapter 3B, Section II)**, VIC aggregates were encapsulated in 10 or 20 w/v% Gel-MOD and photopolymerization of small constructs was performed in the presence of 2 mol% Irgacure or 20 mol% VA (relative to the methacrylamide chains).

Stability and viability of microtissues-laden constructs

Solid crosslinked hydrogel constructs were generated and gel fraction analysis showed that 85.5-87.3% (10-20 w/v% VA-crosslinked gels) or 90.5-97.5% (10-20 w/v% Irg-crosslinked gels) of the Gel-MOD was incorporated into the 3D network. Unfortunately, during the follow-up of the encapsulated microtissues, early disintegration of VA-crosslinked gels was noticed (around day 7 or 14, for 10 or 20 w/v% gels respectively), while Irg-crosslinked gels were stable for at least 14 days. This was unexpected since the concentration of 20 mol% VA has previously been shown to efficiently crosslink 3D bioprinted cell-laden gel-MOD constructs which were stable up to 14 days [255].

Further analysis of the hydrogels revealed that, although solid gels could be generated, the crosslinking extent was far less when VA was used, indicated by the remarkable higher swelling ratio compared to Irg-crosslinked gels. This could explain the early degeneration since less crosslinked gels could be more susceptible to solubilization at 37°C.

Nevertheless, microtissues remained viable in all gels during the complete study duration and viability was not influenced by the type of PI.

Influence of gel stiffness on proliferation, migration and fusion of the microtissues

Stiffness of the different hydrogels was determined and it was shown that 10 w/v% gels and VA-crosslinked gels were softer (lower compressive moduli) compared to 20 w/v% gels and Irgacure-crosslinked gels (higher compressive moduli). Based on the fact that stiffer hydrogels have denser networks and can delay the cell spreading process [353, 354], it was hypothesized that softer gels could enhance proliferation of VIC in microtissues and could be more favorable for VIC migration into the gel.

As expected, there were only a limited number of $Ki67^+$ cells found at the outer edges of the microtissues and the amount of these proliferative cells decreased over-time and with increasing stiffness of the gels. In addition, migration of VIC from microtissues into the gel was most pronounced in the softest 10 w/v% VA-crosslinked gels (5.0 kPa). Although not investigated in this thesis, it is likely that the softer hydrogels had larger and maybe interconnected pores which can also have favored migration. This is suggested since previous studies have already visualized an increase

in pore size and interconnectivity by decreasing gel-MOD concentration [353] and larger, but unconnected, pores were noticed in gel-MOD hydrogels when crosslinked using lower Irgacure concentrations [226].

As the overall goal is to generate a larger macro-scale valvular tissue, microtissues should be able to fuse in the hydrogel. For this reason, and based on the proliferation and migration capacity of VIC, which were more apparent in the soft gels, microtissues were encapsulated at a high density in 10 w/v% VA-crosslinked gels to investigate the potential fusion capacity.

With this preliminary and limited experiment we provided a proof of concept as we have shown that microtissues in these hydrogels were able to fuse within 3 days and larger valvular microtissues were formed in various sizes (±150-1400µm). These valvular microtissues also showed time-dependent increase of valve-related ECM components.

Impact of the bio-ink on cell phenotype and ECM production

We previously stated that to ultimately produce a functional living tissue, microtissues should mimic the native cell phenotype and native tissue composition and showed that microtissues were able to produce valve related ECM components while remaining in a quiescent state. Yet it was expected that the bio-ink itself and especially gel stiffness could possibly interfere or induce changes in cell phenotype and ECM production.

It is important to note that in contrast to 2D cultured VIC which are activated on stiff substrates (see: Generation of valvular microtissues: viability and the problem of calcification), encapsulated VIC respond differently to their substrate and show a reverse correlation between gel stiffness and VIC activation. It has previously been shown that; VIC express more α-SMA in 1.86 kPa gels compared to 5.19 kPa gels [227], VIC express very low α-SMA in 120 kPa gels [235], and dynamic stiffening of gels (0.24 to 13 kPa) can reduce the activation level of the encapsulated VIC [222]. The reported fibroblast-myofibroblast transitional modulus in 3D cultured encapsulated VIC is 4.80–9.60 kPa [406] or ~7 kPa [241] and takes place in the reverse direction compared to 2D cultured VIC. Also, this phenotype transition is somewhat unexpected since softer gels more reflect the *in vivo* mechanical properties of the native leaflets (±0.25-13.02 kPa [11, 12]), yet other biophysical signals including nanotopography, degradation mediated cellular traction, cellular attachment and spreading, anchoring of matrix fibers, and hydrogel type should also be considered as contributing factors in directing cell fate and should be further investigated.

In this research we have shown that the Gel-MOD encapsulated valvular microtissues were still able to produce heart valve related ECM components and there were no indications of calcification. In

addition, remodeling capacity and as expected also low α-SMA expression (~qVIC) was evidenced when encapsulated in Irgacure-crosslinked hydrogels (106.6kPa). However, some differences were noticed between encapsulated and non-encapsulated microtissues. First, encapsulated microtissues showed lower MMP-1/2/3/9 and TIMP-1 mRNA expression levels, indicating lower remodeling capacity. Secondly, more GAG production and elevated mRNA expression levels of HA, biglycan and decorin were noticed, while the expression or production of the other investigated ECM components remained the same, demonstrating selective stimulation of certain ECM molecules. Thirdly, a significant increase of Sox9 mRNA expression was noticed. The transcription factor Sox9 is required for ECM organization and plays an essential role in heart valve development [360, 361] but it is also an early chondrogenic marker and required for cartilage formation [362]. Yet we are not convinced that VIC did differentiate towards a chondrocyte phenotype, since mature chondrocyte specific collagen type II mRNA was not expressed [414] and further research is necessary to elucidate the role of Sox9 in encapsulated microtissues.

We have demonstrated that by encapsulating microtissues, changes in ECM formation and gene expression can be induced. Although only a limited amount of histological stainings were performed and mRNA expression was only analyzed on microtissues encapsulated in the stiffest Irgacure-crosslinked hydrogels, we believe that ECM production and possibly also VIC phenotype in the encapsulated microtissues could be influenced by the hydrogel stiffness, yet this needs to be further investigated. We also want to acknowledge that it is likely that the hydrogel type (Gel-MOD), and not only the stiffness, can enhance/inhibit ECM formation as it is already shown by Duan et al., that GAG content only significantly increased in Gel-MOD/HA-MA hybrid gels compared to pure HA-MA gels [227].

Conclusion

We have successfully applied a completely cell driven 3D approach that generated high-quality valvular microtissues (Ø 150µm) which resembled the native valve composition and contained native-like quiescent VIC that were able to produce and to remodel the ECM.

We also evidenced that Gel-MOD is a good encapsulation material for these microtissues and provided a proof of concept for the formation of larger valvular tissue by showing that microtissues were able to randomly assemble in soft gels and to fuse into larger microtissues (150-1400µm). For this reason, we believe that soft microtissues-laden Gel-MOD hydrogels (<5kPa) are suitable as a bio-ink for future biofabrication of larger-scale valvular macrotissue with predefined shapes, through directed assembly by bioprinting.

Study limitations and future perspectives

It is hypothesized that oxidative stress-induced cell death leads to the spontaneous dystrophic calcification of microtissues, since calcification can be prevented by the addition of the anti-oxidant AA. However, more evidence is needed (e.g. determination of ROS production/inhibition) before it can be stated that oxidative stress is indeed the driving factor behind the initiation and progression of this *in vitro* calcification.

We also want to point out that it is highly likely that optimization of the stability of soft VA-crosslinked Gel-MOD hydrogels will alter the mechanical properties which could potentially results in an undesirable increase of gel stiffness that could prevent fusion. For this reason, and the fact that it seems that the type of hydrogel can influence ECM formation, other soft gels should be evaluated in order to select the most appropriate one. In addition it is imperative to also investigate phenotype of soft gel-encapsulated microtissues.

CLINICAL RELEVANCE OF THE PRESENTED EXPERIMENTAL WORK

As already extensively discussed in the general introduction/discussion there is a need for a viable bio-active TEHV, that has growth, remodeling and regeneration capacity, is readily (off-the-shelf) available and is compatible with minimally invasive valve surgery since this may confer better outcomes than standard sternotomy [415, 416].

The TD-TE approach applied in this thesis used biological tissues as a starting point for the generation of completely cell free xenogeneic tissues. Decellularized tissues can be used to fabricate both conventional as well as minimally invasive valve replacement [416]. The discussed literature indicates that decellularization of allografts prior to implantation one day will become the standard pretreatment of allografts. However, we are not yet convinced that decellularized xenografts, regardless their off-the-shelf potential, will ever replace or outperform the conventional crosslinked porcine BHV and much more research should be performed regarding xeno-compatibility.

Currently there is an ongoing debate whether or not these tissues need to be pre-seeded prior to implantation and the questions still remain whether bio-active allografts could outperform the decellularized stand-alone allograft valves, whether ‘humanized’ xenografts could overcome the current problems of the stand-alone xenogeneic BHV but most important, especially for the pediatric population, whether these TEHV will indeed have growth capacity. If ‘humanizing’ xenogeneic scaffolds would appear not to be possible, then researchers should take a step back and more efforts should be made in the repopulation of already commercially available GA crosslinked BHV or in

finding an optimal alternative crosslinker, that improves both the longevity as well as the repopulation potential.

In the last 20 years there has not been any research group yet who succeeded in the generation of a completely repopulated biological heart valve, which makes us wonder if this will ever be possible. Yet the presented experimental work seems promising. Cells were distributed throughout all the layers of HVL and cell density reached almost native levels when VIC were used and satisfactory levels with BM-MSC. Although we acknowledge that there is still room for improvement, future efforts should now be made to extrapolate the proof-of-concept seeding of heart valve leaflets to complete heart valves, so that the above mentioned questions can finally be answered. However, it is worth mentioning that from a clinical point of view, this approach requires the utilization of autologous (stem) cells, and require the necessary complex infrastructure and time for cell isolation, cultivation and maturation of the seeded scaffolds prior to implantation.

To overcome the limitations of this traditional, non-off-the-shelf- approach that relies on resource-intensive, cell-based manufacturing, which increases cost and hinders clinical translation, other *in situ* tissue engineering approaches have emerged that aim to develop automated approaches for rapidly producing biomimetic heart valve scaffolds that elicit endogenous tissue remodeling, repair and potentially also growth (e.g. JetValves [417], dTEHV [159, 418, 419], etc.). Some of these valves have already been implanted in sheep [419] and the non-human primate model [159, 418] using minimally invasive techniques. Although the first results seem promising, they have yet to be replicated in humans.

The completely cell driven BU-TE approach applied in this thesis, resulted in the formation of bio-active quiescent valvular microtissues that can be encapsulated in a gelatin hydrogel and will ultimately be printed into larger valvular macrotissues with predefined shapes (ideally into hemodynamically competent viable valves upon implantation). Although bioprinting is not new in the domain of HVTE, and efforts are already being made to bioprint anatomically accurate viable valves, the approach of using microtissues instead of single cells is. In addition, in this approach the hydrogel acts as a temporary support material and tissue formation relies on fusion of the microtissues within and degradation of the gel, whereas other groups are investigating the possibility of bioprinting hydrogel encapsulated single cells and where the hydrogel acts as a viable scaffold.

We want to acknowledge that we are aware that we have just made the very first step and it is too early to state if a complex bio-active HV will ever be generated with this approach, and it is too soon to predict if bottom-up generated viable valves could be an alternative to the devices that are already largely employed in the field, as still so many things need to be explored (bio inks, cell types,

fusion capacity, ECM formation, viability of the tissues, degradation of the gel etc.). Regardless the fact that printing is a relatively low-cost technology, the bottom-up approach used in this work does not offer an 'off-the-shelf' valve replacement, since this approach also requires the utilization of autologous (stem) cells. However, the *in vitro* generation of an autologous viable heart valve that is made from scratch, is readily available for transplantation without the presence of any scaffold material so that it does not rely on scaffold recolonization or scaffold degradation, could be a tremendous asset.

We also want to highlight that this is the first time that 3D valvular microtissues were generated and that they could potentially not only be used for modular engineering, but might also offer a new platform to provide insights into valve (patho)biology. Almost all studies (mainly calcification studies) are currently performed, starting from 2D monolayer cultured highly α-SMA positive cells and a relevant native-like 3D model for toxicological/disease studies is still lacking. Findings from a 3D model that more accurately reflect the native heart valve are more likely to translate into improved clinical outcomes.

Overall we believe that TD-HVTE with biological tissues as a starting point, has made a lot of progression in developing better alternative HV substitutes. We are also slowly making progression towards a completely repopulated, bio-active TEHV, but we are definitely not there yet. Although alternatives for the adult population have emerged, we are still far away from developing an optimal bio-active TEHV with growth capacity, for the pediatric population, and other more "off-the-shelf" approaches should also be explored. Minimally invasive, low-cost and off-the-shelf available therapeutic technologies could have a tremendous impact on patients' lives across age-, social-, and geographical boundaries. We also want to state that although the proposed BU approach will never provide a clinical 'off-the-shelf" valve replacement, it is worth to further investigate the potential of biofabricating valvular tissue from the bottom-up, since a scaffold free, patient's own, functional, *in vitro* biofabricated heart valve could definitely be worth the cost. This technology could have invaluable clinical benefits in minimizing the number of (pediatric) re-operations even though it currently might seems a bit futuristic.

REFERENCES

1. Hinton RB, Yutzey KE. Heart valve structure and function in development and disease. Annual review of physiology. 2011;73:29-46.
2. Coffey S, Cairns BJ, Iung B. The modern epidemiology of heart valve disease. Heart. 2016;102(1):75-85.
3. Iung B, Vahanian A. Epidemiology of acquired valvular heart disease. The Canadian journal of cardiology. 2014;30(9):962-70.
4. Thubrikar M. The aortic valve. Boca Raton CRC press. 1990.
5. Charitos EI, Sievers HH. Anatomy of the aortic root: implications for valve-sparing surgery. Annals of cardiothoracic surgery. 2013;2(1):53-6.
6. Misfeld M, Sievers HH. Heart valve macro- and microstructure. Philosophical transactions of the Royal Society of London Series B, Biological sciences. 2007;362(1484):1421-36.
7. Sievers HH, Hemmer W, Beyersdorf F, Moritz A, Moosdorf R, Lichtenberg A, Misfeld M, Charitos EI, Working Group for Aortic Valve Surgery of German Society of T, Cardiovascular S. The everyday used nomenclature of the aortic root components: the tower of Babel? European journal of cardio-thoracic surgery : official journal of the European Association for Cardio-thoracic Surgery. 2012;41(3):478-82.
8. Vesely I. The role of elastin in aortic valve mechanics. Journal of biomechanics. 1998;31(2):115-23.
9. Leopold JA. Cellular mechanisms of aortic valve calcification. Circulation Cardiovascular interventions. 2012;5(4):605-14.
10. Acharya G, Armstrong M, McFall C, Quinn RW, Hilbert SL, Converse GL, Toth PB, Sherman AK, Lee CH, Lofland GK, Hopkins RA. Calcium and phosphorus concentrations in native and decellularized semilunar valve tissues. The Journal of heart valve disease. 2014;23(3):259-70.
11. Zhao R, Sider KL, Simmons CA. Measurement of layer-specific mechanical properties in multilayered biomaterials by micropipette aspiration. Acta biomaterialia. 2011;7(3):1220-7.
12. Vesely I, Noseworthy R. Micromechanics of the fibrosa and the ventricularis in aortic valve leaflets. Journal of biomechanics. 1992;25(1):101-13.
13. Latif N, Sarathchandra P, Taylor PM, Antoniw J, Yacoub MH. Localization and pattern of expression of extracellular matrix components in human heart valves. The Journal of heart valve disease. 2005;14(2):218-27.
14. Liu AC, Joag VR, Gotlieb AI. The emerging role of valve interstitial cell phenotypes in regulating heart valve pathobiology. The American journal of pathology. 2007;171(5):1407-18.
15. Gross L, Kugel MA. Topographic Anatomy and Histology of the Valves in the Human Heart. The American journal of pathology. 1931;7(5):445-74 7.
16. Butcher JT, Mahler GJ, Hockaday LA. Aortic valve disease and treatment: the need for naturally engineered solutions. Advanced drug delivery reviews. 2011;63(4-5):242-68.
17. Eckert CE, Fan R, Mikulis B, Barron M, Carruthers CA, Friebe VM, Vyavahare NR, Sacks MS. On the biomechanical role of glycosaminoglycans in the aortic heart valve leaflet. Acta biomaterialia. 2013;9(1):4653-60.
18. Gupta V, Tseng H, Lawrence BD, Grande-Allen KJ. Effect of cyclic mechanical strain on glycosaminoglycan and proteoglycan synthesis by heart valve cells. Acta biomaterialia. 2009;5(2):531-40.
19. Schoen FJ. Cardiac valves and valvular pathology: update on function, disease, repair, and replacement. Cardiovascular pathology : the official journal of the Society for Cardiovascular Pathology. 2005;14(4):189-94.
20. Balguid A, Driessen NJ, Mol A, Schmitz JP, Verheyen F, Bouten CV, Baaijens FP. Stress related collagen ultrastructure in human aortic valves--implications for tissue engineering. Journal of biomechanics. 2008;41(12):2612-7.
21. Yoshioka J, Lee RT. Vascularization as a potential enemy in valvular heart disease. Circulation. 2008;118(17):1694-6.
22. Schoen FJ. Evolving concepts of cardiac valve dynamics: the continuum of development, functional structure, pathobiology, and tissue engineering. Circulation. 2008;118(18):1864-80.
23. Weind KL, Ellis CG, Boughner DR. The aortic valve blood supply. The Journal of heart valve disease. 2000;9(1):1-7.
24. Schoen FJ. Aortic valve structure-function correlations: role of elastic fibers no longer a stretch of the imagination. The Journal of heart valve disease. 1997;6(1):1-6.
25. Cole WG, Chan D, Hickey AJ, Wilcken DE. Collagen composition of normal and myxomatous human mitral heart valves. Biochem J. 1984;219(2):451-60.
26. Grande-Allen KJ, Calabro A, Gupta V, Wight TN, Hascall VC, Vesely I. Glycosaminoglycans and proteoglycans in normal mitral valve leaflets and chordae: association with regions of tensile and compressive loading. Glycobiology. 2004;14(7):621-33.

27. Murata K. Acidic glycosaminoglycans in human heart valves. Journal of molecular and cellular cardiology. 1981;13(3):281-92.
28. Rothenburger M, Volker W, Vischer P, Glasmacher B, Scheld HH, Deiwick M. Ultrastructure of proteoglycans in tissue-engineered cardiovascular structures. Tissue engineering. 2002;8(6):1049-56.
29. Schoen FJ. Future directions in tissue heart valves: impact of recent insights from biology and pathology. The Journal of heart valve disease. 1999;8(4):350-8.
30. Deck JD. Endothelial cell orientation on aortic valve leaflets. Cardiovascular research. 1986;20(10):760-7.
31. Miragoli M, Yacoub MH, El-Hamamsy I, Sanchez-Alonso JL, Moshkov A, Mongkoldhumrongkul N, Padala M, Paramagurunathan S, Sarathchandra P, Korchev YE, Gorelik J, Chester AH. Side-specific mechanical properties of valve endothelial cells. American journal of physiology Heart and circulatory physiology. 2014;307(1):H15-24.
32. Simmons CA, Grant GR, Manduchi E, Davies PF. Spatial heterogeneity of endothelial phenotypes correlates with side-specific vulnerability to calcification in normal porcine aortic valves. Circulation research. 2005;96(7):792-9.
33. Rabkin E, Aikawa M, Stone JR, Fukumoto Y, Libby P, Schoen FJ. Activated interstitial myofibroblasts express catabolic enzymes and mediate matrix remodeling in myxomatous heart valves. Circulation. 2001;104(21):2525-32.
34. Hinton RB, Jr., Lincoln J, Deutsch GH, Osinska H, Manning PB, Benson DW, Yutzey KE. Extracellular matrix remodeling and organization in developing and diseased aortic valves. Circulation research. 2006;98(11):1431-8.
35. Rabkin-Aikawa E, Farber M, Aikawa M, Schoen FJ. Dynamic and reversible changes of interstitial cell phenotype during remodeling of cardiac valves. The Journal of heart valve disease. 2004;13(5):841-7.
36. Aikawa E, Whittaker P, Farber M, Mendelson K, Padera RF, Aikawa M, Schoen FJ. Human semilunar cardiac valve remodeling by activated cells from fetus to adult: implications for postnatal adaptation, pathology, and tissue engineering. Circulation. 2006;113(10):1344-52.
37. Latif N, Sarathchandra P, Chester AH, Yacoub MH. Expression of smooth muscle cell markers and co-activators in calcified aortic valves. European heart journal. 2015;36(21):1335-45.
38. Horne TE, VandeKopple M, Sauls K, Koenig SN, Anstine LJ, Garg V, Norris RA, Lincoln J. Dynamic Heterogeneity of the Heart Valve Interstitial Cell Population in Mitral Valve Health and Disease. Journal of cardiovascular development and disease. 2015;2(3):214-32.
39. Dreger SA, Taylor PM, Allen SP, Yacoub MH. Profile and localization of matrix metalloproteinases (MMPs) and their tissue inhibitors (TIMPs) in human heart valves. The Journal of heart valve disease. 2002;11(6):875-80.
40. Koullias GJ, Korkolis DP, Ravichandran P, Psyrri A, Hatzaras I, Elefteriadesa JA. Tissue microarray detection of matrix metalloproteinases, in diseased tricuspid and bicuspid aortic valves with or without pathology of the ascending aorta. Eur J Cardio-Thorac. 2004;26(6):1098-103.
41. Fondard O, Detaint D, Lung B, Choqueux C, Adle-Biassette H, Jarraya M, Hvass U, Couetil JP, Henin D, Michel JB, Vahanian A, Jacob MP. Extracellular matrix remodelling in human aortic valve disease: the role of matrix metalloproteinases and their tissue inhibitors. European heart journal. 2005;26(13):1333-41.
42. Latif N, Quillon A, Sarathchandra P, McCormack A, Lozanoski A, Yacoub MH, Chester AH. Modulation of human valve interstitial cell phenotype and function using a fibroblast growth factor 2 formulation. PloS one. 2015;10(6):e0127844.
43. Porras AM, van Engeland NC, Marchbanks E, McCormack A, Bouten CV, Yacoub MH, Latif N, Masters KS. Robust Generation of Quiescent Porcine Valvular Interstitial Cell Cultures. Journal of the American Heart Association. 2017;6(3).
44. Witt W, Buttner P, Jannasch A, Matschke K, Waldow T. Reversal of myofibroblastic activation by polyunsaturated fatty acids in valvular interstitial cells from aortic valves. Role of RhoA/G-actin/MRTF signalling. Journal of molecular and cellular cardiology. 2014;74:127-38.
45. Rajamannan NM, Subramaniam M, Rickard D, Stock SR, Donovan J, Springett M, Orszulak T, Fullerton DA, Tajik AJ, Bonow RO, Spelsberg T. Human aortic valve calcification is associated with an osteoblast phenotype. Circulation. 2003;107(17):2181-4.
46. Wirrig EE, Hinton RB, Yutzey KE. Differential expression of cartilage and bone-related proteins in pediatric and adult diseased aortic valves. Journal of molecular and cellular cardiology. 2011;50(3):561-9.
47. Caira FC, Stock SR, Gleason TG, McGee EC, Huang J, Bonow RO, Spelsberg TC, McCarthy PM, Rahimtoola SH, Rajamannan NM. Human degenerative valve disease is associated with up-regulation of low-

density lipoprotein receptor-related protein 5 receptor-mediated bone formation. Journal of the American College of Cardiology. 2006;47(8):1707-12.
48. Hjortnaes J, Goettsch C, Hutcheson JD, Camci-Unal G, Lax L, Scherer K, Body S, Schoen FJ, Kluin J, Khademhosseini A, Aikawa E. Simulation of early calcific aortic valve disease in a 3D platform: A role for myofibroblast differentiation. Journal of molecular and cellular cardiology. 2016;94:13-20.
49. Bowler MA, Merryman WD. In vitro models of aortic valve calcification: solidifying a system. Cardiovascular pathology : the official journal of the Society for Cardiovascular Pathology. 2015;24(1):1-10.
50. Nkomo VT, Gardin JM, Skelton TN, Gottdiener JS, Scott CG, Enriquez-Sarano M. Burden of valvular heart diseases: a population-based study. Lancet. 2006;368(9540):1005-11.
51. Benjamin EJ, Blaha MJ, Chiuve SE, Cushman M, Das SR, Deo R, de Ferranti SD, Floyd J, Fornage M, Gillespie C, Isasi CR, Jimenez MC, Jordan LC, Judd SE, Lackland D, Lichtman JH, Lisabeth L, Liu S, Longenecker CT, Mackey RH, Matsushita K, Mozaffarian D, Mussolino ME, Nasir K, Neumar RW, Palaniappan L, Pandey DK, Thiagarajan RR, Reeves MJ, Ritchey M, Rodriguez CJ, Roth GA, Rosamond WD, Sasson C, Towfighi A, Tsao CW, Turner MB, Virani SS, Voeks JH, Willey JZ, Wilkins JT, Wu JH, Alger HM, Wong SS, Muntner P, American Heart Association Statistics C, Stroke Statistics S. Heart Disease and Stroke Statistics-2017 Update: A Report From the American Heart Association. Circulation. 2017.
52. Ford ES, Ajani UA, Croft JB, Critchley JA, Labarthe DR, Kottke TE, Giles WH, Capewell S. Explaining the decrease in U.S. deaths from coronary disease, 1980-2000. The New England journal of medicine. 2007;356(23):2388-98.
53. Iung B, Baron G, Tornos P, Gohlke-Barwolf C, Butchart EG, Vahanian A. Valvular heart disease in the community: a European experience. Current problems in cardiology. 2007;32(11):609-61.
54. Bonow RO, Carabello BA, Chatterjee K, de Leon AC, Faxon DP, Freed MD, Gaasch WH, Lytle BW, Nishimura RA, O'Gara PT, O'Rourke RA, Otto CM, Shah PM, Shanewise JS, Nishimura RA, Carabello BA, Faxon DP, Freed MD, Lytle BW, O'Gara PT, Sidney C, Jacobs AK, Buller CE, Creager MA, Ettinger SM, Krumholz HM, Kushner FG, Nishimura RA, Page RL, Tarkington LG, Yancy CW. 2008 focused update incorporated into the ACC/AHA 2006 guidelines for the management of patients with valvular heart disease - A report of the American College of Cardiology American Heart Association task force on practice guidelines (writing committee to revise the 1998 guidelines for the management of patients with valvular heart disease) - Endorsed by the Society of Cardiovascular Anesthesiologists, Society for Cardiovascular Angiography and Interventions, and Society of Thoracic Surgeons. J Am Coll Cardiol. 2008;52(13):E1-E142.
55. Thaden JJ, Nkomo VT, Enriquez-Sarano M. The global burden of aortic stenosis. Progress in cardiovascular diseases. 2014;56(6):565-71.
56. Helms AS, Bach DS. Heart valve disease. Primary care. 2013;40(1):91-108.
57. Wallby L, Steffensen T, Jonasson L, Broqvist M. Inflammatory Characteristics of Stenotic Aortic Valves: A Comparison between Rheumatic and Nonrheumatic Aortic Stenosis. Cardiology research and practice. 2013;2013:895215.
58. Mohammadi H, Mequanint K. Prosthetic aortic heart valves: modeling and design. Medical engineering & physics. 2011;33(2):131-47.
59. Zoghbi WA, Enriquez-Sarano M, Foster E, Grayburn PA, Kraft CD, Levine RA, Nihoyannopoulos P, Otto CM, Quinones MA, Rakowski H, Stewart WJ, Waggoner A, Weissman NJ, American Society of E. Recommendations for evaluation of the severity of native valvular regurgitation with two-dimensional and Doppler echocardiography. Journal of the American Society of Echocardiography : official publication of the American Society of Echocardiography. 2003;16(7):777-802.
60. Yacoub MH, Takkenberg JJ. Will heart valve tissue engineering change the world? Nature clinical practice Cardiovascular medicine. 2005;2(2):60-1.
61. Pibarot P, Dumesnil JG. Prosthetic heart valves: selection of the optimal prosthesis and long-term management. Circulation. 2009;119(7):1034-48.
62. Vongpatanasin W, Hillis LD, Lange RA. Prosthetic heart valves. The New England journal of medicine. 1996;335(6):407-16.
63. Gravel JA. Surgical treatment of aortic insufficiency. Can Med Assoc J. 1955;72(8):599-601.
64. Hufnagel CA, Harvey WP, Rabil PJ, Mc DT. Surgical correction of aortic insufficiency. Surgery. 1954;35(5):673-83.
65. Starr A, Edwards ML. Mitral Replacement - Clinical Experience with a Ball-Valve Prosthesis. Ann Surg. 1961;154(4):726-&.
66. Hammermeister KE, Sethi GK, Henderson WG, Oprian C, Kim T, Rahimtoola S. A comparison of outcomes in men 11 years after heart-valve replacement with a mechanical valve or bioprosthesis. Veterans

Affairs Cooperative Study on Valvular Heart Disease. The New England journal of medicine. 1993;328(18):1289-96.
67. Ribeiro PA, Al Zaibag M, Idris M, Al Kasab S, Davies G, Mashat E, Wareham E, Al Fagih M. Antiplatelet drugs and the incidence of thromboembolic complications of the St. Jude Medical aortic prosthesis in patients with rheumatic heart disease. The Journal of thoracic and cardiovascular surgery. 1986;91(1):92-8.
68. Halkos ME, Puskas JD. Are all bileaflet mechanical valves equal? Curr Opin Cardiol. 2009;24(2):136-41.
69. Tillquist MN, Maddox TM. Cardiac crossroads: deciding between mechanical or bioprosthetic heart valve replacement. Patient preference and adherence. 2011;5:91-9.
70. Matthews AM. The development of the Starr-Edwards heart valve. Texas Heart Institute journal / from the Texas Heart Institute of St Luke's Episcopal Hospital, Texas Children's Hospital. 1998;25(4):282-93.
71. Leon MB, Smith CR, Mack M, Miller DC, Moses JW, Svensson LG, Tuzcu EM, Webb JG, Fontana GP, Makkar RR, Brown DL, Block PC, Guyton RA, Pichard AD, Bavaria JE, Herrmann HC, Douglas PS, Petersen JL, Akin JJ, Anderson WN, Wang D, Pocock S. Transcatheter aortic-valve implantation for aortic stenosis in patients who cannot undergo surgery. The New England journal of medicine. 2010;363(17):1597-607.
72. Filova E, Straka F, Mirejovsky T, Masin J, Bacakova L. Tissue-engineered heart valves. Physiological research / Academia Scientiarum Bohemoslovaca. 2009;58 Suppl 2:S141-58.
73. O'Brien MF, Stafford EG, Gardner MA, Pohlner PG, McGiffin DC. A comparison of aortic valve replacement with viable cryopreserved and fresh allograft valves, with a note on chromosomal studies. The Journal of thoracic and cardiovascular surgery. 1987;94(6):812-23.
74. Murray G. Homologous aortic-valve-segment transplants as surgical treatment for aortic and mitral insufficiency. Angiology. 1956;7(5):466-71.
75. Ross DN. Homograft replacement of the aortic valve. Lancet. 1962;2(7254):487.
76. Delmo Walter EM, de By TM, Meyer R, Hetzer R. The future of heart valve banking and of homografts: perspective from the Deutsches Herzzentrum Berlin. HSR proceedings in intensive care & cardiovascular anesthesia. 2012;4(2):97-108.
77. Mitchell RN, Jonas RA, Schoen FJ. Pathology of explanted cryopreserved allograft heart valves: comparison with aortic valves from orthotopic heart transplants. The Journal of thoracic and cardiovascular surgery. 1998;115(1):118-27.
78. Ross DN. Replacement of aortic and mitral valves with a pulmonary autograft. Lancet. 1967;2(7523):956-8.
79. Kouchoukos NT, Masetti P, Nickerson NJ, Castner CF, Shannon WD, Davila-Roman VG. The Ross procedure: long-term clinical and echocardiographic follow-up. The Annals of thoracic surgery. 2004;78(3):773-81.
80. El-Hamamsy I, Eryigit Z, Stevens LM, Sarang Z, George R, Clark L, Melina G, Takkenberg JJ, Yacoub MH. Long-term outcomes after autograft versus homograft aortic root replacement in adults with aortic valve disease: a randomised controlled trial. Lancet. 2010;376(9740):524-31.
81. Simon P, Aschauer C, Moidl R, Marx M, Keznickl FP, Eigenbauer E, Wolner E, Wollenek G. Growth of the pulmonary autograft after the Ross operation in childhood. European journal of cardio-thoracic surgery : official journal of the European Association for Cardio-thoracic Surgery. 2001;19(2):118-21.
82. Cameron DE, Vricella LA. What is the proper place of the Ross procedure in our modern armamentarium? Current cardiology reports. 2007;9(2):93-8.
83. Grunkemeier GL, Bodnar E. Comparative assessment of bioprosthesis durability in the aortic position. The Journal of heart valve disease. 1995;4(1):49-55.
84. Grunkemeier GL, Bodnar E. Comparison of structural valve failure among different 'models' of homograft valves. The Journal of heart valve disease. 1994;3(5):556-60.
85. Duran CG, Gunning AJ. Heterologous Aortic-Valve Transplantation in the Dog. Lancet. 1965;2(7403):114-5.
86. Binet JP, Duran CG, Carpenter A, Langlois J. Heterologous aortic valve transplantation. Lancet. 1965;2(7425):1275.
87. Ionescu MI, Wooler GH, Smith DR, Grimshaw VA. Mitral valve replacement with aortic heterografts in humans. Thorax. 1967;22(4):305-13.
88. Carpentier A, Lemaigre G, Robert L, Carpentier S, Dubost C. Biological factors affecting long-term results of valvular heterografts. The Journal of thoracic and cardiovascular surgery. 1969;58(4):467-83.
89. Siddiqui RF, Abraham JR, Butany J. Bioprosthetic heart valves: modes of failure. Histopathology. 2009;55(2):135-44.

90. Schmidt D, Stock UA, Hoerstrup SP. Tissue engineering of heart valves using decellularized xenogeneic or polymeric starter matrices. Philosophical transactions of the Royal Society of London Series B, Biological sciences. 2007;362(1484):1505-12.
91. Ionescu MI, Pakrashi BC, Holden MP, Mary DA, Wooler GH. Results of aortic valve replacement with frame-supported fascia lata and pericardial grafts. The Journal of thoracic and cardiovascular surgery. 1972;64(3):340-53.
92. McKinley OL. Human Anatomy.Third edition.
93. Ishihara T, Ferrans VJ, Jones M, Boyce SW, Roberts WC. Structure of bovine parietal pericardium and of unimplanted Ionescu-Shiley pericardial valvular bioprostheses. The Journal of thoracic and cardiovascular surgery. 1981;81(5):747-57.
94. Courtman DW, Pereira CA, Kashef V, McComb D, Lee JM, Wilson GJ. Development of a pericardial acellular matrix biomaterial: biochemical and mechanical effects of cell extraction. Journal of biomedical materials research. 1994;28(6):655-66.
95. Schoen FJ, Levy RJ. Founder's Award, 25th Annual Meeting of the Society for Biomaterials, perspectives. Providence, RI, April 28-May 2, 1999. Tissue heart valves: current challenges and future research perspectives. Journal of biomedical materials research. 1999;47(4):439-65.
96. Hammermeister K, Sethi GK, Henderson WG, Grover FL, Oprian C, Rahimtoola SH. Outcomes 15 years after valve replacement with a mechanical versus a bioprosthetic valve: final report of the Veterans Affairs randomized trial. Journal of the American College of Cardiology. 2000;36(4):1152-8.
97. Rahimtoola SH. Choice of prosthetic heart valve in adults an update. Journal of the American College of Cardiology. 2010;55(22):2413-26.
98. Grauss RW, Hazekamp MG, Oppenhuizen F, van Munsteren CJ, Gittenberger-de Groot AC, DeRuiter MC. Histological evaluation of decellularised porcine aortic valves: matrix changes due to different decellularisation methods. European journal of cardio-thoracic surgery : official journal of the European Association for Cardio-thoracic Surgery. 2005;27(4):566-71.
99. Nichol JW, Khademhosseini A. Modular Tissue Engineering: Engineering Biological Tissues from the Bottom Up. Soft matter. 2009;5(7):1312-9.
100. Lu T, Li Y, Chen T. Techniques for fabrication and construction of three-dimensional scaffolds for tissue engineering. International journal of nanomedicine. 2013;8:337-50.
101. Lu TL, Li YH, Chen T. Techniques for fabrication and construction of three-dimensional scaffolds for tissue engineering. International Journal of Nanomedicine. 2013;8:337-50.
102. Jana S, Tranquillo RT, Lerman A. Cells for tissue engineering of cardiac valves. Journal of tissue engineering and regenerative medicine. 2016;10(10):804-24.
103. Somers P, de Somer F, Cornelissen M, Thierens H, Van Nooten G. Bioactive porcine matrices in heart valve tissue engineering. The Journal of heart valve disease. 2012;21(4):535-43.
104. Tudorache I, Calistru A, Baraki H, Meyer T, Hoffler K, Sarikouch S, Bara C, Gorler A, Hartung D, Hilfiker A, Haverich A, Cebotari S. Orthotopic replacement of aortic heart valves with tissue-engineered grafts. Tissue engineering Part A. 2013;19(15-16):1686-94.
105. Iop L, Renier V, Naso F, Piccoli M, Bonetti A, Gandaglia A, Pozzobon M, Paolin A, Ortolani F, Marchini M, Spina M, De Coppi P, Sartore S, Gerosa G. The influence of heart valve leaflet matrix characteristics on the interaction between human mesenchymal stem cells and decellularized scaffolds. Biomaterials. 2009;30(25):4104-16.
106. Engelmayr GC, Jr., Sales VL, Mayer JE, Jr., Sacks MS. Cyclic flexure and laminar flow synergistically accelerate mesenchymal stem cell-mediated engineered tissue formation: Implications for engineered heart valve tissues. Biomaterials. 2006;27(36):6083-95.
107. Ramaswamy S, Boronyak SM, Le T, Holmes A, Sotiropoulos F, Sacks MS. A novel bioreactor for mechanobiological studies of engineered heart valve tissue formation under pulmonary arterial physiological flow conditions. Journal of biomechanical engineering. 2014;136(12):121009.
108. Ruel J, Lachance G. A new bioreactor for the development of tissue-engineered heart valves. Annals of biomedical engineering. 2009;37(4):674-81.
109. Merryman WD. Development of a tissue engineered heart valve for pediatrics: a case study in bioengineering ethics. Science and engineering ethics. 2008;14(1):93-101.
110. Causa F, Netti PA, Ambrosio L. A multi-functional scaffold for tissue regeneration: the need to engineer a tissue analogue. Biomaterials. 2007;28(34):5093-9.
111. Sodian R, Hoerstrup SP, Sperling JS, Daebritz S, Martin DP, Moran AM, Kim BS, Schoen FJ, Vacanti JP, Mayer JE, Jr. Early in vivo experience with tissue-engineered trileaflet heart valves. Circulation. 2000;102(19 Suppl 3):III22-9.

112. Rabkin E, Schoen FJ. Cardiovascular tissue engineering. Cardiovascular pathology : the official journal of the Society for Cardiovascular Pathology. 2002;11(6):305-17.
113. Ulery BD, Nair LS, Laurencin CT. Biomedical Applications of Biodegradable Polymers. Journal of polymer science Part B, Polymer physics. 2011;49(12):832-64.
114. Neuenschwander S, Hoerstrup SP. Heart valve tissue engineering. Transplant immunology. 2004;12(3-4):359-65.
115. Rosso F, Marino G, Giordano A, Barbarisi M, Parmeggiani D, Barbarisi A. Smart materials as scaffolds for tissue engineering. Journal of cellular physiology. 2005;203(3):465-70.
116. Rosso F, Marino G, Giordano A, Barbarisi M, Parmeggiani D, Barbarisi A. Smart materials as scaffolds for tissue engineering. Journal of cellular physiology. 2005;203(3):465-70.
117. Fallahiarezoudar E, Ahmadipourroudposht M, Idris A, Mohd Yusof N. A review of: application of synthetic scaffold in tissue engineering heart valves. Materials science & engineering C, Materials for biological applications. 2015;48:556-65.
118. Brody S, Pandit A. Approaches to heart valve tissue engineering scaffold design. Journal of biomedical materials research Part B, Applied biomaterials. 2007;83(1):16-43.
119. Murphy SV, Atala A. Organ engineering--combining stem cells, biomaterials, and bioreactors to produce bioengineered organs for transplantation. BioEssays : news and reviews in molecular, cellular and developmental biology. 2013;35(3):163-72.
120. Sewell-Loftin MK, Chun YW, Khademhosseini A, Merryman WD. EMT-inducing biomaterials for heart valve engineering: taking cues from developmental biology. Journal of cardiovascular translational research. 2011;4(5):658-71.
121. Taylor PM, Allen SP, Dreger SA, Yacoub MH. Human cardiac valve interstitial cells in collagen sponge: a biological three-dimensional matrix for tissue engineering. The Journal of heart valve disease. 2002;11(3):298-306.
122. Badylak SF. Xenogeneic extracellular matrix as a scaffold for tissue reconstruction. Transplant immunology. 2004;12(3-4):367-77.
123. Brown BN, Badylak SF. Extracellular matrix as an inductive scaffold for functional tissue reconstruction. Translational research : the journal of laboratory and clinical medicine. 2014;163(4):268-85.
124. Nimni ME, Cheung D, Strates B, Kodama M, Sheikh K. Chemically modified collagen: a natural biomaterial for tissue replacement. Journal of biomedical materials research. 1987;21(6):741-71.
125. O'Brien TK, Gabbay S, Parkes AC, Knight RA, Zalesky PJ. Immunological reactivity to a new glutaraldehyde tanned bovine pericardial heart valve. Transactions - American Society for Artificial Internal Organs. 1984;30:440-4.
126. Yannas IV, Ratner BD, Hoffman AS, Schoen FJ, Lemons JE. Biomaterial Science. 1997:84-94.
127. Schmidt CE, Baier JM. Acellular vascular tissues: natural biomaterials for tissue repair and tissue engineering. Biomaterials. 2000;21(22):2215-31.
128. Galili U, Shohet SB, Kobrin E, Stults CL, Macher BA. Man, apes, and Old World monkeys differ from other mammals in the expression of alpha-galactosyl epitopes on nucleated cells. The Journal of biological chemistry. 1988;263(33):17755-62.
129. Knight RL, Wilcox HE, Korossis SA, Fisher J, Ingham E. The use of acellular matrices for the tissue engineering of cardiac valves. Proceedings of the Institution of Mechanical Engineers Part H, Journal of engineering in medicine. 2008;222(1):129-43.
130. Badylak SF. Decellularized allogeneic and xenogeneic tissue as a bioscaffold for regenerative medicine: factors that influence the host response. Annals of biomedical engineering. 2014;42(7):1517-27.
131. Vesely I. Heart valve tissue engineering. Circulation research. 2005;97(8):743-55.
132. Moroni F, Mirabella T. Decellularized matrices for cardiovascular tissue engineering. American journal of stem cells. 2014;3(1):1-20.
133. Gilbert TW, Sellaro TL, Badylak SF. Decellularization of tissues and organs. Biomaterials. 2006;27(19):3675-83.
134. Arenas-Herrera JE, Ko IK, Atala A, Yoo JJ. Decellularization for whole organ bioengineering. Biomedical materials. 2013;8(1):014106.
135. Seddon AM, Curnow P, Booth PJ. Membrane proteins, lipids and detergents: not just a soap opera. Biochimica et biophysica acta. 2004;1666(1-2):105-17.
136. Gilbert TW. Strategies for tissue and organ decellularization. Journal of cellular biochemistry. 2012;113(7):2217-22.

137. Wainwright JM, Czajka CA, Patel UB, Freytes DO, Tobita K, Gilbert TW, Badylak SF. Preparation of cardiac extracellular matrix from an intact porcine heart. Tissue engineering Part C, Methods. 2010;16(3):525-32.
138. Crapo PM, Gilbert TW, Badylak SF. An overview of tissue and whole organ decellularization processes. Biomaterials. 2011;32(12):3233-43.
139. O'Brien MF, Goldstein S, Walsh S, Black KS, Elkins R, Clarke D. The SynerGraft valve: a new acellular (nonglutaraldehyde-fixed) tissue heart valve for autologous recellularization first experimental studies before clinical implantation. Seminars in thoracic and cardiovascular surgery. 1999;11(4 Suppl 1):194-200.
140. Simon P, Kasimir MT, Seebacher G, Weigel G, Ullrich R, Salzer-Muhar U, Rieder E, Wolner E. Early failure of the tissue engineered porcine heart valve SYNERGRAFT in pediatric patients. European journal of cardio-thoracic surgery : official journal of the European Association for Cardio-thoracic Surgery. 2003;23(6):1002-6.
141. Kasimir MT, Rieder E, Seebacher G, Wolner E, Weigel G, Simon P. Presence and elimination of the xenoantigen gal (alpha1, 3) gal in tissue-engineered heart valves. Tissue engineering. 2005;11(7-8):1274-80.
142. Elkins RC, Dawson PE, Goldstein S, Walsh SP, Black KS. Decellularized human valve allografts. The Annals of thoracic surgery. 2001;71(5 Suppl):S428-32.
143. Dohmen PM, Ozaki S, Verbeken E, Yperman J, Flameng W, Konertz WF. Tissue engineering of an auto-xenograft pulmonary heart valve. Asian cardiovascular & thoracic annals. 2002;10(1):25-30.
144. Bloch O, Golde P, Dohmen PM, Posner S, Konertz W, Erdbrugger W. Immune response in patients receiving a bioprosthetic heart valve: lack of response with decellularized valves. Tissue engineering Part A. 2011;17(19-20):2399-405.
145. Wiles K, Fishman JM, De Coppi P, Birchall MA. The Host Immune Response to Tissue-Engineered Organs: Current Problems and Future Directions. Tissue engineering Part B, Reviews. 2016;22(3):208-19.
146. Schoen FJ, Golomb G, Levy RJ. Calcification of bioprosthetic heart valves: a perspective on models. The Journal of heart valve disease. 1992;1(1):110-4.
147. Gallegos RP, Nockel PJ, Rivard AL, Bianco RW. The current state of in-vivo pre-clinical animal models for heart valve evaluation. The Journal of heart valve disease. 2005;14(3):423-32.
148. Zaragoza C, Gomez-Guerrero C, Martin-Ventura JL, Blanco-Colio L, Lavin B, Mallavia B, Tarin C, Mas S, Ortiz A, Egido J. Animal models of cardiovascular diseases. J Biomed Biotechnol. 2011;2011:497841.
149. Goodman SL. Sheep, pig, and human platelet-material interactions with model cardiovascular biomaterials. Journal of biomedical materials research. 1999;45(3):240-50.
150. Gross DR. Thromboembolic phenomena and the use of the pig as an appropriate animal model for research on cardiovascular devices. The International journal of artificial organs. 1997;20(4):195-203.
151. Honge JL, Funder J, Hansen E, Dohmen PM, Konertz W, Hasenkam JM. Recellularization of aortic valves in pigs. European journal of cardio-thoracic surgery : official journal of the European Association for Cardio-thoracic Surgery. 2011;39(6):829-34.
152. Honge JL, Funder JA, Pedersen TB, Kronborg MB, Hasenkam JM. Degenerative processes in bioprosthetic mitral valves in juvenile pigs. Journal of cardiothoracic surgery. 2011;6:72.
153. Grehan JF, Hilbert SL, Ferrans VJ, Droel JS, Salerno CT, Bianco RW. Development and evaluation of a swine model to assess the preclinical safety of mechanical heart valves. The Journal of heart valve disease. 2000;9(5):710-9.
154. Swan H, Piermattei DL. Technical aspects of cardiac transplantation in the pig. The Journal of thoracic and cardiovascular surgery. 1971;61(5):710-23.
155. Salerno CT, Droel J, Bianco RW. Current state of in vivo preclinical heart valve evaluation. The Journal of heart valve disease. 1998;7(2):158-62.
156. Flameng W, Meuris B, Yperman J, De Visscher G, Herijgers P, Verbeken E. Factors influencing calcification of cardiac bioprostheses in adolescent sheep. The Journal of thoracic and cardiovascular surgery. 2006;132(1):89-98.
157. Ali ML, Kumar SP, Bjornstad K, Duran CM. The sheep as an animal model for heart valve research. Cardiovascular surgery. 1996;4(4):543-9.
158. Hopkins RA, Bert AA, Hilbert SL, Quinn RW, Brasky KM, Drake WB, Lofland GK. Bioengineered human and allogeneic pulmonary valve conduits chronically implanted orthotopically in baboons: hemodynamic performance and immunologic consequences. The Journal of thoracic and cardiovascular surgery. 2013;145(4):1098-107.
159. Weber B, Dijkman PE, Scherman J, Sanders B, Emmert MY, Grunenfelder J, Verbeek R, Bracher M, Black M, Franz T, Kortsmit J, Modregger P, Peter S, Stampanoni M, Robert J, Kehl D, van Doeselaar M, Schweiger M, Brokopp CE, Walchli T, Falk V, Zilla P, Driessen-Mol A, Baaijens FP, Hoerstrup SP. Off-the-shelf

human decellularized tissue-engineered heart valves in a non-human primate model. Biomaterials. 2013;34(30):7269-80.
160. Weber B, Scherman J, Emmert MY, Gruenenfelder J, Verbeek R, Bracher M, Black M, Kortsmit J, Franz T, Schoenauer R, Baumgartner L, Brokopp C, Agarkova I, Wolint P, Zund G, Falk V, Zilla P, Hoerstrup SP. Injectable living marrow stromal cell-based autologous tissue engineered heart valves: first experiences with a one-step intervention in primates. European heart journal. 2011;32(22):2830-40.
161. Trantina-Yates A, Weissenstein C, Human P, Zilla P. Stentless bioprosthetic heart valve research: sheep versus primate model. The Annals of thoracic surgery. 2001;71(5 Suppl):S422-7.
162. Lehner G, Fischlein T, Baretton G, Murphy JG, Reichart B. Endothelialized biological heart valve prostheses in the non-human primate model. European journal of cardio-thoracic surgery : official journal of the European Association for Cardio-thoracic Surgery. 1997;11(3):498-504.
163. Zhang LG, Zhong DH, Zhang Y, Li CZ, Kisaalita WS, Wu ZZ. A microwell pattern for C17.2 cell aggregate formation with concave cylindrical surface induced cell peeling. Biomaterials. 2014;35(35):9423-37.
164. Knight E, Przyborski S. Advances in 3D cell culture technologies enabling tissue-like structures to be created in vitro. J Anat. 2015;227(6):746-56.
165. Mazzoleni G, Di Lorenzo D, Steimberg N. Modelling tissues in 3D: the next future of pharmaco-toxicology and food research? Genes & nutrition. 2009;4(1):13-22.
166. Huh D, Hamilton GA, Ingber DE. From 3D cell culture to organs-on-chips. Trends Cell Biol. 2011;21(12):745-54.
167. Gunter J, Wolint P, Bopp A, Steiger J, Cambria E, Hoerstrup SP, Emmert MY. Microtissues in Cardiovascular Medicine: Regenerative Potential Based on a 3D Microenvironment. Stem cells international. 2016;2016:9098523.
168. Jakab K, Norotte C, Marga F, Murphy K, Vunjak-Novakovic G, Forgacs G. Tissue engineering by self-assembly and bio-printing of living cells. Biofabrication. 2010;2(2):022001.
169. Murphy SV, Atala A. 3D bioprinting of tissues and organs. Nature biotechnology. 2014;32(8):773-85.
170. Achilli TM, Meyer J, Morgan JR. Advances in the formation, use and understanding of multi-cellular spheroids. Expert opinion on biological therapy. 2012;12(10):1347-60.
171. Moreira Teixeira LS, Leijten JC, Sobral J, Jin R, van Apeldoorn AA, Feijen J, van Blitterswijk C, Dijkstra PJ, Karperien M. High throughput generated micro-aggregates of chondrocytes stimulate cartilage formation in vitro and in vivo. European cells & materials. 2012;23:387-99.
172. Mol A, Bouten CV, Baaijens FP, Zund G, Turina MI, Hoerstrup SP. Review article: Tissue engineering of semilunar heart valves: current status and future developments. The Journal of heart valve disease. 2004;13(2):272-80.
173. Schenke-Layland K, Opitz F, Gross M, Doring C, Halbhuber KJ, Schirrmeister F, Wahlers T, Stock UA. Complete dynamic repopulation of decellularized heart valves by application of defined physical signals-an in vitro study. Cardiovascular research. 2003;60(3):497-509.
174. Asahara T, Murohara T, Sullivan A, Silver M, van der Zee R, Li T, Witzenbichler B, Schatteman G, Isner JM. Isolation of putative progenitor endothelial cells for angiogenesis. Science. 1997;275(5302):964-7.
175. Ii M. Bone marrow-derived endothelial progenitor cells: isolation and characterization for myocardial repair. Methods in molecular biology. 2010;660:9-27.
176. Schmidt D, Achermann J, Odermatt B, Genoni M, Zund G, Hoerstrup SP. Cryopreserved amniotic fluid-derived cells: a lifelong autologous fetal stem cell source for heart valve tissue engineering. The Journal of heart valve disease. 2008;17(4):446-55.
177. Schmidt D, Achermann J, Odermatt B, Breymann C, Mol A, Genoni M, Zund G, Hoerstrup SP. Prenatally fabricated autologous human living heart valves based on amniotic fluid derived progenitor cells as single cell source. Circulation. 2007;116(11 Suppl):I64-70.
178. Schmidt D, Mol A, Odermatt B, Neuenschwander S, Breymann C, Gossi M, Genoni M, Zund G, Hoerstrup SP. Engineering of biologically active living heart valve leaflets using human umbilical cord-derived progenitor cells. Tissue engineering. 2006;12(11):3223-32.
179. Aggarwal S, Pittenger MF. Human mesenchymal stem cells modulate allogeneic immune cell responses. Blood. 2005;105(4):1815-22.
180. Desai VD, Hsia HC, Schwarzbauer JE. Reversible modulation of myofibroblast differentiation in adipose-derived mesenchymal stem cells. PloS one. 2014;9(1):e86865.
181. Tamama K, Sen CK, Wells A. Differentiation of bone marrow mesenchymal stem cells into the smooth muscle lineage by blocking ERK/MAPK signaling pathway. Stem cells and development. 2008;17(5):897-908.
182. Oswald J, Boxberger S, Jorgensen B, Feldmann S, Ehninger G, Bornhauser M, Werner C. Mesenchymal stem cells can be differentiated into endothelial cells in vitro. Stem cells. 2004;22(3):377-84.

183. Colazzo F, Sarathchandra P, Smolenski RT, Chester AH, Tseng YT, Czernuszka JT, Yacoub MH, Taylor PM. Extracellular matrix production by adipose-derived stem cells: implications for heart valve tissue engineering. Biomaterials. 2011;32(1):119-27.
184. Ku CH, Johnson PH, Batten P, Sarathchandra P, Chambers RC, Taylor PM, Yacoub MH, Chester AH. Collagen synthesis by mesenchymal stem cells and aortic valve interstitial cells in response to mechanical stretch. Cardiovascular research. 2006;71(3):548-56.
185. Latif N, Sarathchandra P, Thomas PS, Antoniw J, Batten P, Chester AH, Taylor PM, Yacoub MH. Characterization of structural and signaling molecules by human valve interstitial cells and comparison to human mesenchymal stem cells. The Journal of heart valve disease. 2007;16(1):56-66.
186. Hoerstrup SP, Kadner A, Melnitchouk S, Trojan A, Eid K, Tracy J, Sodian R, Visjager JF, Kolb SA, Grunenfelder J, Zund G, Turina MI. Tissue engineering of functional trileaflet heart valves from human marrow stromal cells. Circulation. 2002;106(12 Suppl 1):I143-50.
187. Cushing MC, Liao JT, Anseth KS. Activation of valvular interstitial cells is mediated by transforming growth factor-beta1 interactions with matrix molecules. Matrix biology : journal of the International Society for Matrix Biology. 2005;24(6):428-37.
188. Choi KM, Seo YK, Yoon HH, Song KY, Kwon SY, Lee HS, Park JK. Effect of ascorbic acid on bone marrow-derived mesenchymal stem cell proliferation and differentiation. J Biosci Bioeng. 2008;105(6):586-94.
189. Antonucci I, Iezzi I, Morizio E, Mastrangelo F, Pantalone A, Mattioli-Belmonte M, Gigante A, Salini V, Calabrese G, Tete S, Palka G, Stuppia L. Isolation of osteogenic progenitors from human amniotic fluid using a single step culture protocol. BMC Biotechnol. 2009;9:9.
190. Abumaree MH, Al Jumah MA, Kalionis B, Jawdat D, Al Khaldi A, AlTalabani AA, Knawy BA. Phenotypic and functional characterization of mesenchymal stem cells from chorionic villi of human term placenta. Stem cell reviews. 2013;9(1):16-31.
191. Buzzi M, Alviano F, Campioni D, Stignani M, Melchiorri L, Rotola A, Tazzari P, Ricci F, Vaselli C, Terzi A, Pagliaro PP, Cuneo A, Lanza F, Bontadini A, Baricordi OR, Rizzo R. Umbilical cord blood CD34(+)cell-derived progeny produces human leukocyte antigen-G molecules with immuno-modulatory functions. Hum Immunol. 2012;73(2):150-5.
192. Wang HS, Hung SC, Peng ST, Huang CC, Wei HM, Guo YJ, Fu YS, Lai MC, Chen CC. Mesenchymal stem cells in the Wharton's jelly of the human umbilical cord. Stem cells. 2004;22(7):1330-7.
193. Ferretti C, Mattioli-Belmonte M. Periosteum derived stem cells for regenerative medicine proposals: Boosting current knowledge. World journal of stem cells. 2014;6(3):266-77.
194. Seo BM, Miura M, Gronthos S, Bartold PM, Batouli S, Brahim J, Young M, Robey PG, Wang CY, Shi S. Investigation of multipotent postnatal stem cells from human periodontal ligament. Lancet. 2004;364(9429):149-55.
195. Gronthos S, Mankani M, Brahim J, Robey PG, Shi S. Postnatal human dental pulp stem cells (DPSCs) in vitro and in vivo. Proceedings of the National Academy of Sciences of the United States of America. 2000;97(25):13625-30.
196. Morsczeck C, Gotz W, Schierholz J, Zeilhofer F, Kuhn U, Mohl C, Sippel C, Hoffmann KH. Isolation of precursor cells (PCs) from human dental follicle of wisdom teeth. Matrix biology : journal of the International Society for Matrix Biology. 2005;24(2):155-65.
197. Guo J, Weng J, Rong Q, Zhang X, Zhu S, Huang D, Li X, Chen S. Investigation of multipotent postnatal stem cells from human maxillary sinus membrane. Scientific reports. 2015;5:11660.
198. Orciani M, Di Primio R. Skin-derived mesenchymal stem cells: isolation, culture, and characterization. Methods in molecular biology. 2013;989:275-83.
199. Gullo F, De Bari C. Prospective purification of a subpopulation of human synovial mesenchymal stem cells with enhanced chondro-osteogenic potency. Rheumatology (Oxford). 2013;52(10):1758-68.
200. Cohnheim J. Über Entzündung und Eiterung. 1867;40:1-79.
201. Friedenstein AJ, Chailakhyan RK, Latsinik NV, Panasyuk AF, Keiliss-Borok IV. Stromal cells responsible for transferring the microenvironment of the hemopoietic tissues. Cloning in vitro and retransplantation in vivo. Transplantation. 1974;17(4):331-40.
202. Prockop DJ. Marrow stromal cells as stem cells for nonhematopoietic tissues. Science. 1997;276(5309):71-4.
203. Dominici M, Le Blanc K, Mueller I, Slaper-Cortenbach I, Marini F, Krause D, Deans R, Keating A, Prockop D, Horwitz E. Minimal criteria for defining multipotent mesenchymal stromal cells. The International Society for Cellular Therapy position statement. Cytotherapy. 2006;8(4):315-7.
204. Mendelson K, Schoen FJ. Heart valve tissue engineering: concepts, approaches, progress, and challenges. Annals of biomedical engineering. 2006;34(12):1799-819.

205. Lindroos B, Suuronen R, Miettinen S. The potential of adipose stem cells in regenerative medicine. Stem cell reviews. 2011;7(2):269-91.
206. Vincentelli A, Wautot F, Juthier F, Fouquet O, Corseaux D, Marechaux S, Le Tourneau T, Fabre O, Susen S, Van Belle E, Mouquet F, Decoene C, Prat A, Jude B. In vivo autologous recellularization of a tissue-engineered heart valve: are bone marrow mesenchymal stem cells the best candidates? The Journal of thoracic and cardiovascular surgery. 2007;134(2):424-32.
207. Fraser JK, Zhu M, Wulur I, Alfonso Z. Adipose-derived stem cells. Methods in molecular biology. 2008;449:59-67.
208. Baer PC, Geiger H. Adipose-derived mesenchymal stromal/stem cells: tissue localization, characterization, and heterogeneity. Stem cells international. 2012;2012:812693.
209. Zhang P, Moudgill N, Hager E, Tarola N, Dimatteo C, McIlhenny S, Tulenko T, DiMuzio PJ. Endothelial differentiation of adipose-derived stem cells from elderly patients with cardiovascular disease. Stem cells and development. 2011;20(6):977-88.
210. Colazzo F, Chester AH, Taylor PM, Yacoub MH. Induction of mesenchymal to endothelial transformation of adipose-derived stem cells. The Journal of heart valve disease. 2010;19(6):736-44.
211. Yoshimura K, Shigeura T, Matsumoto D, Sato T, Takaki Y, Aiba-Kojima E, Sato K, Inoue K, Nagase T, Koshima I, Gonda K. Characterization of freshly isolated and cultured cells derived from the fatty and fluid portions of liposuction aspirates. Journal of cellular physiology. 2006;208(1):64-76.
212. Zuk PA, Zhu M, Mizuno H, Huang J, Futrell JW, Katz AJ, Benhaim P, Lorenz HP, Hedrick MH. Multilineage cells from human adipose tissue: implications for cell-based therapies. Tissue engineering. 2001;7(2):211-28.
213. Moon MH, Kim SY, Kim YJ, Kim SJ, Lee JB, Bae YC, Sung SM, Jung JS. Human adipose tissue-derived mesenchymal stem cells improve postnatal neovascularization in a mouse model of hindlimb ischemia. Cellular physiology and biochemistry : international journal of experimental cellular physiology, biochemistry, and pharmacology. 2006;17(5-6):279-90.
214. DiMuzio P, Tulenko T. Tissue engineering applications to vascular bypass graft development: the use of adipose-derived stem cells. Journal of vascular surgery. 2007;45 Suppl A:A99-103.
215. Lee RH, Kim B, Choi I, Kim H, Choi HS, Suh K, Bae YC, Jung JS. Characterization and expression analysis of mesenchymal stem cells from human bone marrow and adipose tissue. Cellular physiology and biochemistry : international journal of experimental cellular physiology, biochemistry, and pharmacology. 2004;14(4-6):311-24.
216. Oedayrajsingh-Varma MJ, van Ham SM, Knippenberg M, Helder MN, Klein-Nulend J, Schouten TE, Ritt MJ, van Milligen FJ. Adipose tissue-derived mesenchymal stem cell yield and growth characteristics are affected by the tissue-harvesting procedure. Cytotherapy. 2006;8(2):166-77.
217. Suga H, Matsumoto D, Eto H, Inoue K, Aoi N, Kato H, Araki J, Yoshimura K. Functional implications of CD34 expression in human adipose-derived stem/progenitor cells. Stem cells and development. 2009;18(8):1201-10.
218. Cao Y, Sun Z, Liao L, Meng Y, Han Q, Zhao RC. Human adipose tissue-derived stem cells differentiate into endothelial cells in vitro and improve postnatal neovascularization in vivo. Biochem Biophys Res Commun. 2005;332(2):370-9.
219. Bassi G, Pacelli L, Carusone R, Zanoncello J, Krampera M. Adipose-derived stromal cells (ASCs). Transfusion and apheresis science : official journal of the World Apheresis Association : official journal of the European Society for Haemapheresis. 2012;47(2):193-8.
220. Nguyen KT, West JL. Photopolymerizable hydrogels for tissue engineering applications. Biomaterials. 2002;23(22):4307-14.
221. Wu Y, Puperi DS, Grande-Allen KJ, West JL. Ascorbic acid promotes extracellular matrix deposition while preserving valve interstitial cell quiescence within 3D hydrogel scaffolds. Journal of tissue engineering and regenerative medicine. 2015.
222. Mabry KM, Lawrence RL, Anseth KS. Dynamic stiffening of poly(ethylene glycol)-based hydrogels to direct valvular interstitial cell phenotype in a three-dimensional environment. Biomaterials. 2015;49:47-56.
223. Benton JA, Fairbanks BD, Anseth KS. Characterization of valvular interstitial cell function in three dimensional matrix metalloproteinase degradable PEG hydrogels. Biomaterials. 2009;30(34):6593-603.
224. Gould ST, Anseth KS. Role of cell-matrix interactions on VIC phenotype and tissue deposition in 3D PEG hydrogels. Journal of tissue engineering and regenerative medicine. 2016;10(10):E443-E53.
225. Flanagan TC, Wilkins B, Black A, Jockenhoevel S, Smith TJ, Pandit AS. A collagen-glycosaminoglycan co-culture model for heart valve tissue engineering applications. Biomaterials. 2006;27(10):2233-46.

226. Benton JA, DeForest CA, Vivekanandan V, Anseth KS. Photocrosslinking of gelatin macromers to synthesize porous hydrogels that promote valvular interstitial cell function. Tissue engineering Part A. 2009;15(11):3221-30.
227. Duan B, Hockaday LA, Kapetanovic E, Kang KH, Butcher JT. Stiffness and adhesivity control aortic valve interstitial cell behavior within hyaluronic acid based hydrogels. Acta biomaterialia. 2013;9(8):7640-50.
228. Masters KS, Shah DN, Leinwand LA, Anseth KS. Crosslinked hyaluronan scaffolds as a biologically active carrier for valvular interstitial cells. Biomaterials. 2005;26(15):2517-25.
229. Lee KY, Mooney DJ. Hydrogels for tissue engineering. Chemical reviews. 2001;101(7):1869-79.
230. Hennink WE, van Nostrum CF. Novel crosslinking methods to design hydrogels. Advanced drug delivery reviews. 2002;54(1):13-36.
231. Duan B, Hockaday LA, Kang KH, Butcher JT. 3D bioprinting of heterogeneous aortic valve conduits with alginate/gelatin hydrogels. Journal of biomedical materials research Part A. 2013;101(5):1255-64.
232. Hockaday LA, Kang KH, Colangelo NW, Cheung PY, Duan B, Malone E, Wu J, Girardi LN, Bonassar LJ, Lipson H, Chu CC, Butcher JT. Rapid 3D printing of anatomically accurate and mechanically heterogeneous aortic valve hydrogel scaffolds. Biofabrication. 2012;4(3):035005.
233. Zhang X, Xu B, Puperi DS, Wu Y, West JL, Grande-Allen KJ. Application of hydrogels in heart valve tissue engineering. J Long Term Eff Med Implants. 2015;25(1-2):105-34.
234. Duan B, Kapetanovic E, Hockaday LA, Butcher JT. Three-dimensional printed trileaflet valve conduits using biological hydrogels and human valve interstitial cells. Acta biomaterialia. 2014;10(5):1836-46.
235. Hjortnaes J, Camci-Unal G, Hutcheson JD, Jung SM, Schoen FJ, Kluin J, Aikawa E, Khademhosseini A. Directing valvular interstitial cell myofibroblast-like differentiation in a hybrid hydrogel platform. Advanced healthcare materials. 2015;4(1):121-30.
236. Aizawa Y, Owen SC, Shoichet MS. Polymers used to influence cell fate in 3D geometry: New trends. Progress in Polymer Science. 2012;37(5):645-58.
237. Tibbitt MW, Anseth KS. Hydrogels as extracellular matrix mimics for 3D cell culture. Biotechnology and bioengineering. 2009;103(4):655-63.
238. Rodriguez KJ, Masters KS. Regulation of valvular interstitial cell calcification by components of the extracellular matrix. Journal of biomedical materials research Part A. 2009;90(4):1043-53.
239. Zustiak SP, Leach JB. Hydrolytically degradable poly(ethylene glycol) hydrogel scaffolds with tunable degradation and mechanical properties. Biomacromolecules. 2010;11(5):1348-57.
240. Truong V, Blakey I, Whittaker AK. Hydrophilic and amphiphilic polyethylene glycol-based hydrogels with tunable degradability prepared by "click" chemistry. Biomacromolecules. 2012;13(12):4012-21.
241. Kloxin AM, Benton JA, Anseth KS. In situ elasticity modulation with dynamic substrates to direct cell phenotype. Biomaterials. 2010;31(1):1-8.
242. Lee SH, Moon JJ, Miller JS, West JL. Poly(ethylene glycol) hydrogels conjugated with a collagenase-sensitive fluorogenic substrate to visualize collagenase activity during three-dimensional cell migration. Biomaterials. 2007;28(20):3163-70.
243. Benoit DS, Durney AR, Anseth KS. The effect of heparin-functionalized PEG hydrogels on three-dimensional human mesenchymal stem cell osteogenic differentiation. Biomaterials. 2007;28(1):66-77.
244. Zhu J. Bioactive modification of poly(ethylene glycol) hydrogels for tissue engineering. Biomaterials. 2010;31(17):4639-56.
245. Hahn MS, Taite LJ, Moon JJ, Rowland MC, Ruffino KA, West JL. Photolithographic patterning of polyethylene glycol hydrogels. Biomaterials. 2006;27(12):2519-24.
246. Stern R, Jedrzejas MJ. Hyaluronidases: their genomics, structures, and mechanisms of action. Chemical reviews. 2006;106(3):818-39.
247. Lockhart M, Wirrig E, Phelps A, Wessels A. Extracellular matrix and heart development. Birth defects research Part A, Clinical and molecular teratology. 2011;91(6):535-50.
248. Shu XZ, Ghosh K, Liu Y, Palumbo FS, Luo Y, Clark RA, Prestwich GD. Attachment and spreading of fibroblasts on an RGD peptide-modified injectable hyaluronan hydrogel. Journal of biomedical materials research Part A. 2004;68(2):365-75.
249. Shu XZ, Ahmad S, Liu Y, Prestwich GD. Synthesis and evaluation of injectable, in situ crosslinkable synthetic extracellular matrices for tissue engineering. Journal of biomedical materials research Part A. 2006;79(4):902-12.
250. Sahoo S, Chung C, Khetan S, Burdick JA. Hydrolytically degradable hyaluronic acid hydrogels with controlled temporal structures. Biomacromolecules. 2008;9(4):1088-92.

251. Duan B, Hockaday LA, Das S, Xu C, Butcher JT. Comparison of Mesenchymal Stem Cell Source Differentiation Toward Human Pediatric Aortic Valve Interstitial Cells within 3D Engineered Matrices. Tissue engineering Part C, Methods. 2015;21(8):795-807.
252. Pignatello R. Biomaterials Applications for Nanomedicine. 2011.
253. Lynn AK, Yannas IV, Bonfield W. Antigenicity and immunogenicity of collagen. Journal of biomedical materials research Part B, Applied biomaterials. 2004;71(2):343-54.
254. Occhetta P, Visone R, Russo L, Cipolla L, Moretti M, Rasponi M. VA-086 methacrylate gelatine photopolymerizable hydrogels: A parametric study for highly biocompatible 3D cell embedding. Journal of biomedical materials research Part A. 2015;103(6):2109-17.
255. Billiet T, Gevaert E, De Schryver T, Cornelissen M, Dubruel P. The 3D printing of gelatin methacrylamide cell-laden tissue-engineered constructs with high cell viability. Biomaterials. 2014;35(1):49-62.
256. Mosadegh B, Xiong G, Dunham S, Min JK. Current progress in 3D printing for cardiovascular tissue engineering. Biomedical materials. 2015;10(3):034002.
257. Lueders C, Jastram B, Hetzer R, Schwandt H. Rapid manufacturing techniques for the tissue engineering of human heart valves. European journal of cardio-thoracic surgery : official journal of the European Association for Cardio-thoracic Surgery. 2014;46(4):593-601.
258. Nakayama Y, Takewa Y, Sumikura H, Yamanami M, Matsui Y, Oie T, Kishimoto Y, Arakawa M, Ohmuma K, Tajikawa T, Kanda K, Tatsumi E. In-body tissue-engineered aortic valve (Biovalve type VII) architecture based on 3D printer molding. Journal of biomedical materials research Part B, Applied biomaterials. 2015;103(1):1-11.
259. Seol YJ, Kang HW, Lee SJ, Atala A, Yoo JJ. Bioprinting technology and its applications. European journal of cardio-thoracic surgery : official journal of the European Association for Cardio-thoracic Surgery. 2014;46(3):342-8.
260. Giannopoulos AA, Mitsouras D, Yoo SJ, Liu PP, Chatzizisis YS, Rybicki FJ. Applications of 3D printing in cardiovascular diseases. Nature reviews Cardiology. 2016;13(12):701-18.
261. Zhang YS, Oklu R, Dokmeci MR, Khademhosseini A. Three-Dimensional Bioprinting Strategies for Tissue Engineering. Cold Spring Harbor perspectives in medicine. 2017.
262. Zhang X, Zhang Y. Tissue Engineering Applications of Three-Dimensional Bioprinting. Cell biochemistry and biophysics. 2015;72(3):777-82.
263. Malda J, Visser J, Melchels FP, Jungst T, Hennink WE, Dhert WJ, Groll J, Hutmacher DW. 25th anniversary article: Engineering hydrogels for biofabrication. Advanced materials. 2013;25(36):5011-28.
264. Cui X, Dean D, Ruggeri ZM, Boland T. Cell damage evaluation of thermal inkjet printed Chinese hamster ovary cells. Biotechnology and bioengineering. 2010;106(6):963-9.
265. Pereira FR, Bártolo JP. 3D bioprinting of photocrosslinkable hydrogel constructs. J Appl Polym Sci. 2015.
266. Barron JA, Wu P, Ladouceur HD, Ringeisen BR. Biological laser printing: a novel technique for creating heterogeneous 3-dimensional cell patterns. Biomed Microdevices. 2004;6(2):139-47.
267. Go AS, Mozaffarian D, Roger VL, Benjamin EJ, Berry JD, Blaha MJ, Dai S, Ford ES, Fox CS, Franco S, Fullerton HJ, Gillespie C, Hailpern SM, Heit JA, Howard VJ, Huffman MD, Judd SE, Kissela BM, Kittner SJ, Lackland DT, Lichtman JH, Lisabeth LD, Mackey RH, Magid DJ, Marcus GM, Marelli A, Matchar DB, McGuire DK, Mohler ER, 3rd, Moy CS, Mussolino ME, Neumar RW, Nichol G, Pandey DK, Paynter NP, Reeves MJ, Sorlie PD, Stein J, Towfighi A, Turan TN, Virani SS, Wong ND, Woo D, Turner MB, American Heart Association Statistics C, Stroke Statistics S. Heart disease and stroke statistics--2014 update: a report from the American Heart Association. Circulation. 2014;129(3):e28-e292.
268. Maganti K, Rigolin VH, Sarano ME, Bonow RO. Valvular heart disease: diagnosis and management. Mayo Clinic proceedings. 2010;85(5):483-500.
269. Al-Atassi T, Toeg H, Ruel M. Should we anticoagulate after bioprosthetic aortic valve replacement? Expert review of cardiovascular therapy. 2013;11(12):1649-57.
270. Schenke-Layland K, Vasilevski O, Opitz F, Konig K, Riemann I, Halbhuber KJ, Wahlers T, Stock UA. Impact of decellularization of xenogeneic tissue on extracellular matrix integrity for tissue engineering of heart valves. Journal of structural biology. 2003;143(3):201-8.
271. Erdbrugger W, Konertz W, Dohmen PM, Posner S, Ellerbrok H, Brodde OE, Robenek H, Modersohn D, Pruss A, Holinski S, Stein-Konertz M, Pauli G. Decellularized xenogenic heart valves reveal remodeling and growth potential in vivo. Tissue engineering. 2006;12(8):2059-68.
272. Park CS, Oh SS, Kim YE, Choi SY, Lim HG, Ahn H, Kim YJ. Anti-alpha-Gal antibody response following xenogeneic heart valve implantation in adults. The Journal of heart valve disease. 2013;22(2):222-9.
273. Manji RA, Ekser B, Menkis AH, Cooper DK. Bioprosthetic heart valves of the future. Xenotransplantation. 2014;21(1):1-10.

274. Rieder E, Seebacher G, Kasimir MT, Eichmair E, Winter B, Dekan B, Wolner E, Simon P, Weigel G. Tissue engineering of heart valves: decellularized porcine and human valve scaffolds differ importantly in residual potential to attract monocytic cells. Circulation. 2005;111(21):2792-7.
275. Somers P, Roosens A, De Somer F, Cornelissen M, Van Nooten G. Non-Cytotoxic Crosslinkers for Heart Valve Tissue Engineering. The Journal of heart valve disease. 2015;24(1):92-100.
276. Kasimir MT, Weigel G, Sharma J, Rieder E, Seebacher G, Wolner E, Simon P. The decellularized porcine heart valve matrix in tissue engineering: platelet adhesion and activation. Thrombosis and haemostasis. 2005;94(3):562-7.
277. Zhou J, Fritze O, Schleicher M, Wendel HP, Schenke-Layland K, Harasztosi C, Hu S, Stock UA. Impact of heart valve decellularization on 3-D ultrastructure, immunogenicity and thrombogenicity. Biomaterials. 2010;31(9):2549-54.
278. Mendoza-Novelo B, Avila EE, Cauich-Rodriguez JV, Jorge-Herrero E, Rojo FJ, Guinea GV, Mata-Mata JL. Decellularization of pericardial tissue and its impact on tensile viscoelasticity and glycosaminoglycan content. Acta biomaterialia. 2011;7(3):1241-8.
279. Liao J, Joyce EM, Sacks MS. Effects of decellularization on the mechanical and structural properties of the porcine aortic valve leaflet. Biomaterials. 2008;29(8):1065-74.
280. Oliveira AC, Garzon I, Ionescu AM, Carriel V, Cardona Jde L, Gonzalez-Andrades M, Perez Mdel M, Alaminos M, Campos A. Evaluation of small intestine grafts decellularization methods for corneal tissue engineering. PloS one. 2013;8(6):e66538.
281. Dohmen PM, Lembcke A, Hotz H, Kivelitz D, Konertz WF. Ross operation with a tissue-engineered heart valve. The Annals of thoracic surgery. 2002;74(5):1438-42.
282. Cebotari S, Tudorache I, Jaekel T, Hilfiker A, Dorfman S, Ternes W, Haverich A, Lichtenberg A. Detergent decellularization of heart valves for tissue engineering: toxicological effects of residual detergents on human endothelial cells. Artificial organs. 2010;34(3):206-10.
283. Bloch O, Erdbrugger W, Volker W, Schenk A, Posner S, Konertz W, Dohmen PM. Extracellular matrix in deoxycholic acid decellularized aortic heart valves. Medical science monitor : international medical journal of experimental and clinical research. 2012;18(12):BR487-92.
284. Carriel VS, Aneiros-Fernandez J, Arias-Santiago S, Garzon IJ, Alaminos M, Campos A. A novel histochemical method for a simultaneous staining of melanin and collagen fibers. The journal of histochemistry and cytochemistry : official journal of the Histochemistry Society. 2011;59(3):270-7.
285. Ragaert K, De Somer F, Somers P, De Baere I, Cardon L, Degrieck J. Flexural mechanical properties of porcine aortic heart valve leaflets. Journal of the mechanical behavior of biomedical materials. 2012;13:78-84.
286. Yang M, Chen CZ, Wang XN, Zhu YB, Gu YJ. Favorable effects of the detergent and enzyme extraction method for preparing decellularized bovine pericardium scaffold for tissue engineered heart valves. Journal of biomedical materials research Part B, Applied biomaterials. 2009;91(1):354-61.
287. Yu BT, Li WT, Song BQ, Wu YL. Comparative study of the Triton X-100-sodium deoxycholate method and detergent-enzymatic digestion method for decellularization of porcine aortic valves. European review for medical and pharmacological sciences. 2013;17(16):2179-84.
288. Dong J, Li Y, Mo X. The study of a new detergent (octyl-glucopyranoside) for decellularizing porcine pericardium as tissue engineering scaffold. The Journal of surgical research. 2013;183(1):56-67.
289. Dohmen PM, Ozaki S, Nitsch R, Yperman J, Flameng W, Konertz W. A tissue engineered heart valve implanted in a juvenile sheep model. Medical science monitor : international medical journal of experimental and clinical research. 2003;9(4):BR97-BR104.
290. Booth C, Korossis SA, Wilcox HE, Watterson KG, Kearney JN, Fisher J, Ingham E. Tissue engineering of cardiac valve prostheses I: development and histological characterization of an acellular porcine scaffold. The Journal of heart valve disease. 2002;11(4):457-62.
291. Kasimir MT, Rieder E, Seebacher G, Silberhumer G, Wolner E, Weigel G, Simon P. Comparison of different decellularization procedures of porcine heart valves. The International journal of artificial organs. 2003;26(5):421-7.
292. Bader A, Schilling T, Teebken OE, Brandes G, Herden T, Steinhoff G, Haverich A. Tissue engineering of heart valves--human endothelial cell seeding of detergent acellularized porcine valves. European journal of cardio-thoracic surgery : official journal of the European Association for Cardio-thoracic Surgery. 1998;14(3):279-84.
293. Gilpin SE, Guyette JP, Gonzalez G, Ren X, Asara JM, Mathisen DJ, Vacanti JP, Ott HC. Perfusion decellularization of human and porcine lungs: bringing the matrix to clinical scale. The Journal of heart and lung transplantation : the official publication of the International Society for Heart Transplantation. 2014;33(3):298-308.

294. Lee TC, Midura RJ, Hascall VC, Vesely I. The effect of elastin damage on the mechanics of the aortic valve. Journal of biomechanics. 2001;34(2):203-10.
295. Vashi AV, White JF, McLean KM, Neethling WM, Rhodes DI, Ramshaw JA, Werkmeister JA. Evaluation of an established pericardium patch for delivery of mesenchymal stem cells to cardiac tissue. Journal of biomedical materials research Part A. 2014.
296. Lam MT, Nauta A, Meyer NP, Wu JC, Longaker MT. Effective delivery of stem cells using an extracellular matrix patch results in increased cell survival and proliferation and reduced scarring in skin wound healing. Tissue engineering Part A. 2013;19(5-6):738-47.
297. Dohmen PM, da Costa F, Lopes SV, Vilani R, Bloch O, Konertz W. Successful implantation of a decellularized equine pericardial patch into the systemic circulation. Medical science monitor basic research. 2014;20:1-8.
298. Cheung DY, Duan B, Butcher JT. Current progress in tissue engineering of heart valves: multiscale problems, multiscale solutions. Expert opinion on biological therapy. 2015;15(8):1155-72.
299. Kasimir MT, Rieder E, Seebacher G, Nigisch A, Dekan B, Wolner E, Weigel G, Simon P. Decellularization does not eliminate thrombogenicity and inflammatory stimulation in tissue-engineered porcine heart valves. The Journal of heart valve disease. 2006;15(2):278-86.
300. Schopka S, Schmid FX, Hirt S, Birnbaum DE, Schmid C, Lehle K. Recellularization of biological heart valves with human vascular cells: in vitro hemocompatibility assessment. Journal of biomedical materials research Part B, Applied biomaterials. 2009;88(1):130-8.
301. Zeltinger J, Landeen LK, Alexander HG, Kidd ID, Sibanda B. Development and characterization of tissue-engineered aortic valves. Tissue engineering. 2001;7(1):9-22.
302. Kajbafzadeh AM, Ahmadi Tafti SH, Mokhber-Dezfooli MR, Khorramirouz R, Sabetkish S, Sabetkish N, Rabbani S, Tavana H, Mohseni MJ. Aortic valve conduit implantation in the descending thoracic aorta in a sheep model: The outcomes of pre-seeded scaffold. International journal of surgery. 2016;28:97-105.
303. Walles T, Lichtenberg A, Puschmann C, Leyh R, Wilhelmi M, Kallenbach K, Haverich A, Mertsching H. In vivo model for cross-species porcine endogenous retrovirus transmission using tissue engineered pulmonary arteries. European journal of cardio-thoracic surgery : official journal of the European Association for Cardio-thoracic Surgery. 2003;24(3):358-63.
304. Roosens A, Somers P, De Somer F, Carriel V, Van Nooten G, Cornelissen R. Impact of Detergent-Based Decellularization Methods on Porcine Tissues for Heart Valve Engineering. Annals of biomedical engineering. 2016;44(9):2827-39.
305. Steinhoff G, Stock U, Karim N, Mertsching H, Timke A, Meliss RR, Pethig K, Haverich A, Bader A. Tissue engineering of pulmonary heart valves on allogenic acellular matrix conduits: in vivo restoration of valve tissue. Circulation. 2000;102(19 Suppl 3):III50-5.
306. Dong X, Wei X, Yi W, Gu C, Kang X, Liu Y, Li Q, Yi D. RGD-modified acellular bovine pericardium as a bioprosthetic scaffold for tissue engineering. Journal of materials science Materials in medicine. 2009;20(11):2327-36.
307. Converse GL, Buse EE, Neill KR, McFall CR, Lewis HN, VeDepo MC, Quinn RW, Hopkins RA. Design and efficacy of a single-use bioreactor for heart valve tissue engineering. Journal of biomedical materials research Part B, Applied biomaterials. 2017;105(2):249-59.
308. Syedain ZH, Bradee AR, Kren S, Taylor DA, Tranquillo RT. Decellularized tissue-engineered heart valve leaflets with recellularization potential. Tissue engineering Part A. 2013;19(5-6):759-69.
309. Phillips CL, Combs SB, Pinnell SR. Effects of ascorbic acid on proliferation and collagen synthesis in relation to the donor age of human dermal fibroblasts. The Journal of investigative dermatology. 1994;103(2):228-32.
310. Rossig L, Hoffmann J, Hugel B, Mallat Z, Haase A, Freyssinet JM, Tedgui A, Aicher A, Zeiher AM, Dimmeler S. Vitamin C inhibits endothelial cell apoptosis in congestive heart failure. Circulation. 2001;104(18):2182-7.
311. Liu J, Yagi T, Sadamori H, Matsukawa H, Sun DS, Mitsuoka N, Yamamura M, Matsuoka J, Jin Z, Yamamoto I, Tanaka N. Annexin V assay-proven anti-apoptotic effect of ascorbic acid 2-glucoside after cold ischemia/reperfusion injury in rat liver transplantation. Acta medica Okayama. 2003;57(5):209-16.
312. Traber MG, Stevens JF. Vitamins C and E: beneficial effects from a mechanistic perspective. Free radical biology & medicine. 2011;51(5):1000-13.
313. Rockey DC, Weymouth N, Shi Z. Smooth muscle alpha actin (Acta2) and myofibroblast function during hepatic wound healing. PloS one. 2013;8(10):e77166.

314. Assmann A, Delfs C, Munakata H, Schiffer F, Horstkotter K, Huynh K, Barth M, Stoldt VR, Kamiya H, Boeken U, Lichtenberg A, Akhyari P. Acceleration of autologous in vivo recellularization of decellularized aortic conduits by fibronectin surface coating. Biomaterials. 2013;34(25):6015-26.
315. Williams JK, Miller ES, Lane MR, Atala A, Yoo JJ, Jordan JE. Characterization of CD133 Antibody-Directed Recellularized Heart Valves. Journal of cardiovascular translational research. 2015;8(7):411-20.
316. Tudorache I, Theodoridis K, Baraki H, Sarikouch S, Bara C, Meyer T, Hoffler K, Hartung D, Hilfiker A, Haverich A, Cebotari S. Decellularized aortic allografts versus pulmonary autografts for aortic valve replacement in the growing sheep model: haemodynamic and morphological results at 20 months after implantation. European journal of cardio-thoracic surgery : official journal of the European Association for Cardio-thoracic Surgery. 2016;49(4):1228-38.
317. Baraki H, Tudorache I, Braun M, Hoffler K, Gorler A, Lichtenberg A, Bara C, Calistru A, Brandes G, Hewicker-Trautwein M, Hilfiker A, Haverich A, Cebotari S. Orthotopic replacement of the aortic valve with decellularized allograft in a sheep model. Biomaterials. 2009;30(31):6240-6.
318. Yau JW, Teoh H, Verma S. Endothelial cell control of thrombosis. BMC cardiovascular disorders. 2015;15:130.
319. Ge L, Sotiropoulos F. Direction and magnitude of blood flow shear stresses on the leaflets of aortic valves: is there a link with valve calcification? Journal of biomechanical engineering. 2010;132(1):014505.
320. Ghazvini-Boroujerdi M, Clark J, Narula N, Palmatory E, Connolly JM, DeFelice S, Xu J, Jian B, Hazelwood S, Levy RJ. Transcription factor Egr-1 in calcific aortic valve disease. The Journal of heart valve disease. 2004;13(6):894-903.
321. Liu AC, Gotlieb AI. Characterization of cell motility in single heart valve interstitial cells in vitro. Histology and histopathology. 2007;22(8):873-82.
322. Yperman J, De Visscher G, Holvoet P, Flameng W. Molecular and functional characterization of ovine cardiac valve-derived interstitial cells in primary isolates and cultures. Tissue engineering. 2004;10(9-10):1368-75.
323. Walker GA, Masters KS, Shah DN, Anseth KS, Leinwand LA. Valvular myofibroblast activation by transforming growth factor-beta: implications for pathological extracellular matrix remodeling in heart valve disease. Circulation research. 2004;95(3):253-60.
324. Gevaert E, Dolle L, Billiet T, Dubruel P, van Grunsven L, van Apeldoorn A, Cornelissen R. High throughput micro-well generation of hepatocyte micro-aggregates for tissue engineering. PloS one. 2014;9(8):e105171.
325. Goll DE, Hoekstra WG, Bray RW. Age-Associated Changes in Muscle Composition - Isolation and Properties of a Collagenous Residue from Bovine Muscle. J Food Sci. 1963;28(5):503-&.
326. Schenke-Layland K, Riemann I, Opitz F, Konig K, Halbhuber KJ, Stock UA. Comparative study of cellular and extracellular matrix composition of native and tissue engineered heart valves. Matrix biology : journal of the International Society for Matrix Biology. 2004;23(2):113-25.
327. Taylor PM, Allen SP, Yacoub MH. Phenotypic and functional characterization of interstitial cells from human heart valves, pericardium and skin. The Journal of heart valve disease. 2000;9(1):150-8.
328. Xu S, Liu AC, Kim H, Gotlieb AI. Cell density regulates in vitro activation of heart valve interstitial cells. Cardiovascular pathology : the official journal of the Society for Cardiovascular Pathology. 2012;21(2):65-73.
329. Cirka HA, Uribe J, Liang V, Schoen FJ, Billiar KL. Reproducible in vitro model for dystrophic calcification of cardiac valvular interstitial cells: insights into the mechanisms of calcific aortic valvular disease. Lab on a chip. 2017;17(5):814-29.
330. Yip CY, Chen JH, Zhao R, Simmons CA. Calcification by valve interstitial cells is regulated by the stiffness of the extracellular matrix. Arterioscler Thromb Vasc Biol. 2009;29(6):936-42.
331. Subramani T, Yeap SK, Ho WY, Ho CL, Omar AR, Aziz SA, Rahman NM, Alitheen NB. Vitamin C suppresses cell death in MCF-7 human breast cancer cells induced by tamoxifen. J Cell Mol Med. 2014;18(2):305-13.
332. Shima N, Kimoto M, Yamaguchi M, Yamagami S. Increased proliferation and replicative lifespan of isolated human corneal endothelial cells with L-ascorbic acid 2-phosphate. Investigative ophthalmology & visual science. 2011;52(12):8711-7.
333. Du CB, Liu JW, Su W, Ren YH, Wei DZ. The protective effect of ascorbic acid derivative on PC12 cells: involvement of its ROS scavenging ability. Life Sci. 2003;74(6):771-80.
334. Phillips CL, Tajima S, Pinnell SR. Ascorbic acid and transforming growth factor-beta 1 increase collagen biosynthesis via different mechanisms: coordinate regulation of pro alpha 1(I) and Pro alpha 1(III) collagens. Archives of biochemistry and biophysics. 1992;295(2):397-403.

335. Ushiki T. Collagen fibers, reticular fibers and elastic fibers. A comprehensive understanding from a morphological viewpoint. Arch Histol Cytol. 2002;65(2):109-26.
336. Sacks MS, Schoen FJ, Mayer JE. Bioengineering challenges for heart valve tissue engineering. Annual review of biomedical engineering. 2009;11:289-313.
337. Arakawa E, Hasegawa K, Irie J, Ide S, Ushiki J, Yamaguchi K, Oda S, Matsuda Y. L-ascorbic acid stimulates expression of smooth muscle-specific markers in smooth muscle cells both in vitro and in vivo. Journal of cardiovascular pharmacology. 2003;42(6):745-51.
338. Lee WC, Rubin JP, Marra KG. Regulation of alpha-smooth muscle actin protein expression in adipose-derived stem cells. Cells, tissues, organs. 2006;183(2):80-6.
339. Langenbach F, Handschel J. Effects of dexamethasone, ascorbic acid and beta-glycerophosphate on the osteogenic differentiation of stem cells in vitro. Stem cell research & therapy. 2013;4(5):117.
340. Reumann MK, Strachna O, Lukashova L, Verdelis K, Donnelly E, Boskey AL, Mayer-Kuckuk P. Early growth response gene 1 regulates bone properties in mice. Calcif Tissue Int. 2011;89(1):1-9.
341. Benton JA, Kern HB, Anseth KS. Substrate properties influence calcification in valvular interstitial cell culture. The Journal of heart valve disease. 2008;17(6):689-99.
342. Gould ST, Darling NJ, Anseth KS. Small peptide functionalized thiol-ene hydrogels as culture substrates for understanding valvular interstitial cell activation and de novo tissue deposition. Acta biomaterialia. 2012;8(9):3201-9.
343. Kaden JJ, Kilic R, Sarikoc A, Hagl S, Lang S, Hoffmann U, Brueckmann M, Borggrefe M. Tumor necrosis factor alpha promotes an osteoblast-like phenotype in human aortic valve myofibroblasts: a potential regulatory mechanism of valvular calcification. Int J Mol Med. 2005;16(5):869-72.
344. Balachandran K, Sucosky P, Jo H, Yoganathan AP. Elevated Cyclic Stretch Induces Aortic Valve Calcification in a Bone Morphogenic Protein-Dependent Manner. American Journal of Pathology. 2010;177(1):49-57.
345. Merryman WD, Lukoff HD, Long RA, Engelmayr GC, Jr., Hopkins RA, Sacks MS. Synergistic effects of cyclic tension and transforming growth factor-beta1 on the aortic valve myofibroblast. Cardiovascular pathology : the official journal of the Society for Cardiovascular Pathology. 2007;16(5):268-76.
346. Fisher CI, Chen J, Merryman WD. Calcific nodule morphogenesis by heart valve interstitial cells is strain dependent. Biomechanics and modeling in mechanobiology. 2013;12(1):5-17.
347. Harris C, Croce B, Cao C. Tissue and mechanical heart valves. Annals of cardiothoracic surgery. 2015;4(4):399.
348. Liu JS, Gartner ZJ. Directing the assembly of spatially organized multicomponent tissues from the bottom up. Trends Cell Biol. 2012;22(12):683-91.
349. Baker BM, Chen CS. Deconstructing the third dimension: how 3D culture microenvironments alter cellular cues. Journal of cell science. 2012;125(Pt 13):3015-24.
350. Roosens A, Puype I, Cornelissen R. Scaffold-free high throughput generation of quiescent valvular microtissues. Journal of molecular and cellular cardiology. 2017;106:45-54.
351. Tejavibulya N, Youssef J, Bao B, Ferruccio TM, Morgan JR. Directed self-assembly of large scaffold-free multi-cellular honeycomb structures. Biofabrication. 2011;3(3):034110.
352. Rago AP, Dean DM, Morgan JR. Controlling cell position in complex heterotypic 3D microtissues by tissue fusion. Biotechnology and bioengineering. 2009;102(4):1231-41.
353. Chen MB, Srigunapalan S, Wheeler AR, Simmons CA. A 3D microfluidic platform incorporating methacrylated gelatin hydrogels to study physiological cardiovascular cell-cell interactions. Lab on a chip. 2013;13(13):2591-8.
354. Kang LH, Armstrong PA, Lee LJ, Duan B, Kang KH, Butcher JT. Optimizing Photo-Encapsulation Viability of Heart Valve Cell Types in 3D Printable Composite Hydrogels. Annals of biomedical engineering. 2017;45(2):360-77.
355. Gevaert E, Billiet T, Declercq H, Dubruel P, Cornelissen R. Galactose-functionalized gelatin hydrogels improve the functionality of encapsulated HepG2 cells. Macromol Biosci. 2014;14(3):419-27.
356. Su K, Wang C. Recent advances in the use of gelatin in biomedical research. Biotechnol Lett. 2015;37(11):2139-45.
357. Van Den Bulcke AI, Bogdanov B, De Rooze N, Schacht EH, Cornelissen M, Berghmans H. Structural and rheological properties of methacrylamide modified gelatin hydrogels. Biomacromolecules. 2000;1(1):31-8.
358. Rouillard AD, Berglund CM, Lee JY, Polacheck WJ, Tsui Y, Bonassar LJ, Kirby BJ. Methods for photocrosslinking alginate hydrogel scaffolds with high cell viability. Tissue Eng Part C Methods. 2011;17(2):173-9.

359. Tan HP, Marra KG. Injectable, Biodegradable Hydrogels for Tissue Engineering Applications. Materials. 2010;3(3):1746-67.
360. Garside VC, Cullum R, Alder O, Lu DY, Vander Werff R, Bilenky M, Zhao Y, Jones SJ, Marra MA, Underhill TM, Hoodless PA. SOX9 modulates the expression of key transcription factors required for heart valve development. Development. 2015;142(24):4340-50.
361. Lincoln J, Kist R, Scherer G, Yutzey KE. Sox9 is required for precursor cell expansion and extracellular matrix organization during mouse heart valve development. Dev Biol. 2007;305(1):120-32.
362. Bi W, Deng JM, Zhang Z, Behringer RR, de Crombrugghe B. Sox9 is required for cartilage formation. Nat Genet. 1999;22(1):85-9.
363. Harken DE, Taylor WJ, Lefemine AA, Lunzer S, Low HB, Cohen ML, Jacobey JA. Aortic valve replacement with a caged ball valve. The American journal of cardiology. 1962;9:292-9.
364. Reardon MJ, David TE. Stentless xenograft aortic valves. Curr Opin Cardiol. 1999;14(2):84-9.
365. Schoen FJ, Levy RJ. Tissue heart valves: Current challenges and future research perspectives. Journal of biomedical materials research. 1999;47(4):439-65.
366. Langer R, Vacanti JP. Tissue engineering. Science. 1993;260(5110):920-6.
367. Dohmen PM, Konertz W. Tissue-engineered heart valve scaffolds. Annals of thoracic and cardiovascular surgery : official journal of the Association of Thoracic and Cardiovascular Surgeons of Asia. 2009;15(6):362-7.
368. O'Brien FJ. Biomaterials and scaffolds for tissue engineering. Materials Today. 2011;14(3):88-95.
369. Hoerstrup SP, Sodian R, Daebritz S, Wang J, Bacha EA, Martin DP, Moran AM, Guleserian KJ, Sperling JS, Kaushal S, Vacanti JP, Schoen FJ, Mayer JE, Jr. Functional living trileaflet heart valves grown in vitro. Circulation. 2000;102(19 Suppl 3):III44-9.
370. Somers P, De Somer F, Cornelissen M, Bouchez S, Gasthuys F, Narine K, Cox E, Van Nooten G. Genipin blues: an alternative non-toxic crosslinker for heart valves? The Journal of heart valve disease. 2008;17(6):682-8.
371. Yoo JS, Kim YJ, Kim SH, Choi SH. Study on genipin: a new alternative natural crosslinking agent for fixing heterograft tissue. The Korean journal of thoracic and cardiovascular surgery. 2011;44(3):197-207.
372. Connolly JM, Bakay MA, Alferiev IS, Gorman RC, Gorman Iii JH, Kruth HS, Ashworth PE, Kutty JK, Schoen FJ, Bianco RW, Levy RJ. Triglycidyl Amine Crosslinking Combined With Ethanol Inhibits Bioprosthetic Heart Valve Calcification. The Annals of thoracic surgery. 2011;92(3):858-65.
373. Dohmen PM, Lembcke A, Holinski S, Kivelitz D, Braun JP, Pruss A, Konertz W. Mid-term clinical results using a tissue-engineered pulmonary valve to reconstruct the right ventricular outflow tract during the Ross procedure. The Annals of thoracic surgery. 2007;84(3):729-36.
374. Cicha I, Ruffer A, Cesnjevar R, Glockler M, Agaimy A, Daniel WG, Garlichs CD, Dittrich S. Early obstruction of decellularized xenogenic valves in pediatric patients: involvement of inflammatory and fibroproliferative processes. Cardiovascular pathology : the official journal of the Society for Cardiovascular Pathology. 2011;20(4):222-31.
375. Simionescu DT. Prevention of calcification in bioprosthetic heart valves: challenges and perspectives. Expert opinion on biological therapy. 2004;4(12):1971-85.
376. Yamada S, Sugahara K. Potential therapeutic application of chondroitin sulfate/dermatan sulfate. Curr Drug Discov Technol. 2008;5(4):289-301.
377. Brown JW, Elkins RC, Clarke DR, Tweddell JS, Huddleston CB, Doty JR, Fehrenbacher JW, Takkenberg JJ. Performance of the CryoValve SG human decellularized pulmonary valve in 342 patients relative to the conventional CryoValve at a mean follow-up of four years. The Journal of thoracic and cardiovascular surgery. 2010;139(2):339-48.
378. Brown JW, Ruzmetov M, Eltayeb O, Rodefeld MD, Turrentine MW. Performance of SynerGraft decellularized pulmonary homograft in patients undergoing a Ross procedure. The Annals of thoracic surgery. 2011;91(2):416-22.
379. Bechtel JF, Gellissen J, Erasmi AW, Petersen M, Hiob A, Stierle U, Sievers HH. Mid-term findings on echocardiography and computed tomography after RVOT-reconstruction: comparison of decellularized (SynerGraft) and conventional allografts. European journal of cardio-thoracic surgery : official journal of the European Association for Cardio-thoracic Surgery. 2005;27(3):410-5.
380. Bechtel JF, Stierle U, Sievers HH. Fifty-two months' mean follow up of decellularized SynerGraft-treated pulmonary valve allografts. The Journal of heart valve disease. 2008;17(1):98-104.
381. Zehr KJ, Yagubyan M, Connolly HM, Nelson SM, Schaff HV. Aortic root replacement with a novel decellularized cryopreserved aortic homograft: postoperative immunoreactivity and early results. The Journal of thoracic and cardiovascular surgery. 2005;130(4):1010-5.

382. Cebotari S, Tudorache I, Ciubotaru A, Boethig D, Sarikouch S, Goerler A, Lichtenberg A, Cheptanaru E, Barnaciuc S, Cazacu A, Maliga O, Repin O, Maniuc L, Breymann T, Haverich A. Use of fresh decellularized allografts for pulmonary valve replacement may reduce the reoperation rate in children and young adults: early report. Circulation. 2011;124(11 Suppl):S115-23.
383. Sarikouch S, Horke A, Tudorache I, Beerbaum P, Westhoff-Bleck M, Boethig D, Repin O, Maniuc L, Ciubotaru A, Haverich A, Cebotari S. Decellularized fresh homografts for pulmonary valve replacement: a decade of clinical experience. European journal of cardio-thoracic surgery : official journal of the European Association for Cardio-thoracic Surgery. 2016;50(2):281-90.
384. Tudorache I, Horke A, Cebotari S, Sarikouch S, Boethig D, Breymann T, Beerbaum P, Bertram H, Westhoff-Bleck M, Theodoridis K, Bobylev D, Cheptanaru E, Ciubotaru A, Haverich A. Decellularized aortic homografts for aortic valve and aorta ascendens replacement. European journal of cardio-thoracic surgery : official journal of the European Association for Cardio-thoracic Surgery. 2016;50(1):89-97.
385. Konertz W, Angeli E, Tarusinov G, Christ T, Kroll J, Dohmen PM, Krogmann O, Franzbach B, Pace Napoleone C, Gargiulo G. Right ventricular outflow tract reconstruction with decellularized porcine xenografts in patients with congenital heart disease. The Journal of heart valve disease. 2011;20(3):341-7.
386. Ruffer A, Purbojo A, Cicha I, Glockler M, Potapov S, Dittrich S, Cesnjevar RA. Early failure of xenogenous de-cellularised pulmonary valve conduits--a word of caution! European journal of cardio-thoracic surgery : official journal of the European Association for Cardio-thoracic Surgery. 2010;38(1):78-85.
387. Perri G, Polito A, Esposito C, Albanese SB, Francalanci P, Pongiglione G, Carotti A. Early and late failure of tissue-engineered pulmonary valve conduits used for right ventricular outflow tract reconstruction in patients with congenital heart disease. European journal of cardio-thoracic surgery : official journal of the European Association for Cardio-thoracic Surgery. 2012;41(6):1320-5.
388. Voges I, Brasen JH, Entenmann A, Scheid M, Scheewe J, Fischer G, Hart C, Andrade A, Pham HM, Kramer HH, Rickers C. Adverse results of a decellularized tissue-engineered pulmonary valve in humans assessed with magnetic resonance imaging. European journal of cardio-thoracic surgery : official journal of the European Association for Cardio-thoracic Surgery. 2013;44(4):e272-9.
389. Kneib C, von Glehn CQ, Costa FD, Costa MT, Susin MF. Evaluation of humoral immune response to donor HLA after implantation of cellularized versus decellularized human heart valve allografts. Tissue antigens. 2012;80(2):165-74.
390. Iop L, Bonetti A, Naso F, Rizzo S, Cagnin S, Bianco R, Dal Lin C, Martini P, Poser H, Franci P, Lanfranchi G, Busetto R, Spina M, Basso C, Marchini M, Gandaglia A, Ortolani F, Gerosa G. Decellularized allogeneic heart valves demonstrate self-regeneration potential after a long-term preclinical evaluation. PloS one. 2014;9(6):e99593.
391. Fallon AM, Goodchild TT, Cox JL, Matheny RG. In vivo remodeling potential of a novel bioprosthetic tricuspid valve in an ovine model. The Journal of thoracic and cardiovascular surgery. 2014;148(1):333-40 e1.
392. Della Barbera M, Valente M, Basso C, Thiene G. Morphologic studies of cell endogenous repopulation in decellularized aortic and pulmonary homografts implanted in sheep. Cardiovascular pathology : the official journal of the Society for Cardiovascular Pathology. 2015;24(2):102-9.
393. Quinn RW, Hilbert SL, Bert AA, Drake BW, Bustamante JA, Fenton JE, Moriarty SJ, Neighbors SL, Lofland GK, Hopkins RA. Performance and morphology of decellularized pulmonary valves implanted in juvenile sheep. The Annals of thoracic surgery. 2011;92(1):131-7.
394. Dohmen PM, da Costa F, Holinski S, Lopes SV, Yoshi S, Reichert LH, Villani R, Posner S, Konertz W. Is there a possibility for a glutaraldehyde-free porcine heart valve to grow? European surgical research Europaische chirurgische Forschung Recherches chirurgicales europeennes. 2006;38(1):54-61.
395. Hof A, Raschke S, Baier K, Nehrenheim L, Selig JI, Schomaker M, Lichtenberg A, Meyer H, Akhyari P. Challenges in developing a reseeded, tissue-engineered aortic valve prosthesis. European journal of cardio-thoracic surgery : official journal of the European Association for Cardio-thoracic Surgery. 2016;50(3):446-55.
396. Bertipaglia B, Ortolani F, Petrelli L, Gerosa G, Spina M, Pauletto P, Casarotto D, Marchini M, Sartore S, Vitalitate Exornatum Succedaneum Aorticum Labore Ingenioso Obtenibitur P. Cell characterization of porcine aortic valve and decellularized leaflets repopulated with aortic valve interstitial cells: the VESALIO Project (Vitalitate Exornatum Succedaneum Aorticum Labore Ingenioso Obtenibitur). The Annals of thoracic surgery. 2003;75(4):1274-82.
397. Santoro R, Consolo F, Spiccia M, Piola M, Kassem S, Prandi F, Vinci MC, Forti E, Polvani G, Fiore GB, Soncini M, Pesce M. Feasibility of pig and human-derived aortic valve interstitial cells seeding on fixative-free decellularized animal pericardium. Journal of biomedical materials research Part B, Applied biomaterials. 2016;104(2):345-56.

398. Liu ZZ, Wong ML, Griffiths LG. Effect of bovine pericardial extracellular matrix scaffold niche on seeded human mesenchymal stem cell function. Scientific reports. 2016;6:37089.
399. Theodoridis K, Tudorache I, Calistru A, Cebotari S, Meyer T, Sarikouch S, Bara C, Brehm R, Haverich A, Hilfiker A. Successful matrix guided tissue regeneration of decellularized pulmonary heart valve allografts in elderly sheep. Biomaterials. 2015;52:221-8.
400. Lichtenberg A, Tudorache I, Cebotari S, Suprunov M, Tudorache G, Goerler H, Park JK, Hilfiker-Kleiner D, Ringes-Lichtenberg S, Karck M, Brandes G, Hilfiker A, Haverich A. Preclinical testing of tissue-engineered heart valves re-endothelialized under simulated physiological conditions. Circulation. 2006;114(1 Suppl):I559-65.
401. Lichtenberg A, Cebotari S, Tudorache I, Sturz G, Winterhalter M, Hilfiker A, Haverich A. Flow-dependent re-endothelialization of tissue-engineered heart valves. The Journal of heart valve disease. 2006;15(2):287-93.
402. Dohmen PM, Lembcke A, Holinski S, Pruss A, Konertz W. Ten years of clinical results with a tissue-engineered pulmonary valve. The Annals of thoracic surgery. 2011;92(4):1308-14.
403. Cebotari S, Mertsching H, Kallenbach K, Kostin S, Repin O, Batrinac A, Kleczka C, Ciubotaru A, Haverich A. Construction of autologous human heart valves based on an acellular allograft matrix. Circulation. 2002;106(12 Suppl 1):I63-I8.
404. Napolitano AP, Chai P, Dean DM, Morgan JR. Dynamics of the self-assembly of complex cellular aggregates on micromolded nonadhesive hydrogels. Tissue engineering. 2007;13(8):2087-94.
405. Berneel E, Philips C, Declercq H, Cornelissen R. Redifferentiation of High-Throughput Generated Fibrochondrocyte Micro-Aggregates: Impact of Low Oxygen Tension. Cells, tissues, organs. 2016;202(5-6):369-81.
406. Quinlan AM, Billiar KL. Investigating the role of substrate stiffness in the persistence of valvular interstitial cell activation. Journal of biomedical materials research Part A. 2012;100(9):2474-82.
407. Wang H, Haeger SM, Kloxin AM, Leinwand LA, Anseth KS. Redirecting valvular myofibroblasts into dormant fibroblasts through light-mediated reduction in substrate modulus. PloS one. 2012;7(7):e39969.
408. Benton JA, Kern HB, Leinwand LA, Mariner PD, Anseth KS. Statins block calcific nodule formation of valvular interstitial cells by inhibiting alpha-smooth muscle actin expression. Arterioscler Thromb Vasc Biol. 2009;29(11):1950-7.
409. Jian B, Narula N, Li QY, Mohler ER, 3rd, Levy RJ. Progression of aortic valve stenosis: TGF-beta1 is present in calcified aortic valve cusps and promotes aortic valve interstitial cell calcification via apoptosis. The Annals of thoracic surgery. 2003;75(2):457-65.
410. Liberman M, Bassi E, Martinatti MK, Lario FC, Wosniak J, Jr., Pomerantzeff PM, Laurindo FR. Oxidant generation predominates around calcifying foci and enhances progression of aortic valve calcification. Arterioscler Thromb Vasc Biol. 2008;28(3):463-70.
411. Miller JD, Chu Y, Brooks RM, Richenbacher WE, Pena-Silva R, Heistad DD. Dysregulation of antioxidant mechanisms contributes to increased oxidative stress in calcific aortic valvular stenosis in humans. Journal of the American College of Cardiology. 2008;52(10):843-50.
412. Farrar EJ, Huntley GD, Butcher J. Endothelial-derived oxidative stress drives myofibroblastic activation and calcification of the aortic valve. PloS one. 2015;10(4):e0123257.
413. Branchetti E, Sainger R, Poggio P, Grau JB, Patterson-Fortin J, Bavaria JE, Chorny M, Lai E, Gorman RC, Levy RJ, Ferrari G. Antioxidant enzymes reduce DNA damage and early activation of valvular interstitial cells in aortic valve sclerosis. Arterioscler Thromb Vasc Biol. 2013;33(2):e66-74.
414. Gomez-Leduc T, Hervieu M, Legendre F, Bouyoucef M, Gruchy N, Poulain L, de Vienne C, Herlicoviez M, Demoor M, Galera P. Chondrogenic commitment of human umbilical cord blood-derived mesenchymal stem cells in collagen matrices for cartilage engineering. Scientific reports. 2016;6:32786.
415. Castrovinci S, Emmanuel S, Moscarelli M, Murana G, Caccamo G, Bertolino EC, Nasso G, Speziale G, Fattouch K. Minimally invasive aortic valve surgery. Journal of geriatric cardiology : JGC. 2016;13(6):499-503.
416. Glauber M, Ferrarini M, Miceli A. Minimally invasive aortic valve surgery: state of the art and future directions. Annals of cardiothoracic surgery. 2015;4(1):26-32.
417. Capulli AK, Emmert MY, Pasqualini FS, Kehl D, Caliskan E, Lind JU, Sheehy SP, Park SJ, Ahn S, Weber B, Goss JA, Hoerstrup SP, Parker KK. JetValve: Rapid manufacturing of biohybrid scaffolds for biomimetic heart valve replacement. Biomaterials. 2017;133:229-41.
418. Driessen-Mol A, Emmert MY, Dijkman PE, Frese L, Sanders B, Weber B, Cesarovic N, Sidler M, Leenders J, Jenni R, Grunenfelder J, Falk V, Baaijens FP, Hoerstrup SP. Transcatheter implantation of homologous "off-the-shelf" tissue-engineered heart valves with self-repair capacity: long-term functionality and rapid in vivo remodeling in sheep. Journal of the American College of Cardiology. 2014;63(13):1320-9.

419. Syedain Z, Reimer J, Schmidt J, Lahti M, Berry J, Bianco R, Tranquillo RT. 6-month aortic valve implantation of an off-the-shelf tissue-engineered valve in sheep. Biomaterials. 2015;73:175-84.
420. Aguiari P, Iop L, Favaretto F, Fidalgo CM, Naso F, Milan G, Vindigni V, Spina M, Bassetto F, Bagno A, Vettor R, Gerosa G. In vitro comparative assessment of decellularized bovine pericardial patches and commercial bioprosthetic heart valves. Biomedical materials. 2017;12(1):015021.
421. Lichtenberg A, Tudorache I, Cebotari S, Ringes-Lichtenberg S, Sturz G, Hoeffler K, Hurscheler C, Brandes G, Hilfiker A, Haverich A. In vitro re-endothelialization of detergent decellularized heart valves under simulated physiological dynamic conditions. Biomaterials. 2006;27(23):4221-9.
422. Yang M, Chen CZ, Shu YS, Shi WP, Cheng SF, Gu YJ. Preseeding of human vascular cells in decellularized bovine pericardium scaffold for tissue-engineered heart valve: an in vitro and in vivo feasibility study. Journal of biomedical materials research Part B, Applied biomaterials. 2012;100(6):1654-61.
423. Mirsadraee S, Wilcox HE, Watterson KG, Kearney JN, Hunt J, Fisher J, Ingham E. Biocompatibility of acellular human pericardium. The Journal of surgical research. 2007;143(2):407-14.
424. Mirsadraee S, Wilcox HE, Korossis SA, Kearney JN, Watterson KG, Fisher J, Ingham E. Development and characterization of an acellular human pericardial matrix for tissue engineering. Tissue engineering. 2006;12(4):763-73.
425. Dohmen PM, Hauptmann S, Terytze A, Konertz WF. In-vivo repopularization of a tissue-engineered heart valve in a human subject. The Journal of heart valve disease. 2007;16(4):447-9.
426. Korossis SA, Booth C, Wilcox HE, Watterson KG, Kearney JN, Fisher J, Ingham E. Tissue engineering of cardiac valve prostheses II: biomechanical characterization of decellularized porcine aortic heart valves. The Journal of heart valve disease. 2002;11(4):463-71.
427. Rieder E, Kasimir MT, Silberhumer G, Seebacher G, Wolner E, Simon P, Weigel G. Decellularization protocols of porcine heart valves differ importantly in efficiency of cell removal and susceptibility of the matrix to recellularization with human vascular cells. The Journal of thoracic and cardiovascular surgery. 2004;127(2):399-405.
428. Numata S, Fujisato T, Niwaya K, Ishibashi-Ueda H, Nakatani T, Kitamura S. Immunological and histological evaluation of decellularized allograft in a pig model: comparison with cryopreserved allograft. The Journal of heart valve disease. 2004;13(6):984-90.
429. Jordan JE, Williams JK, Lee SJ, Raghavan D, Atala A, Yoo JJ. Bioengineered self-seeding heart valves. The Journal of thoracic and cardiovascular surgery. 2012;143(1):201-8.
430. Gallo M, Naso F, Poser H, Rossi A, Franci P, Bianco R, Micciolo M, Zanella F, Cucchini U, Aresu L, Buratto E, Busetto R, Spina M, Gandaglia A, Gerosa G. Physiological performance of a detergent decellularized heart valve implanted for 15 months in Vietnamese pigs: surgical procedure, follow-up, and explant inspection. Artificial organs. 2012;36(6):E138-50.
431. Assmann A, Akhyari P, Delfs C, Flogel U, Jacoby C, Kamiya H, Lichtenberg A. Development of a growing rat model for the in vivo assessment of engineered aortic conduits. The Journal of surgical research. 2012;176(2):367-75.
432. Quinn RW, Hilbert SL, Converse GL, Bert AA, Buse E, Drake WB, Armstrong M, Moriarty SJ, Lofland GK, Hopkins RA. Enhanced Autologous Re-endothelialization of Decellularized and Extracellular Matrix Conditioned Allografts Implanted Into the Right Ventricular Outflow Tracts of Juvenile Sheep. Cardiovascular engineering and technology. 2012;3(2):217-27.
433. Navarro FB, Costa FD, Mulinari LA, Pimentel GK, Roderjan JG, Vieira ED, Noronha L, Miyague NI. Evaluation of the biological behavior of decellularized pulmonary homografts: an experimental sheep model. Revista brasileira de cirurgia cardiovascular : orgao oficial da Sociedade Brasileira de Cirurgia Cardiovascular. 2010;25(3):377-87.
434. Hopkins RA, Jones AL, Wolfinbarger L, Moore MA, Bert AA, Lofland GK. Decellularization reduces calcification while improving both durability and 1-year functional results of pulmonary homograft valves in juvenile sheep. The Journal of thoracic and cardiovascular surgery. 2009;137(4):907-13, 13e1-4.
435. Costa F, Dohmen P, Vieira E, Lopes SV, Colatusso C, Pereira EW, Matsuda CN, Cauduro S. Ross Operation with decellularized pulmonary allografts: medium-term results. Revista brasileira de cirurgia cardiovascular : orgao oficial da Sociedade Brasileira de Cirurgia Cardiovascular. 2007;22(4):454-62.
436. Iwai S, Torikai K, Coppin CM, Sawa Y. Minimally immunogenic decellularized porcine valve provides in situ recellularization as a stentless bioprosthetic valve. Journal of artificial organs : the official journal of the Japanese Society for Artificial Organs. 2007;10(1):29-35.
437. Takagi K, Fukunaga S, Nishi A, Shojima T, Yoshikawa K, Hori H, Akashi H, Aoyagi S. In vivo recellularization of plain decellularized xenografts with specific cell characterization in the systemic circulation: histological and immunohistochemical study. Artificial organs. 2006;30(4):233-41.

438. Miller DV, Edwards WD, Zehr KJ. Endothelial and smooth muscle cell populations in a decellularized cryopreserved aortic homograft (SynerGraft) 2 years after implantation. The Journal of thoracic and cardiovascular surgery. 2006;132(1):175-6.
439. Meyer SR, Nagendran J, Desai LS, Rayat GR, Churchill TA, Anderson CC, Rajotte RV, Lakey JR, Ross DB. Decellularization reduces the immune response to aortic valve allografts in the rat. The Journal of thoracic and cardiovascular surgery. 2005;130(2):469-76.
440. Ota T, Sawa Y, Iwai S, Kitajima T, Ueda Y, Coppin C, Matsuda H, Okita Y. Fibronectin-hepatocyte growth factor enhances reendothelialization in tissue-engineered heart valve. The Annals of thoracic surgery. 2005;80(5):1794-801.
441. Costa FDAD, Dohmen P, Lopes SV, Pohl F, Vilani R, Vieira E, Costa MBAD, Konertz SYW. Estudo experimental com heteroenxertos valvares descelularizados: a prótese do futuro. Brazilian Journal of Cardiovascular Surgery. 2004;19:74-82.
442. Wilson GJ, Courtman DW, Klement P, Lee JM, Yeger H. Acellular matrix: a biomaterials approach for coronary artery bypass and heart valve replacement. The Annals of thoracic surgery. 1995;60(2 Suppl):S353-8.
443. Mabry KM, Schroeder ME, Payne SZ, Anseth KS. Three-Dimensional High-Throughput Cell Encapsulation Platform to Study Changes in Cell-Matrix Interactions. ACS applied materials & interfaces. 2016;8(34):21914-22.
444. Duan B, Yin Z, Hockaday Kang L, Magin RL, Butcher JT. Active tissue stiffness modulation controls valve interstitial cell phenotype and osteogenic potential in 3D culture. Acta biomaterialia. 2016;36:42-54.
445. Zhang X, Xu B, Puperi DS, Yonezawa AL, Wu Y, Tseng H, Cuchiara ML, West JL, Grande-Allen KJ. Integrating valve-inspired design features into poly(ethylene glycol) hydrogel scaffolds for heart valve tissue engineering. Acta biomaterialia. 2015;14:11-21.
446. Durst CA, Cuchiara MP, Mansfield EG, West JL, Grande-Allen KJ. Flexural characterization of cell encapsulated PEGDA hydrogels with applications for tissue engineered heart valves. Acta biomaterialia. 2011;7(6):2467-76.
447. Shah DN, Recktenwall-Work SM, Anseth KS. The effect of bioactive hydrogels on the secretion of extracellular matrix molecules by valvular interstitial cells. Biomaterials. 2008;29(13):2060-72.

SUPPLEMENTARY TABLES

Table S1: Overview of *in vitro* repopulation studies of decellularized scaffolds

	Decellularization	Scaffold (+additives) Cells	Repopulation protocol (Static/Rotation/Dynamic)	In vivo	Decellularization & Recellularization
Roosens et al. (2017)	**Detergent:** • Triton X-100 **Enzyme:** • Trypsin • RNase and DNase	**Scaffold:** • **p**AVL • **p**PER **Cells:** • **p**VIC • **p**BM-MSC • **p**ADSC • **p**VEC	**Static:** • $1*10^6$ cells/cm² (VIC/MSC), • After 7d ➔ • $2*10^5$ cells/cm² (VEC), 7d • Cells were seeded onto LV (HVL) and fibrosa side (PER) • MSC ± AA		**Decell:** • HE: cell free • Preservation ECM and acellularity evaluated in [304] **Recell:** • HVL: complete repopulation interstitium with VIC and BM-MSC (+AA) + monolayer of $CD31^+$ EC (no repopulation with ADSC) • PER: repopulation fibrosa with VIC and BM-MSC (+AA) + monolayer of $CD31^+$ EC (EC did attach but did not spread)
[420] Aguiari et al. (2017)	**Detergent:** • Triton X-100 • Sodium taurodeoxycholate	**Scaffold:** • **b**PER **Cells:** • **h**ADSC	**Static:** • $0.5*10^6$/cm², 30d		**Decell:** • HE: cell free **Recell:** • Evenly but not complete repopulated PER
[307] Converse et al. (2017)	**Detergent:** • Triton X-100 • Sodium-lauroyl sarcosine **Enzyme:** • Benzoase®	**Scaffold:** • **o**AV **Cells:** • **h**MSC	**Static:** • $5.0*10^6$/10ml, 24h (Group 1), n=3) **Dynamic:** • Cyclic pressure -20-5mmHg, 72h (Group 2, n=6) • positive pressures, 10d (group 3, n=6)		**Decell:** • HE: cell free **Recell:** • Group 1: cells adherent only to the LF and often concentrated within undulations on the surface of the HVL • Group 2: more uniform distribution of cells on the surface and sparse subsurface infiltration into the LF • Group 3: better surface coverage, often on both LF and LV and improved subsurface infiltration. Infiltration not observed in every HVL and cell density remained below native levels
[397] Santoro et al. (2016)	**Detergent:** • SDS **Enzyme:** • RNase and DNase	**Scaffold:** • **p**PER **Cells:** • **p**VIC	**Static:** • $0.6\text{-}3*10^3$ cells,72h		**Decell:** • DAPI: cell free **Recell:** • Cells seeded on serosa side: higher cell adhesion but no ingrowth
[395] Hof et al. (2016)	**Detergent:** • SDS • SDC • ± trypsin treatment • ±laser perforation	**Scaffold:** • **o**VIC **Cells:** • **o**AVL	**Static:** • $0.3\text{-}1*10^6$ cells/50mm²,7d • $4*10^6$/ml,7d (cyclic strain) • On fibrosa or serosa side		**Decell:** • HE: cell free **Recell:** • No VIC adhesion or migration in untreated leaflets • + trypsin treatment = most effective, but no complete repopulation
[398] Liu et al.	**Detergent:** • SDS	**Scaffold:** • **b**PER	**Static:** • $3*10^4$ cells		**Decell:** • No visible nuclei (data not shown)

	Decellularization	Scaffold (+additives) Cells	Repopulation protocol (Static/Rotation/Dynamic)	In vivo	Decellularization & Recellularization
(2016)	**Enzyme:** • RNase and DNase	**Cells:** • **h**BM-MSC	• On fibrosa or serosa side		**Recell:** • No cells on decellularized PER
[302] Kajbafzadeh et al. (2016)	**Detergent:** • Triton X-100 • SDS	**Scaffold:** • **o**PER • **o**AV **Cells:** • **o**BM-MSC	**Dynamic:** • $2*10^6$ cells • Max. flow rate: 2.0L/min • Pressure: 100mmHg • 48h	**Lambs** (n=8) • Aorta descendens thoracalis • 4 non-homograft related deaths (2 after 10m, 2 after 19m) ○ *Post-implantation (18m)*: mild aneurismal formation, no evidence of thrombosis or macroscopic calcification	**Decell:** • HE: cell free; SEM: no cellularity or structure distortion; preserved col type I, no significant deterioration of ECM **Recell:** • *Pre-implantation:* N/I • *Post-implantation*: complete layer EC-like cells covered the surface, and the interstitium was completely recellularized by spindle shaped cells after 18m
[399] Theodoridis et al. (2015)	**Detergent:** • SDC • SDS	**Scaffold:** • **o**PV • CNN1-coating **Cells:** • **o**EC differentiated from **o**MNC	**Static:** • $5.6 \pm 3.2 *10^6$ cells • vertical position, 6h **Rotation:** • Horizontal position • 0.1rpm/min, 6h **Dynamic:** • Max flow 1.0L/min,2d	**Sheep** (each group n=6) • Supravalvular pulmonary position • Group 1: acellular valve • Group 2: acellular valve CNN1 coating • Group 3: acellular valve CNN1 coating + **o**EC • 6 and 12m (no significant difference) ○ *Post-implantation:* calcification in 2 allografts (group 1 and 3), $CD45^+$ cells similar to native PV	**Decell:** • N/I [421] **Recell:** • *Pre-implantation:* N/I • *Post-implantation*: group 1<2<3. Overall: LV surface covered 1/3 with cells, LF coverage less pronounced. Cells in LV and LS not LF. Tendency of better repopulation in group 3. Better *in vivo* repopulation did not influence valve function
[104] Tudorache et al. (2013)	**Detergent:** • SDC • SDS	**Scaffold:** • **o**AV • CNN1-coating **Cells:** • **o**EC	**Rotation:** • $0.5*10^7$ cells/valve vertical position, 6h • Slow rotation 0.05 rpm, 6h **Dynamic:** • Max flow 1.0L/min • Pressure: 80mmHg, 7d	**Young sheep** (n=10) • Orthotopic position • Cryopreserved **o**AV (n=4), Recellularized **o**AV (n=10) ○ *Post-implantation (3m):* Cryopreserved **o**AV = *calcification*, massive infiltration $CD45^+$ cells. Recellularized **o**AV = no signs of inflammation or calcification	**Decell:** • N/I [317] **Recell:** • *Pre-implantation:* complete re-endothelialization ($eNOS^+$, $CD31^+$) • *Post-implantation*: Cryopreserved **o**AV = $CD31^+$ and vWF^+ cells on luminal surface. Recellularized **o**AV = surface covered by $eNOS^+$, vWF^+ and $CD31^+$ cells up to the free margin
[103] Somers et al. (2012)	**Detergent:** • Triton X-100 **Enzyme:** • Trypsin • RNase and DNase	**Scaffold:** • **p**AVL • preloading with heparin and incubation PG **Cells:** • **o**MSC	**Static:** • $1*10^6$ cells/cm², 5d **OR** **Dynamic**: • $6*10^6$ cells/ml, 2d • Average flow rate: 2.7L/min • Pressure: 40mmHg		**Decell:** • N/I **Recell:** • Static: near confluent surface layer of cells on preloaded scaffolds but no cell ingrowth • Dynamic: near confluent surface layer of cells on preloaded scaffolds, limited cell ingrowth in LV
[422] Yang et al. (2012)	**Detergent:** • Triton X-100 **Enzyme:** • RNase and DNase	**Scaffold:** • **b**PER **Cells:** • **h**Vascular cells	**Static:** • $2*10^6$ cells, 7/14/21d	**Mice** (n=10) • Subcutaneous: left side (group 2 = decell), right side (group 1 = recell) • 30d	**Decell:** • HE: cell free **Recell:** • *Pre-implantation:* d7: scaffold covered completely, by d21 also some penetrating cells • *Post-implantation*: more accumulation of cells on PER. Group 1 = large number of infiltrating cells + SEM = monolayer on surface; Group 2 = no cell ingrowth + SEM = monolayer of non-spread cells on surface.

	Decellularization	Scaffold (+additives) Cells	Repopulation protocol (Static/Rotation/Dynamic)	In vivo	Decellularization & Recellularization
[402] Dohmen et al. (2011)	**Detergent:** • SDC	**Scaffold:** • **h**PV • Fibronectin **Cells:** • **h**EC	**Dynamic**: • 4.9±2.5*10^6 cells/valve, 10d • [281]	**Humans** (n=11) • Ross operation • 10y survival = 100% ○ No structural device-specific complication (calcification or degeneration), thromboembolic complication, bleeding events or prosthetic valve endocarditis	**Decell:** • N/I [281] **Recell:** • *Pre-implantation:* Confluent monolayer EC inner surface of seeded heart valves • *Post-implantation:* N/A
[282] Cebotari et al. (2010)	**Detergent:** • SDS • SDC	**Scaffold:** • **p**PV **Cells:** • **h**EC	**Static:** • 3.33*10^5 cells/cm², 72h		**Decell:** • cell free scaffolds (data not shown) **Recell:** • monolayer EC with cobblestone morphology (data not shown)
[306] Dong et al. (2009)	**Detergent:** • Triton X-100 **Enzyme:** • RNase and DNase	**Scaffold:** • **b**PER • acetic acid RGD polypeptide **Cells:** • **h**BM-MSC	**Static:** • 1.0*10^6 cells/10mL, 20h		**Decell:** • HE: complete removal of cells; Acetic acid treatment significantly increased pore size **Recell:** • Only single layer of cells on acellular PER. Cells grow deep into the scaffold of acetic acid treated and RGD modified acellular PER.
[105] Iop et al. (2009)	**Detergent:** • Triton X-100 • Sodium cholate (=TRICOL) **Enzyme:** • Endonucleases	**Scaffold:** • **p**PVL • **h**PVL • FBS • Fibronectin **Cells:** • **h**BM-MSC	**Static:** • 2*10^6 cells/cm², 30d		**Decell:** • HE/HOECHST: cell free; α-gal: negative; decreased leaflet thickness (loss GAG), Col I/III and elastin fibers well preserved **Recell:** • LV/LF behave differently regards cell proliferation, differentiation and survival (LV=more cell ingrowth) • Homotypic cell seeding is more effective

[423] Mirsadraee et al. (2007)	**Detergent:**
	• SDS
	Enzyme:
	• Nuclease treatment
		Scaffold:
		• Group 1: Fresh/frozen **h**PER
		• Group 2: **h**PER
		• Group 3: GA-**h**PER
		Cells:
		• **h**Fb
			Static:
			• 6.25*10^5 cells/cm², 5w
				Mice (each group n=3)
				• Subcutaneous
				  ○ *Post-implantation (*3m): Group 1: 50-60% $CD3^+$, $CD4^+$ and $CD11b^+$ cells. Group 2: 11% $CD3^+$/$CD4^+$ cells 28% $CD11b^+$ and higher $CD34^+$ cells compared to group 1. Group 3: 30% $CD3^+$, $CD4^+$ and $CD11b^+$ cells, low $CD34^+$ cells but high polymorphonuclear cells
					Decell:
					• N/I [424]
					Recell:
					• *Pre-implantation:* after 4w, more than half of the tissue thickness repopulated
					• *Post-implantation:*
					  ○ Group 1: tissue encapsulated with a high number of host cells
					  ○ Group 2: host cells deep into the tissue, little signs of capsular formation
					  ○ Group 3: completely encapsulated with a high number of host cells

[425] Dohmen et al. (2007)	**Detergent:** • SDC	**Scaffold:** • **h**PV • Fibronectin **Cells:** • **h**EC	**Dynamic**: • 5.0*10^6 cells/valve, 7d • [281]	**Human case report** • Female 63j • Ross operation • 6j follow up	**Decell:** • N/I [281] **Recell:** • *Pre-implantation:* Confluent monolayer EC ($CD31^+$) • *Post-implantation (biopsy, 3m):* Confluent monolayer EC ($CD31^+$, vWF^+), ingrowth of interstitial cells in the deeper layers

	Decellularization	Scaffold (+additives) Cells	Repopulation protocol (Static/Rotation/Dynamic)	In vivo	Decellularization & Recellularization
[373] Dohmen et al. (2007)	**Detergent:** • SDC	**Scaffold:** • Group 1: **p**PV (Matrix P) • Group 2: **h**PV • Pronectin F **Cells:** • **h**EC	**Dynamic**: • 5.0*10^6 cells/valve, 10d • [281]	**Humans** (n=12, group 1; n=11, group 2) • Ross operation • 5j follow up • 1 patient died after 3m (arrhythmia) • 1 patient new valve after 4m (inflammatory reaction) ○ *Post-implantation (biopsy? timepoint?):* few $CD68^+$, ECM preserved, little tissue fibrosis, no calcification	**Decell:** N/I [281] **Recell:** • *Pre-implantation:* Confluent monolayer EC inner surface leaflets (both groups) • *Post-implantation:* Confluent monolayer EC ($CD31^+$), ingrowth of interstitial cells in the deeper layers (mainly $CD34^+$) • *No comparison between group 1 and 2*
[206] Vincentelli et al. (2007)	**Detergent:** • SDS	**Scaffold:** • **p**PV **Cells:** • Group 1**:** **o**BM-MSC • Group 2: **o**BM-MNC • n=2/group: PKH67 labeled cells	**In vivo injection of cells:** • 100 ± 50*10^6 MNC • 7.7 ± 3*10^6 MSC	**Lambs** (each group n=7) • Pulmonary artery (cardiopulmonary bypass) • Explanted after 4m or 7d (labeled cells) ○ *Post-implantation (4m):* Group 2: wall thickened with calcifications, fibrous tissue, leaflets slightly thickened and retracted, ECM disorganized, strong $CD68^+$ cell infiltration, many neovessels. Group 1: no calcification, no fibrous tissue, no thickened wall/leaflets, no $CD68^+$ cells, rare neovessels	**Decell:** • N/I [290, 426] **Recell:** • *Post-implantation:* ○ After 7d: early migration of labeled cells in matrix (around injection area), also infiltrated host cells (non-fluorescent), no difference between groups. ○ After 4m, both groups complete re-endothelialization (vWF^+) but more pronounced in group 1. Few recolonizing cells in group 1
[401] Lichtenberg et al. (2006)	**Detergent:** • SDC • SDS	**Scaffold:** • **o**PV **Cells:** • **o**EC	**Rotation:** • 3 seeding steps, total 1.2*10^7 cells/valve, 2d (group 1) • rotation 0.1rpm/min **Dynamic:** • Max flow: 0.5L/min, 2d (group 2); 2.0L/min, 2d (group 3) • Pressure: 25 mmHg		**Decell:** • HE: cell free; ECM preserved **Recell:** • Group 1: incomplete monolayer EC ≥50% (vWF^+, $eNOS^+$) • Group 2: complete monolayer EC >90% (vWF^+, $eNOS^+$) • Group 3: incomplete monolayer EC <50% (only wall, not leaflets) (vWF^+, $eNOS^+$)
[421] Lichtenberg et al. (2006)	**Detergent:** • SDC • SDS	**Scaffold:** • **o**PV **Cells:** • **o**EC	[401] Lichtenberg et al. (2006)		**Decell:** • HE: cell free; DNA less than 5%; ECM preserved **Recell:** • Group 1: incomplete monolayer EC ≥50% (vWF^+) data not shown • Group 2: complete monolayer EC >90% (vWF^+) • Group 3: complete re-endothelialization (SEM)
[400] Lichtenberg et al. (2006)	**Detergent:** • SDC • SDS	**Scaffold:** • **o**PV **Cells:** • **o**EC	[401] Lichtenberg et al. (2006)	**Lambs** (n=14) • Orthotopic position • Group 1 (n=7): decell PV • Group 2 (n=7): recell PV ○ *Post-implantation (3m):* no difference in competence and no signs of calcification. More thrombotic and neointima formation in group 1	**Decell:** • HE/DAPI: cell free; ECM preserved **Recell:** • *Pre-implantation:* Confluent monolayer EC (vWF^+, $eNOS^+$) • *Post-implantation:* Interstitium comparable repopulated, only monolayer EC in group 2

	Decellularization	Scaffold (+additives) Cells	Repopulation protocol (Static/Rotation/Dynamic)	In vivo	Decellularization & Recellularization
[98] Grauss et al. (2005)	**Detergent:** • Group 1: Triton X-100 **Enzyme:** • Group 2: Trypsin	**Scaffold:** • **p**AVL **Cells:** • **p**EC	**Static:** • amount? • on LF • 10d		**Decell:** • Group 1: cell free; Group 2: shrunken cell pyknotic nuclei (data not shown) • Group 2: fragmentation and distortion elastin fibers, col distribution changes, complete washout GAG, laminin and fibronectin; Group 1: less GAG reduction, no distortion elastin fibers, washout laminin and fibronectin **Recell:** • 80% surface covered with monolayer EC (vWF^+), no cell ingrowth. EC layer also positive for fibronectin, laminin and chondroitin sulphate
[427] Rieder et al. (2004)	**Detergent:** • SDS (Group 2) • Triton X-100 AND • SDC (Group 3) **Enzyme:** • RNase and DNase (Group 3) • Trypsin (Group 1)	**Scaffold:** • **p**PV • **p**AV **Cells:** • **h**EC • **h**MFb	**Static:** • $1*10^4$ (**h**EC), 5d • $2*10^4$ (**h**MFb) 10d		**Decell:** • DNA staining: Group 1 still cells. Group 2-3: cell free **Recell:** • Group 1-3: confluent monolayer EC (SEM), Group 2: no cell attachment • Group 3: few interstitial cells (other groups not mentioned)
[428] Numata et al. (2004)	**Detergent:** • Triton X-100 **Enzyme:** • RNase and DNase	**Scaffold:** • **p**PV **Cells:** • **p**EC	**Static:** • $5*10^6$ cells • 48h	**Mini-pigs** (n=6) • Group 1 (n=2): recell PV • Group 2 (n=2): decell PV • Group 3 (n=2): cryopreserved PV • *Post-implantation (4w):* Group 3: $CD68^+$ and $CD3^+$ cells	**Decell:** • N/I **Recell:** • *Pre-implantation:* N/I • *Post-implantation:* Group 1-2: EC coverage (vWF^+), no cell ingrowth Group 3: no recellularization (only inflammatory cells)
[173] Schenke-Layland et al. (2003)	**Enzyme:** • Trypsin	**Scaffold:** • **p**PV **Cells:** • **o**EC • **o**MFb	**Static:** • $3*10^7$ MFb, 2d **Dynamic:** • Flow rate: 3.0L/min, 60/40mmHg, 9 or 16d **Static:** • $9*10^6$ EC, 2d		**Decell:** • HE: almost completely cell free; preservation col and elastin but a decrease in GAG **Recell:** • Complete repopulation after 16d dynamic culture (interstitium: α-SMA^+, surface vWF^+)
[289] Dohmen et al. (2003)	**Detergent:** • SDC	**Scaffold:** • **p**PV (Matrix P) • Fibronectin **Cells:** • **o**EC	**Rotation:** • $1.1*10^6$ cells/cm^3, 4h • rotation 10° steps **Static:** • 7d	**Sheep** (n=8) • RVOT • Explanted at 7d (n=1), 3m (n=4) and 6m (n=3 ○ *Post-implantation (6m):* no encapsulation leaflets, no hematomas, vegetation or thrombotic material, no calcification, minimal inflammation	**Decell:** • HE: completely cell free **Recell:** • *Pre-implantation:* N/I • *Post-implantation (6m):* monolayer EC middle part of leaflets, islands of EC at the free edge, no cell ingrowth
[396] Bertipaglia et al.	**Detergent:** • Triton X-100 • SDC	**Scaffold:** • **p**AVL • FBS • Fibronectin	**Static:** • $2*10^6$ cells • 15d		**Decell:** • HE: completely cell free **Recell:** • Cells on surface and in LF and LS (characteristics of EC, Fb, MFb

	Decellularization	Scaffold (+additives) Cells	Repopulation protocol (Static/Rotation/Dynamic)	In vivo	Decellularization & Recellularization
(2003)		**Cells:** • **p**VIC			and SMC), cell density remained below native levels
[403] Cebotari et al. (2002)	**Enzyme:** • Trypsin	**Scaffold:** • **h**PV • **h**AV **Cells:** • **h**EC	**Rotation:** • $2*10^5$ cells/cm², 12h **Dynamic:** • 15mL/min, 10d		**Decell:** • HE: completely cell free; DNA less than 98%, ECM preserved **Recell:** • Monolayer EC on both sides (vWF^+, VE-cadherin$^+$)
[281] Dohmen et al. (2002)	**Detergent:** • SDC	**Scaffold:** • **h**PV • Pronectin F **Cells:** • **h**EC	**Rotation:** • $1.1*10^6$ cells/cm³, 4h • rotation 10° steps **Static:** • 7d	**Human case report** • Ross operation • 43y old	**Decell:** • N/I **Recell:** • *Pre-implantation:* monolayer EC
[301] Zeltinger et al. (2001)	• Hypo-/hypertonic buffers **Enzyme:** • Trypsin • RNase and DNase	**Scaffold:** • **p**AV • **p**AVL **Cells:** • **h**Fb	**Dynamic:** • shaker (**p**AVL): $2*10^5$ cells, 8w • Bioreactor (**p**AV): $1*10^7$ cells, 8w		**Decell:** • HE: cells largely removed; ECM preserved **Recell:** • Gradual recolonization scaffolds
[305] Steinhoff et al. (2000)	**Enzyme:** • Trypsin	**Scaffold:** • **o**PV **Cells:** • **o**EC • **o**MFb	**Static:** • **o**MFb 6d • **o**EC 2d • amount?	**Lambs** (n=10) • Orthotopic position • Group 1 (n=6): recell • Group 2 (n=4): decell ○ *Post-implantation (3m):* Group 2: 1 died (endocarditis and thrombosis). Both groups: subvalvular calcification (different degree); valvular calcification (1 animal group 2); Group 1: leukocyte infiltration decreases in time	**Decell:** • Almost complete removal of cells **Recell:** • *Pre-implantation:* patchy incomplete seeding of MFb and EC (vWF^+ and α-SMA$^+$) data not shown • *Post-implantation (3m):* ○ Group 2: almost complete monolayer EC (vWF^+), very few cells at the base of interstitium ○ Group 1: monolayer EC (vWF^+), gradual recolonization interstitium with MFb (α-SMA$^+$)
[292] Bader et al. (1998)	**Detergent:** • Triton X-100 **Enzyme:** • RNase and DNase	**Scaffold:** • **p**AVL **Cells:** • **p**EC	**Static:** • $1.2*10^5$ cells/cm², 3d		**Decell:** • TB: Almost complete removal of cells; matrix loosened at interfibrillar zones, fibers grossly maintained **Recell:** • Confluent monolayer EC surface (CD31$^+$), no cell ingrowth

Abbreviations: b = bovine; h = human; o = ovine; p = porcine; SEM = scanning electron microscopy; N/I = not investigated; N/A = not applicable; SDC = sodium deoxycholate; SDS = Sodium dodecyl sulfate; eNOS = endothelial nitric oxide synthase; vWF = von Willebrandfactor; GA = glutaraldehyde; FBS = fetal bovine serum; GAG = glycosaminoglycans; LF = lamina fibrosa; LS = lamina spongiosa; LV = lamina ventricularis; ECM = extracellular matrix; d = days; w = weeks; m = months; y = years; SMC = smooth muscle cells; VIC = valvular interstitial cells; AV = aortic valve; PER = pericardium; BM-MSC = bone marrow derived mesenchymal stem cells; PV = pulmonary valve; MNC = mononuclear cells; EC = endothelial cells; MSC = mesenchymal stem cells; MFb = myofibroblasts; PVL = pulmonary valve leaflet; Fb = fibroblasts; AVL = aortic valve leaflet; α-SMA = α-smooth muscle actin; HE = hematoxylin eosin; RGD = tripeptide Arg-Gly-Asp; AA= ascorbic acid 2-phosphate

Table S2: Overview of *in vivo* repopulation studies of decellularized scaffolds

	Decellularization	Scaffold (+additives)	*In vivo*	Decellularization & Recellularization
[316] Tudorache et al. (2016)	**Detergent:** • SDS • SDC	**Scaffold:** • **o**AV • **o**PV • **o**PV (autograft)	**Sheep** (n=10) • AV replacement; Group 1 (n=5): Ross operation, AV replaced by **o**PV (autograft (PA)) and PV replaced by acellular **o**PV (DPVA); Group 2 (n=5): AV replaced by acellular **o**AV (DAVA). • Explanted after 20m • Only intrinsic calcifications in PA grafts • Very low levels of $CD8^+$ and $CD11b^+$ cells in all grafts, $CD11b^+$ cells mainly in the wall and on surface of the leaflets	**Decell:** • N/I [421] **Recell:** • After 20m, PA grafts had less vWF^+ and $eNOS^+$ cells compared to DAVA and DPVA which showed a monolayer of EC (vWF^+ and $eNOS^+$) especially on the LV of the leaflets • DPVA and DAVA grafts had high α-SMA^+ and pro-col I^+ cells in interstitium of leaflets compared to PA grafts • Cell density was higher in PA than in DAVA and DPVA and full repopulation was observed neither in DAVA nor in DPVA • DAVA: leaflets repopulated in the LV and LS but not LF, wall strongly repopulated in the adventitia layer but no full repopulation in any graft; DPVA: comparable repopulation to DAVA but in the LS to a lesser degree. Wall stronger repopulated than DAVA, in 2 cases reaching a native-like density
[392] Della Barbera et al. (2015)	**Detergent:** • SDS • SDC	**Scaffold:** • **o**AV • **o**PV	**Sheep** (n=8) • Group 1 (n=2): **o**AV; Group 2 (n=6): **o**PV • Explanted after 14-21m • No gross calcification, calcium content slightly higher group 1, no inflammatory infiltrates, no structural deterioration and negligible calcification	**Decell:** • HE: completely cell free; ECM preserved **Recell:** • After 14m, cell repopulation variably occurred in the outer part of the wall, with α-SMA+ and vimentin+ spindle cells. vWF^+ EC present over the intimal surface • Leaflets: cell repopulation in the LV and LS, not LF, cells appeared scattered in the leaflet belly and rare in the leaflet free margin. The endothelial lining restored with vWF^+ cells
[315] Williams et al. (2015)	**Detergent:** • Triton X-100	**Scaffold:** • **p**PV • Matrix conjugated with CD133 monoclonal antibody	**Sheep** (n=39) • Pulmonary valve replacement • Group 1 (n=18): coated **p**PV; Group2 (n=18) non-coated **p**PV; n=3 native valve • Explanted after 4h, 3, 7, 14, 14, 30 and 90d • No calcification or thrombi in any valve	**Decell:** • N/I [429] **Recell:** • Group 2: after 90d, little cell invasion and no monolayer EC ($CD31^+$) • Group 1: by d3, $CD133^+/CD31^-$ cells adhered to the surface of the leaflets, by d30 cells were $CD133^-/CD31^+$ and a monolayer was formed. From d14-90, leaflet interstitium repopulated. After 90d interstitium completely repopulated with 90% α-SMA^+ and 75% $vimentin^+$ cells, periostin and MMP-2 expression comparable to native cells
[390] Iop et al. (2014)	**Detergent:** • Triton X-100 • Sodium cholate (=TRICOL) **Enzyme:** • Endonuclease treatment	**Scaffold:** • **p**AV	**Pigs** (n=11) • RVOT • Explanted after 6 or 15m • No signs of calcification, fibrosis or thrombosis, neovascularization in the wall, reparative M2 macrophages	**Decell:** • N/I [430] **Recell:** • After 6m, intimal layer covered by a dense endothelial lining (vWF^+), and activated fibroblast in the media layer and most leaflets completely re-endothelialized • fibroblast in the leaflet base, migrating towards the free middle and distal portions, in one case after 6m, but in most samples after 15m

	Decellularization	Scaffold (+additives)	*In vivo*	Decellularization & Recellularization
[391] Fallon et al. (2013)	**Detergent:** • N/A	**Scaffold:** • **p**SIS (CorMatrix)	**Sheep** (n=4) • Tricuspid replacement • Explanted after 3, 5, 8, 12m	**Decell:** • N/A **Recell:** • After 3m, elastin formation (annulus), and some eNOS$^+$ cells at the ventricular side, interspersed vimentin+ cells • The endothelial layer progressively developed into a CD31$^+$ and eNOS$^+$ monolayer after 12m • After 5m, collagen reorganization increased and GAG present in the middle of the leaflets • After 8m, vimentin$^+$ cells at the center of the leaflets with some colocalization of α-SMA$^+$ cells. α-SMA$^+$ cells mainly at the ventricular side and in the wall
[314] Assmann et al. (2013)	**Detergent:** • SDS • SDC	**Scaffold:** • **r**AV • Fibronectin coating	**Rats** (each group n=18) • Group 1: coated **r**AV; Group 2: non-coated **r**AV • Systemic circulation • Explanted after 8w • No CD3$^+$, CD68$^+$ cells or thrombosis in both groups • Group 1: micro calcifications in the wall (in regions with extensive hyperplasia)	**Decell:** • N/I [431] **Recell:** • After 8w, luminal re-endothelialization was accelerated in group 1 • Group 1: local MFb hyperplasia with significantly increased ration of intima-media thickness α-SMA$^+$, desmin$^+$, and little vimentin$^+$ cells (aortic wall)
[432] Quinn et al. (2012)	**Detergent:** • Triton X-100 • Sodium-lauroyl sarcosine **Enzyme:** Benzoase®	**Scaffold:** • **o**PV	**Sheep** (n=8) • RVOT • Group 1 (n=4): acellular **o**PV; Group 2 (n=2): cryopreserved allografts; Group 3 (n=2): bioprosthetic porcine valves ○ *Post-implantation (20w):* no cusp calcification in any valve, arterial wall calcification in group 2 (mild/moderate) and group 3 (severe). Group 1: valves slightly stiffer and less extensible than group 2 but comparable hemodynamics	**Decell:** • HE: cell free **Recell:** • Only spontaneous recellularization in group 1 • EC on outflow layer of leaflets (vWF$^+$) • Interstitial cells mainly in arterial wall and variably extending into the leaflets
[151] Honge et al. (2011)	**Detergent:** • SDC	**Scaffold:** • **p**AV	**Pigs** (n=27) • Orthotopic position • Group 1 (n=12): acellular **p**AV; Group 2 (n=15): GA-**p**AV • Explanted at 6m • 14 pigs died due to non-valve related causes and 3 to infective endocarditis • Group 1: valves functioned well, only minor thrombotic depositions, almost complete absence of calcification; Group 2: 2 pigs had severe and 3 had limited thrombosis, all valves had severe calcification, and more inflammatory cells compared to group 1	**Decell:** • N/I **Recell:** • After 6m, only group 1 displayed a confluent layer of EC (vWF$^+$) on surface • Ingrowth fibroblast in the wall and in only the basal part of leaflets

	Decellularization	Scaffold (+additives)	*In vivo*	Decellularization & Recellularization
[393] Quinn et al. (2011)	**Detergent:** • Triton X-100 • Sodium-lauroyl sarcosine **Enzyme:** • Benzoase®	**Scaffold:** • **o**PV	**Sheep** (n=18) • RVOT • Group 1 (n=8): acellular **o**PV; Group 2 (n=6): cryopreserved allografts; Group 3 (n=4): bioprosthetic porcine valves ○ *Post-implantation (20w):* minimal regurgitation similar in all groups, no calcification in group 1 (only arterial wall calcification in group 2/3). Valve performance comparable between group 1 and 2	**Decell:** • HE: cell free; DNA content reduced >99.3%; ECM preserved **Recell:** • Only spontaneous recellularization in group 1, mainly in arterial wall and variably extending into the leaflets
[382] Cebotari et al. (2010)	**Detergent:** • SDS • SDC	**Scaffold:** • **h**PV	**Humans** (n=38) • RVOT • Follow-up 5y (5y freedom explantation=100%) • 1 patient died after 11m (non-valve related cause)	**Decell:** • N/I [401] **Recell:** • After 11m, partial repopulation with autologous cells
[433] Navarro et al. (2010)	**Detergent:** • SDS	**Scaffold:** • **h**PV	**Sheep** (n=8) • orthotopic position • Explanted at 7d, 1, 3 or 6m • Mean diameter valves increased over time • No signs of degeneration or calcification	**Decell:** • N/I **Recell:** • From day 7 until 6m: progressive recellularization valve conduit (wall) • After 6m: repopulation reaching distal end of the leaflet, mainly LV
[317] Baraki et al. (2009)	**Detergent:** • SDC • SDS	**Scaffold:** • **o**AV	**Sheep** (n=18) • Orthotopic position • Group 1 (n=12): acellular **o**AV; Group 2 (n=6): fresh allograft • Explanted at 3 or 9m • Group 1: trivial regurgitation, normal morphology, no signs of dilatation, degeneration or rejection. Some animals (n=2) minimal calcification and in one microthrombi formation on the leaflet surface; group 2: valves thickened, shrunken with marked calcification/degeneration signs, and advanced insufficiency	**Decell:** • HE: complete cell free; ECM preserved **Recell:** • After 9m, wall partially covered with an EC monolayer, incomplete EC layer on leaflets ($eNOS^+$ and vWF^+) • After 3m, partial repopulation interstitium by interstitial cells which increased after 9m
[434] Hopkins et al. (2009)	**Detergent:** • Sodium lauryl sulfate • Triton X-100	**Scaffold:** • **o**PV	**Sheep** (n=10) • pulmonary valve replacement • Group 1 (n=5): cryopreserved **o**PV; group 2 (n=10) acellular **o**PV • Explanted after 1y • Group 1: 1 sheep had leaflet dysfunction, no leaflet calcification in any valve but wall calcification in 1 valve; Group 2: 1 sheep died due to calcified subacute bacterial endocarditis and the other 4 sheep had leaflet and wall calcifications	**Decell:** • N/I **Recell:** • After 1y, recellularization of the pulmonary artery and basal region of the leaflets, focal re-endothelialization on the outflow surface of the leaflets

	Decellularization	Scaffold (+additives)	*In vivo*	Decellularization & Recellularization
[435] Costa et al. (2007)	**Detergent:** • SDC • SDS	**Scaffold:** • **h**PV	**Humans** (n=68) • Study ongoing • Ross operation • Follow-up more than 4y • 1 late and 1 early death, and 2 re-operations for endocarditis ○ *Post-implantation (6m):* inflammatory reaction in the wall	**Decell:** • N/I **Recell:** • After 6m, partial re-endothelialization (data not shown) and partial repopulation of the wall

[436] Iwai et al. (2007)	**Detergent:**
	• Sodium lauryl sulfate
	Triton X-100
		Scaffold:
		• **p**AV
			Rats
			• Piece of valve in subdermal space
			• Explanted at 14 or 60d
			  ○ *Post-implantation (60d):* minimal inflammatory cell infiltration and calcification
			Dogs
			• Pulmonary valve position
			• Explanted 1, 2 and 6m
			  ○ *Post-implantation (6m):* no thrombus formation, no regurgitation
				Decell:
				• HE: effective cell elimination
				Recell:
				• Dogs
				  ○ Spontaneous re-endothelialization ($CD31^+$) of the luminal surface within 1 month. After 2m little cells invade wall and leaflets. After 6m, interstitium of the wall complete repopulated (leaflets only partial)

[394] Dohmen et al. (2006)	**Detergent:** • SDC	**Scaffold:** • **p**PV (Matrix P)	**Sheep** (n=4) • Pulmonary valve replacement • Mean follow-up 9 months • Significant increase diameter annulus • No calcification and low calcium content	**Decell:** • N/I [281] **Recell:** • After 11 months, conduit wall covered with vWF^+ cells, and repopulation of the interstitium with Fb-like cells (No data of valve leaflets)
[437] Takagi et al. (2006)	**Enzyme:** • Trypsin	**Scaffold:** • **I**AV	**Dogs** (n=15) • abdominal aorta • explanted at 4, 12, 24w	**Decell:** • HE: almost completely cell free **Recell:** • After 4w, incomplete endothelial lining (vWF^+), this gradually increased, and after 24w a single layer of EC completely covered the surface of the conduits (no data for the leaflets) • After 24w, the conduit interstitium was almost completely recellularized by fibroblast-like cells (vimentin and/or α-SMA^+) (no data for the leaflets)

[271] Erdbrügger et al. (2006)	**Detergent:**
	• SDC
		Scaffold:
		• **p**PV (Matrix P)
			Sheep (n=10)
			• Ross operation
			• 100% survival rate
			• Explanted at 3m, 6m or 11m
			• Excellent hemodynamic properties, no signs of calcification (time?)
			Humans (n=103)
			• Study ongoing
			• 2 died (36d, 43d) from septic multiorgan failure
			• 1 re-operation (10m)
			• Follow-up more than 2y
				Decell:
				• DAPI: not completely cell free; DNA content reduced by >90%; extractable membrane protein reduced by 75%
				Recell:
				• Sheep:
				  ○ After 3m; luminal surface covered with EC (vWF^+), and interstitial cells started to invade
				  ○ After 11m, confluent EC layer, the entire media was repopulated by host cells (no data repopulation of leaflets)
				• Human:
				  ○ After 10m, repopulation of host cells in vessel wall (+ also leaflets (data not shown)), EC covered the surface (vWF^+)

	Decellularization	Scaffold (+additives)	*In vivo*	Decellularization & Recellularization
[438] Miller et al. (2006)	[139] O'Brien et al. (1999)	**Scaffold:** • CryoValve SG (**h**AV)	**Human case report** • Orthotopic position • Male, 52y ○ *Post-implantation (2y):* leaflets minimal fibrous thickening, focal calcifications, no $CD3^+$, $CD20^+$ or $CD15^+$, only $CD68^+$ in scattered cells, 1mm deep to the endothelium of the leaflets	**Decell:** • N/I **Recell:** • Cells observed lining the valve cusps (endothelial appearance) and showed focal extension into the LS, more prominent at the base of the leaflet (spindle shaped cells)
[439] Meyer et al. (2005)	**Detergent:** • Triton X-100	**Scaffold:** • **r**AV	**Rats** • Infrarenal abdominal aorta • 1 til 4w ○ *Post-implantation (1w):* Untreated valves: early and intense T cell infiltrate and significant thickening leaflets. Decellularized valves: less T cells and no leaflet thickening. Majority of T cells are $CD8^+$ (also $CD3^+$ present), decrease over time	**Decell:** • Complete removal of EC (anti-CD31) and absence of intact cellular elements. Some residual interstitial fragments are noted (anti-vimentin); preserved ECM **Recell:** • N/I
[440] Ota et al. (2005)	**Detergent:** • Sodium lauryl sulfate • Triton X-100	**Scaffold:** • **p**AV • Fibronectin • Hepatocyte GF	**Dogs** (n=39) • Pulmonary arterial trunk • Group 1 (n=15): fibronectin-HGF coated **p**AV; Group 2 (n=12): non-coated **p**AV; Group 3 (n=12): HGF coated **p**AV • 5 dogs died (infection or unknown causes) (3 from group 3, 1 group 1/2) • Explanted at 1w or 1m	**Decell:** • N/I **Recell:** • After 1w, partial re-endothelialization (group 1) • After 1m, complete monolayer EC (vWF^+) in group 1, but inadequate in group 2 and 3 • Partial repopulation interstitium group 1, less in group 2 and little in group 3
[441] Da costa et al. (2004)	**Detergent:** • SDC	**Scaffold:** • **p**PV (Matrix P)	**Sheep** (n=4) • RVOT • Normal function ○ *Post-implantation (5m):* Calcium content higher in cryopreserved grafts and traces of calcification compared to acellular grafts	**Decell:** • He: cell free **Recell:** • Ingrowth of Fb-like cells (50%) and partial re-endothelialization
[140] Simon et al. (2003)	[139] O'Brien et al. (1999)	**Scaffold:** • **p**PV (SynerGraft)	**Human**s (n=4) • RVOT (2 Ross operation) • 3 patients died (1 at 6w and 1 at 1y due to generation of the valve, and 1 at 7d due to rupture of the valve) • In the 4^{th} patient, the valve was explanted after 2d ○ *Post-implantation:* Non-specific severe early inflammatory reaction and a lymphocytic reaction later on; dense fibrous sheets around the grafts	**Decell:** • Incomplete recellularization and calcific deposits **Recell:** • No cell repopulation

	Decellularization	Scaffold (+additives)	*In vivo*	Decellularization & Recellularization
[142] Elkins et al. (2001)	[139] O'Brien et al. (1999)	**Scaffold:** • **o**PV (SynerGraft) • CryoValve SG (**h**PV)	**Sheep** (n=6) • RVOT • Group 1 (n=4): SynerGraft **o**PV; Group 2 (n=2): Cryopreserved **o**PV • 1 from group 2 died (non-valve related infection) • Explanted at 3 and 6m • Trivial-to-mild regurgitation both groups **Humans** (n=32) • Ross operation with CryoValve SG • Study ongoing but so far: no antibody production against donor tissue (follow-up 1 or 3m)	**Decell:** • HE: >99% cell free; MHC I and II markedly reduced **Recell:** • After 6m, matrix recellularization 75% of leaflet length (group 1)
[139] O'Brien et al. (1999)	• Water **Enzyme:** • RNase and DNase	**Scaffold:** • **p**PV (SynerGraft)	**Sheep** (n=7) • RVOT • Hemodynamically functional ○ *Post-implantation (5m)*: small population of lymphocytes (<5%), no calcification	**Decell:** • HE: >95% reduction in histologically demonstrable cellularity **Recell:** • Allografts largely acellular and no re-endothelialization (cell remnants or host cells?) • SynerGraft: ingrowth of fibroblastic cells at the base of the leaflets, distal 1/3 still acellular
[442] Wilson et al. (1995)	**Detergent:** • Triton X-100	**Scaffold:** • **d**AV • **d**PV	**Dogs** (n=6) • Heterotopic position (left main pulmonary artery) ○ *Post-implantation (1m)*: no inflammation	**Decell:** • N/I [94] **Recell:** • Ingrowth at the base of the leaflets with spindle-shaped cells (not through the body to the tip) • Partial re-endothelialization across the base of the leaflets, semi-monolayer at the body

Abbreviations: b = bovine; h = human; o = ovine; p = porcine; r = rat; l = lapine; c = canine; GF = growth factor; AV = aortic valve; PV = pulmonary valve; SIS = small intestine submucosa; PER = pericardium; PA = pulmonary valve autograft; DPVA = decellularized pulmonary valve allograft; DAVA = decellularized aortic valve allograft; MHC = major histocompatibility complex; N/I = not investigated; N/A = not applicable; SDC = sodium deoxycholate; SDS = Sodium dodecyl sulfate; eNOS = endothelial nitric oxide synthase; vWF = von Willebrandfactor; ECM = extracellular matrix; d = days; w = weeks; m = months; y = years; α-SMA = α-smooth muscle actin; HE = hematoxylin eosin; Fb = fibroblasts; MFb = myofibroblasts; EC = endothelial cells; LF = lamina fibrosa; LS = lamina spongiosa; LV = lamina ventricularis; MMP = matrix metalloproteinase.

Table S3: Overview of hydrogels used in HVTE for the encapsulation of VIC

	Hydrogel/Crosslinking	Cell type/Density/Study duration	Results
[354] Kang et al. (2017)	• Hybrid hydrogels: 20 w/v% **Gel-MOD/ PEG-DA (ratio = 1:1)** + 7.5 w/v% **alginate** • Hydrogels discs (Ø8mm*1.5mm) • Crosslinking: 5min, UV-A (365nm), 2mW/cm^2, 0.025-0.1 w/v% Irg, 0.25-1 w/v% VA-086 • (also high powered LED lamp = 136mW/cm²)	• **h**VIC, **h**ADSC, **h**SMC • 2.5*10^6 cells/ml • 7d • Catalase	**Viability** • Highest viability for SMC= 95%, VIC= 93%, ADSC= 93% • Irg had a more detrimental effect on the viability of all cell types than VA-086 • Increased PI concentration = decreased viability **Phenotype** • ADSC spread more than VIC and SMC in Irg gels; VIC circularity increased with increasing Irg; Cells in VA-086 gels spread more • Catalase did reduce oxidative stress but did not improve viability of cells in general • Using LED lamp resulted in decreased numbers of viable cells **Compressive Biomechanics** • CM of hydrogels ranged from ±19.3-120.7 kPa; CM of VA-086 and Irg crosslinked gels with the low intensity light was not significantly affected by increasing PI concentration; lamp light intensity seemed to have saturation points since increased PI concentrations did not increase the CM • Gels with 0.25-0.5 w/v% VA-086 mostly dissolved; crosslinked gels with 0.75-1 w/v% VA-086; 0.025-0.1 w/v% Irg = ok • CM of gels with 1.0 w/v% VA-086 (26kPa) and 0.1 w/v% Irg (80kPa) increased when using LED to ±50 and ±125 kPa respectively • Q decreased when increasing PI concentration and increasing light intensity (only for VA-086)
[443] Mabry et al. (2016)	• 8-arm MMP-degradable **PEGnb** + adhesive peptide (RGDS, IKVAV, RLD) • DS = ~90% • Hydrogels discs (Ø4mm*1mm) • Crosslinking: 2m, UV-A (365nm), 2.5mW/cm^2, 1.7mM LAP	• **p**VIC • 1*10^7 cells/ml • 5d	**Viability** • After 1d cell viability = 75% **Phenotype** • VIC in control gels (without peptides) remained round after 5d; cells in IKVAV gels remained round, while cells in RGDS or RLD gels were elongated; circularity of cells decreased with increasing peptide concentration • VIC in gels without RGDS had low levels of α-SMA; VIC in gels with RGDS were more activated after 3d (MFb-like) **Compressive Biomechanics** • EM= 1 or 6 kPa
[444] Duan et al. (2016)	• Hybrid hydrogels: **HA-MA/Gel-MOD** (0.5/1 w/v%) • DS = 22.5% (HA-MA); 61.1% (Gel-MOD) • Hydrogels discs (Ø 8mm*1mm and 15mm*15mm)	• **h**VIC • 4*10^6 cells/ml • 21d • ± activation medium (TGF-β) • ± osteogenic medium	**Viability** • Viability of the cells did not significantly decrease during the study **Phenotype** • In activation media 3kPa VIC-laden gels (5m crosslinking) had higher GAG, Col, and elastin content than 1kPa VIC-laden gels (1m crosslinking) at d7. At d21 in osteogenic media 1kPa gels had higher GAG, Col, and elastin content than 3kPa gels; Gels in control media = Col and elastin in 3kPa gels higher than in 1kPa gels, • Expression of α-SMA and vim detected in all hydrogels after 21d; VIC in activation or osteogenic media more pronounced α-SMA$^+$ • Increasing gel stiffness resulted in upregulation of α-SMA and downregulation of vim in activation media as well as in osteogenic media (significant in 3kPa gels) • Runx2 and OCN detected only in VIC in osteogenic media and increased with increasing stiffness; VIC in 1kPa hydrogels showed more significant increase of Runx2 and OCN than in 3kPa gels; ALP expression increased with increasing stiffness (higher in 1kPa gels)

	Hydrogel/Crosslinking	Cell type/Density/Study duration	Results
	• Crosslinking: 1 or 5m, UV-A (365nm), 2mW/cm^2, 0.05 w/v% Irg		**Compressive Biomechanics** • CM correlated with crosslinking duration; the stiffness of acellular hybrid hydrogels increased from ±1.33kPa (1m) to ± 3.33kPa (5m) • Stiffness of VIC-laden gels (5m crosslinking) decreased at d1; after 21d VIC-laden gels in control media maintained stiffness, while VIC-laden gels in activation and osteogenic medium increased stiffness; gels in osteogenic media had the highest stiffness • Stiffness of VIC-laden gels (1m crosslinking) similar to stiffness of acellular gels; only VIC-laden gels in osteogenic media increased stiffness; stiffness of gels in osteogenic media from 1m crosslinking had much greater increase in stiffness than gels from 5m crosslinking
[224] Gould et al. (2016)	• 2.5 mM MMP-degradable 8-arm **PEGnb** + adhesive peptides (RGDS/VGVAPG/P15) • DS > 95% • • Crosslinking: 10m, UV-A (365nm), 8.5mW/cm^2, 0.2 mM Irg	• **p**VIC • 15*10^6 cells/ml • 42d	**Viability** • Viability cells after 14d = 95% regardless the adhesive peptides **Phenotype** • VIC metabolic activity in RGDS-gel slightly > than other gels at d14 • At d14, VIC in RGDS-gel more elongated than in VGVAPG/P15-gels • At d2, VIC in RGDS-gels had slightly higher MMP activity compared to VGVAPG/P15-gels; cell spreading appeared to correlate with MMP activity: cell spreading by d14 in P15 gels + increased MMP expression • At d14 VIC α-SMA$^+$ RGDS-gel (33%), VGVAPG-gel (56%) and P15-gel (38%); VIC in VGVAPG-gels < Col I but > Col X and chondroitin sulphate than RGDS-gel • After 42d, Col deposition in RGDS-gels > than VGVAPG-gels and P15-gels; Col X/ Col I ratio in RGDS-gels < than VGVAPG-gels and P15-gels **Compressive Biomechanics** • CM = 2kPa
[48] Hjortnaes et al. (2016)	• Hybrid hydrogels: **HA-MA/Gel-MOD** (1/5 w/v%) • DS = ±20% HA-MA; 80% Gel-MOD • Hydrogel discs (Ø8mm*450µm) • Crosslinking: 30s, UV-A (365nm), 2.5mW/cm^2, 0.1 w/v% Irg	• **p**VIC • 21d	**Viability** • Viability cells d1=95%; d21=90% **Phenotype** • VIC quiescent in 3D hydrogels: low α-SMA
[445] Zhang et al. (2015)	• 5, 10, 20 w/v% MMP-degradable **PEG-DA +** adhesive peptide (RGDS) • DS >95% • Hydrogels discs (Ø 8mm*1mm) • Crosslinking: 3m, UV-A (360-480nm), 7.2mW/cm2, 0.3 w/v% Irg • Crosslinking: 3m, white light exposure, 1.5 w/v% TEA, 10 µM Eosin Y, 0.375 w/v% NVP	• **p**VIC • 3*10^7 cells/ml • 28d	**Viability** • Cell viability >80% in all conditions; cell viability decreased with lower amount of peptide **Phenotype** • Increasing the amount of RGDS resulted in decrease of cell circularity and increase cell area • VIC activation = higher level of α-SMA found in gels with higher RGDS; amount of RGDS had little effect on vim • PEG hydrogels were degraded by VIC; MMP2 was detected in culture medium **Compressive Biomechanics** • CM dependent on crosslinking time; Q of 10 w/v% dependent on PEG-DA MW (lower Q for stiffer 3.4kDa gels, higher Q for weaker 20kDa gels • EM of cell-laden hydrogels was significantly higher at d21 and 28 than at d1 to d14

	Hydrogel/Crosslinking	Cell type/Density/Study duration	Results
[235] Hjortnaes et al. (2015)	• 1 and 2 w/v% **HA-MA** • 5 and 10 w/v% **gel-MOD** • Hybrid hydrogels: **HA-MA/Gel-MOD** (1/5 w/v% and 2/10 w/v%) • DS = ±20% HA-MA; 80% Gel-MOD • Hydrogel discs (Ø8mm*450µm) • Crosslinking: 30-90s, UV-A (320-480nm), 2.5mW/cm^2, 0.5 w/v% Irg	• **p**VIC • 1*10^7 cells/ml • ±5ng/ml TGF-β1 • 21d	**Viability** • Cells viable up to 21d (>80%); viability cells 2/10 w/v% gel (77.7%) < 1/5 w/v% gel (87.4%) • Amount of cells decreased in all gels from d1 till d21 except in 5w/v% gel-MOD **Phenotype** • Cells in 5w/v % Gel-MOD spread the most; increased α-SMA, Col I, and MMP-9 expression (MFb-like); same levels of vim expression in all gels; Col I expression increased in all gels with gel-MOD • aVIC in 5w/v % Gel-MOD; qVIC in hybrid- and HA-MA gels • TGF-β1 upregulated α-SMA, Col I, and MMP-9 expression in hybrid gels (qVIC/Fb-like to aVIC/MFb-like) **Compressive Biomechanics and Q** • 1 compared to 2% HA-MA and 5 to 10% Gel-MOD showed 30% decrease in Q • CM increased with concentration of gel (5-120kPa); highest CM in hybrid hydrogels; CM inversely proportional to Q and pore size in independent hydrogels
[251] Duan et al. (2015)	• Hybrid hydrogels: **HA-MA/Gel-MOD** (0.5/1 w/v%) • DS = 22.5% HA-MA; 61.1% Gel-MOD • Hydrogel discs (Ø8mm*1mm) • Crosslinking: 5m, UV-A (365nm), 2mW/cm^2, 0.05 w/v% Irg	• **p**VIC • **h**BM-MSC • **h**ADSC • 2.5*10^6 cells/ml • 28d	**Viability** • All cell types viable up to 28d (>85%); Viability ADSC significantly > than BM-MSC **Phenotype** • Spreading and circularity VIC and ADSC > BM-MSC; at d28 VIC show the greatest spreading (lowest circularity) • GAG content of all cell types increased (d7-14), stable d14-d28; ADSC lowest GAG production • No significant changes in Col I content of VIC and ADSC; Col I content of BM-MSC peaked at d14; ADSC highest Col I • Elastin content of ADSC increased (d7-14) and stable d14-28; VIC and BM-MSC elastin production stable, but increased d28; ADSC highest elastin after d28
[222] Mabry et al. (2015)	• MMP-degradable 8-arm **PEGnb** + adhesive peptide (RGDS) • Hydrogel discs? (6mm mold) • Crosslinking: 3m, UV-A (365nm), 2mW/cm^2, 1.7 mM LAP	• **p**VIC • 1*10^7 cells/ml • 14d	**Viability** • Viability cells only evaluated after 2d: in soft gels ±90%; in stiff gels ±60% **Phenotype** • After 2d, only cell spreading in soft gels • Inverse relationship between gel stiffness and α-SMA/F-actin fibers expression; cells in stiffer gels more FSP-1 expression; VIC in soft gels MFb-like; VIC in stiff gel Fb-like; more MMP1 expression in stiff gels than soft gels; Col I expression is independent of gel-stiffness **Biomechanics** • EM gels: 0.24 kPa - 13kPa
[221] Wu et al. (2015)	• 4w/v% MMP-degradable **PEG-A** + adhesive peptide (RGDS) • Hydrogel discs (380µm-thick) • Crosslinking: 25s, white light exposure, 10µM eosin Y,1.5% v/v TEA and 3.5µl/ml NVP	• **p**VIC • 1*10^7 cells/ml • 28d • ±50µg/ml AA	**Viability** • Viability cells only evaluated after 3d=98% **Phenotype** • AA increased cell spreading by ±18%, MMP-2 production by 40%, and cell proliferation (amount of cells) by ±76% at d28 (compared to ±33% -AA) • Caspase 3/7 expression lower in AA-treated VIC than non-treated VIC; Col I and Col III production increased due to AA treatment; AA had no influence on α-SMA and ALP expression **Compressive Biomechanics** • At d1 CM of cell-laden hydrogel < than cell-free hydrogel; at d21 or d28 CM of cell-laden hydrogel increased and = CM of cell-free hydrogel • CM: 4.3-6.0 kPa

	Hydrogel/Crosslinking	Cell type/Density/Study duration	Results
[234] Duan et al. (2014)	• Hybrid hydrogels: **HA-MA/Gel-MOD** (2,4,6,6,10,12 w/v%) • DS = 22.5% HA-MA; 61.1% Gel-MOD Hydrogel discs (Ø8mm*1mm) Crosslinking: 5m, UV-A (365nm), 2mW/cm^2, 0.05 w/v% Irg	• **p**VIC • 5*10^6 cells/ml • 7d	**Viability** • Cells viable up to 7d (>90%) **Phenotype** • Circularity VIC in gels with lower stiffness < gels with higher stiffness • d3 VIC in stiffer gels > proliferation than VIC in soft gels; d7 no significant difference in cell proliferation between gels; GAG content on d7>d3 • VIC in stiffer gels expressed less α-SMA, vim, periostin; vim gene expression increased with decreasing gel stiffness; no difference in Col I expression of cells in different gels; upregulation Col I, vim, periostin and α-SMA after 7d **Compressive Biomechanics** • CM decreased with increasing Gel-MOD concentration; CM increased with increasing HA-MA concentration • Highest stiffness: 4% HA-MA/6% Gel-MOD (13.0kPa); lowest stiffness: 6% HA-MA/12% Gel-MOD (4.2kPa)
[227] Duan et al. (2013)	• 0.75 w/v% $O_{0.1}$**HA-MA** or $O_{0.05}$HA-MA or HA-MA • Hybrid hydrogels: + 1 w/v% **Gel-MOD** • DS = 22.5% HA-MA; 29% $O_{0.05}$HA-MA; 30.7% $O_{0.1}$HA-MA • Hydrogel discs (Ø8mm*2mm) • Crosslinking: 5m, UV-A (365nm), 2mW/cm^2, 0.03 w/v% Irg	• **p**VIC • 5*10^6 cells/ml • Spheroids = 5*10^6 cells/ml (hanging drop, 20µl) • 14d • 7d spheroid	**Viability** • Cells viable up to 14d (>75%); addition of Gel-MOD slightly increased cell viability **Phenotype** • At d14, cells more proliferative in softer hydrogels than in stiffer hydrogels; proliferation increased in hybrid hydrogels; circularity decreased in hybrid hydrogels and with decreasing CM • After 14d, GAG content in hybrid gels > than pure hydrogels; only significant increase of GAG content in HA-MA/Gel-MOD; α-SMA, periostin, and hyaluronidase I expression increased with decreasing stiffness of pure hydrogels; addition of Gel-MOD did not influence α-SMA expression, but vim expression slightly increased • Periostin and hyaluronidase expressions increased with decreasing stiffness of hybrid hydrogels • Cells from spheroids in hybrid hydrogels showed extensive spreading and fastest migration rate • HA-MA: α-SMA strongly expressed in VIC inside spheroids, migrated VIC showed more vim expression; Hybrid gels: cells inside spheroid more vim and less α-SMA, but migrated VIC showed more α-SMA **Compressive Biomechanics and Q** • CM correlated with MW HA (HA-MA (2.74kPa) > $O_{0.05}$HA-MA > $O_{0.1}$HA-MA (1.86kPa)) • Addition of gel-MOD increased CM: $O_{0.1}$HA-MA /Gel-MOD (5.19kPa) > HA-MA /Gel-MOD (3.93kPa) • Lower CM = higher Q; addition of gel-MOD lowers Q (levels of crosslinks increased)
[353] Chen et al. (2013)	• Microfluidic: 5, 10, 15 w/v% **Gel-MOD** • DS = 94% • Channel (2000*300µm = WxH) • Crosslinking: 30s (5 w/v% gel), 25 s (10 w/v% gel), and 15s (15 w/v% gel), UV-A (360-480nm), 7.2mW/cm^2, 0.5, 1, 2 w/v% Irg	• Co-culture: **p**VIC-**p**VEC • 1.5*10^6 cells/ml • 21d	**Viability** • Cell viability after 4d = 84% • Concentration of gel-MOD had no significant influence on the cell viability; cell viability decreased with increasing PI concentration (94% viability with 0.5% PI; 0% viability with 2%PI) **Phenotype** • VIC in 5 w/v% gels had the highest spreading; cell spreading decreased with increasing PI concentration and with increasing UV irradiation time • After 3d, VEC formed a confluent monolayer; VEC remained viable and did not migrate • Static cultured VIC = 78% α-SMA$^+$, static co-cultured VIC = 29% α-SMA$^+$, shear-stressed co-cultured VIC 17% = α-SMA$^+$) **Compressive Biomechanics** • EM ranged from 2.5kPa (5 w/v% gels) to ~30kPa (15 w/v%); pores in 5 w/v% gels are heterogeneous in size and distribution, and interconnected; pores in 15 w/v% gels were uniform in size and distribution, and separated by thin walls
[231] Duan et al.	• Hybrid hydrogel: **Gel-Alg** • (0.06g/ml-0.05g/ml) Hydrogel discs (Ø8mm*1mm)	• **p**VIC • **h**SMC • 2*10^6 cells/ml	**Viability** • Viability cells d1=91%; d7=86%; SMC d1=91%; d7= 85% **Phenotype** • Circularity: VIC d1=90%; d7=76%; SMC d1=91%; d7=80% • VIC expressed significantly higher vim than α-SMA (Fb-like), while SMC expressed significantly higher α-SMA than vim (MFb-

	Hydrogel/Crosslinking	Cell type/Density/Study duration	Results
(2013)	• Crosslinking: 5m, 300mM $CaCl_2$	• 7d	like) **Tensile Biomechanics** • Ultimate TS and EM at d1 was significantly > in cell free hydrogels (TS=0.8MPa; EM=1.4MPa); at d7 values were statistically = between both groups (TS±0.35 MPa; EM±1 MPa)
[446] Durst et al. (2011)	• 5/10/15 w/v% of different MW **PEG-DA** • Hydrogel discs (6x44x0.88mm = WxHxT) • Crosslinking: 10m, UV-A (365nm), 10mW/cm^2, 3 w/v% 2-hydroxy-40-(2-hydroxyethoxy)-2-methylpropiophenone	• **p**VIC • 22*10^6 cells/ml • 21d	**Phenotype** • α-SMA expression decreased with increasing stiffness of gels **Compressive and Flexure Biomechanics** • Cell-free hydrogels stiffer than cell-laden hydrogels
[223] Benton et al. (2009)	• 5 and 10 w/v% MMP-degradable 4-arm **PEGnb +** adhesive peptide (RGDS) • Hydrogels discs (Ø7mm*1mm) • Crosslinking: 10m, UV-A (352nm), 5mW/cm^2, 0.05 w/v% Irg	• **p**VIC • 15*10^6 cells/ml • 14d • ±5ng/ml TGF-β1	**Viability** • VIC still viable after 14d in both gel concentrations; 5 w/v% gels more viable cells than 10 w/v% gels **Phenotype** • VIC were proliferative and showed random migration in gels • VIC in 5 w/v% gels spread faster (less circular) than VIC in 10 w/v% (14d) • VIC spread more in gels with higher RGD concentration • + TGF-β1= increased α-SMA and Col I expression
[226] Benton et al. (2009)	• 10 w/v% **Gel-MOD** • DS =57% • Crosslinking: 10m, UV-A (365nm), 5mW/cm^2, 0.05-0.5 w/v% Irg • Hydrogel discs (Ø5mm*1mm) • Crosslinking: 10m, UV-A (365nm), 5mW/cm^2, 0.05-0.5 w/v% Irg	• **p**VIC • 1*10^7 cells/ml • ±5ng/ml TGF-β1 • 7w	**Viability** • Cells viable up to 7w (±80%); TGF-β1 did not influence viability **Phenotype** • Spreading and circularity (±90% and 62.5%) of TGF-β1 treated VIC significantly > compared to untreated (±50% and ±50%) • TGF-β1 lead to higher α-SMA and Col I gene expression **Compressive Biomechanics** • CM = 42kPa • Gels with lowest [PI] = largest pores (~1800μm^2); gels with highest [PI]I = smallest pores (~400μm^2)
[447] Shah et al. (2008)	• Hybrid hydrogels: **HA-MA/PEG-diMA** (1.38μM/1.37 to 22.0mM) • DS ~ 85% • Hydrogels discs (Ø5mm*1mm) • Crosslinking: 7m, UV-A (365nm), 5mW/cm^2, 0.0375 w/v% Irg	• **p**VIC • 22*10^6 cells/ml • 6w • ±1.2mg/ml Exogenous HA • ±1U/ml HAase	**Viability** • HA enhanced VIC survival up to 2w at concentration > than 1.38μM **Phenotype** • Col production in HAase-untreated gels only around the cells, while in HAase-treated gels better Col distribution away from the cell body, throughout the gel and cell number increase • Elastin production was apparent after 4w in HAase-treated gels; no apparent elastin staining in the untreated gels • Exogenous HA reduced Col production in HAase-treated gels compared to untreated gels and increased elastin production in both gels **Compressive Biomechanics** • Total macromere mass increased with increasing PEG concentration; dry mass HA decreased with increasing PEG concentration • Increasing PEG concentration caused decrease in Q (Q = 12.4-37.3)

	Hydrogel/Crosslinking	Cell type/Density/Study duration	Results
[228] Masters et al. (2005)	• 2 w/v% **HA-MA** • 10 w/v% **PEG-DA** • Hybrid hydrogels: **HA-MA/PEG-DA** (2/5 w/v% and 2/10 w/v%) • DS = 1.5%, 54%, 100% HA-MA • Crosslinking: 3m, UV-A (365nm), 5mW/cm^2, 0.05 w/v% Irg	• **p**VIC • 40*10^6 cells/ml • 6w • ±5 HA-MA degradation products	**Viability** • VIC were viable after one week of encapsulation **Phenotype** • Addition of HA degradation products influenced VIC proliferation; VIC proliferation increased with decreasing MW HA degradation products • At d3, total matrix production of VIC (+ degraded HA) was similar to the control gels; at d20 there was significant difference in total matrix production and composition • At d3, elastin production of VIC (+ degraded low MW HA) increased compared to untreated control cells; at d20, increase of elastin more apparent in almost all gels supplemented with HA of different MW • Encapsulated VIC showed significant elastin production after 6w **Compressive Biomechanics** • Increasing MA → decreased Q, increased CM and increased degradation time • Highest Q: 2% HA-MA (79.9); lowest Q: 2% HA-MA + 10% PEG-DA (9.69); Highest CM: 2% HA-MA (12.61 kPa); lowest CM: 2% HA-MA + 10% PEG-DA (6.5 kPa)

Abbreviations: p = porcine; h = human; d = days; w = weeks; m = minutes; s = seconds; VIC = valvular interstitial cells; SMC = smooth muscle cells; α-SMA = alpha smooth muscle; vim = vimentin; Fb = fibroblasts; MFb = myofibroblasts; MOD = modified; Gel = gelatin; MA = methacrylamide; Alg = alginate; TS = tensile strength; EM = elastic modulus; DS = degree of substitution; CM = compressive modulus; HA = hyaluronic acid; Abs = absorbance; GAG = glycosaminoglycans; Col = collagen; OHA = oxidized hyaluronic acid; Q = swelling ratio; Irg = Irgacure 2959; MW = molecular weight; PI = photoinitiator; BM-MSC = bone marrow derived mesenchymal stem cells; ADSC = adipose derived mesenchymal stem cells; MMP = matrix metalloproteinase; PEG = polyethylene glycol; Hep = heparin; PEGDA: polyethylene glycol diacrylate; PEGnb = polyethylene glycol norbornene; TEA = triethanolamine; NVP = 1-vinyl-2-pyrrolidinone; LAP = lithium phenyl-2,4,6-trimethylbenzoylphosphinate; W = width; H = height; T = thickness; PEG-diMA = polyethylene glycol dimethacrylate; PEG-A = polyethylene glycol acrylate; HAase = hyaluronidase.

CURRICULUM VITAE

Curriculum Vitae

Annelies **Roosens**

PERSONALIA

Sint-Amandstraat 22 Box 1
9000 Ghent
23th of August 1989
+32 472/23.56.28
roosens.annelies@gmail.com

EDUCATION AND DEGREES

2013-2017 **PhD fellowship**
Department of Basic Medical Sciences
Tissue Engineering Group
Ghent University

PhD thesis: Towards the development of a bio-active tissue engineered heart valve
Promotor: prof. dr. Maria Cornelissen & Co-promotor: dr. Pamela Somers

2011-2013 **MSc in Biomedical Sciences**
Major Degeneration and Regeneration

Master thesis: Generation of transgenic embryonic stem cell lines for the study of human hematopoiesis
Promotor: prof. dr. Bart Vandekerckhove & Co-promotor: dr. Katrien De Mulder

2007-2011 **BSc in Biomedical Sciences**

ADDITIONAL TRAINING

Specialist Course: Laboratory Animal Science (Cat. C), Ghent University
Specialist Course: From qPCR experiment design to data analysis, Biogazelle, Ghent
Intermediate Academic English, Ghent University (UCT)

SCIENTIFIC OUTPUT
A1 publications

1. Charlot P, Campos F, **Roosens A**, Cornelissen R, Carriel V. Evaluation of a novel detergent-based method for decellularization of peripheral nerve allografts. (Manuscript in preparation for Journal of Tissue Engineering and Regenerative Medicine, 2017)

2. **Roosens A**, Handoyo Y, Declercq H, Cornelissen R. Impact of modified gelatin on valvular microtissues (Submitted: Journal of Tissue Engineering and Regenerative Medicine, June 2017)

3. **Roosens A**, Asadian M, De Geyter N, Somers P, Cornelissen R. Complete static repopulation of decellularized porcine tissues for heart valve engineering – an in vitro study. (In press: Cells Tissues Organs)

4. **Roosens A**, Puype I, Cornelissen R. Scaffold-free high throughput generation of quiescent valvular microtissues. Journal of molecular and cellular cardiology. 2017;106:45-54.

5. **Roosens A**, Somers P, De Somer F, Carriel V, Van Nooten G, Cornelissen R. Impact of Detergent-Based Decellularization Methods on Porcine Tissues for Heart Valve Engineering. Annals of biomedical engineering. 2016;44(9):2827-39.

6. Somers P, **Roosens A**, De Somer F, Cornelissen M, Van Nooten G. Non-Cytotoxic Crosslinkers for Heart Valve Tissue Engineering. The Journal of heart valve disease. 2015;24(1):92-100.

SCIENTIFIC OUTPUT
Conferences

1. Tissue Engineering and Regenerative Medicine International Society, European Chapter meeting 2017 (TERMIS-EU 2017); 26-30 June 2017, Davos, Switzerland

   Poster presentation: Evaluation of a novel detergent-based method for decellularization of peripheral nerve allografts. Charlot P, Campos F, **Roosens A**, Cornelissen R, Carriel V.

2. Tissue Engineering and Regenerative Medicine International Society, European Chapter meeting 2017 (TERMIS-EU 2017); 26-30 June 2017, Davos, Switzerland

   Oral presentation: High throughput generation of quiescent valvular interstitial cell micro-aggregates for biofabrication of heart halve tissue. **Roosens A**, Puype I, Philips C, Cornelissen R.

3. Tissue Engineering and Regenerative Medicine International Society, 4th World congress (TERMIS 2015); 8-11 September 2015, Boston, USA

   Poster presentation: Tissue engineering of heart valves: valvular or pericardial matrix? **Roosens A**, Somers P, De Somer F, Carriel V, Van Nooten G, Cornelissen R.

4. 3th Belgian Symposium on Tissue Engineering (BSTE) 2015
   19-20 March 2015, Louvain, Belgium

   Poster presentation: Histological, biochemical and mechanical evaluation of decellularized heart valve leaflets. **Roosens A**, Somers P, Cornelissen R.

5. Tissue Engineering and Regenerative Medicine International Society, European Chapter meeting 2014 (TERMIS-EU 2014); 10-13 June 2014, Genova, Italy

   Poster presentation: Histochemical and biochemical evaluation of porcine decellularized heart valves and pericardium. **Roosens A**, Carriel V, Somers P, Cornelissen R.

6. 2nd Belgian Symposium on Tissue Engineering (BSTE) 2013
   24-25 October 2013, Louvain, Belgium

   Attendance

DANKWOORD

"It always seems impossible until it's done"
~ Nelson Mandela (°1918 - †2013)

Dit is het dan, de ultieme kers op de taart: het dankwoord met de allerlaatste woorden die ik ooit zal neerpennen in dit boekje. Aangezien ervaring leert dat dit de meest gelezen pagina's zijn van een thesis alvorens die bij velen in een boekenkast verdwijnt, heb ik er dan ook met veel plezier uitgebreid mijn tijd voor genomen.

Allereerst had ik graag mijn promotor en co-promotor bedankt:

Prof. dr. R. Cornelissen, jij gaf me de mogelijkheid om te doctoreren. Vanaf dag één mocht ik jou aanspreken met **Ria** en jouw deur stond steeds open. Deze familiare sfeer zorgde ervoor dat ik met veel plezier elke dag naar het werk kwam. Je gaf me ook de vrijheid om geheel zelfstandig nieuwe ideeën uit te werken en stond steeds geduldig te wachten op de resultaten. Toen je mij in februari voorstelde om mijn doctoraat nog zowel af te ronden, als te verdedigen binnen het huidige academiejaar, dient eerlijkheid mij toch te gebieden om te zeggen dat er een weekje lang chaos heerste in mijn hoofd. Nog twee papers, een masterstudent met bijhorende thesis, labowerk én een doctoraat finaliseren...ik zag niet direct hoe ik dit gedaan moest krijgen. Na een lijstje te maken met al de voordelen, zijn we er voor de volle 100%, zeg maar 200%, voor gegaan. Bedankt voor de steun tijdens dit toch wel druk half jaartje en de hulp bij de laatste loodjes.

Dr. Somers, Pamela, dat het tussen ons klikte vanaf dag één, zag iedereen. We hebben spijtig genoeg slechts een dik jaar samengewerkt voordat je besloot andere oorden in de privatieve sector op te zoeken. Graag wil ik jou bedanken om me te begeleiden en te helpen mijn eerste stapjes te zetten in de wondere wereld van de cardiale tissue engineering. Full-time mama, full-time job.. bedankt voor de tijd die je kon vrijmaken voor mij tijdens het finaliseren van dit doctoraat.

Vervolgens wil ik graag heel wat mensen in de bloemetjes zetten die de voorbije jaren mijn pad gekruist hebben en die elk op hun manier (op de voor- of achtergrond, soms bewust of onbewust) een belangrijke rol hebben gespeeld om mij tot op dit punt te brengen.

"Whether success or failure, you need to move forward. The momentum is what is critical"
~ Frederique Dame (~2017)

Op de vraag die me vroeger veel gesteld is: "Wat wil jij later worden?", zijn vele antwoorden de revue gepasseerd: van juffrouw, dierenarts, bioloog, tot fysicus. Tegen de tijd dat ik in het 5^{e}-6^{e}-middelbaar aanbelandde stond de keuze min of meer vast: regentaat wiskunde-fysica. Weinigen onder jullie weten dit, maar het was op aanraden van **Meneer Detremerie,** mijn toenmalige leerkracht fysica, dat ik toch voor Universitaire studies koos. Regentaat wiskunde-fysica maakte plaats maken voor Biomedische Wetenschappen. Meneer Detremerie, bedankt om altijd en overal het beste in uw leerlingen naar boven te halen, om me te inspireren en te motiveren, maar vooral bedankt om in mij te geloven!

"I'd give my right arm to know the secret of regeneration"
~ Oscar E. Schotte (°1895 - †1988)

Het studentenleven in Gent beviel me zo hard dat ik ineens besloot om er iets langer te blijven door mijn eerste jaar zo goed als te dubbelen. Maar verstand -en in mijn geval discipline- komt met de jaren! Na de bachelor succesvol afgerond te hebben, koos ik resoluut en met volle overtuiging voor de Major Degeneratie en Regeneratie. Wat ik niet in de hand had, was het onderwerp voor onze masterthesis. Door complete willekeur kwam ik terecht in het labo van **prof. dr. Vandekerckhove** onder de begeleiding van **dr. Katrien De Mulder**. Het bovenstaande citaat is dan ook eentje met een dikke knipoog naar haar. Zonder Katrien had ik nooit gestaan waar ik nu sta. Bedankt om me de passie voor het wetenschappelijk onderzoek bij te brengen, om me te introduceren in de wondere wereld van de celcultuur en moleculaire biologie, om me de kneepjes van het vak bij te brengen, maar vooral voor jouw enthousiasme. Wie zich afvraagt van wie of waar ik mijn drive heb…. I learned it from the best!

"Women love to wonder, and that is the seed of science"
~ adapted from Ralph Waldo Emerson (°1803 - †1882)

Februari 2013 zat er een mailtje in mijn inbox van dr. Pamela Somers: "naar aanleiding van de start van een nieuw BOF project dit jaar zoek ik een geschikte doctoraatsstudent (cardiale tissue engineering)". Datzelfde weekend gingen mijn CV en motivatiebrief nog de deur uit en na een aangenaam gesprek met prof. dr. Cornelissen en dr. Somers werd ik weerhouden voor de positie. Zo kwam ik in oktober terecht op **de Dienst Histologie**, een dienst waar ik met open armen ben verwelkomd (behalve de ochtend van mijn allereerste werkdag toen ik, nog voor ik iets kon zeggen, vriendelijk werd doorverwezen naar het gebouw ernaast omdat ze dachten dat ik een verloren gelopen studente was. **Leen** het is je bij deze al lang vergeven!).

"Reason, Observation, and Experience — the Holy Trinity of Science"
~ Robert G. Ingersoll (°1833 - †1899)

De Dienst Histologie, ons labo!
The girls: **Annelot, Charlot en Lise**, drie doctorandae waarmee ik niet alleen een bureauruimte maar ook lief en leed gedeeld heb. Bedankt om vele uurtjes samen met mij te knallen, om me ook wel vele uurtjes gewoon bezig te houden met gekwebbel (al moet ik daarvoor eerder met de vinger naar mezelf wijzen), om samen nieuwe studies te bedenken of om me te helpen bij de interpretatie van data, maar vooral om me te steunen tijdens dit laatste toch wel hectisch half jaartje. Annelot mag zichzelf ondertussen al doctor noemen, Lise en Charlot hebben nog een (lange) weg te gaan. Mijn advies: ni neute, ni pleuje! Vooral blijven knallen, altijd denken zoals een proton en alles komt goed! Ik wil dit ook **Stephanie** toewensen; jij bent nog niet zo heel lang onder ons, maar ik weet zeker dat (zeker nu je verhuisd bent naar onze bureau) ook jij daar een toffe periode tegemoet gaat!

The boys: **Matthias**, mijn pauzebuddy! Bedankt om me te leren relativeren en om me te prikkelen om terug de wijde wereld in te trekken, maar vooral voor die carte blanche die ik gekregen heb en ooit echt wel ga inzetten! **Jeroen**, het is altijd een verrassing om jou hier tegen te komen aangezien je het meeste van je tijd in het MRB doorbrengt en jij je plaatsje in onze bureau hebt vrijgemaakt voor **Bram.** Jullie beiden wil ik graag bedanken voor de plezante bureau momentjes en om ervoor te zorgen dat het niet áltijd over vrouwenzaken ging! Van wat ik hoor en zie, zijn jullie allemaal goed bezig! Veel succes nog!

Mijn surrogaatmamaatjes: **Greet, Johanna en Leen.** Bedankt om steeds mijn onderzoek mee te helpen ondersteunen (qPCR, IHC, celcultuur), maar ook om op persoonlijk vlak er steevast te staan. Bedankt voor de vele babbeltjes, berichtjes en peptalks. Ook bedankt om ontelbare keren te vragen of jullie iets voor mij konden doen en om ermee om te kunnen dat ik soms veeleisend kan zijn en de dingen liever vandaag dan morgen zie gebeuren. De (toekomstige) doctoraatstudenten mogen echt hun 'pollekes kussen' met jullie, want zo maken ze er niet veel!

De techneuten: **Toke en Chris.** Toke, bedankt om steeds zo behulpzaam te zijn en voor het inscannen van mijn preparaatjes met de virtuele microscoop. Chris, jij hebt ons team pas het laatste jaar vervoegd maar het voelt aan alsof je al veel langer deel uitmaakt van onze onderzoeksgroep. Bedankt voor die dagelijkse glimlach, de oprechte interesse en de uitgevoerde mechanische analyses!

De post-docs: **Julie en Heidi**. Julie, jij hebt er heel recent voor gekozen om full-time voor het onderwijs te kiezen en de onderzoeksgroep te verlaten. Toch heb ik de kans gekregen om je beter te leren kennen. Zo goed zelfs dat je me je drie schatjes van patatjes toevertrouwt. Het is een waar genoegen om al vier jaar deel uit te maken van jouw en hun leven en hen te zien groot worden. Top-mama = top-kindjes! Bij deze, je mag me nog lang op je lijstje met babysitters laten staan. Heidi, bedankt voor het gezelschap tijdens ons werktripje naar Boston en voor het kritisch nalezen van mijn laatste paper. De recent opgerichte Bioprint Core Facility heeft voor jou nieuwe deuren geopend. Ik ben al benieuwd welke (bio)scaffolds er de komende jaren geprint zullen worden!

Het is echt met pijn in het hart dat ik jullie allemaal 'achterlaat'. Denk eens aan mij als jullie nog eens een labo-uitstapje doen!

"First we eat, then we do everything else"
~ M.F.K. Fisher (°1908 - †1992)

Aan al de **cafetaria ladies**: *Eat good, feel good* zegt men, en ze hebben nog gelijk ook! Na een tijdje had niemand van jullie nog veel woorden nodig om te weten dat ik elke middag 'the usual' kwam halen. Bedankt voor de vele korte babbeltjes, ook bedankt om mijn salade vaak spontaan te verrijken met extra patatjes, selder en perziken, maar vooral bedankt om me steeds met een glimlach te bedienen en voor de extra support bij de laatste loodjes. Ik ga die dagelijkse bezoekjes echt missen!

" A clean place, makes a happy space"
~ author unknown

Aan onze poetsmannen: **Pierre en Samir**. Bedankt om mijn bureau steeds zo netjes te houden. Mijn vuilniszakjes en papiermand werden steevast sneller geledigd dan dat ik ze kon vullen, bedankt!

"So often you find that students you are trying to inspire are the ones that end up inspiring you"
~ Sean Junkins (~2013)

De afgelopen jaren heb ik me ook door heel wat studenten laten inspireren. 11 studenten (**Maïté**, **Joke & Ilia**, **Thomas & Camille**, **Arne & Lotte & Arthur**, **Maarten**, en mijn laatste twee toppertjes: **Inès** en **Yohana**) resulteerden in een totaal van zeven masterscripties. Bedankt om me kritische (soms onmogelijke) vragen te stellen, om over de lat te springen die ik elk van jullie boven het hoofd hield, om me te leren dat ieder van jullie op een andere manier benaderd diende te worden, om al mijn revisies keer op keer aan te passen (goed wetende dat ik hoogstwaarschijnlijk nog wel weer met nieuwe opmerkingen zou afkomen). Ook bedankt voor de vele lieve berichtjes en kaartjes op mijn prikbord en voor de (soms intercontinentale) cadeautjes. Het was een voorrecht om jullie begeleidster te mogen zijn en weet dat ieder van jullie heeft bijgedragen tot dit proefschrift! Het ga jullie goed!

"The old order changeth, yielding place to the new"
~Alfred Lord Tennyson (°1809 - †1892)

Een universitair team is een dynamisch team. Er zijn dan ook enkele mensen die ik graag wil bedanken maar die ondertussen niet meer aanwezig zijn op onze dienst. **Elien, Elke, Karolien en Sylvia,** bedankt voor de vele tips & tricks bij aanvang van dit doctoraat.

Prof. dr. ir. Ans Baeyens, jij hebt recent de fakkel van prof. dr. Thierens overgenomen en komt het team Radiobiologie versterken. Bedankt voor jouw gedrevenheid, de vele babbeltjes over de middag en voor jouw steun. Samen met **prof. dr. Anne Vral**, een even hard werkende professor, ben ik zeker dat je deze groep naar nieuwe hoogtepunten zal brengen. Veel succes!

Ria, jij staat aan het einde van je carrière en kan binnenkort genieten van je emeritaat. Alhoewel je onze Alma Mater het komende jaar nog niet helemaal wilt/kan loslaten en je nog betrokken zal blijven bij een lopende studie, wens ik jou toch vele gelukkige werkvrije jaren toe.

Seba, you went back to Granada.. whish you all the best with your girls! Whenever I'll find the time, I promise, I will come and vistit you. Thanks again for all the support and for letting me use your brain once in a while!

"Friendschip is only real when shared"
~Christopher McCandless (°1968 - †1992) #IntoTheWild

Lieve topvriendinnetjes: **Alieke, Aurélie, Charlotte C, Charlotte D, Ellen, Evelien, Hanneke, Kerensa, Lina, Michèle, Mumu, Sofie**, mijn steun en toeverlaat: over ieder van jullie valt meer dan een pagina te schrijven! Jullie hebben me, vooral dan het laatste jaar, geregeld moeten missen -wegens te druk-. Ik maak alleen beloftes die ik kan nakomen: wij gaan schade inhalen komende jaar! Nogmaals dikke merci om er steeds onvoorwaardelijk te zijn, om mijn gedachten te verzetten wanneer dat nodig was, om me te helpen met de voorbereidingen van de receptie of de lay-out van dit proefschrift, om te babysitten op mijn ratjes terwijl ik op congres was, om mijn middagpauzes op het UZ op te fleuren, om af en toe gewoon simpelweg eens te vragen hoe alles liep, om me te vergeven dat ik niet zoveel heb kunnen helpen bij de voorbereidingen van de vrijgezellen-weekendjes, om me af en toe te doen beseffen dat er meer was dan een doctoraat alleen, en om zó veel meer! Big love <3!

"Science is organized knowledge. Wisdom is organized life"
~ Immanuel Kant (°1724 - †1804)

Eindigen doe ik met de állerbelangrijkste mensen. Onvoorwaardelijke liefde en steun krijg je van je familie. **Mama & Papa**, **Dorien & Robin**, **Emma & Jonas** bedankt om de laatste vier jaar interesse te tonen in mijn onderzoek (ondanks dat jullie er waarschijnlijk vaak geen jota van verstonden), om huishoudelijke taken van mij over te nemen op de drukke momenten (de was en strijk, boodschappen…), om af en toe mijn diepvries te komen vullen met huisbereide maaltijden, om deeltjes van dit proefschrift na te lezen, om de receptie mee te helpen organiseren, maar simpelweg ook om er gewoon te zijn! Ik heb het misschien soms te weinig benadrukt maar weet dat dit een enorme hulp was! Van **Opa & Oma** hebben we helaas in de afgelopen periode afscheid moeten nemen, maar ik weet dat ze heel trots zouden zijn. We mochten dan weer wel twee nieuwe kleine wondertjes verwelkomen. **Matthis & Mila,** bedankt om me te laten beseffen wat écht telt in het leven: familie!

Uit de diepste grond van mijn hart nogmaals allemaal bedankt!!

Annelies

The future belongs to those who believe

in the beauty of their dreams

~ Eleanor Roosevelt (°1884 - †1962)